# Structure-Function-Dynamics Relationships of Protein-Polymer Conjugates: Improving Activity and Stability in Non-Native Environments

Submitted in partial fulfillment of the requirements for

the degree of

Doctor of Philosophy

in

Department of Biomedical Engineering

Stefanie L. Baker

B.S., Chemical Engineering, Oregon State University

Carnegie Mellon University
Pittsburgh, PA

August, 2019

## ACKNOWLEDGEMENTS

**ABSTRACT**

Evolution has optimized the activities and selectivities of proteins at the cost of stability. Certain organisms, known as extremophiles, contain specially adapted proteins that thrive in extreme conditions such as high temperature or high salt; however, the majority of proteins are only able to survive in moderate environments. Thus, protein engineers have long been interested in modifying proteins to increase their stabilities in non-native environments. One method of protein modification is attaching synthetic polymers to the protein surface. There are two main approaches to create these protein-polymer conjugates. Pre-synthesized polymers can be grafted to the protein surface or polymers can be grown from a protein macro-initiator monomer by monomer to a desired length using a controlled radical polymerization technique. Covalently attaching polymers to a protein alters the protein's physicochemical properties (size, bioactivity, stability, solubility), but not always in a predictable way. The key to rationally designing protein-polymer conjugates that display a desired property is to understand the underlying protein-polymer interfacial interactions that drive changes in protein function. In this work, the structure-function-dynamics relationships of grafted from protein-polymer conjugates were investigated using experimental and computational methods in order to improve their activities, stabilities, and solubilities in non-native environments. In Chapter 2, various charged polymers of varying lengths were grown from α-chymotrypsin. Different polymer types altered enzyme bioactivity by changing substrate affinity. Additionally, a mechanism was developed to explain how polymers stabilized proteins at low pH. Zwitterionic and positively charged polymers prevented protein unfolding and assisted in protein refolding to increase stability at pH 1. In Chapter 3, the effect of atom-transfer radical polymerization (ATRP) initiator structure on protein and protein-polymer conjugates was determined. Positively charged ATRP initiators restored the native

surface charge of proteins, when targeting surface accessible amino groups, which increased the protein-initiator and subsequent protein-polymer conjugate activities and stabilities at low pH and high temperature. In Chapter 4, the solubility of lysozyme was predictably tuned by polymer conjugation. Zwitterionic polymers increased lysozyme solubility and prevented precipitation in fully saturated ammonium sulfate salt with maintained bioactivity while amphiphilic polymers decreased solubility. Zwitterionic polymers displayed an anti-polyelectrolyte effect in increasing salt which increased the number of hydration layers around the conjugate to increase solubility. Amphiphilic polymers collapsed around the protein surface in increasing salt concentrations and decreased in hydration which promoted precipitation. The differences in solubilities were utilized to purify mixtures of native protein and protein-polymer conjugates into homogeneous components. In all of these Chapters, atomistic molecular dynamics simulations were employed to enhance the mechanistic understanding of protein-polymer conjugate structure-function-dynamics relationships. The knowledge gained through these combined studies helps to demystify how covalently attached polymers impact protein function which can lead to new applications of protein-polymer conjugates in therapeutic and biotechnological industries.

# TABLE OF CONTENTS

# LIST OF TABLES

# LIST OF FIGURES

# Chapter 1.   **Introduction to Protein-Polymer Conjugates**

## 1.1   **Protein-Polymer Conjugates**

Proteins, the workhorses of living systems, have been the foundation of advances in fields as diverse as paper manufacturing and pharmaceuticals. These extraordinary biomacromolecules sacrifice longevity for exquisite selectivity and activity, and in that molecular sensitivity lies a challenge that has vexed biochemists for decades: how can we engineer proteins to be robust catalysts and binding agents *ex vivo*? The race to ruggedization has gone through phases of discovery during which proteins and enzymes have been immobilized on solid supports, embedded in polymers, reacted with polymers, and protein engineered by random or site-directed mutagenesis. Just three decades ago, it could take dozens of scientists a year to successfully engineer a protein, but with modern protein science there has been an order of magnitude improvement in the pace of progress. One of the most remarkable marriages between the biologic and synthetic worlds has been the generation of protein-polymer bioconjugates. In the late 1960's, Frank Davis from Rutgers University was the first to suggest that poly(ethylene glycol) (PEG) could be attached to proteins for benefit.[1] Then in the 1970's, the ideas became a reality.[2,3] The straightforward chemistry, coupled with significant advances in the synthetic purity of PEG (driven originally by Union Carbide and then later by Prof. Milton Harris and Shearwater Polymers[4]), opened the door to therapeutic applications in which injected protein-polymer conjugates could retain activity while extending lifetime and improving biocompatibility. Between 1990 and 2019, the FDA approved 17 PEGylated therapeutics for human use and it is estimated to be a multi-billion-dollar market. Although this progress has been exponential and exciting, it is vital to continue our exploration of the convergence of chemical, biological, and materials science at the nano- and molecular scale. Further progress

and rational design of biotic-abiotic hybrid biomacromolecules will open the door to the synthesis of multifunctional "biohybrid" materials that combine components of living systems with desired synthetic polymer properties. This means that we must move beyond PEG and introduce proteins to the full breadth of synthetic polymer chemistry. Readers with a specific interest in learning more about protein PEGylation can find a number of excellent reviews on that topic.[5-8]

Biomacromolecules with controlled sequences, such as proteins, polysaccharides, and nucleic acids, provide the diversity, complexity and adaptability of living organisms. Billions of years of molecular evolution have directed nature to synthesize polymers with controlled sequences and configurations. Learning from nature, advances in polymer synthesis have led to reversible deactivation radical polymerization (RDRP) techniques, such as atom-transfer radical polymerization (ATRP) or reversible addition-fragmentation chain transfer (RAFT), that can precisely and reproducibly control the length, monomer content and, to some degree, monomer sequence. Almost two decades ago, scientists began to explore whether RDRP techniques could be initiated from the surface of proteins. Briefly, the vision was to graft polymers from initiators that had been covalently coupled to, or incorporated in, proteins. Often unrecognized in the academic literature is the key work of Andrew Lewis and colleagues at Biocompatibles Ltd who grew polymers from covalently coupled protein-initiators in 2003.[9] Russell and Matyjaszewski began exploring biologic uses of ATRP at the turn of the century and in 2005 published the first report of an active protein-polymer conjugate grown from the surface of an enzyme.[10-13] The Maynard group, taking advantage of the exquisite tight binding of biotin and avidin, used a non-covalently bound biotinylated initiator to grow polymers from the surface of streptavidin-biotin complexes.[14] Since the early pioneering work of these groups, growing of polymers from the

surface of proteins has significantly expanded in scope and complexity. Although the field is now well beyond its infancy, to a large extent, the current chemical design of protein-polymer hybrids has been artful guesswork. There is a need to develop fundamental structure-function-dynamic relationships for biomacromolecule-polymer hybrid structures using computational simulations, and then design and exploit controlled polymer synthetic techniques to enhance the function of biological molecules, cells, and tissues.

## 1.2   Protein-Polymer Conjugate Synthesis

Grafting-from polymerization entails the growth of polymer chains directly from pre-installed initiating sites on a polymer backbone[15], nanoparticle[16], or protein.[17–19] Compared to a grafting-to approach, where coupling occurs between a protein and polymer and after which removal of excess macromolecular species can be difficult, a grafting-from approach allows facile purification of the protein conjugate since reaction byproducts are usually low-molar mass species (**Figure 1.1**). Additionally, mild polymerization conditions afford a range of polymer-protein conjugates with minimal effects on protein integrity or function.[18] Recent developments in controlled radical polymerization (CRP, also termed reversible deactivation radical polymerization, RDRP),[20] especially in ATRP and RAFT polymerization, permit precise control of molecular mass, dispersity, as well as preservation of chain-end functionality. Perhaps one of the most interesting opportunities for bioconjugates is offered by macromolecular engineering and precise control of polymer composition, functionality and topology.[21] Thus, not only linear homopolymers and random copolymers, but also block and gradient copolymers, and various smart polymers with thermal (LCST and UCST) or pH or light responsiveness can be grown from proteins.[22]
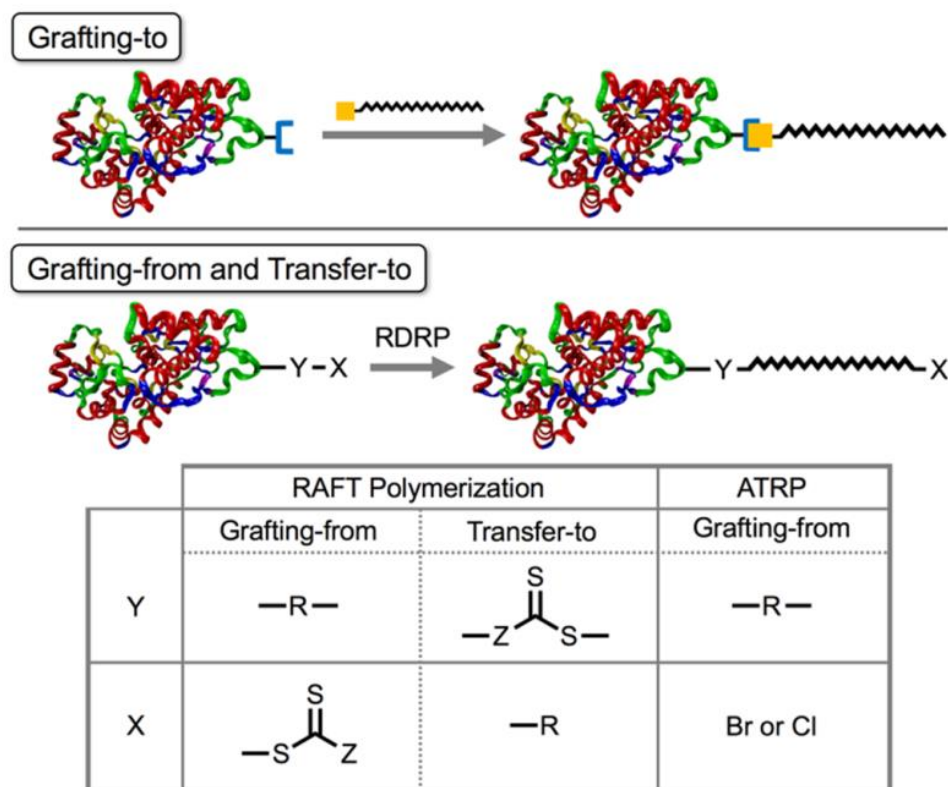
**Figure 1.1.** Grafting-to and grafting-from conjugation techniques for protein-polymer synthesis. In grafting-to, a pre-formed polymer is reacted with a protein. In grafting-from, polymers are grown from initiator modified proteins, using RDRP techniques, including ATRP and RAFT. ATRP uses alkyl halide initiators and Cu catalysts while RAFT uses chain transfer agents and radical initiators. In both cases, these agents must be coupled to the protein prior to polymer growth.

### 1.2.1 Atom-transfer radical polymerization

ATRP employs reversible intermittent activation of dormant alkyl bromides or chlorides with $Cu^I/L$ species as activator. Ligands, L, are typically branched multidentate alkyl amines or pyridines such as tris(2-pyridylethyl)amine, TPMA. The resulting alkyl radicals after addition of a few monomer units (propagation) are deactivated with $Br-Cu^{II}/L$ species back to a dormant state. This provides controlled polymerization and concurrent growth of all polymer chains anchored to protein. Originally, Cu catalysts at concentrations nearly equimolar to alkyl halides were used. However, recently, ATRP with very small amounts (ppm) of Cu catalysts is possible

in the presence of various reducing agents. They include ascorbic acid or sugars, but also various external stimuli such as light, ultrasound, or electrical current.[23,24]

### 1.2.2 Reversible addition-fragmentation chain transfer polymerization

Grafting-from using RAFT polymerization leads to well-defined polymers where propagation and degenerative chain-transfer occur distal to the site of polymer-protein conjugation.[25] This method involves chain-transfer events between the ends of polymer chains in solution, so the chain transfer agent (CTA) R-group is conjugated to the protein.[26] The alternative transfer-to approach, in which the CTA is conjugated to the protein via the Z-group,[27] is more sterically demanding because chain-transfer events must occur between a propagating polymer chain and a thiocarbonylthio group situated between a polymer and protein. Since RAFT polymerizations require external radical initiators, many examples of grafting-from and transfer-to have relied on azo initiators with low degradation temperatures or redox initiators to avoid degrading the protein. However, reports using visible light,[28] photoredox catalysts,[29,30] *etc.*, to initiate RAFT polymerizations have also recently proven to be promising routes to achieve polymer-protein conjugates.

### 1.2.3 Biorelevant polymerization reaction conditions

Macromolecular engineering in aqueous systems does require some special conditions, such as lower pH for RAFT polymerizations or addition of salts with halide counterions (e.g. PBS buffer) for ATRP, to carry out polymerizations under biorelevant conditions.[31] In all cases, the chemistry used must be amiable for proteins, specifically diluted aqueous systems with reasonable temperatures (~4-40°C) and pH (6-8). Monomers typically include various substituted acrylamides, acrylates, or methacrylates.

### 1.2.4 Approaches for site-selective macroinitiator synthesis

Controlling the location of polymer attachment so as not to destabilize or inactivate a protein or enzyme has represented a major challenge in the synthesis of protein-polymer conjugates. In addition to preventing the disruption of structure and activity, such control may enable regulation of protein or enzyme stability and/or dynamics. For instance, if conjugated proximal to the active site or critical residues, polymers that act as actuators may be used to control the dynamics of enzymes and, in turn, modulate activity. While there are many proteins and enzymes where such control may be relevant, a prominent example involves acetylcholinesterase (AChE). Interestingly, the active site of AChE is situated in a crevice that may be opened or closed via molecular motions involving sub-domains of the enzyme, which, in principle, may be controlled via the attachment of polymers at precise locations near the hinge region.[32,33] Once we understand where to grow polymers on proteins, we must develop the tools to target their location.

Conjugating the CTA or ATRP initiator to a protein prior to polymerization is typically accomplished by targeting naturally-occurring nucleophilic (*N*-terminus, lysine, *etc.*) residues on the protein.[17] Various activated esters (such as N-hydroxysuccinimide, NHS) carrying ATRP initiators (α-bromoisobutyrate or α-bromoisobutyramide) and CTAs can be used to react with amino groups on proteins. This approach is advantageous when a dense modification is desired, but disadvantageous when wanting to selectively modify just a few selective sites. In a recent advance, an understanding of how to control the reactivity of surface amino groups with activated ATRP initiators has emerged using blocking agents.[34] Another technique is to specifically target the amino group on the *N*-terminus by reducing the reaction pH.[35] Carbodiimide coupling is also frequently used to conjugate an acid-containing CTA or ATRP

initiator to amine-containing protein residues. In addition to amino groups, protein modification can also be performed on free thiols (cysteines as well as reduced disulfide bonds), hydroxyl groups (serine or threonine), or carboxylic acids (aspartic or glutamic acid as well as the C-terminus) (**Figure 1.2**).[36] Analogous carbodiimide chemistry can be performed at the C-terminus and at acid-containing residues using amine containing polymerization moieties. Moreover, chemical groups that are in low abundance, such as cysteines, are well-suited for site-specific modifications. Disulfide formation is extensively used to conjugate disulfide-containing CTAs or ATRP initiators to free thiols of cysteine residues via thiol-disulfide exchange.

Strategies for site-selective growth have emerged using recombinant proteins where non-natural amino acids are incorporated into the protein sequence at a specific site so that further modification can be performed solely from this location.[37] Using genetic code expansion, Peeler and co-workers[38] have previously demonstrated the successful incorporation of an initiator in proteins at programmable locations. In this case, the initiator was incorporated via introducing a non-canonical amino acid containing a side chain with a bromoisobutyramido group from which polymers were grown via ATRP. Furthermore, conjugating polymers to genetically modified proteins via a reversible cleavable linker, for example using complementary strands of DNA,[39] could subsequently be chain-extended to demonstrate a different approach. More recently, we have developed an analogous approach based on the use of an enzymatic ligation reaction, which can be used to attach multiple reactive handles anywhere in a protein, including internal sites.[40] This approach relies on the insertion of an acceptor peptide to which azide groups may be appended through the activity of lipoic acid ligase. The azide groups may subsequently be used to attach an initiator for growing polymers from as well as attaching polymers to via azide-alkyne click chemistry. Notably, using this approach, initiators may be incorporated in multiple

sites, including internal sites, simultaneously, which represents a major advantage over other enzyme ligation approaches. In addition to lipoic acid ligase, sortase and tyrosinase have also been widely exploited to site-specifically modify proteins, and pre-date the use of lipoic acid ligase for protein modification.

Sortase is a transpeptidase that cleaves between threonine and glycine in an LPXTG motif, and then subsequently ligates the carboxyl group of the threonine to an amine group. This reaction has been used to covalently conjugate a protein/peptide with an LPXTG signaling motif to an aminoglycine protein/peptide.[41,42] Tyrosinase is an oxidase that performs hydroxylation on the phenolic group on tyrosine to create a catechol intermediate. Following this reaction, the catechol intermediate is *O*-alkylated by catechol-*O*-methyltransferase (COMT). This method is highly specific towards the modification of tyrosine residues in proteins and can be used to subsequently modify the tyrosine residue with a molecule of choice, such as an initiator. Site-specific modifications will be needed in the future to facilitate the understanding of how specific modification at pre-determined positions impact biological function.
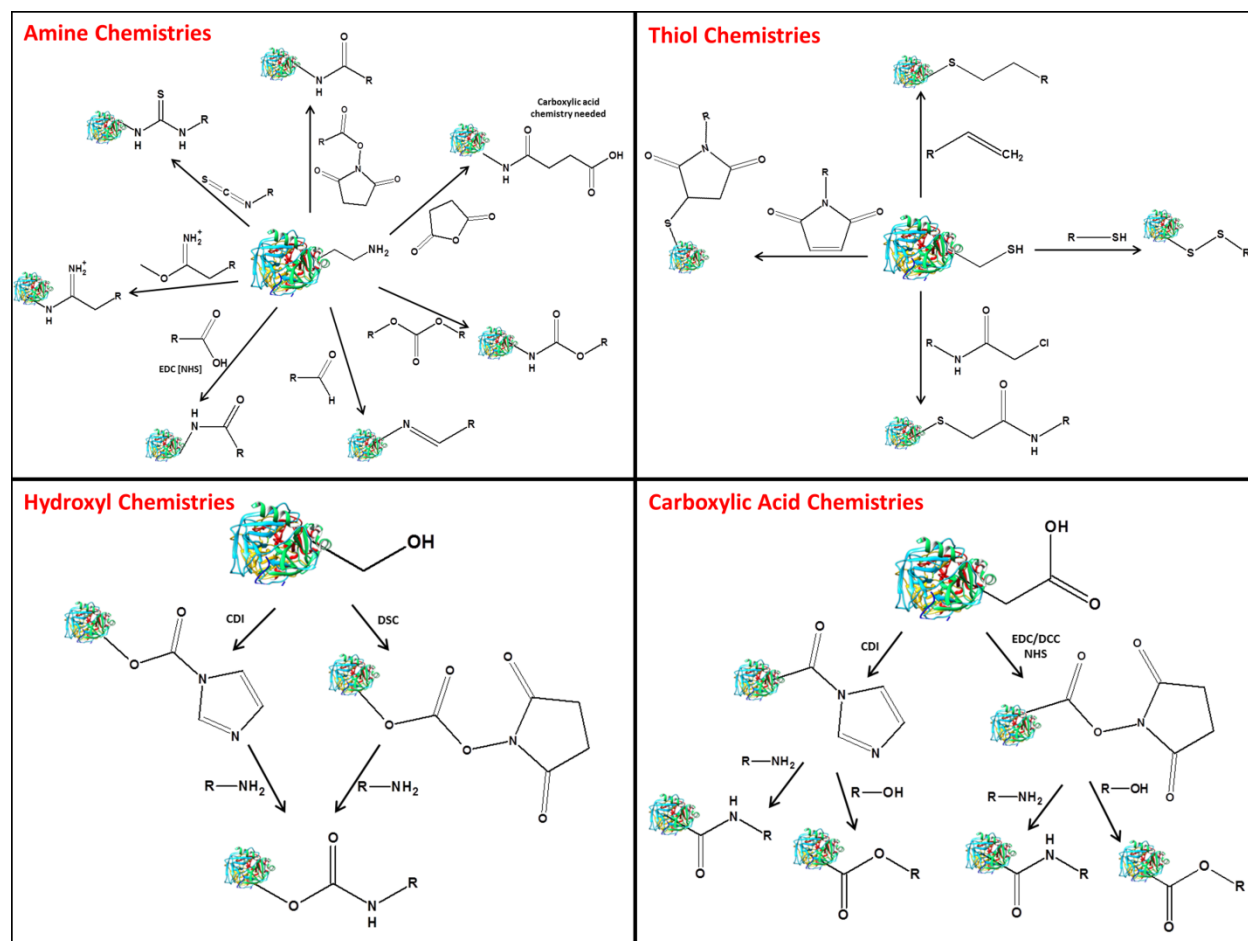
**Figure 1.2.** Conjugation chemistry examples from chemical groups on proteins. The R group would need to contain the initiator for subsequent polymerization. Chemical acronyms: Carbonyldiimidazole (CDI), N,N'-Disuccinimidyl carbonate (DSC), 1-Ethyl-3-(3 dimethylaminopropyl)carbodiimide (EDC), N,N'-Dicyclohexylcarbodiimide (DCC), N-Hydroxysuccinimide (NHS).

### 1.2.5 Oxygen-tolerant controlled polymerization techniques

A major challenge for non-experts in the *in situ* growth of polymers from proteins via ATRP and RAFT is the presence of oxygen, which quenches radicals and thereby inhibits polymerization. A novel approach to overcome this challenge that entailed the sequential enzymatic conversion of oxygen to hydrogen peroxide and finally to carbon dioxide and acetate was recently reported.[43,44] This approach, which emulates the aerobic respiration process used by cells, entailed the use of glucose oxidase to scavenge oxygen. The hydrogen peroxide produced

by glucose oxidase in the presence of pyruvate was then converted to carbon dioxide, acetate and water. Notably, by eliminating oxygen, this approach permitted the synthesis of block copolymers and protein-polymer conjugates in reaction vessels that were open to the air. This approach may significantly reduce the cost and facilitate the scale up of protein-polymer conjugates. Additionally, because cells and tissues generally require oxygen to remain viable, it is interesting to consider how this approach may facilitate the growth of polymers from living biomacromolecules. For example, such an approach may enable the modification of the surface of stem cells or pancreatic islets for cell transplantation therapy, which may protect the cells from the host immune system and, in turn, prevent cell (or graft) rejection. Moreover, through this approach, it may be feasible to encapsulate cells in a polymer matrix (*e.g.*, hydrogel) as scaffolds for tissue engineering where the cells are retained in the polymer network due to the growth of the polymer from the cell surface.

## 1.3    Rational Design of Protein-Polymer Conjugates

Inherent to rational design is an ability to link the chemical structure of a particular polymer to its ultimate effect on the biological molecule. This approach requires an understanding of the chemical nature of the biomolecule-polymer interface, including the interactions of the polymer with moieties on the biomolecule surface. To date, our understanding of these interactions remains elusive, which has severely hindered our ability to predict the impact of polymer chemistry and location of attachment on biomolecule stability. Ultimately, by tuning the polymer chemistry and precisely controlling the location of polymer attachment on a biomolecule, such understanding of fundamental chemistry may be elucidated with unprecedented molecular detail, thereby opening the door to a myriad of exciting applications. The steps to rationally design protein-polymer conjugates are outlined in **Figure 1.3**.
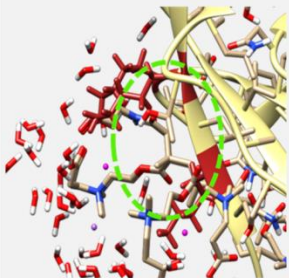
10
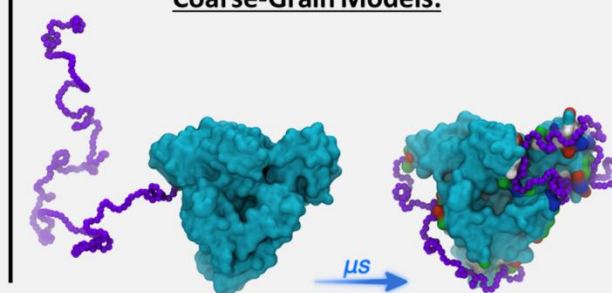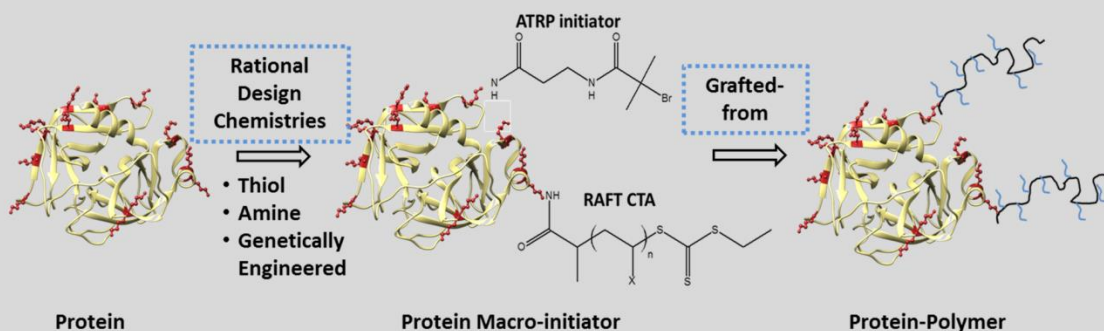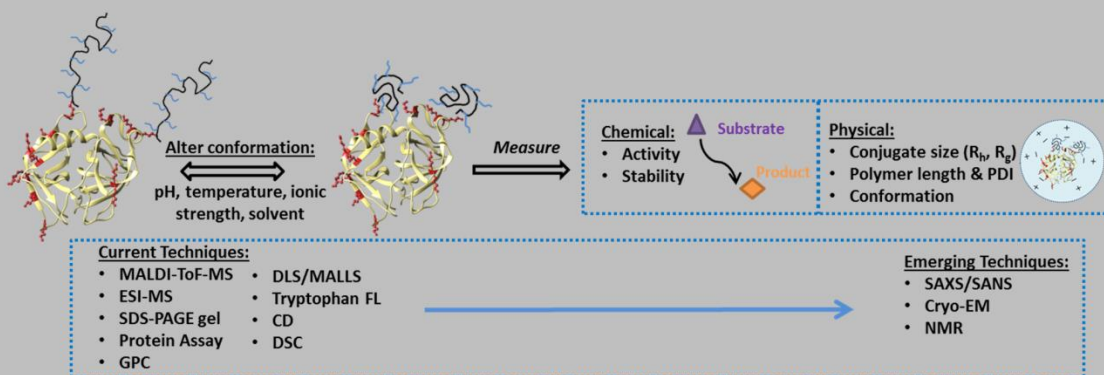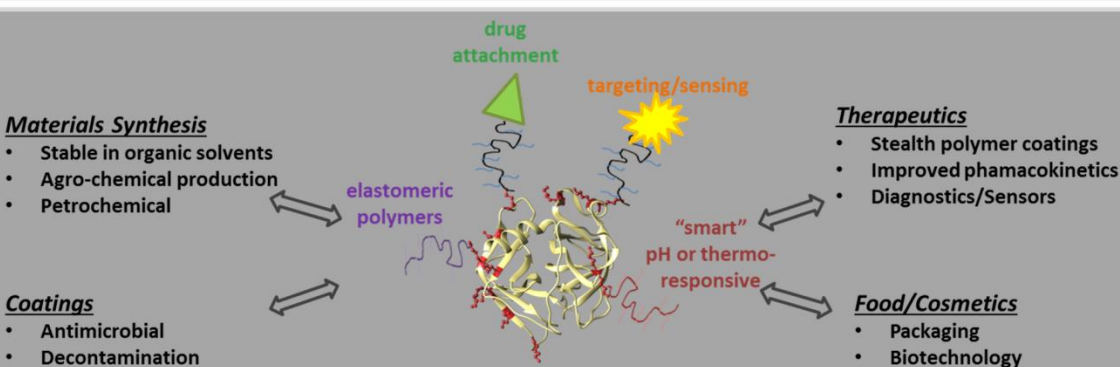
**Figure 1.3.** An overview of protein-polymer conjugate science. Computational studies can be used to predict the structure, dynamics, and interactions of the conjugates using molecular dynamics simulations to help guide the design for conjugate synthesis. The grafting-from synthesis approach utilizes protein-reactive initiators to create macro-initiators from which polymers are grown using either ATRP or RAFT polymerization. Protein-polymer hybrids characterization relies on a combination of techniques that, when performed together, provide a thorough analysis. Finally, protein-polymer conjugates are applied to many different fields including chemical synthesis, materials science, drug development, and biotechnology.

Progress in understanding dynamics of proteins and polymers (separately) has been significant, but there is little knowledge about how molecular motion changes in biotic/abiotic hybrid structures. Protein function in biology is tuned through precise chemical surface modifications (such as glycosylation) that act in concert with the core of the protein. The beauty of protein complexes is how they can communicate this information through sensitive protein interfaces and dynamic conformational changes, but unfortunately these delicate systems have not evolved to be robust. Modification of biomacromolecules with precision-designed synthetic polymers will underpin the next generation of hybrid materials. Specifically, covalent attachment of polymers to proteins can alter the surface and solubility properties of the protein, thereby affecting/improving biocompatibility, stability, activity, delivery, and therapeutic potential. Two decades of research have significantly advanced the ability to combine polymer synthesis with the precision, complexity, and specificity of biomacromolecules. However, our ability to access well-defined polymer bioconjugates as well as to simulate the structure-function-dynamic relationships that govern their performance, are minimal at best.

### 1.3.1  Structure-Function-Dynamics Relationships of Protein-Polymer Conjugates

Structure-function-dynamics relationships are the foundation from which we will expand the impact of protein-polymer conjugates by understanding how specific protein-polymer interactions, at the molecular level, lead to function. Polymers that have been covalently attached

to proteins are in constant dynamic movement in solution, can adopt different conformations (mushroom or extended/brush), and can participate in numerous noncovalent interactions (Coulombic, van der Waals, and hydrogen bonding) between protein-polymer or polymer-polymer. The noncovalent interactions, and thus the degree to which polymers are interacting with the protein surface, are governed by factors including polymer grafting density[45], polymer molecular mass[46,47], polymer physicochemical properties[48,49], attachment site[34], and external bulk environments (solvent, pH, ionic strength, temperature)[50]. Many studies have exploited the unique properties of polymers, such as responsiveness to external stimuli to drive altered protein activity for sensing applications.[51,52] For example, a polymer with a lower critical solution temperature (LCST) will collapse on the protein surface when temperatures are above the critical value leading to lower protein activity.[53,54] From these types of studies, it is obvious that understanding structure-function-dynamics relationships is important and furthermore, controlling them is paramount for synthesizing rationally designed conjugates.

### 1.3.2 Molecular Simulations of Protein-Polymer Conjugates

Unfortunately, however, there are real challenges to predicting how a chosen polymer will affect (either positively or negatively) the protein's function. Molecular simulations (MS) represent a powerful approach to uncover the fundamental mechanisms that govern materials and are playing an increasingly important role in the design of new materials with tailored properties. Among many other contributions, MS have provided invaluable insights within the protein and polymer communities. Studies have been performed on proteins, enzymes, and viruses that can contain several domains or aggregates. On the polymer side, different polymer architectures, molecular masses, entanglements, loops, and dangling chains have been investigated. MS can be designed to mimic *in vitro* conditions by systematically varying different variables such as

temperature, pH, ionic strength, *etc*. These efforts have allowed the understanding, prediction and design of hundreds of materials in both communities.

The modeling and simulation of protein-polymer conjugates is a complex task. Crystal structures are available for many proteins and serve as starting points from where atomic positions for MS can be generated. However, the generation of amorphous polymeric structures in solutions, blends, or in the glassy state requires special-purpose algorithms to generate the initial structure on both the atomistic and mesoscale levels. After the model has been generated, the simulation parameters must be carefully determined. Different force-fields (FFs) have been developed (based on experimental data or high level quantum calculations) for the understanding, prediction and design of polymers and proteins, but they are essentially designed specific to each community. Thus, the identification of FFs that are appropriate for simulating both the protein and polymer simultaneously represents a critical challenge. In order to model a vast array of protein-polymer conjugates, a unifying approach to molecular (dynamic) simulations is required.

Computational studies have been used previously to investigate dynamics of protein/polymer systems where the polymers are conjugates to the protein or free in solution. These studies have exposed the challenges of extending FFs developed in the protein community (Amber, CHARMM, *etc.*) to polymers, as shown for the "simple" and very-well known PEG.[55–57] At the atomistic level, the latest CHARMM ether FF is one of the best in reproducing conformational populations of dimethoxyethane, and has also been shown to achieve quantitative agreement with experimental values such as persistence length and hydrodynamic radii for poly(ethylene oxide) and poly(ethylene glycol).[58] Atomistic simulations are too slow, however, to couple with experimental synthesis for the rapid identification of the "right" polymer

architecture, binding density, and protein-polymer dynamics. Coarse-grain protocols are needed to facilitate rapid identification of dynamic properties that impact polymer-protein interactions. Coarse-grained (CG) models can significantly expand the length and time scales of the system compared with all-atom models, and are desirable for modeling bioconjugates dynamics of diverse systems. Several CG models have also been developed for proteins and polymers independently, however, studies that tackle the cross between proteins and polymers are scarce. For example, modifications of the Martini approach[59] have proven to be defiant when used to develop CG models for PEG chains attached to bovine serum albumin. Despite the lack of a unified approach, MS have been used to determine the local effect of interactions at the polymer-protein interface level[60] over multiple time and length scales. Additionally, atomistic and phenomenological CG models have been used to explain shifts in LCST-like phase transitions.[61,62]

To develop more accurate and reliable models for protein-polymer conjugates that can be used to compare and guide experimental efforts, five main factors are required:

1) Development of FFs or effective potential functions that predict polymer-protein interactions correctly;

2) Generation of complex topologies that mimic experimental samples;

3) Development of mapping/reverse mapping procedures that allow cross-communication between the atomistic scale and the mesoscale (CG models);

4) Use of advanced techniques to perform appropriate conformational sampling (*e.g.* the use of steered molecular dynamics (SMD) simulation to speed up the encounter of reactive pairs and graphical representations to track the system's topology), and;

5) Incorporation of accelerated sampling methods including metadynamics or replica exchange MD.

## 1.4   Protein-Polymer Characterization Techniques

Various characterization techniques can be employed to help experimentally derive structure-function-dynamic relationships for a library of conjugates including, but not limited to, light scattering (dynamic light scattering, static light scattering, multi-angle laser light scattering for size), conjugate activity (*e.g.* Michaelis-Menten kinetics or protein activity assays), conjugate stability (conformational, thermal, chemical stability measured by residual activity over time), circular dichroism (conjugate secondary structure), and tryptophan fluorescence (conjugate tertiary structure).[63] These analysis techniques can also be validated through computational models of conjugates. As an example, multi-angle laser light scattering (MALLS) when coupled with size exclusion chromatography provides information on conjugate molar mass and radius of gyration ($R_g$) while dynamic light scattering (DLS) data provides information on hydrodynamic radius ($R_h$). When combining MALLS and DLS data, the conformation of the attached polymer around the protein can be determined by calculating the $R_g/R_h$ shape ratio.[64] This is extremely useful characterization technique for determining structure-function-dynamic relationships because one can determine if the polymer is wrapped tightly around the protein surface or fully extended into the surrounding solution.

Although DLS is used routinely for conjugate size characterization, it has many intricacies that are rarely discussed. Briefly, DLS measures the translational diffusion coefficient of the particles in Brownian motion by measuring the dynamic fluctuations in scattered light over time. The fluctuations are dependent on particle size where smaller particles will have a higher frequency of fluctuations since they diffuse quicker than larger particles. This dynamic

16

information is captured mathematically in an autocorrelation function. Various analysis techniques are then used to derive the hydrodynamic diameter distribution from the autocorrelation function including the methods of cumulants (most common) and CONTIN (also known as non-negatively constrained least squares (NNLS)). Specifically, the CONTIN algorithm was designed to handle multimodal, heterogeneous samples. In any case, the DLS measurements will derive hydrodynamic diameters based on intensity, volume, and number distributions. The intensity distribution output is the size value that is directly measured by the instrument based on the intensity of the scattered light (*e.g.*, larger particles scatter more light). The intensity distribution is then converted to volume and number distributions using Mie theory which provides information on the relative amount of sub-populations weighted by individual particle volumes or the number of those particles in the sample. This conversion, however, has a few assumptions that should be noted: 1) all particles are spherical, 2) optical properties (refractive index and absorption) of the particle are known, and 3) all particles are homogeneous. Each of these distributions provides useful information and when analyzed together, can provide insight into the true nature of a sample. If the sample was perfectly homogeneous, which is rarely the case for protein-polymer conjugates, then the intensity, volume, and number distributions would be the same. In heterogeneous samples, these distributions are different. For example, a few agglomerates in a sample will scatter much more light than the remaining individual particles and shift the intensity distribution to much higher values. When additionally analyzing the volume and number distributions, however, the sub-populations of smaller particles will be highlighted. One thing should be immediately apparent, and that is that all published reports of hydrodynamic diameter for protein polymer conjugates are not useful without clearly indicating whether the numbers are intensity, volume or number based.

17

As an example, protein-polymer conjugates were synthesized using chymotrypsin and poly(carboxybetaine methacrylate) with increasing degrees of polymerization and all conjugates were initially modified with four initiators. **Figure 1.4** shows the difference in hydrodynamic diameter versus degree of polymerization when analyzing either intensity, volume, or number distributions in relation to the size of the protein-initiator complex (dotted line). From these plots, the differences in hydrodynamic diameters between the different distributions are apparent.
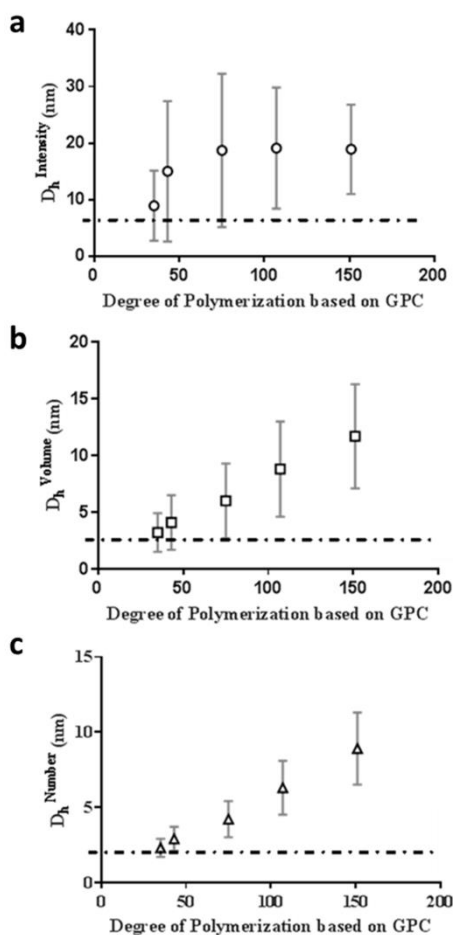


**Figure 1.4.** Hydrodynamic diameters of chymotrypsin-poly(carboxybetaine methacrylate) conjugates with 4 polymer chains and increasing degrees of polymerization as reported by a) intensity distribution, b) volume distribution, and c) number distribution. Dotted lines correspond to the hydrodynamic diameter of the chymotrypsin-initiator complex: $6.2 \pm 3.8$ nm (intensity), $2.6 \pm 1.3$ nm (volume), and $1.9 \pm 0.5$ (number). Data provided by Jill Anderson, CMU.

Since there is no standard operating procedure to characterize conjugates via DLS, the distribution to report is decided by the user and more often than not, only one type of distribution is reported. It is also not common practice to report which type of distribution was used, so it is often a mystery to the reader. It is also worth mentioning that hydrodynamic diameters highly depends on the ionic strength of the solution since ions compress the electric double layer and alter how the particles diffuse in solution. Thus, it is critical that scientists are transparent when reporting DLS data and their methods so that comparisons between experimental and literature values can be more easily made. We have highlighted the pitfalls for DLS, but other analysis techniques also have their downfalls. For example, many researchers study protein-polymer conformation by measuring tryptophan fluorescence, but they ignore the fact that bromine (the natural terminating moiety that remains at the end of ATRP-grown polymers) quenches tryptophan fluorescence. This highlights the need for a simple, high-throughput analytical characterization technique for protein-polymer conjugates, which could then be adapted into standard operating procedures for all scientists.

Characterization techniques that have been used traditionally in structural biology are emerging as new techniques to characterize conjugates and hold a lot of potential. Nuclear magnetic resonance spectroscopy (NMR), small-angle X-ray scattering (SAXS), and cryo-electron microscopy (cryo-EM) are some of the frontrunners. SAXS can provide structural information of conjugates including morphology, size, distributions, dynamics, and can further provide insight into self-assembly.[52,65] NMR can also provide similar information as SAXS, but has historically been limited to relatively small proteins. The introduction of transverse relaxation-optimized spectroscopy, however, has increased its working range to larger complexes

up to 900 kDa.[66] Cryo-EM is a powerful technique that won the 2017 Nobel Prize in Chemistry and it is designed to image biomolecular structures.[67] It is advantageous over conventional X-ray crystallography because the biomolecules are frozen in solution and do not need to be crystallized. This feature is highly attractive for conjugates since polymers typically cannot crystallize. The determination of structure-function-dynamic relationships can be validated through combined computational and experimental studies as shown in **Figure 1.5**.
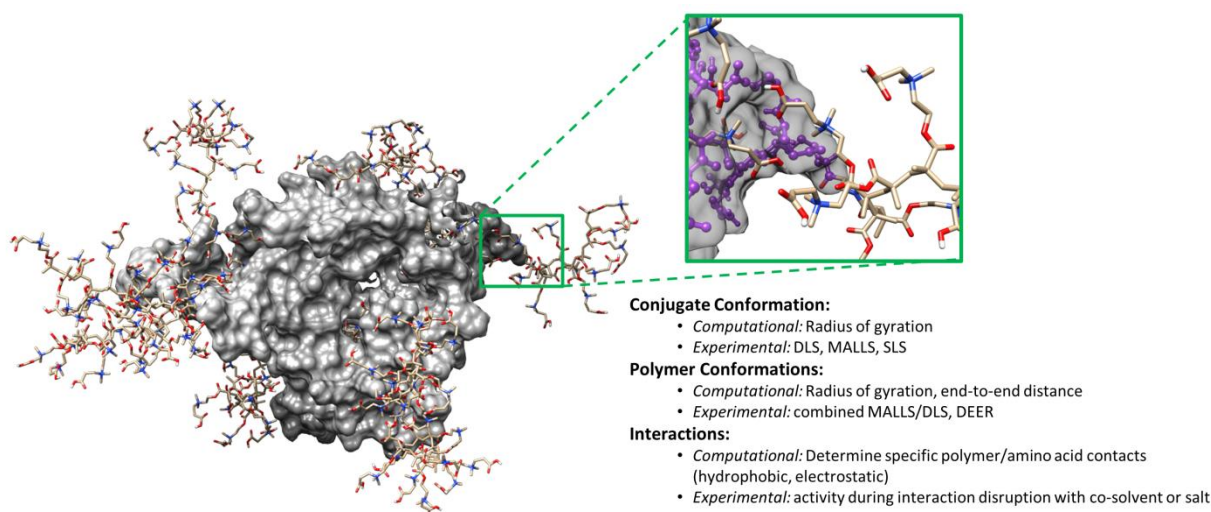


**Figure 1.5.** Depiction of a protein-polymer conjugate with zoomed-in view showing specific contacts between a polymer chain and nearby protein residues (purple). Molecular dynamics simulations can be used to validate experimental characterizations while providing point source information. Acronyms: dynamic light scattering (DLS), multi-angle laser light scattering (MALLS), static light scattering (SLS), double electron electron resonance (DEER).

## 1.5 Applications of Protein-Polymer Conjugates

### 1.5.1 Therapeutic Applications

In the realm of bioconjugate therapeutics, the technique of PEGylation, or attaching a pre-formed polyethylene glycol (PEG) polymer chain to a drug biomolecule of choice, has dominated the consumer market since 1990 with the release of Adagen. PEGylation is performed

to improve pharmacokinetics and reduce immunogenicity by altering the physiochemical properties of the biomolecule by coating it with polymer. The increasing knowledge of the functions of protein-polymer conjugates, new chemistries to create bioconjugates, and broadened range of polymer types, including "smart materials," enabled multiple potential applications of protein-polymer conjugates in medicine including drug delivery, sensing/detection, and incorporation into complex matrices.

A common approach for creating drug delivery vehicles using amphiphilic protein-polymer conjugates relies on the ability of the particles to self-assemble into nanostructures. One important feature is that these structures must be degradable so that the therapeutic can be released from the nanostructure once it has reached its destination. An example of a degradable self-assembled nanocarrier used conjugates of hydrophilic bovine serum albumin (BSA) and hydrophobic poly($\varepsilon$-caprolactone) (PCL) loaded with the cancer drug, doxorubicin (DOX). When decorated with cetuximab as a targeting ligand, these biohybrids showed enhanced antitumor activity in comparison to free DOX.[68] In another study, *in situ* growth was used to create protein-polymer nanostructures with tunable morphologies including spheres, worms, and vesicles by changing the polymer molecular mass. Poly(2-hydroxypropyl methacrylate) was grown from the surface of human serum albumin (HSA) using ATRP and upon self-assembly, green fluorescent protein was encapsulated which allowed tracking for intracellular delivery.[69] Instead of creating self-assembled nanostructures, protein-polymer conjugates can be used as their own drug delivery vehicles as well. For example, albumins (BSA or HSA) function as transporter proteins of small hydrophobic molecules in blood plasma. Therefore, drugs, such as DOX, can be loaded into the albumin binding pockets through physical adsorption and then polymers can be attached either by grafting-to or grafting-from techniques. The chosen polymer

can be designed to provide stealth to increase circulation time or provide functionality by incorporating targeting moieties. Finally, another study used phenylpiperazine-containing polymers, which are known permeation enhancers, conjugated to BSA. These conjugates were used to facilitate transport across intestinal membranes to allow passage of therapeutic proteins that would have been previously impenetrable without the polymer.[70]

Protein-polymer conjugates can also be designed for applications in sensing and detection. In one case, thermo-responsive polymer-antibody conjugates, using poly(N-isopropylacrylamide) (PNIPAAm), were used in a microfluidic immunoassay for detection and purification of specific biomarkers. This strategy would be easily employed in diagnostic assays for various diseases.[71] Another application took advantage of the self-assembly behavior of BSA-PCL conjugates to encapsulate $CuInS_2$/ZnS quantum dots. This hybrid material was used as a near-infrared fluorescent nanoprobe that could be used for *in vivo* imaging.[72] Semiconducting polymers can also be used for detection purposes since changes in their conformation lead to varying degrees of spectral shifts. In one application, recombinant cationic proteins were associated along an anionic π-conjugated polyelectrolyte polymer to introduce steric hindrance and alter the polymer conformation as detected by a shift in the vibronic spectra. This structure was used to detect the polymer's encapsulation into a protein capsid.[73] Lastly, enzyme-based glucose biosensors were created using glucose oxidase conjugated with redox-containing polymers. These conjugates were further linked to HSA and mixed within a chitosan solution and then drop cast onto carbon paper to create the sensor.[74]

In addition to solution-based syntheses, protein-polymer conjugates can be created as hydrogels to perform similar functions. There are many scenarios where this would be advantageous, such as incorporation of protein-polymers into complex matrices in tissue

engineering or degradable hydrogels for controlled drug release. PNIPAAm has a lower critical solution temperature (LCST) around 32 °C and is used for many biomedical hydrogel applications because it displays phase transitions around the temperature of the human body at 37 °C.[75] In one example, NIPAAm and itaconic acid monomers were copolymerized by free radical polymerization to form a stimuli responsive hydrogel with entrapped lipase as a model protein. Higher levels of lipase were able to be released at pH 6.8 in comparison to pH 2.2, enabling this biomaterial to be used as an oral drug delivery system.[76] In another example, NIPAAm was copolymerized into a hydrogel with (ethylene glycol) methacrylate and entrapped urease. This hydrogel displayed reversible thermo-responsive phase behavior, enzyme temperature-dependent activity, and increased storage stability of urease.[76]

Protein-polymer conjugate self-assembly and organization into higher ordered 3-dimensional hydrogel structures are a couple of areas that hold exciting potential for new therapeutic applications. With the advancement and rising interest in 3D printing, specifically in tissue engineering for the creation of artificial organs, there is potential to incorporate these conjugates into complex matrices or create 3D hydrogel delivery systems that are designed and printed for each patient depending on their individual therapeutic needs.

### 1.5.2  Industrial Applications

Polymer-based protein engineering has emerged as a powerful tool in protein scientists' toolbox to improve enzyme properties to facilitate their use in industrial enzyme applications as well. To broaden the application of proteins for industrial applications beyond the medical field, research has been focused on methods to generate stable, selective and productive proteins and enzymes, which can accept a variety of substrates and transform them into novel materials, high-value chemicals, and renewable biofuels. It has been shown that covalent attachment of a water-

soluble polymer to a protein improves physical stability, proteolytic stability, and pharmacokinetics in therapeutic applications. The same approach has been applied in biocatalysis, where polymer-grafted enzymes displayed increased solution and thermal stability, as well as improved performance in non-aqueous solvents.[77] Such enzyme-polymer based biocatalysts can be promising tools for active pharmaceutical ingredients synthesis, commodity and specialty chemicals synthesis, waste remedication, coatings and packaging applications.

Modification of enzymes with stimuli-responsive polymers was shown to generate conjugates with enhanced behavior over a broad range of conditions such as varied pH or increased temperature. Growing a pH-sensitive polymer from chymotrypsin resulted in the formation of a conjugate whose activity was 10-fold higher than the activity of the unmodified enzyme under acidic conditions (pH=5).[78] Additionally, the affinity of the modified enzyme towards its substrate could be increased over a targeted pH range of 5-8. Chymotrypsin modified with temperature-responsive polymers maintained its activity while its stability to autolysis and denaturation was increased.[22,79] In another example, lipase modified with a range of acrylamides preserved up to 20% of its activity upon heating up to 70$^{\circ}$C in comparison to fully deactivated native enzyme.[80] Furthermore, conjugation of several enzymes within single polymer system demonstrated benefits of this approach for cascade reactions.[81] In the case of acid phosphatase, its activity was increased 20-fold when conjugated in multi-enzyme-poly(acrylic acid) system possibly due to a more favorable exposure of the active site to a substrate.[82]

Improving enzymatic activity in organic solvents can be beneficial for development of biocatalytic tools for more diverse types of substrates including more hydrophobic molecules. Genetic engineering and immobilization are commonly used to address enzymatic stabilization in organic solvents. However, a number of recent reports demonstrated that polymer conjugation

results in improved enzyme dissolution and activity in both polar and non-polar organic solvents. Laccase-poly(2-methyloxazoline) with modified active center metal was shown to catalyze styrene dihydroxylation with enantioselectivity over 90%.[83] In another example, chymotrypsin modified with pDMAEMA was soluble in several organic solvents such as acetonitrile, dichloromethane and others, exhibited good substrate binding, and had an activity 100 times higher than that of the insoluble native enzyme.[84] Amphiphilic block copolymer Pluronic was used to modify two types of lipases and cytochrome C, and final conjugates showed solubility in toluene and increase in activity of about 60- and 670-fold respectively.[85]

Finally, application of protein-polymer conjugates also include specialty areas such as fuel cells, sensors and coatings. An antifouling zwitterionic coating was prepared by electromediated ATRP on the surface of glucose oxidase immobilized on an electrode surface.[86] Polymer coating on such biosensor repelled over 99% of nonspecific protein adsorption, and the final biosensor had low sensitivity drift in comparison to polyurethane coatings. In another report, glucose oxidase was modified with ferrocene-containing polymers followed by adsorption to an electrode.[87] The resulting system showed 24-fold increase in current generation efficiency in comparison to the native enzyme due to the use of the redox mediator-containing polymers. Application of protein-polymer conjugates in coatings is another promising area due to the interest in biocatalytic coatings for synthetic applications, sensors or smart packaging. Such enzyme-containing coatings can be produced by flow coating of enzyme-polymer conjugates. One can utilize self-assembly processes to generate 5-10 times more active coatings in comparison to more traditional approaches.[88]

# Chapter 2.   Intramolecular Interactions of Conjugated Polymers Mimic Molecular Chaperones to Stabilize Protein-Polymer Conjugates

## 2.1   Chapter Summary

The power and elegance of protein-polymer conjugates has solved many vexing problems for society.  Rational design of these complex covalent hybrids depends on a deep understanding of how polymer physicochemical properties impact the conjugate structure-function-dynamic relationships.   We have generated a large family of chymotrypsin-polymer conjugates which differ in polymer length and charge, using grafting-from atom-transfer radical polymerization, to elucidate how the polymers influenced enzyme structure and function at pH's that would unfold and inactivate the enzyme.   We also used molecular dynamics simulations to deepen our understanding of protein-polymer intramolecular interactions.   Remarkably, the data revealed that, contrary to current thoughts on how polymers stabilize proteins, appropriately designed polymers actually stabilize partially-unfolded intermediates and assist in refolding to an active conformation.   Long, hydrophilic polymers minimized interfacial interactions in partially-unfolded conjugates leading to increased stabilization.   The design of covalently attached intramolecular biomimetic chaperones that drive protein refolding could have far reaching consequences.

## 2.2  Introduction

The interface of synthetic chemistry and biology has created interest in protein-polymer conjugates in industries as diverse as therapeutics[89,90], diagnostics[91], sensing[50], synthetic synthesis[92], food and cosmetics[93], and biotechnology[92,94]. There has also been increasing interest in whether polymer conjugation could enhance enzyme activity and stability in non-native environments[95,96]. The absence of a fundamental understanding of how polymers enhance biologic activity has limited our ability to rationally design bioconjugates that survive in extreme environments. The first reported protein-polymer conjugate was synthesized in 1977 by covalently attaching poly(ethylene glycol) (PEG) to bovine serum albumin[2,97]. More recently, efforts have focused on fully exploiting the properties of polymers to create functional and responsive "smart conjugates"[50,53,91,98,99]. Protein-polymer conjugates have been designed to alter the temperature[50,53,54] and pH[47] dependence of activity, solubility and stability. The rational design of protein-polymer conjugates has also been enhanced by the development of predictive tools[34] and the breadth of synthetic tools that can attach polymers to proteins is rapidly expanding.[100] In the grafting-from approach, an initiator is first reacted with the surface of a protein, typically using surface accessible primary amines, and polymer chains are grown from the initiator sites using controlled radical polymerization[49,99,101–104]. Grafting-from is particularly attractive when seeking to increase modification density, control polymer architecture (length and monomer type), and enhance control over attachment site resulting in uniform conjugates. Over the past decade, we have studied many grafted-from protein-polymer conjugates synthesized using atom-transfer radical polymerization (ATRP), but have struggled to develop a molecular understanding of how the conjugated polymers influence the activity and stability of the protein.[49,53,54,101,105]

Although several reports have described how the attachment of polymers to protein increased protein stability[57,106–110], other studies have yielded contradictory results[48,49,111,112]. There are also many different hypotheses as to the mechanism by which conjugated polymers increase stability[49,56,109,112,113]. The significant lack of agreement and breadth of hypotheses are summarized in **Table 2.1**. One oft-described hypothesis is that polymers that preferentially interact with the protein surface will stabilize proteins through that interaction[48,56,57,114]. Some confusion has arisen since the effect of polymer on conjugate activity versus residual activity (stability) are easily confused. That said, until now, the descriptions of how the polymer stabilizes a protein under extreme conditions have generally assumed that the polymer exerts its influence on the active native structure of the protein.

Although interest in protein-polymer conjugate structure-function relationships has driven creative research, the stabilizing effects of electrostatic interactions in conjugates have been mostly overlooked. Electrostatic interactions become an important factor, however, when studying charged polymers in conditions where both the polymer and protein are changing protonation states (acidic or basic environments). Stabilization of protein-polymer conjugates at extremes of pH is relevant for both medicinal and industrial applications. For example, therapeutic conjugates delivered orally would need to remain active in the acidic environment of the stomach and xylanase conjugates would need to be active in alkaline conditions during the bleaching step in the pulp and paper industry.

In order to fully understand structure-function relationships of conjugates, molecular dynamics (MD) simulations can be employed, especially in conjunction with experimental data, because specific interactions can be determined and visualized with atomic resolution over time. MD simulations have traditionally been used to study the dynamics of native protein structure at

both the all-atom and coarse-grain level of detail and can be designed to mimic experimental conditions (solvent, temperature, pH, ionic strength). Recent advances in this area have expanded into studying protein-polymer hybrids in systems where polymers were either covalently or non-covalently attached. This computational work was driven by the desire to understand PEGylated proteins and more specifically, how the chain length and attachment site of PEG affected protein stability. The work in this area had led to the development and validation of appropriate force fields for PEGylated proteins at the atomistic (CHARMM, Amber, OPLS) and meso-scales (MARTINI). The field of protein-polymer conjugates has advanced beyond PEGylated systems, but unfortunately, computational models of proteins with other polymer types is virtually non-existent. This is because force fields for other unique polymers of interest, as well as for hybrid protein-polymer systems, are rare and nearly impossible to validate without experimental data. Protein-polymer conjugates are in constant dynamic movement in solution and MD simulations have the ability to predict polymer conformations around a protein surface, protein-polymer interactions, dynamic changes over time, and subtle polymer-induced changes to protein structure. Demystifying this type of information through MD simulations would be of significant value.

In this Chapter, we sought to unravel the network of competing hypotheses of conjugate stabilization (**Table 2.1**) by using protein-ATRP to synthesize a library of fifteen protein-polymer conjugates using α-chymotrypsin (CT) as a model protein. We varied the charge (zwitterionic, positive, negative, and neutral), hydrophobicity, and molecular masses for each polymer type. Michaelis-Menten kinetics were measured over a range of pH (4-10) to determine the polymer's impact on activity. Stability against acid (pH 1) and base (pH 12) was also determined by measuring residual activity after exposure to the denaturing environment.

Residual activities were then correlated with observed changes in tertiary structure measured by tryptophan fluorescence. Finally, we performed molecular dynamic simulations on the conjugates to explore the structure-function-dynamic relationships that governed the observed properties.

**Table 2.1.** Summary of protein-polymer conjugate stability mechanistic hypotheses.

| Protein | Polymer | Polymer Size | Polymer Density | Stability Type | Hypothesized Stabilizing Mechanism | Stability increases with polymer $M_W$? | Ref. |
|---|---|---|---|---|---|---|---|
| Chymotrypsin | PEG | 0.7, 2, 5 kDa | 10-65% of amino groups | Thermal | PEG increased protein thermal stability by decreasing structural dynamics because hydrophobic regions of PEG bind the protein surface, exclude water, and make the protein more rigid. Stability increased with the density of polymer modification | No | 57 |
| | Spermidine (noncovalent) | 0.25 kDa | 0-1 mM was added | Thermal | Bound spermidine interacts with the protein through VDWs and H-bonding leading to increased thermal stability | - | 114 |
| | pCBAm | 30.7 kDa | 80% of amino groups | Acid | Conjugate stability against acid was increased due to extension of polymer from the protein surface to minimize electrostatic interactions | - | 49 |
| | pQA | 19.1 kDa | | | | | |
| | pSMA | 9.6 kDa | | | | | |
| | pOEGMA | 11.6 kDa | | | | | |
| Trypsin | PEG | 5 kDa | 80% of amino groups | Thermal and Detergent | Thermal and detergent stability increased from the formation of a highly H-bonded structure around the enzyme | - | 106 |
| | Dextrin | Dextrin: 17 or 64 kDa | 1 or 2 chains | Thermal and Autolytic | Conjugates showed increased thermal stability and better stability to autolysis. Higher MW polymer enhanced protection from autolytic attack due to steric hindrance and H-bonding | Yes | 108 |
| | ST-HPMA | ST-HPMA: 12 kDa | | | | | |
| Lysozyme | PEG | 5 kDa | 1 chain | Thermal | Thermal stability of conjugates increased due to H-bonding between the ethylene oxide groups and the protein | - | 107 |
| | Am | Low and High $M_W$ Range: ~0.6-53 kDa | 90% of amino groups | Thermal and Chemical | Conjugates, independent of polymer charge, had decreased thermal stability and higher molecular mass further decreased thermal stability. This was attributed to the larger polymers causing unfavorable folding entropy. Increased polymer molecular mass increased chemical stability. Ionic polymers improve stability by interacting with the protein surface in comparison to nonionic polymers of similar molecular mass. | Thermal: No Chemical: Yes | 48 |
| | DMAm | | | | | | |
| | OEOA | | | | | | |
| | Am/PCMA | | | | | | |
| | Am/AA | | | | | | |
| | Am/DMAEMA | | | | | | |
| | AGA | | | | | | |
| | PEG | 2, 5, 10 kDa | 1 or 2 chains | Thermal | Polymer conjugation did not improve thermal stability | No | 111 |
| Pyrophosphatase | pOEGMA | 4, 8, 12 kDa | 1 chain | Thermal | High polymer molecular masses increase thermal stability. Polymer length needs to be longer than the distance between the attachment site and active center. pOEGMA stabilized the protein at high temperatures by forming a hydration layer around the protein to reduce aggregation. | Yes | 110 |
| | pNIPAAm | | | | | | |
| | via host-guest interactions (non-covalent) | | | | | | |

| | | | | | | | |
|---|---|---|---|---|---|---|---|
| | pNIPAAm | $M_W$ conjugate: ~50 kDa | 1 chain | Thermal | Thermal stability was increased due to the hydrophobic collapse of pNIPAAm above its LCST. This conformation helped protect the protein structure. | - | 115 |
| Staphylokinase | PEG | 5, 20 kDa | 1 chain | Conformational | PEG remains flexible, but forms a hydration layer around the protein which results in steric shielding. | Yes | 113 |
| Cytochrome c | PEG | 5 kDa | 80% of amino groups | Thermal and Conformational | Conjugation caused thermodynamic destabilization, but polymers energetically trapped the destabilized protein conformation | - | 112 |
| Insulin | PEG | 10, 50, 100, 200 ethylene oxide units | - | Conformational | PEG-protein interactions are driven by hydrophobic interactions causing water to be excluded from the protein surface to increase structural stability. | Yes | 56 |
| WW domain of human protein Pin 1 | PEG | 1-45 ethylene oxide units | 1 chain | Conformational | PEG disrupts the solvent-shell structure and water is released into the bulk. Stability is dependent on polymer attachment site and molecular mass. PEG provides stability by favorable interactions with protein surface residues in a transition state. | Yes | 116 |
| Methionyl-granulocyte colony stimulating factor | PEG | 20 kDa | 1 chain | Thermal | Thermal stability of conjugates was increased due to a reduction in propensity to aggregate | - | 109 |
| Rec. human factor VIIa | glycoPEG | Linear: 10 kDa  Branched: 40 kDa | Linear: 3 chains  Branched: 2 chains | Thermal | Thermal stability of conjugates was increased, but was independent of PEG molecular mass. This occurs because PEG postpones thermally induced aggregation leading to irreversible inactivation. | No | 117 |
| Cellulase | Am  DMAm  DMAm-AA  DMAm-DMAEMA | 2.6 kDa  3.7 kDa  3.4 kDa  4.7 kDa | Low density: 1-3 chains  High density:2-5 chains | Thermal and Chemical | Polymer conjugation did not improve thermal or chemical stability | - | 118 |

The table is color-coded where matching colors correspond to similar hypotheses. Poly(ethylene glycol) (PEG), poly(carboxybetaine acrylamide) (pCBAm), poly(quarternary ammonium methacrylate) (pQA), poly (sulfonate methacrylate) (pSMA), poly(oligoethylene glycol methacrylate) (pOEGMA), semi-telechelic poly[N-(2-hydroxypropyl)methacrylamide (ST-HPMA), acrylamide (Am), dimethyl acrylamide (DMAm), oligo(ethylene oxide) methyl ether acrylate (OEOA), phosphoroylcholine methacrylate (PCMA), acrylic acid (AA), dimethylaminoethoxy methacrylate (DMAEMA), N-acryloyl-D-glucosamine (AGA), poly(N-isopropylacrylamide) (pNIPAAm)

## 2.3   Materials and Methods

α-Chymotrypsin (CT) from bovine pancreas (type II) was purchased from Sigma Aldrich (St Louis, MO). Protein surface active ATRP initiator (NHS-Br initiator) was prepared as described previously.[47] Copper (I) bromide (Cu(I)Br), copper (II) bromide (Cu(II)Br), copper (I) chloride (Cu(I)Cl), copper (II) chloride (Cu(II)Cl), sodium ascorbate (NaAsc) 1,1,4,7,10,10-Hexamethyltriethylenetetramine (HMTETA), and 2,2'-Bypyridyl (bpy) were purchased from

Sigma Aldrich. HMTETA was purified prior to use using a basic alumina column. 3-[[2-(Methacryloyloxy) ethyl] dimethylammonio] propionate (CBMA) was purchased from TCI America. 3-sulfopropyl methacrylate potassium salt (SMA) was purchased through Sigma Aldrich. All materials were purchased from Sigma Aldrich (St Louis, MO) and used without further purification unless stated otherwise. Dialysis tubing (Spectra/Por, Spectrum Laboratories Inc., CA) was purchased from ThermoFisher (Waltham, MA).

### 2.3.1 Initiator modification and characterization

Initiator modified CT (CT-Br) was synthesized by reacting NHS-Br (469 mg, 1.4 mmol) and CT (1.0 g, 0.04 mmol protein, 0.56 mmol primary amines) in 100 mM sodium phosphate buffer (pH 8, 100 mL). The solution was stirred at 4 °C for 3 hours, then dialyzed against deionized water (MWCO 15 kDa) overnight, then lyophilized.

CT-Br was characterized using MALDI-ToF MS. MALDI-ToF-MS measurements were recorded using a PerSeptive Voyager STR MS with nitrogen laser (337 nm) and 20 kV accelerating voltage with a grid voltage of 90 %. 300 laser shots covering the spot were accumulated for each spectrum. The matrix was composed of sinapinic acid (20 mg/mL) in 50% acetonitrile with 0.4% trifluoroacetic acid. Protein solutions of native CT and CT-Br (1.0 mg/mL) were mixed with an equal volume of matrix and 2 µL of the resulting mixture was spotted on a sterling silver target plate. Apomyoglobin, cytochrome C, and aldolase were used as calibration samples. Number of initiator modifications was determined by taking the difference in peak m/z between native CT and CT-Br and dividing by the molecular mass of the initiator (220.9 Da).

### 2.3.2 ATRP from initiator modified sites

A summary of ATRP reaction conditions are provided in Supplementary Table 1. After the reaction stopped via exposure to air, all conjugates were purified using dialysis (MWCO 25 kDa) against deionized water for 48 h at 4 °C followed by lyophilization. Lengths were varied by increasing the target degree of polymerization (DP) by increasing the monomer to initiator ratio.

*Synthesis of CT-pCBMA.* CT-pCBMA was synthesized by adding CT-Br (50 mg, 4.7 mg initiator) and CBMA (dependent on target DP) to 16.4 mL of 100 mM sodium phosphate buffer (pH 8). This solution was stirred on ice and bubbled under argon for 30 minutes to deoxygenate the system. In a separate flask, Cu(I)Br (6.02 mg) was added to 4.6 mL of deionized water and the solution bubbled under argon for 30 minutes with HMTETA (13.7 µL). The 4.6 mL of catalyst solution was added to the CBMA/CT-Br solution. The reaction was stirred at 4 °C for 2 hours. Target DPs were 30, 125, and 220 for short, medium, and long length conjugates.

*Synthesis of CT-pOEGMA.* Poly(ethylene glycol) methyl ether methacrylate ($M_n$ = 500, OEGMA) was filtered through basic alumina column to remove inhibitor prior to use. CT-pOEGMA was synthesized by adding CT-Br (50 mg, 4.7 mg initiator) and OEGMA (dependent on target DP) to 16.4 mL of deionized water. This solution was stirred on ice and bubbled under argon for 30 minutes to deoxygenate the system. In a separate flask, Cu(II)Br (23.45 mg) was added to 4.6 mL of deionized water and the solution bubbled under argon for 30 minutes with HMTETA (68.5 µL). NaAsc (5 mg) was added to the catalyst solution, then the 4.6 mL of catalyst solution was added to the OEGMA/CT-Br solution. The reaction was stirred at 4 °C for 4 hours. Target DPs were 12 and 220 for short and long length conjugates, respectively. The medium length conjugate was synthesized using a catalyst solution of Cu(I)Cl/Cu(II)Cl/bpy (5 mM/45 mM/110 mM) and was reacted for 18 hours (target DP=125). All other conditions were similar to the synthesis of short and long conjugates.

*Synthesis of CT-pDMAEMA.* (Dimethylamino) ethyl methacrylate (DMAEMA) was filtered through a basic alumina column prior to use. CT-pDMAEMA was synthesized by adding CT-Br (50 mg, 4.7 mg initiator) and DMAEMA (dependent on target DP) to 15 mL of deionized water. This solution was stirred on ice and bubbled under argon for 30 minutes to deoxygenate the system. In a separate flask, Cu(I)Cl (10 mg) was added to 5 mL of deionized water and the solution bubbled under argon for 30 minutes with HMTETA (27.5 µL). The 5 mL of catalyst solution was added to the DMAEMA/CT-Br solution. The reaction was stirred at 4 °C for 18 hours. Target DPs were 12, 100, and 200 for short, medium, and long length conjugates.

*Synthesis of CT-pQA.* Quaternary ammonium methacrylate (QA) was synthesized as previously described.[103] CT-pQA was synthesized by adding CT-Br (50 mg, 4.7 mg initiator) and QA (dependent on target DP) to 25 mL of 64 mM sodium sulfate buffer (pH 8). This solution was stirred on ice and bubbled under argon for 30 minutes to deoxygenate the system. In a separate flask, Cu(I)Br (3.7 mg) was added to 2 mL of deionized water and the solution bubbled under argon for 30 minutes with HMTETA (8.74 µL). The 2 mL of catalyst solution was added to the QA/CT-Br solution. The reaction was stirred at 4 °C for 2 hours. Target DPs were 35, 154, and 243 for short, medium, and long length conjugates.

*Synthesis of CT-pSMA.* CT-pSMA was synthesized by adding CT-Br (50 mg, 4.7 mg initiator) and SMA (dependent on target DP) to 16.4 mL of 100 mM sodium phosphate buffer (pH 8). This solution was stirred on ice and bubbled under argon for 30 minutes to deoxygenate the system. In a separate flask, Cu(II)Br (23.45 mg) was added to 4.6 mL of deionized water and the solution bubbled under argon for 30 minutes before NaAsc (5 mg) was added. After addition of HMTETA (68.5 µL), the 4.6 mL of catalyst solution was added to the SMA/CT-Br solution.

The reaction was stirred at 4 °C for 2 hours. Target DPs were 25, 100, and 175 for short, medium, and long length conjugates.

### 2.3.3 Prediction of logD and p$K_a$

ChemAxon was used to calculate the hydrophobicity (logD) and $pK_a$ of the monomers. The $pK_a$ was estimated from the inflection point of the logD versus pH plot. This is the point at which the protonation state changes as evidenced by a sharp change in logD.

### 2.3.4 Conjugate determination of protein content

Protein content of CT-conjugates was determined in triplicate using a bichinchoninic acid (BCA) assay according to Sigma Aldrich microplate protocol. Briefly, 0.5-1.0 mg/mL of CT-conjugates were prepared in deionized water along with native CT standards. To each well, 25 μL of sample was added to 200 μL of working solution (1:8 ratio). The plate was covered and incubated at 37 °C for 30 minutes followed by measuring the absorbance at 562 nm using a BioTek Synergy H1 Plate Reader. The degree of polymerization was determined as previously described.[53]

### 2.3.5 Polymer cleavage from conjugates

Polymers were cleaved from the surface of CT using acid hydrolysis as previously described.[53] Briefly, CT-conjugates (20 mg/mL) were dissolved in 6 N HCl and incubated at 110 °C under vacuum for 24 hours. Cleaved polymers were purified from CT by dialysis (MWCO 1 kDa) for 24 hours against deionized water, then lyophilized until a powder.

### 2.3.6 Molecular mass and uniformity of cleaved polymer

Gel permeation chromatography (GPC) was used to determine number ($M_n$) and weight average ($M_w$) molecular masses and polydispersity index ($M_w/M_n$) of cleaved polymer. GPC was performed on a Waters 2695 Series with a data processor and a refractive index (RI) detector. Running buffers varied with polymer type: 100 mM phosphate buffer (pH 7.0) and 0.01 v/v% $NaN_3$ (pCBMA, pOEGMA), 100 mM sodium phosphate (pH 2.0) and 0.5% trifluoroacetic acid (pDMAEMA, pQA), and 80 v/v% sodium phosphate (pH 9.0) and 20 v/v% acetonitrile (pSMA). Running buffers were set to a 1 mL/min flowrate. Pullulan narrow standards were used for calibration.

### 2.3.7 Conjugate hydrodynamic diameter

CT-conjugates, native CT, and CT-Br (0.5-1.0 mg/mL) were prepared in 100 mM sodium phosphate buffer (pH 8) and filtered using a 0.22 μM cellulose acetate syringe filter. Hydrodynamic diameter was measured using Particulate Systems NanoPlus (Micromeritics) dynamic light scattering at 25 °C with 25 accumulations in triplicate. The hydrodynamic diameters, as determined by dynamic light scattering, were reported in number distribution. Volume and intensity values are also often reported when using dynamic light scattering and can provide more insight into the composition of the sample. For example, native CT had number, volume, and intensity distribution diameters of 1.8 ± 0.5, 2.5 ± 1.2, and 5.9 ± 3.5 nm, respectively. Since the values were different, this implied that the protein was not perfectly homogenous. The same holds true for all conjugate hydrodynamic diameters. All conjugate hydrodynamic diameters were reported by number distribution.

### 2.3.8 Michaelis-Menten kinetics

N-succinyl-Ala-Ala-Pro-Phe p-nitroanilide (Suc-AAPF-pNA) was used as a substrate for CT hydrolysis. Substrate (0-20 mg/mL in DMSO, 30 μL) was added to a 1.5 mL cuvette with 100 mM sodium phosphate buffer (pH 4, 6, 8, or 10). Native CT or CT-conjugates (0.1 mg/mL protein, 4 μM, 10 μL) was added to the cuvette with substrate and buffer. The initial substrate hydrolysis rate was measured by recording the increase in absorbance at 412 nm over the first 90 seconds after mixing using a Lambda 2 Perkin Elmer ultraviolet-visible spectrometer equipped with a temperature-controlled cell holder at 37 °C. Michaelis-Menten parameters were determined using nonlinear curve fitting of initial hydrolysis rate versus substrate concentration in GraphPad. Kinetics were measured in triplicate.

### 2.3.9 Residual activity kinetics

CT-conjugates, native CT, and CT-Br (1 mg/mL, 40 μM protein) were dissolved in 100 mM sodium phosphate buffer (pH 8). Samples were then diluted in triplicate to 4 μM using either 167 mM HCl (pH 1) or 10 mM NaOH (pH 12) and incubated in a circulating water bath at 37 °C. Aliquots of 10 μL were removed at specific time points over 60 min and residual activity was measured in 100 mM sodium phosphate buffer (pH 8, 960 μL) using Suc-AAPF-pNA as a substrate (6 mg/mL, 30 μL, 288 μM in DMSO). Initial hydrolysis rate was determined by measuring the increase in absorbance at 412 nm over 40 seconds and data was normalized to its optimal activity at time 0. For disrupting electrostatic and hydrophobic interactions, either 1.0 M NaCl or 10 v/v% DMSO was added to the cuvette during incubation at pH 1. This was performed for each of the short length conjugates.

### 2.3.10 Tryptophan fluorescence refolding

CT-conjugates, native CT, and CT-Br (1 mg/mL, 40 μM protein) were dissolved in 100 mM sodium phosphate buffer (pH 8). Samples were diluted (0.1 mg/mL, 4 μM) using either 167 mM HCL (pH 1) or 10 mM NaOH (pH 12) and incubated at 37 °C using a circulating water bath. After 40 min incubation, samples were diluted back to pH 8 (0.01 mg/mL, 0.4 μM) using 100 mM sodium phosphate (pH 8) into a 96 well plate in triplicate. Changes in pH were verified by measurement with a pH meter. The fluorescence intensity was measured by excitation at 270 nm and emission at 330 nm and 350 nm. The ratio of the emitted fluorescence intensity was calculated (350 nm/330 nm) and compared to the sample's original fluorescence intensity at time 0 (no incubation at pH 1 or 12). Percent change was calculated to determine refolding ability. Fluorescence was measured using a BioTek Synergy H1 Plate Reader at 37 °C.

### 2.3.11 Tryptophan fluorescence kinetic unfolding

CT-conjugates, native CT, and CT-Br (1 mg/mL, 40 μM protein) were dissolved in 100 mM sodium phosphate buffer (pH 8). Samples were diluted to 0.1 mg/mL (4 μM protein) in a 96 well plate in triplicate using either 167 mM HCl (pH 1) or 10 mM NaOH (pH 12) (e.g. 30 μL sample and 270 μL of pH 1 or pH 12 solution). Fluorescence intensity was measured every 2 minutes over 40 minutes (excitation at 270 nm, emission at 330 nm and 350 nm). The ratio of emission (350 nm/330 nm) was plotted over time with time 0 as the fluorescence intensity of the sample at pH 8 (no incubation in pH 1 or pH 12). The temperature was held constant at 37 °C over 40 minutes and measurements were made using a BioTek Synergy H1 Plate Reader.

### 2.3.12 Molecular Dynamics Simulations

The chymotrypsin model was constructed from a crystallographic structure (PDB ID "4CHA" in the protein data bank).[119] Polymer chains of pQA, pSMA and pCBMA were

constructed using a force field assisted linear self avoiding random walk method implemented in the PySimm software.[120] The topology files of CT and CT-conjugates were prepared using the psfgen tool in the VMD software.[121] Once the conjugate initial structures were prepared, each system was solvated with TIP3P water molecules in a rectangular box with a buffering distance of 14Å. $Na^+$ and $Cl^-$ ions were added to neutralize each system and maintain an ionic strength of approximately 0.1 M. The protein was modeled using the CHARMM C36m force field[122] and the initiator and polymer chains were modeled using the CGenFF force field.[123] Molecular dynamics simulations were performed using NAMD 2.12.[124] Energy minimizations were carried out with the protein backbone restrained using the conjugate gradient for 10,000 steps followed by another 10,000 steps without any restraint. Each system was then gradually heated to 310.15 K with 50 K increments and a 20 ps interval in a NVT ensemble. The system was subjected to an additional 500 ps of simulation in the NVT ensemble before switching to NPT simulations at 1 bar. A cutoff of 14 Å and a switching distance of 12 Å were used for non-bonded interactions. Particle mesh Ewald summation was applied to incorporate long range electrostatic interactions.[125] Langevin thermostat with a 1.0 $ps^{-1}$ collision frequency was used to maintain the system temperature at 310.15 K. The SETTLE algorithm was used to constrain bond lengths involving hydrogen atoms and a 1 fs time step was used. All of the analysis was carried out using VMD software.

The diameters for CT-pCBMA conjugates were validated by calculating the contour lengths of the polymers obtained from molecular simulations of the monomer multiplied by the DP plus the length of the initiator. Considering that the polymer chains are dispersed across the surface of the protein, the overall diameter of the conjugate was estimated. The lengths of initiator and monomer were approximately 6.2 Å and 2.6 Å, respectively. Therefore, for DPs of

10, 46, and 112, the contour lengths of each pCBMA chain, including the initiator, are approximately 3.2, 12.6, and 29.7 nm. Further, the atomistic dynamics simulation results showed that although the polymer chains were dispersed across the entire surface of CT and could vary in conformations depending on interactions with the protein surface, each other, and the solvent, a majority of the polymer chains were extended into the solvent. Therefore, the radii of gyrations and hydrodynamic diameters of the conjugates were expected to grow with the length of the polymer chains. The average radius of gyration of CT, CT-pCBMA 10, CT-pQA 10, and CT-pSMA 14 obtained from atomistic dynamic simulations were 1.7, 2.7, 2.8, and 3.0 nm, respectively.

## 2.4    Results and Discussion

A family of fifteen chymotrypsin-polymer conjugates were synthesized (**Figure 2.1**) with varying polymer charge, hydrophobicity (**Figure 2.2**) and molecular mass (*i.e.* chain length) using protein-ATRP. First, 12 surface accessible primary amine groups (determined through matrix assisted laser desorption/ionization time-of flight mass spectroscopy (MALDI-ToF MS) analysis (**Figure 2.3**))[34] were modified with an ATRP initiator (NHS-Br) as described previously[47].    Next, zwitterionic poly(carboxybetaine methacrylate) (pCBMA), neutral poly(oligoethylene glycol methacrylate) (pOEGMA), neutral to positive poly(dimethylaminoethyl methacrylate) (pDMAEMA),  positive poly(quarternary ammonium methacrylate) (pQA), or negative poly(sulfonate methacrylate) (pSMA) were grown from the surface of CT-Br using ATRP with copper catalysts (**Table 2.2**). For each polymer type, three conjugates of increasing chain length, or degree of polymerization (DP), were synthesized: short, medium, and long.
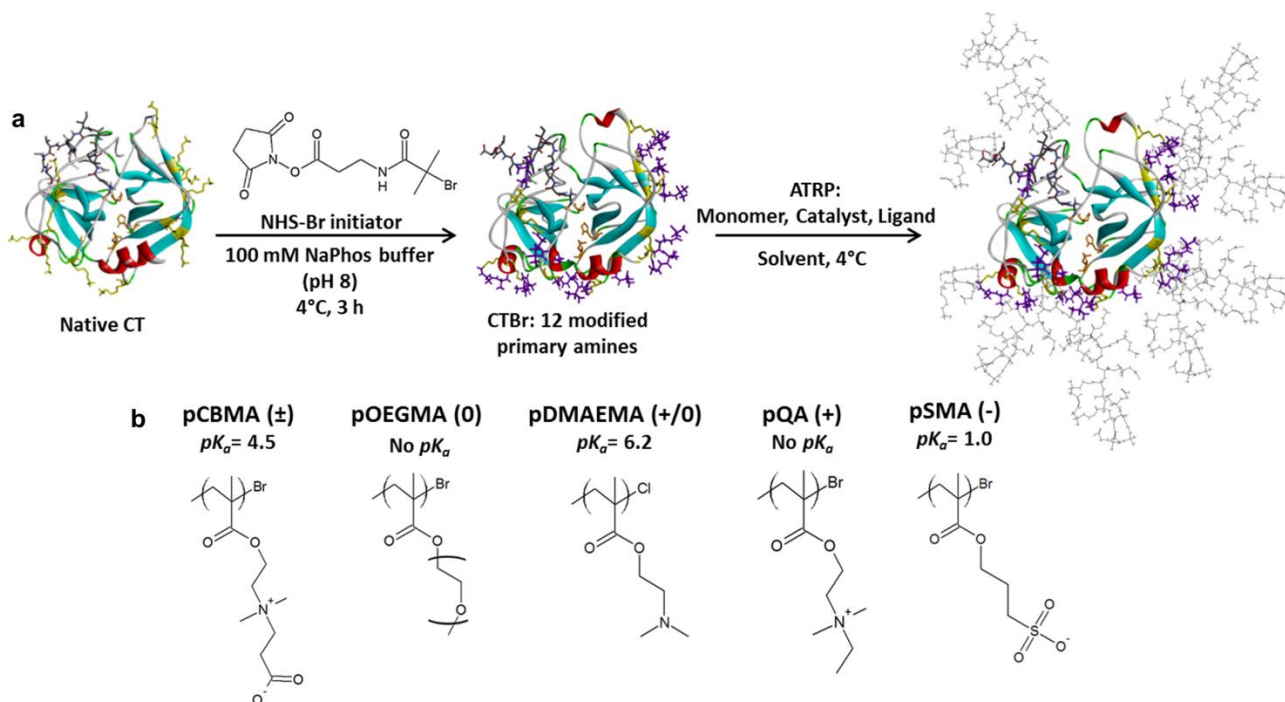
**Figure 2.1.** Synthesis and characterization of chymotrypsin-polymer conjugates. a, Synthesis scheme to prepare "grafted-from" conjugates. The first step is initiator immobilization using surface accessible primary amines followed by atom-transfer radical polymerization (ATRP) from the initiator modified sites. b, Polymers of varying charge and hydrophobicity used to create conjugates using ATRP. Three conjugates with increasing chain length were created for each monomer type.
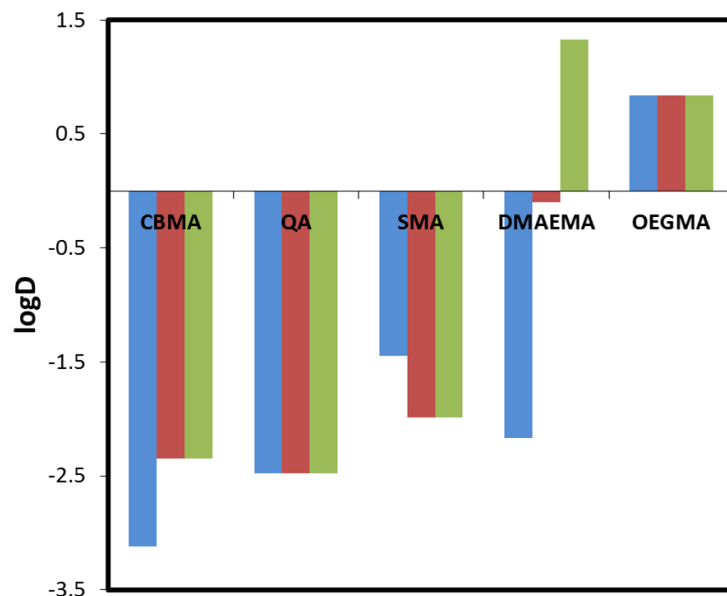
**Figure 2.2.** Monomer hydrophobicity as the distribution coefficient between octanol and water (logD) determined using ChemAxon at pH 1 (blue), 7 (red), and 12 (green). Hydrophobicity increases at pH 7 from QA < CBMA < SMA < DMAEMA < OEGMA.
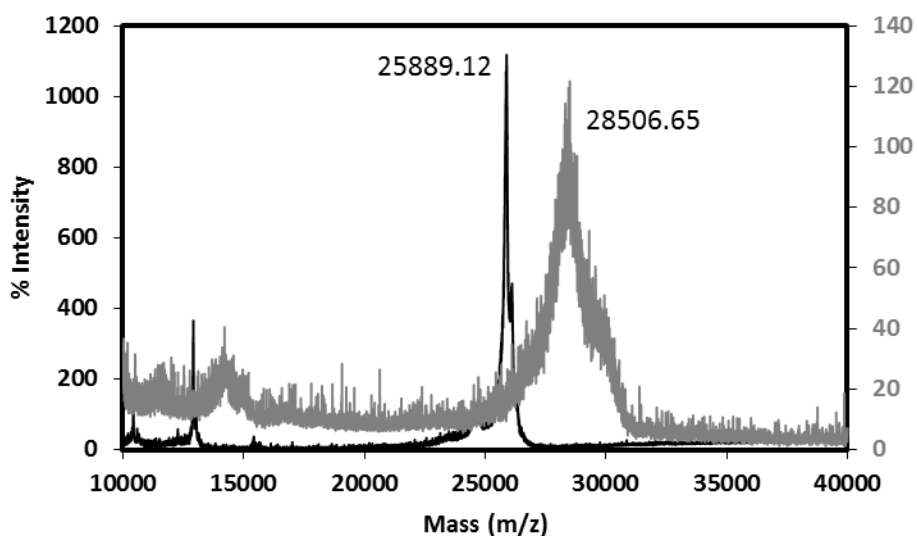


**Figure 2.3.** Matrix assisted laser desorption/ionization time-of-flight mass spectroscopy (MALDI-ToF MS) of native CT (black) and initiator modified CT (CT-Br, gray). The difference in m/z allows calculation of how many modification sites were achieved. The conjugated initiator adds a mass of 220.5 Da per modification site. Peak labels are in Da. CT was modified with 12 initiators for atom-transfer radical polymerization.

**Table 2.2.** Atom-transfer radical polymerization conditions for conjugate synthesis. Reactions were performed at 4 °C to prevent CT autolysis. Increasing chain length was achieved by increasing the initiator to monomer ratio ([I]:[M]).

| Conjugate | Catalyst | Ligand | Final Concentration (mM) [M]:[I]:[Cu(I)]:[Cu(II)]:[L] | Reaction Time (h) |
|---|---|---|---|---|
| CT-pDMAEMA$_9$ | Cu(I)Cl | HMTETA | 14 : 1.15 : 5 : 0 : 5 | 18 |
| CT-pDMAEMA$_{46}$ | Cu(I)Cl | HMTETA | 115 : 1.15 : 5 : 0 : 5 | 18 |
| CT-pDMAEMA$_{89}$ | Cu(I)Cl | HMTETA | 230 : 1.15 : 5 : 0 : 5 | 18 |
| CT-pSMA$_{14}$ | Cu(II)Br + NaAsc (1.21 mM) | HMTETA | 25 : 1 : 0 : 5 : 12 | 2 |
| CT-pSMA$_{48}$ | Cu(II)Br + NaAsc (1.21 mM) | HMTETA | 100 : 1 : 0 : 5 : 12 | 2 |
| CT-pSMA$_{113}$ | Cu(II)Br + NaAsc (1.21 mM) | HMTETA | 175 : 1 : 0 : 5 : 12 | 2 |
| CT-pQA$_{10}$ | Cu(I)Br | HMTETA | 25 : 0.72 : 1 : 0 : 1.2 | 2 |
| CT-pQA$_{43}$ | Cu(I)Br | HMTETA | 111 : 0.72 : 1 : 0 : 1.2 | 2 |
| CT-pQA$_{89}$ | Cu(I)Br | HMTETA | 175 : 0.72 : 1 : 0 : 1.2 | 2 |
| CT-pOEGMA$_9$ | Cu(II)Br + NaAsc (1.21 mM) | HMTETA | 12 : 1 : 0 : 5 : 12 | 4 |
| CT-pOEGMA$_{53}$ | Cu(I)Cl/Cu(II)Cl | bpy | 125 : 1 : 1.1 : 9.9 : 24.1 | 18 |
| CT-pOEGMA$_{97}$ | Cu(II)Br + NaAsc (1.21 mM) | HMTETA | 220 : 1 : 0 : 5 : 12 | 4 |
| CT-pCBMA$_{10}$ | Cu(I)Br | HMTETA | 30 : 1 : 2 : 0 : 2.4 | 2 |
| CT-pCBMA$_{46}$ | Cu(I)Br | HMTETA | 125 : 1 : 2 : 0 : 2.4 | 2 |
| CT-pCBMA$_{112}$ | Cu(I)Br | HMTETA | 220 : 1 : 2 : 0 : 2.4 | 2 |

After purification via dialysis, conjugates were characterized with a bicinchoninic acid (BCA) assay to determine protein content and DP. We also performed acid-induced polymer cleavage followed by gel permeation chromatography to determine relative polymer molecular mass and polymer dispersity index (Đ) (**Figure 2.4**).
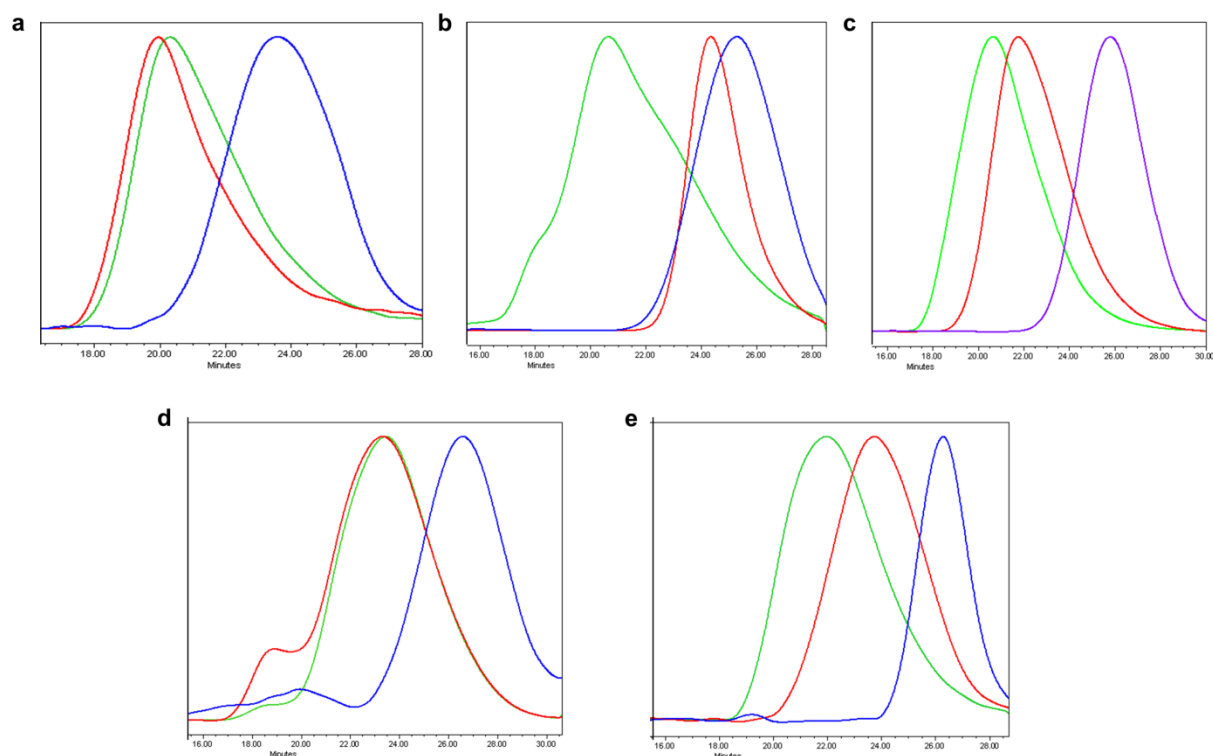
**Figure 2.4.** Gel permeation traces for cleaved polymer of varying molecular masses after acid hydrolysis for a, pCBMA b, pOEGMA c, pDMAEMA d, pQA e, pSMA. Molecular masses were relative to pullulan narrow standards.

Finally, we used dynamic light scattering (DLS) to determine the hydrodynamic diameter of the bioconjugates (**Table 2.3**). The percent conversions for the ATRP reactions, as determined by BCA assays, were on average 40% (pCBMA), 54% (pOEGMA), 50% (pDMAEMA), 43% (pQA), and 56% (pSMA). As DP increased for each conjugate type, the molecular mass increased while maintaining reasonable Đ's. The hydrodynamic diameter ($D_h$) also increased with molecular mass of the attached polymers. Native CT has a $D_h$ of $1.8 \pm 0.5$ nm by number distribution and the conjugates grew in size as the degree of polymerization increased. For example, the apparent $D_h$ values by number distribution for CT-pCBMA short, medium, and long conjugates were $8.8 \pm 2.6$, $14.8 \pm 4.1$, and $25.8 \pm 7.2$ nm, respectively.

**Table 2.3.** Conjugate characterization using bicinchoninic acid (BCA) assay for protein content, estimated degree of polymerization (DP) from BCA, cleaved polymer molecular mass and uniformity from gel permeation chromatography, and number intensity hydrodynamic diameter ($D_h$, number distribution). Conjugates increased in DP for each monomer type with a corresponding increase in molecular mass and $D_h$. Conjugate characterization was compared to native CT and initiator modified CT (CT-Br).

| | % Protein from BCA | Calculated DP | Cleaved Polymer $M_n$ (kDa) | Cleaved Polymer Đ ($M_w/M_n$) | $D_h$ (nm) |
|---|---|---|---|---|---|
| **Native CT** | - | - | - | - | $1.8 \pm 0.5$ |
| **CT-Br** | - | - | - | - | $1.8 \pm 0.5$ |
| **CT-pCBMA (±)** | 50.8 | 10 | 21.2 | 1.52 | $8.8 \pm 2.6$ |
| | 18.2 | 46 | 85.5 | 1.92 | $14.8 \pm 4.1$ |
| | 8.30 | 112 | 106.5 | 1.69 | $25.8 \pm 7.2$ |
| **CT-pOEGMA (0)** | 31.8 | 9 | 11.1 | 1.63 | $6.8 \pm 1.9$ |
| | 8.10 | 53 | 20.0 | 1.28 | $13.5 \pm 3.3$ |
| | 4.60 | 97 | 85.9 | 1.59 | $27.8 \pm 7.6$ |
| **CT-pDMAEMA (+/0)** | 60.9 | 9 | 14.8 | 1.51 | $3.7 \pm 1.0$ |
| | 22.9 | 46 | 83.3 | 1.68 | $15.9 \pm 4.4$ |
| | 13.8 | 89 | 170.0 | 2.08 | $21.4 \pm 5.9$ |
| **CT-pQA (+)** | 51.2 | 10 | 11.1 | 1.67 | $3.9 \pm 1.1$ |
| | 17.5 | 43 | 40.2 | 1.94 | $12.7 \pm 3.2$ |
| | 10.0 | 89 | 45.8 | 1.66 | $21.9 \pm 6.1$ |
| **CT-pSMA (-)** | 40.0 | 14 | 8.8 | 1.19 | $5.2 \pm 1.4$ |
| | 16.5 | 48 | 27.4 | 1.58 | $8.8 \pm 2.5$ |
| | 7.70 | 113 | 69.7 | 1.61 | $21.4 \pm 6.0$ |

## 2.4.1   Polymer effect on enzyme activity

The covalent coupling of polymers to enzymes has been shown to influence both the pH-dependence of activity as well as the rate of pH-induced irreversible inactivation of enzymes. We first used the family of conjugates to determine the relative effect of charge and length on the pH-dependence of CT activity. Serine proteases, like CT, have a mechanism that converts a normally inert serine hydroxyl group into an active nucleophile.  The active site has a catalytic triad (including the serine) in which the active site histidine must be uncharged for the enzyme to be active.  It has been suggested that engineering the surface charge of the enzyme might alter

the p$K_a$ of that active site histidine and thereby alter the p$K_a$ of the enzyme itself.[126] It is common to observe reduced enzyme activity upon polymer conjugation and many groups have proposed that polymers could cause structural stiffening of the protein, thereby reducing intrinsic activity[57]. It could also possible that the nucleophilicity of the active site could be reduced by subtle polymer-induced changes in structure. In an attempt to distinguish between these effects and gain further insight into structure-function-dynamic relationships, we designed molecular dynamic (MD) simulations of the shortest polymer conjugates at neutral pH.

### 2.4.2  Simulation of Conjugate Molecular Dynamics

CT is composed of 3 chains (A: 13 residues, B: 131 residues, and C: 97 residues) that are each connected by a single inter-chain disulfide bond to form the overall structure (PDB: 4CHA). From the 12 total initiator modified sites, 1 is on chain A, 6 are on chain B, and 5 are on chain C. The reactivity of each of these 12 amino groups with ATRP initiator were predicted as previously described.[34] Further, CT's specificity and activity arises from substrate binding to the hydrophobic S$_1$ pocket which then positions the amide bond to be cleaved by the catalytic triad in the active site (His 57, Asp 102, Ser 195). CT cleaves the amide bonds on the carbonyl side of large hydrophobic residues which means that it is also susceptible to autolysis. Native CT and short polymer chain conjugate models were created for CT-pCBMA, CT-pQA, and CT-pSMA and dynamics were simulated to mimic experimental conditions (37 °C, pH 8, 0.1M salt concentration) using NAMD 2.12 with CHARMM c36m and CGenFF force fields over 500 ns. Simulation force fields were validated against experimental size data. The root mean square deviation (RMSD) was analyzed for native CT and conjugates to determine the effect of polymer attachment on the structural motions of the protein core. Additionally, to determine the conformation of individual polymer chains around the surface of CT, the polymer end-to-end

46

distributions were calculated for the 12 polymer chains in each of the conjugates. Higher end-to-end distances would imply that the polymers adopted a more rigid, extended conformation while lower end-to-end distances would imply that the chains were more flexible.

The RMSD of the protein core in CT-pCBMA was significantly smaller and more stable than native CT, CT-pQA and CT-pSMA conjugates, suggesting a potentially enhanced structural stability in the CT-pCBMA conjugate (**Figure 2.5a**). A deeper analysis of the data revealed that the unique dynamic properties of CT-pCBMA were coupled to a specific interaction of Lys202-pCBMA with chain A of the protein (**Figure 2.5b**).
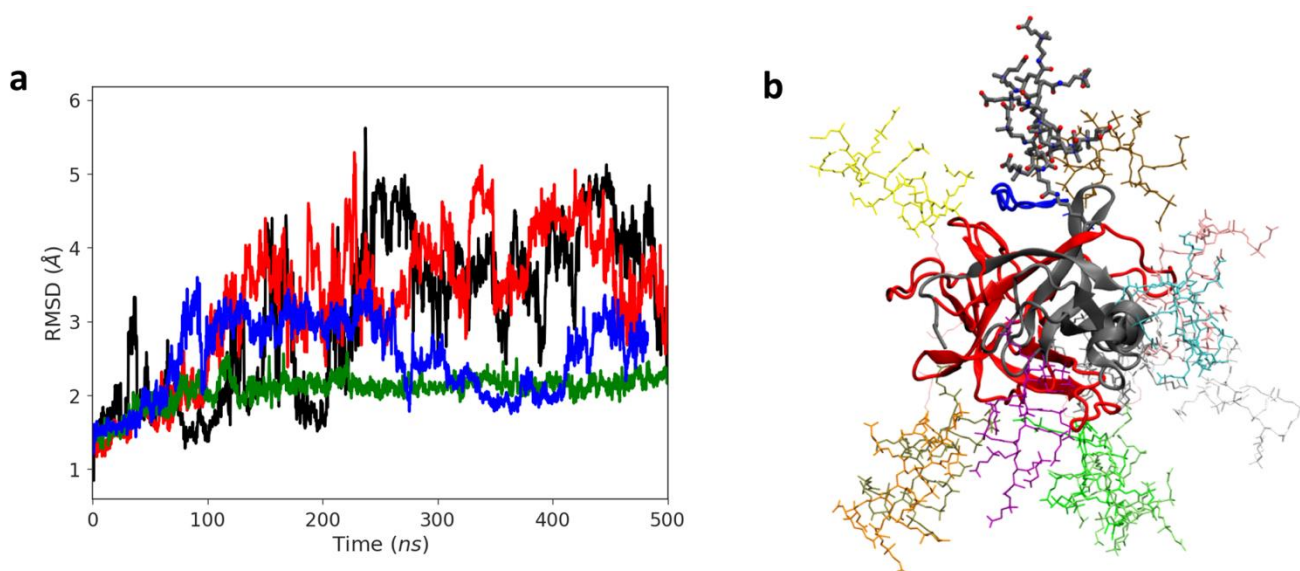


**Figure 2.5.** a, Root mean square deviation of backbone atoms from molecular dynamics simulations in native CT (black), CT-pCBMA 10 (green), CT-pQA 10 (red), and CT-pSMA 14 (blue) compared to the crystal structure. Short chain lengths were used to model each conjugate. pCBMA was shown to stabilize the overall protein structure compared to the native CT and other conjugates. The RMSD of CT-pCBMA was smaller and more stable in comparison to the highly dynamic CT, CT-pQA, and CT-pSMA. b, Snapshot showing the interaction of Lys202-pCBMA (grey) with chain A (blue), promoting the stabilization of the CT.

Chain A is the shortest chain and is highly flexible because it does not have a defined secondary structure. The stabilizing interaction of Lys202-pCBMA with chain A restricted its

fluctuations and created a more conformationally stable conjugate. Analysis of the trajectories of CT-pCBMA showed that the polymers formed some interactions with the protein surface over time, but there was no interference with the hydrophobic $S_1$ binding pocket, most likely due to pCMBA's super-hydrophilicity, which could enhance substrate affinity. The pCBMA polymer chains were also very flexible, as seen in the relatively shorter end-to-end distances, and their conformations depended on the attachment site (**Figure 2.6**). For example, the average end-to-end distances of pCBMA's attached to Lys 202 and Lys 175 were approximately 12 Å and 23 Å, respectively.
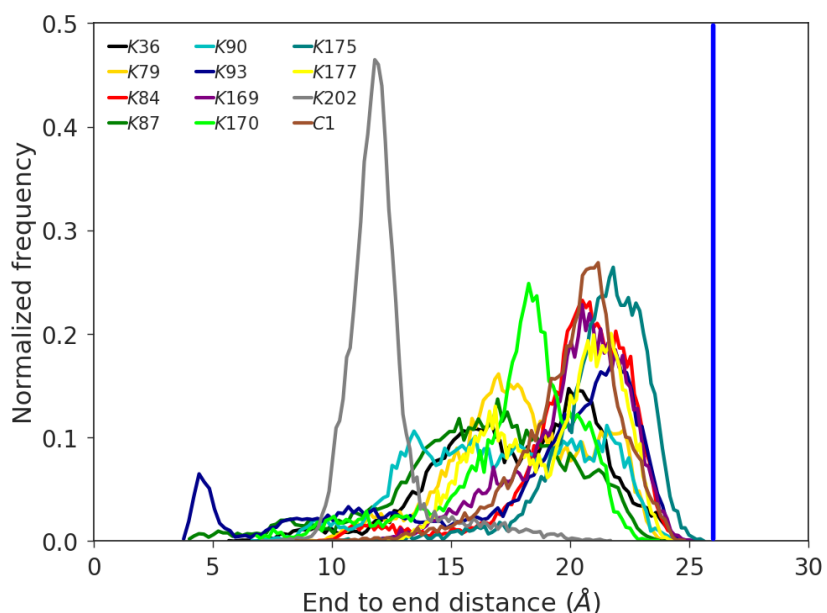


**Figure 2.6.** End to end distribution of each polymer in CT-pCBMA . pCBMA chains were highly flexible as seen by the large distribution in end-to-end distances between different polymer chains. pCBMA chains were shown to interact with the protein surface.

The RMSD data for the protein core of the CT-pQA conjugate showed high dynamic fluctuations, similar to native CT. There were slight interactions between pQA polymers and the protein surface over time, but not anything unique that could have increased conformational stability. No direct interactions were observed between pQA chains and the hydrophobic $S_1$

binding pocket, which in addition to a positively charged micro environment, could help

accelerate the diffusion of a negatively charged substrate towards the active site of CT. The

polymer chain end-to-end distances were highly dependent on attachment site and ranged on

average from 15 to 24 Å, similar to CT-pCBMA chains (**Figure 2.7**).
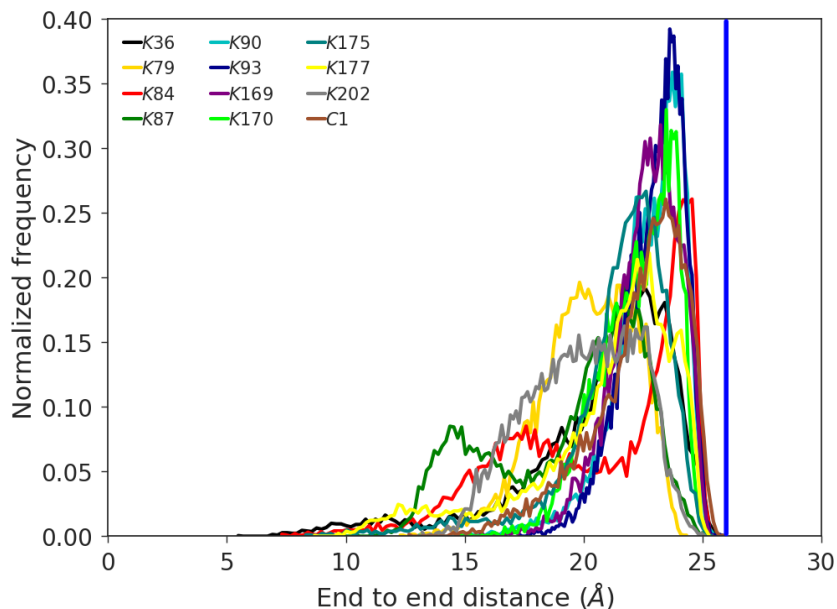


**Figure 2.7.** End to end distribution of each polymer in CT-pQA . The average end-to-end distances are different for different polymers. For example, the average end-to-end distances are ~15 and ~24 Å for K87 and K170, respectively. This indicated that pQA polymers were more flexible and were more likely to interact with the protein surface.

Finally, the RMSD data for the CT-pSMA conjugate showed high dynamic fluctuations

and upon further analysis, most of the pSMA chains adopted a rather rigid and extended form on

CT due to electrostatic repulsions between the negatively charged sulfonate groups. Accordingly,

the end-to end distances were relatively high and did not depend on attachment site (**Figure 2.8**).

All of the pSMA chains had similar distributions with an average end-to-end distance of

approximately 30 Å. Hence, little to no interactions were formed with the protein surface which

caused a highly dynamic RMSD. The only exception was the pSMA chain conjugated to Lys170, which was found to interact with the residues located near the $S_1$ binding pocket of CT (**Figure 2.9**).[127] Since the $S_1$ pocket is responsible for substrate binding, the simulation suggested that the enzyme's affinity for the substrate could be impacted. Moreover, the spatial arrangement of the repelled pSMA polymer chains created a uniform negatively charged micro environment around the CT surface, which would reduce the affinity of a negatively charged substrate towards the enzyme.
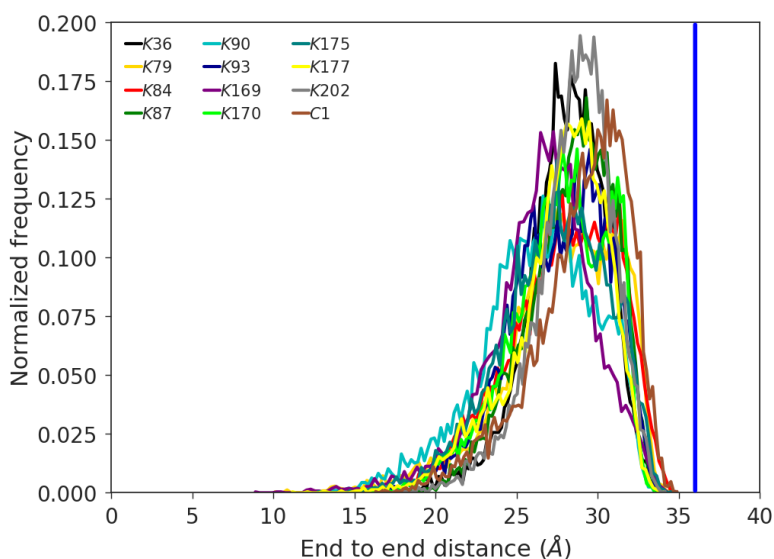


**Figure 2.8.** End to end distribution of each polymer in CT-pSMA. All chains had similarly high end-to-end distances indicating that the polymer chains were extended into solution, most likely due to unfavorable electrostatic interactions between sulfonate groups.
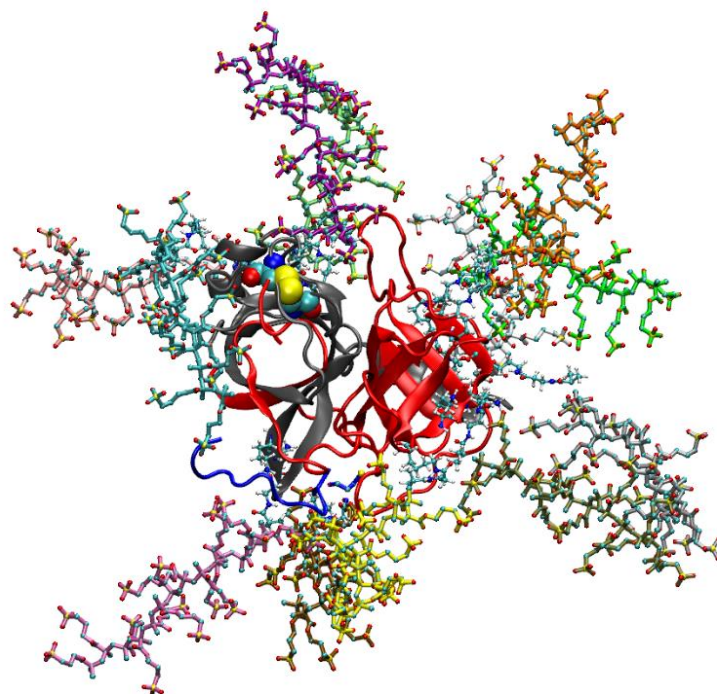
**Figure 2.9.** A snap shot of the CT-pSMA conjugate showing the pSMA chain conjugated to Lys170 (cyan), chain A (blue), B (grey) and C (red) of CT. The S1 binding pocket is near the two Cys residues in CPK representation.

### 2.4.3   pH-Dependence of Conjugate Activity

In order to experimentally confirm what was predicted *in silico* and gain a better understanding of how the conjugated polymers impact CT activity across a range of pH values, Michaelis-Menten kinetics were determined for native CT and CT-polymer conjugates as a function of pH (4, 6, 8, 10) at 37 °C (**Figure 2.10**). A hydrophobic, negatively charged substrate, *N*-succinyl-L-Ala-L-Ala-L-Pro-L-Phe-p-nitroanilide (suc-AAPF-pNA), was used for enzyme hydrolysis.
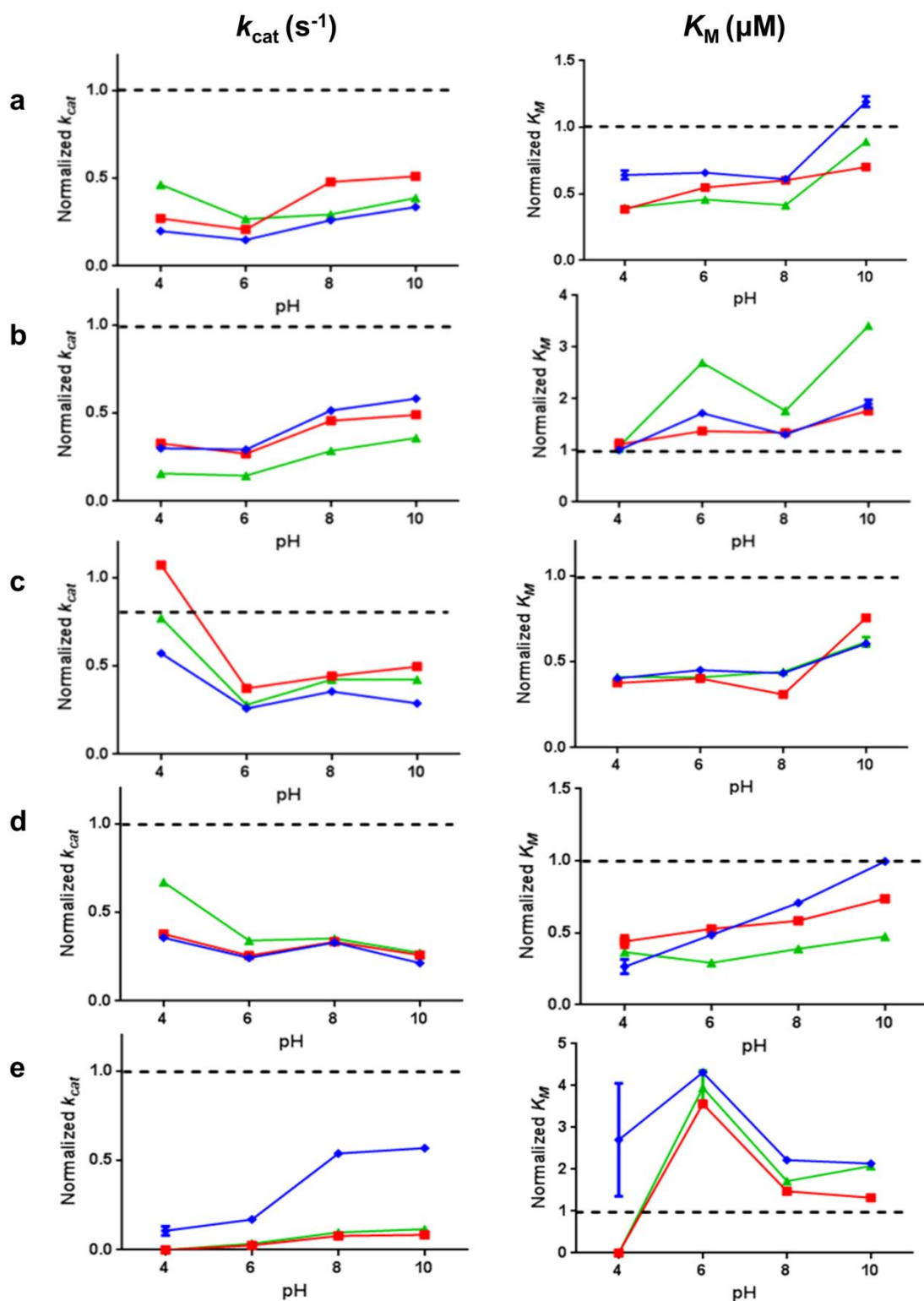
**Figure 2.10.** Michaelis-Menten kinetics of CT conjugates at pH 4, 6, 8, and 10 (x-axis) in comparison to native CT for turnover rate ($k_{cat}$, s$^{-1}$, 1$^{st}$ column) and Michaelis constant ($K_M$, μM, 2$^{nd}$ column). a, Kinetics of CT-pCBMA (±) normalized to native CT. b, Kinetics of CT-pOEGMA (0) normalized to native CT. c, Kinetics of CT-pDMAEMA (+/0) normalized to native CT. d, Kinetics of CT-pQA (+) normalized to

native CT. e, Kinetics of CT-pSMA (-) normalized to native CT. Normalized native CT (dashed black line), short length conjugates (blue diamonds), medium length conjugates (red squares), and long length conjugates (green triangles). Changes in activity derived from changes in $K_M$ due to polymer charge and were not length dependent. Error bars represent the standard deviation from triplicate measurements.

When normalized to native CT at each pH (**Figure 2.11a-c**), all conjugates showed decreased intrinsic activity ($k_{cat}$). The MD simulation studies showed structural stiffening only for CT-pCBMA, which could correlate with the lower intrinsic activity, while the other conjugates and native CT displayed high dynamic fluctuations. Therefore, the reduction in $k_{cat}$ for the majority of conjugates was most likely due to subtle changes in the protein structure that altered the nucleophilicity of the active site. An increase in activity at lower pH was observed for conjugates with positively charged polymers, namely pQA and pDMAEMA. pDMAEMA becomes positively charged at pH's below the $pK_a$ (6.2). Increasing surface positive charge has been shown to increase enzyme activity at low pH's, most likely as a result of long range electrostatic interactions between the surface and the active site histidine to reduce the $pK_a$ of the active site.[126]
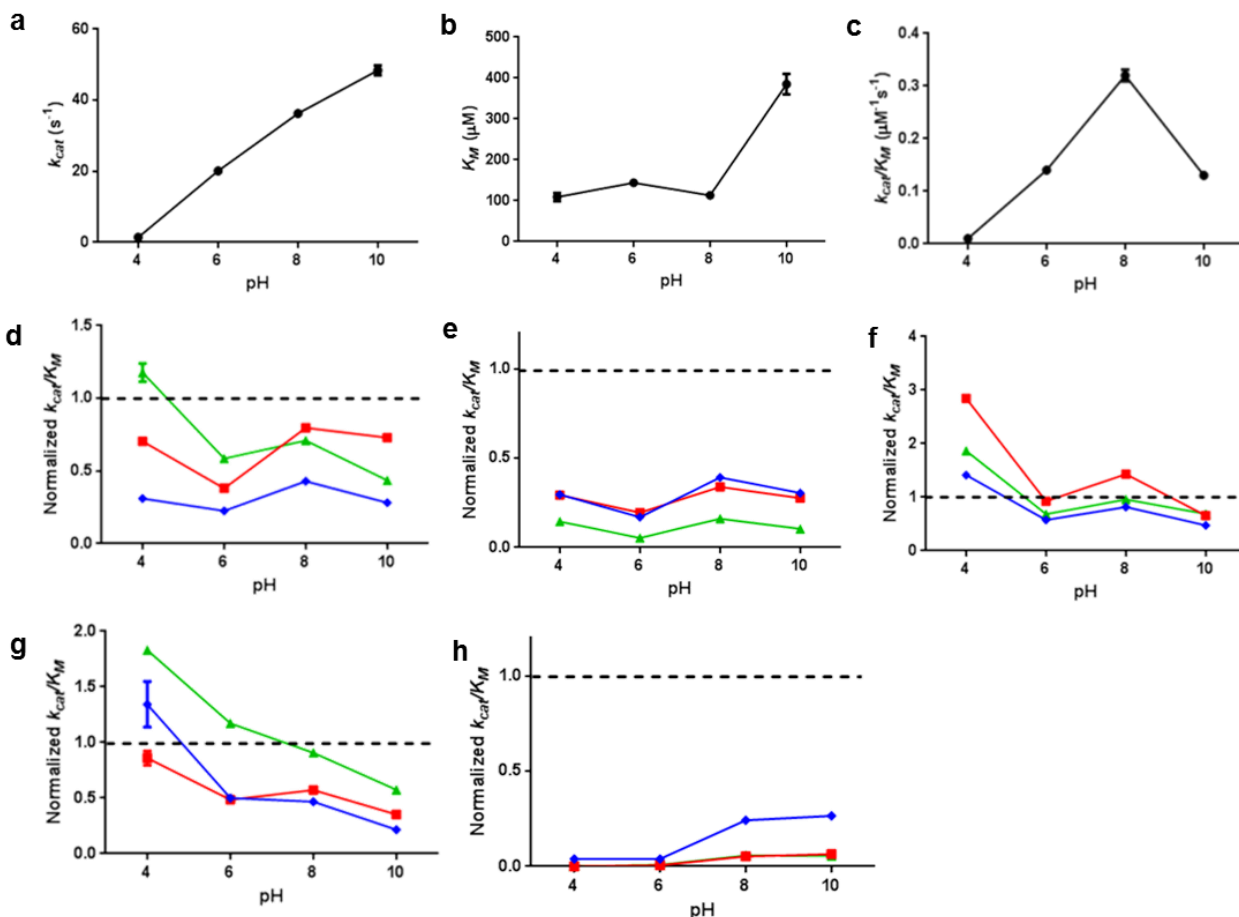
**Figure 2.11.** a, $k_{cat}$, s$^{-1}$ of native CT. b, $K_M$, μM of native CT. Overall catalytic efficiency ($k_{cat}/K_M$, μM$^{-1}$ s$^{-1}$) for c, native CT d, CT-pCBMA, e, CT-pOEGMA f, CT-pDMAEMA g, CT-pQA h, CT-pSMA. d-h are normalized to native CT at each pH. Normalized native CT (dashed black line), short length conjugates (blue diamonds), medium length conjugates (red squares), and long length conjugates (green triangles). Error bars represent the standard deviation from triplicate measurements.

It has been known for many years that the attachment of polymers to proteins can have direct and indirect effects on the ability of an enzyme to bind substrates and inhibitors. In our family of conjugates, substrate affinity ($K_M$) was highly dependent on polymer properties. CT-pCBMA (**Figure 2.10a**) had increased substrate affinity (lower $K_M$'s) compared to native CT at pH 4, 6, and 8. At pH 10, the $K_M$ of the native and CT-pCBMA enzymes were similar. Zwitterionic polymer super-hydrophilicity, that might displace water molecules from the active

site, has been suggested as a mechanism that explained increased substrate affinity. The movement of water molecules from the $S_1$ binding pocket to the polymer phase would have increased the hydrophobicity of the binding pocket.[128,129] The neutral conjugate, CT-pOEGMA, showed increased $K_M$'s compared to native CT (**Figure 2.10b**). The amphiphilicity of PEG-protein conjugates has been proposed to reduce the hydrophobic-hydrophobic driving force of the substrate binding to the active site.[128] The hydrophobic-hydrophobic interactions between the substrate and pOEGMA chains combined with possible steric hindrance as the substrate diffuses through the polymer layer would also explain the decreased $K_M$. The affinity of CT-pDMAEMA for its negatively charged substrate was stronger than that for native CT (**Figure 2.10c**). The positively charged conjugate, CT-pQA, (**Figure 2.10d**) had similar pH dependence of functionality to CT-pDMAEMA. As expected, the affinity of a negatively charged substrate for a positively charged conjugate was significantly increased. Finally, the negatively charged conjugate, CT-pSMA, (**Figure 2.10e**) was significantly less active than native chymotrypsin. Indeed, activity was undetectable at pH 4 and 6, except for the shortest CT-pSMA conjugate. Substrate affinity was also damaged by the negatively charged polymer and partial blockage of the $S_1$ binding pocket, as determined through MD simulations.

Overall, CT-pCBMA, CT-pDMAEMA, and CT-pQA, maintained the most activity while CT-pOEGMA and CT-pSMA had the least activity (**Figure 2.11d-h**). Of particular note, polymer length did not have a significant effect on overall activity. The pH dependent changes in conjugate function were driven almost exclusively by changes in substrate affinity versus intrinsic activity. We were also interested in whether or not there was a correlation between conjugates maintaining the most activity and providing the most stabilization, so we next investigated irreversible inactivation of the conjugates.

### 2.4.4 pH-Dependence of Irreversible Inactivation

Proteins are known to unfold in a two-step process in which the first step is reversible (**Figure 2.12a**). Protein unfolding at extremes of pH is predominantly, but not exclusively, due to disruption of protonation states on the protein surface which disrupt hydrogen-bonding and electrostatic interactions. Protein folding has classically been described in terms of hydrophobic collapse, with surface charges thought to be less important than the protein core because the residues hydrogen-bonding with the solvent will be the same in the folded and unfolded states.[130] However, it has also been suggested that surface charge could be an important factor because each charged side chain could be involved in electrostatic interactions that maintain optimal folding.[131] In a basic environment, previous studies of myoglobin unfolding found that, as a result of heme dissociation, there was no intermediate state in the unfolding process.[132] Another study investigated the unfolding of barstar protein at pH 12 and hypothesized that deprotonation of tyrosine ($pK_a$= 10.5), lysine ($pK_a$ = 10.8), and arginine ($pK_a$= 12.5) residues caused mutual charge repulsion causing rapid destabilization and simultaneous unrecoverable loss in tertiary and secondary structure.[133] This effect was further evidenced in the unfolding of lectin at high pH.[134] It is also known that hydrogen-bonding that holds secondary structures together, such as alpha helices and beta sheets, depends on pH.[135] We already knew from our previous reports with CT-conjugates that polymers could stabilize the protein in acid, with varying degrees dependent on polymer type[49], but it was unclear whether or not that would hold true when denaturing in base.

We postulated that protein stability could be altered by controlling the amount of added charge to the protein through the choice and length of conjugated polymer. We further hypothesized that the unfolding pathways would be different for conjugates at the two ends of the pH scale where polymers would stabilize proteins at pH 1, but not pH 12. Moreover, we

hypothesized that polymer conjugation could impact irreversible inactivation by either altering

the rate of complete unfolding or the rate of refolding (**Figure 2.12b,c**).
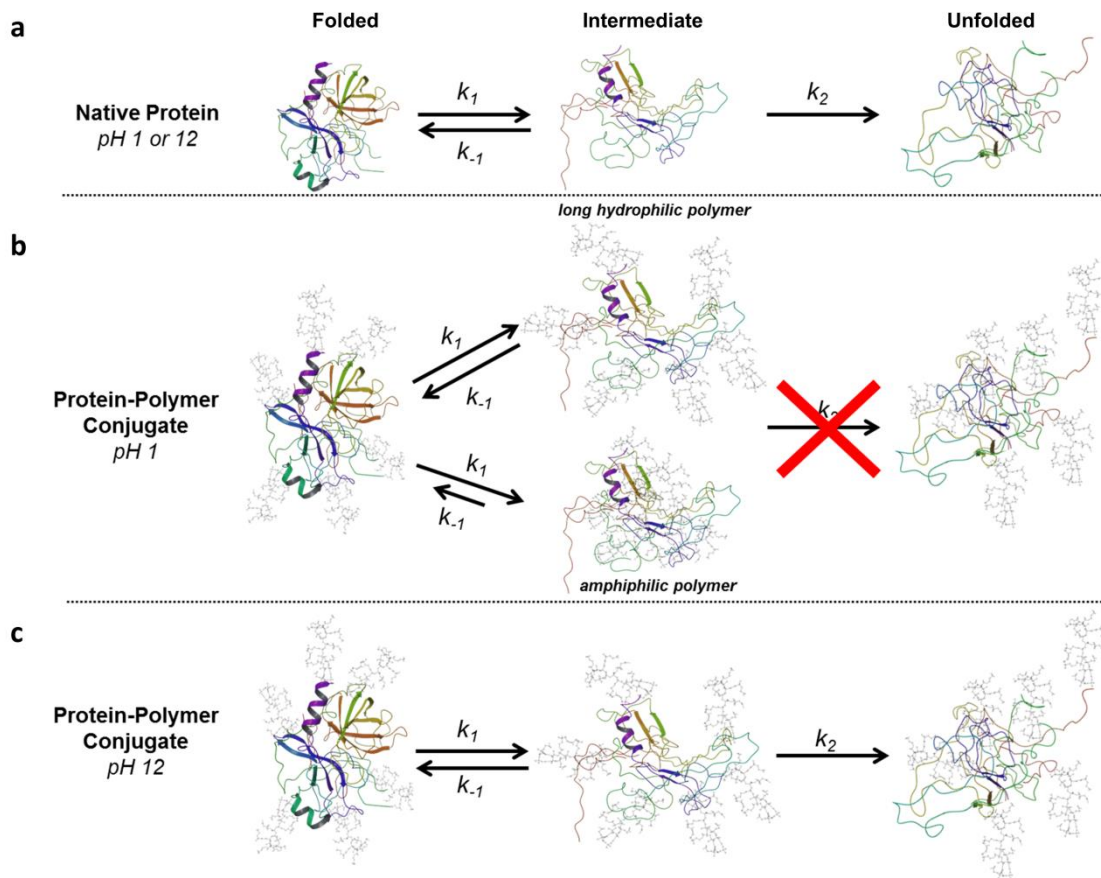


**Figure 2.12.** Mechanistic hypothesis of unfolding pathways for native CT and CT-conjugates at extremes of pH. a, Unfolding pathway of native protein at pH 1 and pH 12. b, Unfolding pathway of a protein-polymer conjugate at pH 1. Polymers stabilize partially unfolded states and prevent irreversible denaturation at pH 1. Conjugate refolding is dependent on polymer physiochemical properties where long, hydrophilic polymers enhance the refolding rate in comparison to amphiphilic polymers c, Unfolding pathway of a protein-polymer conjugate at pH 12. Polymers are not able to stabilize the intermediate state when denaturing at pH 12 and complete unfolding proceeds.

To test this, the conjugates were exposed to low pH (pH 1) or high pH (pH 12) at 37 °C,

then residual activity was determined after the protein was restored to its optimal pH 8.  Serine

proteases would be inactive at pH's below the $pK_a$ of the active site histidine, even if the protein

was perfectly folded.  Thus, these experiments determined the degree to which native CT, initiator modified CT, and CT-conjugates could unfold and refold.

### 2.4.5   Acid-induced inactivation

Comparing the residual activity of native CT to CT-Br (**Figure 2.13a**), we immediately noticed that CT-Br that had been exposed to acid for just two minutes had irreversibly inactivated.  CT-Br was the protein from which all conjugates were grown and therefore, when considering stability, we compared the effect of conjugation to both the native and initiated forms of the enzyme.  The initiated enzyme had lost 12 of the 15 positive charges on the protein surface, and given its dramatically reduced stability at low pH, the idea of a charged polymer restoring the electrostatic environment and stabilizing the protein was of interest.

The rate of acid-induced inactivation of CT-pCBMA (**Figure 2.13b**) and CT-pQA (**Figure 2.13e**) was significantly less than for native enzyme.  In both cases, longer polymers were particularly effective at preventing irreversible inactivation. The longest CT-pCBMA maintained ~65% of its activity while the longest CT-pQA maintained ~55% of its activity after 60 minutes. We found it interesting that, for these conjugates, the activity loss after refolding reached a constant value but did not appear to approach zero.  This indicated that either the conjugates had refolded to a less active state or the mechanisms of inactivation for native and conjugated forms of the enzyme were different.

CT-pOEGMA, CT-pDMAEMA, and CT-pSMA all stabilized the enzyme against acid-induced irreversible inactivation as indicated by the residual activities reaching constant values. However, the degree of stabilization was far less than the zwitterionic and positively charged protein-polymer conjugates (**Figure 2.13c,d,f**). Indeed, some of these conjugates lost more activity than the native enzyme during the 60 minute timeframe. As native CT would eventually

irreversibly inactivate and approach zero at longer times, all of the conjugates did provide

stabilization and are expected to remain active over longer incubation times in acid.
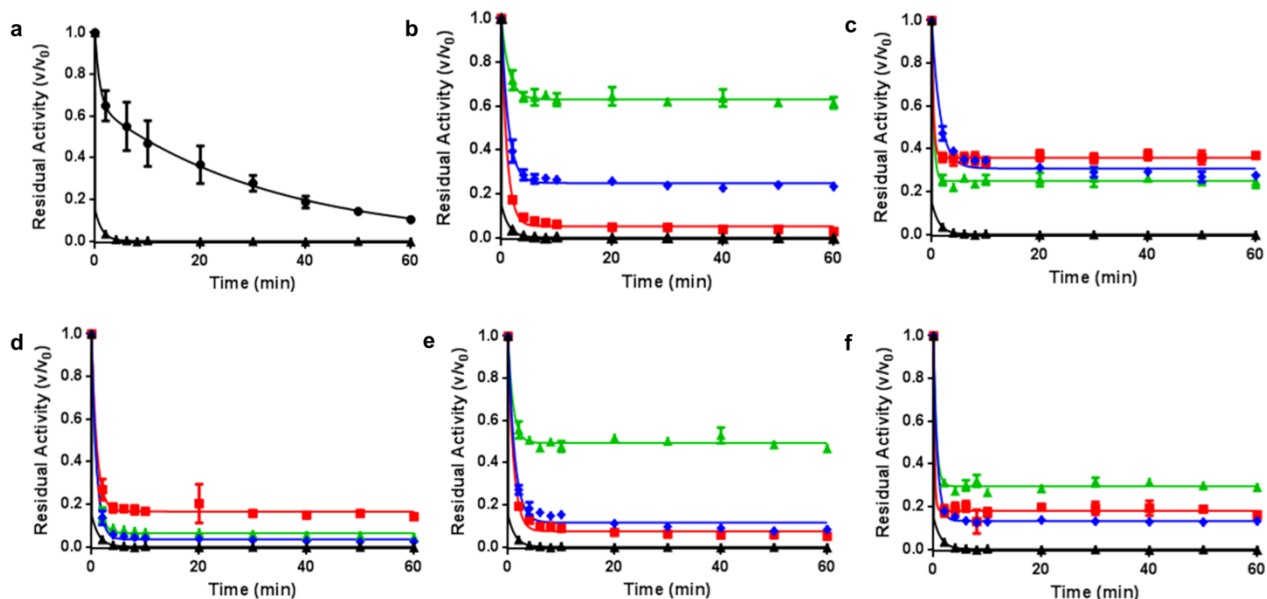


**Figure 2.13.** Conjugate acid stabilities at pH 1 (167 mM HCl) in comparison to native CT (black circles) and CT-Br (black triangles in all plots) in terms of residual activity over 60 minutes. Residual activity for a, native CT (black circles) and CT-Br (black triangles). b, CT-pCBMA (±). c, CT-pOEGMA (0). d, CT-pDMAEMA (+/0). e, CT-pQA (+). f, CT-pSMA (-). CT-Br (black triangles), short length conjugates (blue diamonds), medium length conjugates (red squares), and long length conjugates (green triangles). Long, hydrophilic polymers, pCBMA and pQA, stabilized conjugates the most at pH 1. All conjugates followed one-phase decays where native CT followed a two-phase decay. Error bars represent standard error of the mean from triplicate measurements.


In our prior work, we had concluded that conjugate stability was likely a function of how

the attached polymers interacted with the surface of the folded enzyme by altering the hydration

layer around the enzyme surface.[49]  It is also important to note that for CT, autolysis is also a

factor that could influence stability, however, this effect is minimized due to steric hindrance by

the dense polymer coating. Thus we focused on the various possible noncovalent interactions at

the protein-polymer interface. These interactions, if present, would be driven by noncovalent

interactions including electrostatic and/or hydrophobic (van der Waals). Thus, in order to explore

whether disruption of electrostatic or hydrophobic interactions would influence the stabilizing

effects of the polymers, we measured residual activity while independently doping the enzymes with either 1.0 M NaCl (to diminish electrostatic interactions) or 10 v/v% dimethyl sulfoxide (DMSO) (to diminish hydrophobic interactions) during incubation at pH 1 (**Figure 2.14**). If a noncovalent interaction between the polymer and protein surface lead to the observed stabilization, then disrupting them independently should cause dramatic changes in their stabilizing ability. The addition of DMSO to native CT increased stability against the acid while NaCl caused rapid destabilization. The addition of NaCl has been found to cause conformational changes in proteins[136] which could explain the increased destabilization of CT in acid. Conversely, at low concentrations (≤10%), DMSO has been shown to cause compaction of the folded protein[137] which could explain the observed increased stability for native CT. The stability of each conjugate decreased slightly with the addition of NaCl and DMSO. NaCl and DMSO were then added to the refolding buffer at pH 8 and stability of CT-pCBMA 112 was assessed at pH 1 (**Figure 2.15**). Stability decreased when salt and co-solvent were added into the refolding buffer. Since there were no dramatic increases in stability for any of the conjugates, regardless of polymer type, and recognizing that NaCl and DMSO both affect protein conformation, we surmised that conjugate acid stabilization was not strictly driven by the polymer's interaction with the surface of a folded protein, but conformational changes could also be involved.
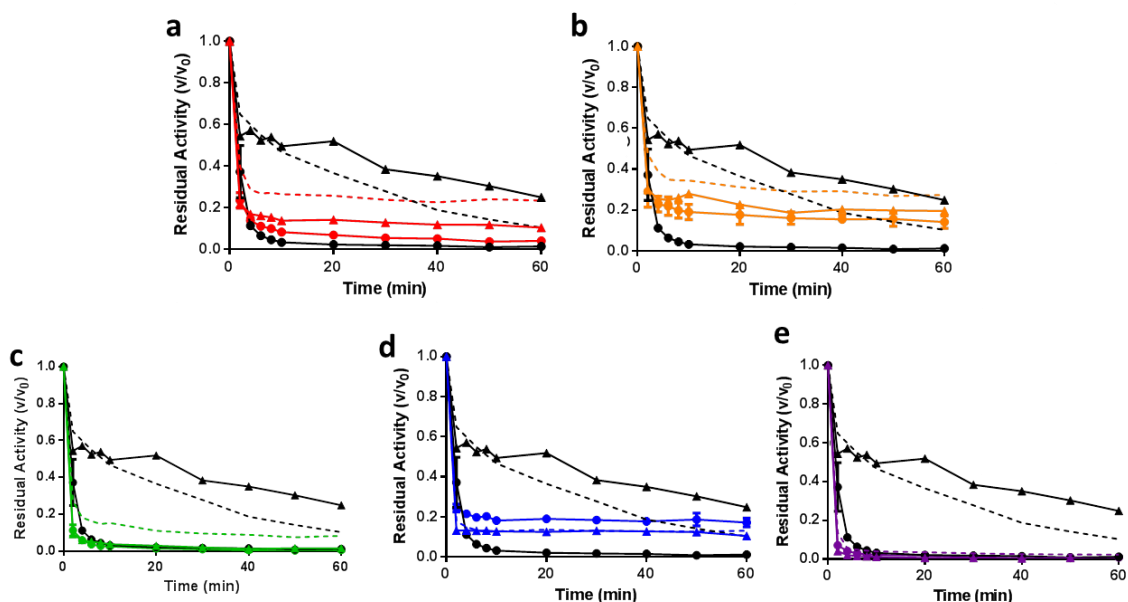
**Figure 2.14.** Residual activity measurements for stability of short length CT-conjugates at pH 1 while independently doping in 1.0 M NaCl or 10 v/v% dimethyl sulfoxide (DMSO) to disrupt electrostatic and hydrophobic interactions, respectively. In all plots a-e, native CT (dashed black line), native CT with NaCl (black circles), and native CT with DMSO (black triangles). a, CT-pCBMA (±) (red). b, CT-pOEGMA (0) (orange). c, CT-pQA (+) (green). d, CT-pSMA (-) (blue). e, CT-pDMAEMA (+/0) (purple). In all plots, stability of conjugates without NaCl or DMSO (colored dashed lines), conjugates with NaCl (colored circles), and conjugates with DMSO (colored triangles). The addition of NaCl and DMSO did not increase stability indicating an alternative mechanism for conjugate stabilization. Error bars represent standard error of the mean from triplicate measurements.
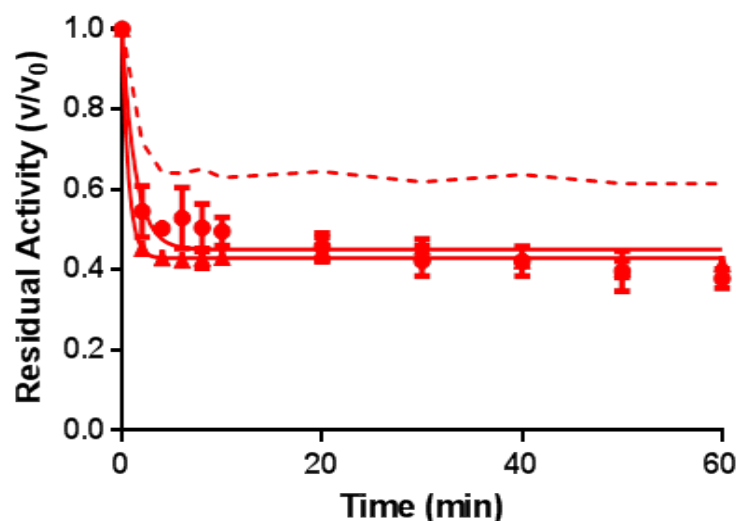
**Figure 2.15.** Residual activity measurements for stability of long length CT-pCBMA 112 at pH 1 while independently doping in 1.0 M NaCl or 10 v/v% dimethyl sulfoxide (DMSO) to disrupt electrostatic and hydrophobic interactions, respectively. NaCl and DMSO were also added in the refolding buffer (pH 8, sodium phosphate). CT-pCBMA 112 at pH 1 (red dashed line), CT-pCBMA 112 incubated with 1.0 M NaCl and refolded in buffer with 1.0 M NaCl (red circles), and CT-pCBMA 112 incubated with 10 v/v% DMSO and refolded in buffer with 10 v/v% DMSO (red triangles). Error bars represent standard error of the mean from triplicate measurements.

Upon reflecting further on the unique shape of the residual activity profiles for the conjugates compared to native CT, and the elimination of electrostatic and hydrophobic polymer-surface interactions as the driver of the observed behavior, we decided to explore the changes in the structure of chymotrypsin upon exposure to acid and subsequent refolding at neutral pH. Changes in enzyme tertiary structure can be measured by following tryptophan fluorescence (FL). We measured tryptophan fluorescence over 40 minutes incubation at pH 1 and then also after the conjugates had been diluted back into pH 8 buffer (similar to residual activity measurements) (**Table 2.4**). We observed that the conjugates that were able to maintain the most activity after incubation at pH 1, also had the lowest percent change in refolding FL

62

after 40 minutes, implying that these conjugates were able to either maintain or refold back to their native form most effectively. This was the case for longer chain CT-pCBMA and CT-pQA conjugates. Similarly, changes in FL for CT-pOEGMA and CT-pDMAEMA followed similar trends to changes in their residual activity after exposure to acid.

**Table 2.4.** Tryptophan fluorescence (FL) intensity (em.350 nm/em.330 nm) percent change from 40 minutes at pH 1 to its time 0 (pH 8) indicating ability to refold for all conjugates. Blue represents short length conjugates, red represents medium length conjugates, and green represents long length conjugates. Long, hydrophilic polymers, pCBMA and pQA, stabilized conjugates the most at pH 1 and were able to refold the greatest (corresponding to the lowest FL % change). Error bars represent standard error of the mean from triplicate measurements.

| *pH 1:* FL Intensity % Change at t=40 min | | | | | | |
|---|---|---|---|---|---|---|
| **CT** | **CT-Br** | **CT-pCBMA** | **CT-pOEGMA** | **CT-pDMAEMA** | **CT-pQA** | **CT-pSMA** |
| 22 ± 13 | 24 ± 5 | 21 ± 3 | 16 ± 6 | 40 ± 5 | 28 ± 3 | 29 ± 11 |
| | | 31 ± 5 | 11 ± 4 | 26 ± 13 | 31 ± 4 | 2 ± 5 |
| | | 8 ± 4 | 12 ± 3 | 20 ± 9 | 12 ± 3 | 9 ± 12 |

In order to further investigate conjugate dynamics, FL was also monitored kinetically during incubation at pH 1 over 40 minutes (**Figure 2.16**). The shapes of the curves highly mimicked the residual activity curves, where there were immediate increases in FL indicating unfolding, followed by relatively stable intensities. This data confirmed that polymers enabled conjugates to reversibly unfold and refold. It was also interesting to observe that, opposite of residual activity measurements, there was no length dependence for changes in FL of CT-pCBMA and CT-pQA. Only CT-pSMA had a unique FL profile in that the conjugate was unfolded even at time zero. In acid, the negatively charged polymer will start to become more neutral as it approaches its expected $pK_a$ (~1.0). Since we already knew that removal of surface

positive charge, as in CT-Br, significantly impairs stability, the results with CT-pSMA were not surprising.
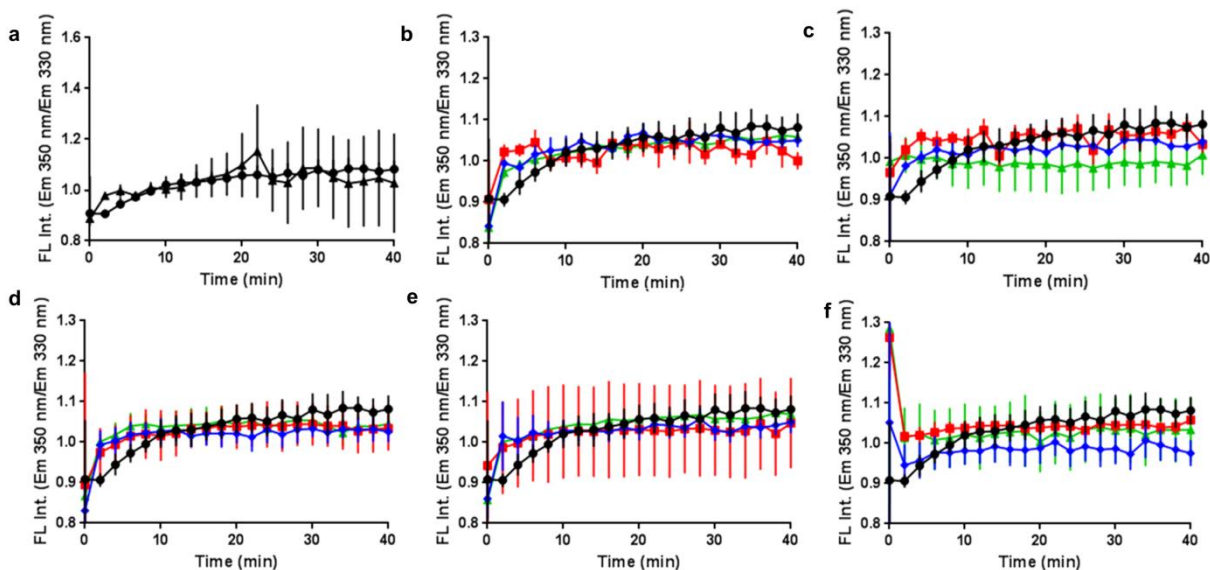


**Figure 2.16.** Tryptophan FL kinetics for a, native CT (black circles) and CT-Br (black triangles). b, CT-pCBMA (±). c, CT-pOEGMA (0). d, CT-pDMAEMA (+/0). e, CT-pQA (+). f, CT-pSMA (-). Native CT (black circles), short length conjugates (blue diamonds), medium length conjugates (red squares), and long length conjugates (green triangles). All conjugates unfold to relatively the same degree independent of length or charge and all unfolding occurs within the first 5 minutes. The ability to reversibly refold depends on polymer hydrophobicity and length. Long, hydrophilic polymers, pCBMA (±) and pQA (+), increase refolding rates by minimizing interactions with the exposed protein core. Error bars represent the standard error of the mean from triplicate measurements.

The irreversible inactivation kinetics for native CT at pH 1 were fit to a classic two step inactivation profile using GraphPad, consistent with the proposed mechanism in **Figure 2.13a**, in which a rapid unfolding to a partially active state ($k_{fast}$, min$^{-1}$) was followed by a slow complete unfolding ($k_{slow}$, min$^{-1}$) as modeled by equation (**2.1**),

$$Y(t) = Ae^{-k_{fast}t} + Be^{-k_{slow}t} + Plateau \quad (\textbf{equation 2.1})$$

where *Y(t)* is the normalized residual activity at time, *t* (min), *A* is *Y(0)-Y(infinity)* accounted for by the fast component, *B* is *Y(0)-Y(infinity)* accounted for by the slow component, $k_{fast}$ is the fast rate constant (min$^{-1}$), $k_{slow}$ is the slow rate constant (min$^{-1}$), and *Plateau* is the *Y* value at infinite time. The first step has been shown to be reversible, whereas the second step yields a protein structure that cannot refold. As shown in **Figure 2.13a**, $k_{fast}$ is associated with the reversible first step in the unfolding pathway from the folded to intermediate state while $k_{slow}$ is associated with the second step in the pathway leading to complete unfolding. The inactivation kinetics of CT-Br at pH 1 were so rapid that $k_{slow}$ became negligible and the observed rate was exclusively $k_{fast}$. This was also the case for all of the conjugates, but unlike CT-Br, activity was not completely eliminated over time. Taking into account all of the FL, activity, and stability data at pH 1, we believe that under acidic conditions, the conjugated enzymes unfold and the polymers then stabilize the partially unfolded state and prevent further irreversible inactivation (**Figure 2.13b**). The FL kinetics showed that all lengths of CT-pCBMA and CT-pQA unfolded to similar degrees, but the refolding FL and stability data showed that the longest conjugates were able to refold most effectively from an activity standpoint. Thus, it appeared that longer hydrophilic polymers (CT-pCBMA and CT-pQA) assisted in the refolding of the partially unfolded form of the protein. Previous reports on conjugate stability, including our own, focused on the interactions between the active protein surface and the attached polymer (or polymers attached to adjacent molecules). We were also interested in whether polymer on one protein molecule might stabilize another protein. We therefore mixed equal parts native CT and long CT-pCBMA, the most stabilizing conjugate, and performed residual activity measurements at pH 1. CT-pCBMA was not able to stabilize native CT in solution showing that the stabilizing effects of polymers on proteins were intramolecular effects versus intermolecular effects (**Figure 2.17**).
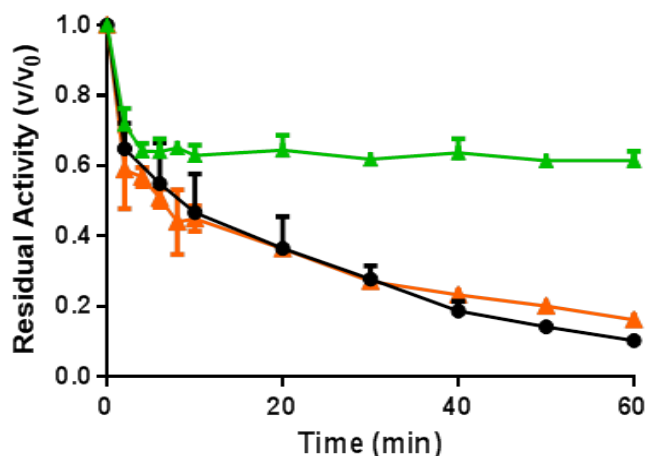
**Figure 2.17.** Residual activity measurements for stability of native CT (black circles), CT-pCBMA 112 (green triangles), and an equal mixture of native CT plus CT-pCBMA 112 (orange triangles). Stabilization is not due to intermolecular interactions between a conjugate and native protein. Error bars represent standard error of the mean from triplicate measurements.

Interestingly, Langevin dynamics simulations have shown that, in the presence of unbound polymer, the kinetics of protein folding follow a two-step mechanism that varies with polymer hydrophobicity.[138] In another study, Monte Carlo simulations investigated tethered polymers on a surface around a binding site and found that longer polymers forced each other into an upright position due to mutual crowding, similar to the formation of polymer brushes.[139] The length of the polymers also had a non-monotonic effect on the brush and depended on grafting density. Our data implied that the conjugates reversibly unfolded to intermediate states, but did not proceed to fully denatured states, where secondary and tertiary structure were lost, in acid. Thus, the polymers stabilized the intermediate form and assisted in the refolding step, which was kinetically dependent on polymer hydrophobicity. More hydrophobic/amphiphilic polymers (pOEGMA and pDMAEMA) would have favorably bound to the aromatic, hydrophobic residues in the protein core once they were exposed. This helped stabilize the partially-unfolded low-activity intermediate form of the protein, but hindered the protein from

66

refolding back to its native conformation. Conversely, more hydrophilic polymers (pCBMA and pQA) both stabilized the intermediate form and promoted more efficient refolding since there was less interaction between the hydrophilic polymer and hydrophobic protein core. Also, the potential degree of interaction decreased as chain length increased past a critical length where the polymers were able to form intramolecular polymer-polymer interactions rather than polymer-protein interactions. This would also be highly dependent on grafting density as well as polymer length. This effect was more prominent for hydrophilic polymers since amphiphilic polymers (pOEGMA and pDMAEMA) would be favorably bound to exposed aromatic residues even at the longest length, which explained why there was no length dependence in the residual activity experiments for these conjugates.

### 2.4.6   Base-induced inactivation

We next sought to determine if irreversible inactivation of CT and CT-Br by base would be the result of rapid unfolding to an unrecoverable structure (as for lectin and barstar), or whether it would mimic more closely the effect of acid on the protein. First, we followed tryptophan fluorescence of the proteins over 40 minutes of exposure to base (pH 12, 10 mM sodium hydroxide). We noticed that the mechanisms for unfolding of native CT and CT-Br were similar at pH 1 and 12, and also observed that once again, changing the surface charge caused an increase in the rate of unfolding (**Figure 2.18**). The unfolding of CT and CT-Br steadily increased over the entire 40 minute timespan. Next, we performed residual activity measurements after refolding at neutral pH to verify that the inactivation profiles were similar for CT and CT-Br at pH 1 and 12 (**Figure 2.19a**). Both CT and CT-Br had detectable $k_{fast}$ and $k_{slow}$ rate constants (**Table 2.5**). The inactivation rates were decreased at pH 12 in comparison to pH 1, especially for CT-Br, alluding to the possibility that surface charge was not the sole

67

contributor in the unfolding process. If either the integrity of the protein core was disrupted or hydrogen bonds were breaking apart, then the covalent attachment of polymer would not be expected to stabilize partially unfolded intermediates at pH 12. Considering all the data, we hypothesized that the rate of partial unfolding would be similar at pH 1 and 12, whereas deprotonation of now exposed tyrosine residues at pH 12 would alter the hydrophobicity of the core preventing correct hydrophobic collapse back to native conformations further causing complete unfolding. We therefore measured protein folding directly using FL at pH 12. The FL kinetic data demonstrated that the conjugates continued to unfold at pH 12 and were not stabilized in a partially unfolded form (**Figure 2.18b-f**).
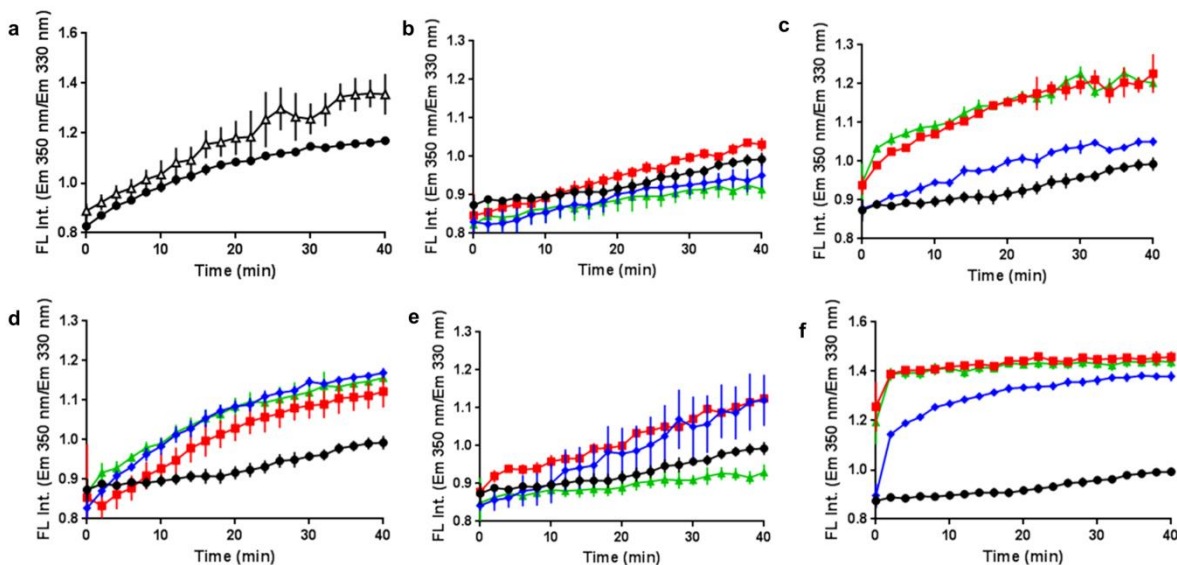


**Figure 2.18.** Conjugate base stabilities at pH 12 (10 mM NaOH) in comparison to native CT (black circles in all plots) and CT-Br in terms of tryptophan fluorescence (FL) intensity over time. Tryptophan FL kinetics for a, native CT (black circles) and CT-Br (black open triangles). b, CT-pCBMA ($\pm$). c, CT-pOEGMA (0). d, CT-pDMAEMA (+/0). e, CT-pQA (+). f, CT-pSMA (-). Native CT (black circles), short length conjugates (blue diamonds), medium length conjugates (red squares), and long length conjugates (green triangles). All conjugates unfold slowly over time independent of polymer type. Conjugated polymers do not stabilize partially unfolded states and irreversible denaturation proceeds, most likely do due deprotonation of exposed tyrosine residues ($pK_a$=10.5) and eventual loss of secondary structure. Error bars represent the standard error of the mean from triplicate measurements.

We next measured residual activity over 60 minutes. Conjugates were incubated at pH 12 and diluted back into pH 8 buffer at specified time points to measure activity (**Figure 2.19b-f**). We also measured the refolding FL at 40 minutes from pH 12 to 8 (**Table 2.6**). As expected, the inactivation profiles were strikingly different than conjugates at pH 1, but were similar to native CT. Whereas the addition of polymers were able to regain the stability lost after initiator modification at pH 1, stability was not regained upon conjugating polymer at pH 12 supporting the mechanistic hypothesis in **Figure 2.12**. We also observed that none of the conjugates were able to refold effectively resulting in a large percent change from the refolding FL intensity at time 0 versus 40 minutes.
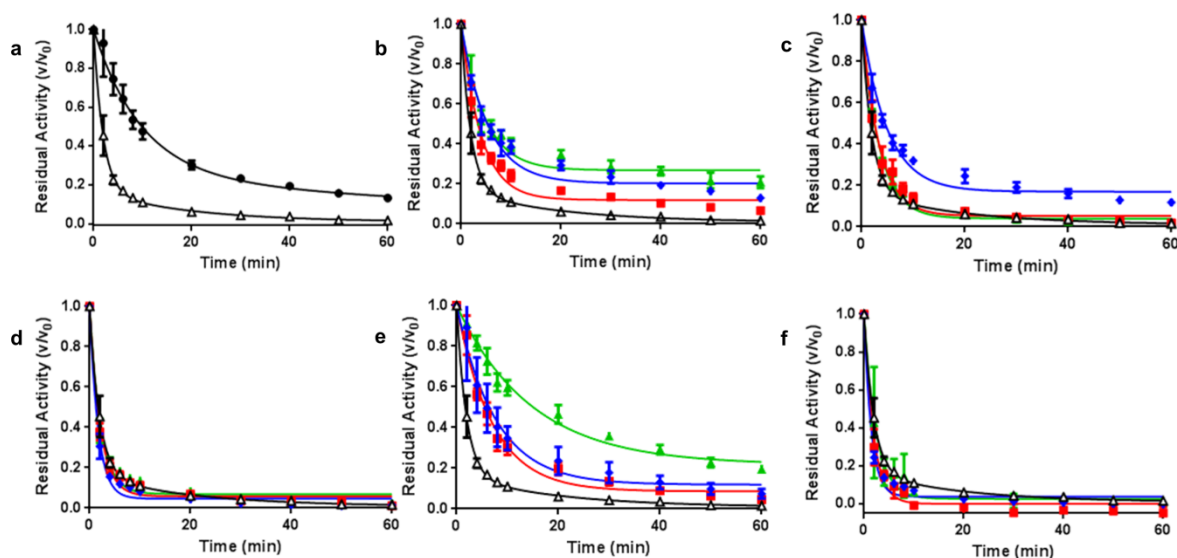


**Figure 2.19.** Conjugate residual activity over 60 minutes in comparison to native CT (black circles) and CT-Br (black open triangles) in all plots. Residual activity for a, native CT (black circles) and CT-Br (black open triangles). b, CT-pCBMA (±). c, CT-pOEGMA (0). d, CT-pDMAEMA (+/0). e, CT-pQA (+). f, CT-pSMA (-). Short length conjugates (blue diamonds), medium length conjugates (red squares), and long length conjugates (green triangles). Error bars represent standard error of the mean from triplicate measurements.

**Table 2.5.** Kinetic rates of residual activity measurements for conjugates at pH 1 and pH 12. Rates were calculated using non-linear fitting in GraphPad. Error bars are standard error of the mean from triplicate measurements.

| | pH 1 | | | pH 12 | |
|---|---|---|---|---|---|
| | $k_{fast}$ (min$^{-1}$) | $k_{slow}$ (min$^{-1}$) | Plateau Value | $k_{fast}$ (min$^{-1}$) | $k_{slow}$ (min$^{-1}$) |
| **Native CT** | 1.128 ± 0.666 | 0.030 ± 0.005 | - | 0.103 ± 0.046 | 0.0101 ± 0.178 |
| **CT-Br** | 1.689 ± 0.049 | - | - | 0.521 ± 0.049 | 0.051 ± 0.034 |
| **CT-pCBMA 10** | 0.804 ± 0.043 | - | 0.248 ± 0.005 | 0.368 ± 0.055 | 0.023 ± 0.015 |
| **CT-pCBMA 46** | 0.999 ± 0.038 | - | 0.051 ± 0.003 | 0.407 ± 0.047 | 0.038 ± 0.019 |
| **CT-pCBMA 112** | 0.726 ± 0.089 | - | 0.630 ± 0.006 | 0.386 ± 0.077 | 0.020 ± 0.023 |
| **CT-pOEGMA 9** | 0.647 ± 0.045 | - | 0.308 ± 0.007 | 0.358 ± 0.045 | 0.034 ± 0.016 |
| **CT-pOEGMA 53** | 3.044 ± 4.554 | - | 0.358 ± 0.004 | 0.528 ± 0.120 | 0.093 ± 0.044 |
| **CT-pOEGMA 97** | 2.704 ± 2.076 | - | 0.249 ± 0.004 | 0.399 ± 0.024 | 0.063 ± 0.020 |
| **CT-pQA 10** | 0.814 ± 0.055 | - | 0.115 ± 0.007 | 0.167 ± 0.149 | 0.020 ± 0.193 |
| **CT-pQA 43** | 0.985 ± 0.046 | - | 0.074 ± 0.004 | 0.179 ± 0.057 | 0.025 ± 0.081 |
| **CT-pQA 89** | 1.055 ± 0.130 | - | 0.493 ± 0.005 | 0.138 ± 0.035 | 0.019 ± 0.006 |
| **CT-pDMAEMA 9** | 1.113 ± 0.036 | - | 0.034 ± 0.002 | 0.836 ± 0.061 | 0.078 ± 0.024 |
| **CT-pDMAEMA 46** | 1.037 ± 0.094 | - | 0.165 ± 0.007 | 0.697 ± 0.045 | 0.065 ± 0.018 |
| **CT-pDMAEMA 89** | 1.171 ± 0.050 | - | 0.063 ± 0.003 | 0.748 ± 0.052 | 0.064 ± 0.015 |
| **CT-pSMA 14** | 1.447 ± 0.059 | - | 0.132 ± 0.002 | 1.109 ± 0.074 | 0.095 ± 0.016 |
| **CT-pSMA 48** | 5.037 ± 270 | - | 0.180 ± 0.006 | 1.813 ± 4.631 | 0.305 ± 0.138 |
| **CT-pSMA 113** | 1.933 ± 0.453 | - | 0.295 ± 0.004 | 0.609 ± 0.246 | 0.087 ± 0.136 |

**Table 2.6.** Tryptophan fluorescence (FL) intensity (em.350 nm/em.330 nm) percent change from 40 minutes at pH 12 to its time 0 (pH 8) indicating ability to refold for all conjugates. Blue represents short length conjugates, red represents medium length conjugates, and green represents long length conjugates. Conjugated polymers did not stabilize CT for any charge or chain length. All conjugates followed a two-phase decay similar to native CT. Error bars represent the standard error of the mean from triplicate measurements.

| pH 12: FL Intensity % Change at t=40 min | | | | | | |
|---|---|---|---|---|---|---|
| CT | CT-Br | CT-pCBMA | CT-pOEGMA | CT-pDMAEMA | CT-pQA | CT-pSMA |
| 50 ± 5 | 42 ± 8 | 32 ± 4 | 30 ± 6 | 42 ± 4 | 44 ± 9 | 46 ± 4 |
| | | 43 ± 5 | 30 ± 6 | 36 ± 11 | 41 ± 5 | 12 ± 9 |
| | | 21 ± 7 | 26 ± 3 | 32 ± 10 | 22 ± 3 | 14 ± 3 |

## 2.5 Conclusions

In this Chapter, polymer-based protein engineering has allowed us to generate a family of related bioconjugates that were used to explore the importance of intramolecular interactions by altering the physicochemical properties of the attached polymers. Structure-function-dynamic relationships were predicted using MD simulations and were in high agreement with experimental activity data. The data revealed that intrinsic activity was reduced by polymer conjugation, but that only polymer charge (versus length) appeared to influence substrate affinity. We were able to broaden the functional pH of the enzyme in more acidic conditions by increasing the number of positive charges on the protein surface. Additionally, we were able to stabilize proteins against acid by engineering the polymer hydrophobicity and length to propose a folding/unfolding mechanism for protein-polymer conjugates.

A protein's function is inherently linked to its dynamic three-dimensional structure. Unstable proteins misfold to lower-energy states with altered conformations, lose their inherent function, and for proteins inside the body, this leads to various disease states including Alzheimer's and Parkinson's. To combat incorrect protein folding, the body employs molecular chaperones to stabilize non-native conformations and assist in correct folding. In this work, we showed how covalently attached synthetic polymers were able to modulate the folding of a protein, emulating molecular chaperones. While native protein folding has been studied for hundreds of years, the field of protein-polymer conjugates is still relatively young. We are just beginning to understand structure-function-dynamic relationships of protein-polymer conjugates, both experimentally and theoretically. As more of these types of fundamental studies are

performed with a scope of different protein-polymer variants, there will be a rapid increase in the pace that we learn about these complex hybrid systems.

# Chapter 3.  A Charge-Preserving ATRP Initiator Rescues the Lost Function of Negatively Charged Protein-Polymer Conjugates

## 3.1  Chapter Summary

When grown from the surface of proteins, negatively charged polymers cause irreversible inactivation, thereby limiting the breadth of the synthetic space that negatively charged protein-polymer conjugates can be applied to.  More broadly speaking, independent of polymer and synthetic approach, almost all protein-polymer conjugates are less active than their precursors. After more than a decade without major advances in understanding why the attachment of some polymers so sharply deactivates enzymes, we focused our attention on a technique to protect enzymes from the growth of a deactivating polymer by restoring the charge at the protein surface during polymer attachment. We synthesized an amino-reactive positively-charged ATRP initiator that inserted a permanent positive charge at the site of bio-macroinitiator attachment. Maintaining surface charge through attachment of the permanent positively charged initiator led to the first observation of activity of enzymes that were coupled to negatively charged homopolymers.

## 3.2 Introduction

The delicate balance of forces that maintain the structure, function, and dynamics of enzymes is at the heart of their remarkable activity and bothersome instability.[140] Although some enzymes have evolved to survive in extreme environments[141], protein engineers that desire to stabilize proteins for therapeutic or industrial uses have generally used molecular biology to dramatically improve function.[142–144] Another compelling approach to protein/enzyme stabilization has been to covalently attach polymers to the protein surface.[2,49,97,101] Polymers can either be covalently coupled to the surface of proteins (commonly referred to as PEGylation; PEG=poly(ethylene glycol)) or grown from the surface of proteins using controlled radical polymerization from protein-initiator constructs, also known as bio-macroinitiators.[14,47,74,90,91,145–150] ATRP has been used to grow dense polymer coatings that "nano-armor" proteins.[21,104] A wide variety of polymers, over a range of molecular masses and densities, have been conjugated with proteins to determine their impact on function, including random copolymers[60], block copolymers[54,88,98], thermoresponsive[47,146,151] or pH responsive polymers[53], branched polymers[152], and charged polymers.[48,49,64] Unfortunately, however, the full diversity of polymers that can be attached to proteins is inaccessible because some polymers almost instantaneously unfold and inactivate proteins. In particular, the growth of negatively charged polymers from the surface of enzymes is not tolerated by proteins.[153]

Interestingly, even while the conjugation of conventional PEG to a protein increases its stability, it is always at the expense of bioactivity.[7] Protecting proteins from conjugated polymer-induced activity loss is a vexing challenge in the field of next generation protein-polymer conjugate design.[154] Since Jiang's work in 2011, zwitterionic polymers have become increasingly attractive for protein conjugation because they improve stability while preserving some degree of bioactivity.[129] Zwitterionic monomers have a one-to-one ratio of positively and

74

negatively charged groups yielding a net neutral molecule and their polymeric forms were found to be stabilizing for proteins by mimicking stabilizing kosmotropic anions and chaotropic cations as defined by the Hofmeister series.[129,155] Previous studies by our group have shown the stabilizing effect of zwitterionic poly(carboxybetaine methacrylate) (pCBMA) along with high stabilities and activity retention with positively charged polymers, such as poly(quaternary ammonium methacrylate) (pQA).[49,153] These polymers contain stabilizing chaotropic cations, $NR_4^+$, aligning with the findings of Jiang. We also found that at low pH, these polymers could act as powerful intramolecular chaperones to drive protein folding and stabilization.[153] We have also shown, however, that negatively charged polymers, such as poly(sulfonate methacrylate) (pSMA), are destabilizing and deactivating.[148,153] pSMA is a hydrophilic, negatively charged polymer containing kosmotropic sulfonate anions, which are defined as stabilizing by the Hofmeister series. Another study used the SMA monomer, copolymerized with three other monomers of varying hydrophobicities, and found the random heteropolymer to be stabilizing due to statistical monomer distribution.[60] The first publication by our group on grafted-from protein-polymer conjugates used a negatively charged homopolymer, poly(sodium 4-styrenesulfonate) to create conjugates with α-chymotrypsin (CT) that also sharply reduced enzyme activity.[101] To our knowledge, there are no reported protein-negatively charged homopolymer conjugates that maintain enzyme stability or activity. Determining why negatively charged homopolymers are deactivating and destabilizing to proteins may enable us to remediate the problem and then use that knowledge to determine if more general protein conjugate-induced activity loss can be reduced when using compatible polymers.

In order to design a polymer conjugation protective strategy, we have focused our attention on how ATRP initiators are coupled to proteins. Our prior work has always focused on

the properties of next generation protein-polymer conjugates, but in doing that work, we routinely used protein macroinitiator constructs as controls. We have observed that although compatible polymers can stabilize enzymes, their biomacromolecular initiator precursors are often less active and stable than the native protein or the conjugate.[153]  Protein-initiator constructs are most often formed by reacting accessible surface amino groups with activated ester alkyl halides.  These reactions, and almost all common PEGylation coupling chemistries, sacrifice the native electrostatic environment of the protein surface for the supposed benefit of the resulting protein-polymer conjugate (**Figure 3.1 and Table 3.1**).
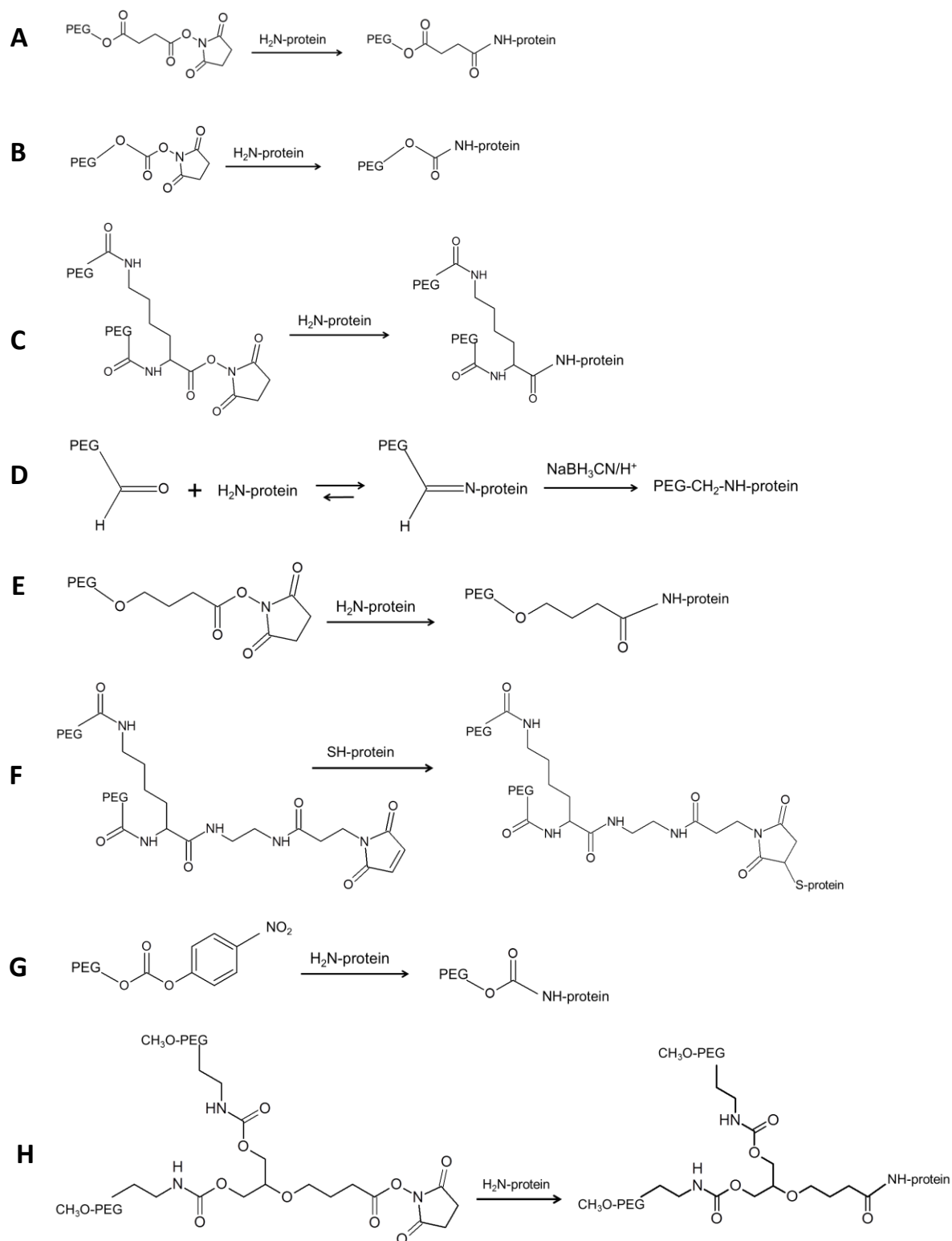
**Figure 3.1.** PEGylation strategies for FDA approved PEGylated therapeutic proteins as of July 2019. Correlate reactions with Supplementary Table 1. [156–165]

**Table 3.1.** PEGylation strategies for FDA approved PEGylated therapeutic proteins as of July 2019. Correlate attachment chemistries with Supplementary Figure 1.[156–165]

| Commercial Name | Company (Approval Year) | Indication | Biologic Type | PEG Type | PEG Size (kDa) | Attachment chemistry (and derivatives) | Positive Charge Maintained? |
|---|---|---|---|---|---|---|---|
| Adagen | Enzon (1990) | Severe combined immunodeficiency disease | Enzyme | Multiple (11-17); Linear | 5 | A | No |
| Oncaspar | Enzon (1994) | Acute lymphoblastic leukemia | Enzyme | Multiple (69-82); Linear | 5 | A | No |
| PEG-INTRON | Schering-Plough (2000) | Hepatitis C | Protein | Single; Linear | 12 | B | No |
| PEGASYS | Roche (2001) | Hepatitis B & C | Protein | Single; Branched | 40 | C | No |
| Neulasta | Amgen (2002) | Neutropenia | Protein | Single; Linear | 20 | D | Yes |
| Somavert | Pfizer (2003) | Acromegaly | Protein | Multiple (4-6); Linear | 5 | A | No |
| Mircera | Roche (2007) | Anemia associated with chronic renal failure | Protein | Single; Linear | 30 | E | No |
| Cimzia | UCB (2008) | Crohn's Disease, rheumatoid arthritis, ankylosing spondylitis, psoriatic arthritis | FAB' fragment | Single; Branched | 40 | F | N/A (thiol reactive) |
| Krystexxa | Savient (2010) | Gout | Enzyme | Multiple (9-11 per monomer); Linear | 10 | G | No |
| Sylatron | Merck (2011) | Melanoma | Protein | Single; Linear | 12 | B | No |
| Plegridy | Biogen (2014) | Multiple Sclerosis | Protein | Single; Linear | 20 | D | Yes |
| Adynovate | Baxalta (2015) | Hemophilia A | Protein | Multiple (2); Branched | 20 | H | No |
| Rebinyn | Novo Nordisk (2017) | Hemophilia B | Enzyme | Single | 40 | Proprietary Enzymatic Ligation (Asn modified) | N/A |
| Palynziq | BioMarin (2018) | Phenylketonuria | Enzyme | Multiple (9); Linear | 20 | E (Nektar's mPEG-SPA) | No |
| Jivi | Bayer (2019) | Hemophilia A | Protein | Single; Branched | 60 | F | N/A (thiol reactive) |

The prevailing view of protein scientists has been that maintaining protein surface charge-charge interactions is less important to protein stability than maintaining the integrity of the hydrophobic core. Indeed, hydrophobic interactions within a protein contribute hundreds of kJ mol$^{-1}$ to maintaining a folded conformation, whereas exposed surface charge-charge interactions only contribute a few kJ mol$^{-1}$.[166–169] Surprisingly, however, rationally optimizing charge-charge interactions can be an effective tool when designing proteins with increased stability.[131,170–175] These charge-charge interactions can either be optimized by increasing

favorable electrostatic interactions or by decreasing the number of unfavorable electrostatic interactions.[176] It has also been observed that long-range electrostatic interactions are just as important as short-range salt bridge interactions.[175] Conversely, others have questioned whether charge-charge interactions are important influencers of stability.[177] Commercially, of the 14 FDA-approved therapeutic protein-polymer conjugates, Neulasta and Plegridy are the only two examples where the nitrogen is still positively charged after PEG attachment by utilizing aldehyde attachment chemistries that result in secondary amines. Two natural questions arise: could we protect an enzyme from the growth of an incompatible polymer by initiating the reaction from a charge-maintaining initiator? And, if so, could that same strategy be used to further enhance the activity and stability of compatible polymer-protein conjugates?

Modeled after successfully commercialized PEGylation reagents, alkyl halide ATRP-initiators usually possess *N*-hydroxysuccinimide (NHS) groups that react with protein primary amines, including the N-terminal and lysine residues. We have developed algorithms that can predict the site of reaction on the protein surface as well as the initiation reaction rates at each amino group.[34] The amino group on the N-terminus has a $pK_a$ in the range of 7.8-8.0 while the $pK_a$'s of lysine side chain amino groups range from approximately 10.5-12.0, depending on their local environment.[178] Therefore, at biologically relevant pH values (6-8), all accessible amino groups will be positively charged almost all of the time (>95%). These positive charges are unfortunately lost when neutral initiators are used to launch protein-ATRP as the nitrogens are converted to amide bonds.[179,180]

We hypothesized that a positively charged ATRP-initiator would restore the positive charges on an enzyme surface, thereby enhancing activity and stability of the enzyme-initiator constructs and the protein-polymer conjugates derived from it. We describe the synthesis of the

first positively charged amine-reactive ATRP-initiator. We used this initiator to study the growth of an incompatible polymer (pSMA) from the surfaces of α-chymotrypsin (CT), uricase, acetylcholinesterase, lysozyme, and avidin. We now understand that the charge of an ATRP-initiator is a crucial parameter to consider in the design of highly active and stable protein-polymer conjugate variants and that negatively charged polymers can now lead to conjugates with high activities and stabilities.

## 3.3    Materials and Methods

α-chymotrypsin (CT) from bovine pancreas (type II), acetylcholinesterase (AChE) from *Electrophorus electricus* (electric eel, type VI-S), uricase from Candida sp., lysozyme from chicken egg white, biotin, and HABA 4'-hydroxyazobenzene-2-carboxylic acid were purchased from Sigma Aldrich (St. Louis, MO). Avidin from egg white was purchased from Lee Biosolutions (Maryland Heights, MO). CT, lysozyme, and avidin were used as received. AChE and uricase were dialyzed in 25 mM sodium phosphate (pH 7.0) using a 25 kDa molecular mass cutoff dialysis tube in a refrigerator for 24 h and were then lyophilized. Copper (II) chloride, sodium ascorbate, 1,1,4,7,10,10-hexamethyltriethylenetetramine (HMTETA), 2-bromo-2-methylpropionyl bromide, 3-(dimethylamino)-1-propylamine, *N,N'*-diisopropylcarbodimine, fluorescamine, acetylthiocholine iodide, and 5,5'-dithiobis(2-nitrobenzoic acid) (DTNB) were purchased from Sigma Aldrich. 4-bromobutyric acid and *N*-hydroxysuccinimide were purchased from TCI USA (Portland, OR). Micro BCA assay kit was purchased from Thermo Fisher Scientific.

### 3.3.1    Instrumentation and Sample Analysis Preparations

$^{1}$H and $^{13}$C NMR were recorded on a spectrometer (500 MHz, 125 MHz, Bruker Avance$^{TM}$ 500) in the NMR facility located in the Center for Molecular Analysis, Carnegie

Mellon University, Pittsburgh, PA, with deuterium oxide ($D_2O$) and DMSO-$d_6$. Routine FT-IR spectra were obtained with a Nicolet Avatar 560 FT-IR spectrometer (Thermo) in the Department of Chemical Engineering at Carnegie Mellon University. Ultraviolet-visible (UV−VIS) spectra were obtained and used for enzyme activity determination using an UV−VIS spectrometer (Lambda 45, PerkinElmer) with a temperature-controlled cell holder. Melting points (mp) were measured with a Laboratory Devices Mel-Temp. Number and weight average molecular masses ($M_n$ and $M_w$) and the polydispersity index ($M_w/M_n$) were estimated by gel permeation chromatography (GPC) on a Water 2695 Series with a data processor, equipped with three columns (Waters Ultrahydrogel Linier, 500 and 250), using Dulbecco's Phosphate Buffered Saline with 0.02 wt% sodium azide for pCBMA and 80 vol% of 100 mM sodium phosphate (pH 9.0) and 20 vol% of acetonitrile for pSMA as an eluent at flow rate of 1.0 mL/min, with detection by a refractive index (RI) detector. Pullulan standards (PSS-Polymer Standards Service − USA Inc, Amherst, MA) were used for calibration. Matrix-Assisted Laser Desorption Ionization Time-of-Flight Spectrometry (MALDI-ToF MS) was performed with a Perseptive Biosystems Voyager Elite MALDI-ToF spectrometer in the Center for Molecular Analysis, Carnegie Mellon University. Dynamic Light Scattering (DLS) data were collected on a Malvern Zetasizer nano-ZS, which was located in the Department of Chemistry, Carnegie Mellon University. The concentration of the sample solution was kept at 0.2 - 1.0 mg/mL. The hydrodynamic diameters of samples were measured three times (15 runs for each measurement).

### 3.3.2 Positive initiator synthesis and characterization

***4-bromobutyryl-N-oxysuccinimide ester synthesis:*** *N,N'*-diisopropylcarbodimine (8.5 mL, 55 mmol) was slowly added to the solution of 4-bromobutyric acid (8.4 g, 50 mmol) and *N*-

hydroxysuccinimide (4.3 g, 55 mmol) in dichloromethane (100 mL) at 0 °C, and then the mixture was stirred at room temperature overnight. Precipitated urea was filtered out and the filtrate was evaporated to remove the solvent. 4-bromobutyryl-*N*-oxysuccinimine ester was isolated by recrystallization in 2-propanol; yield 10.2 g (77 %), mp 49 – 52 °C. $^1$H NMR (500 MHz, DMSO-$d_6$) δ 2.16 (m, 2 H, C=OCH$_2$C*H*$_2$CH$_2$Br), 2.81 (s, 4 H, succinimide), 2.83 (t, 2 H, *J* = 7.0 Hz, C=OC*H*$_2$CH$_2$CH$_2$Br), 3.60 (t, 2 H, *J* = 7.0 Hz, C=OCH$_2$CH$_2$C*H*$_2$Br) ppm; $^{13}$C NMR (125 MHz, DMSO-$d_6$) δ 25.9, 27.9, 29.5, 33.3, 168.7, 170.6 ppm; IR (KBr pellete) 3017, 2948, 2914, 2852, 1812, 1786, 1731, 1382, 1360, 1311, 1202 and 1150 cm$^{-1}$.

*N-(3-N',N'-Dimethylaminopropyl)-2-bromoisobutyramide* *synthesis:* 2-bromo-2-methylpropionyl bromide (3.4 mL, 27 mmol) was slowly added into the solution of 3-(dimethylamino)-1-propylamine (3.1 mL, 24.6 mmol) in deionized water (50 mL) at 0 °C, and then the mixture was stirred at room temperature for 1 h. After the mixture was adjusted to pH 10 with 5 N NaOH aq. at 0 °C, the product was extracted with ethyl acetate (50 mL x 3). The organic phase was washed with 20 wt% potassium carbonate aq. (50 mL × 3) and saturated NaCl aq. (50mL × 2). The organic phase was dried with Na$_2$CO$_3$ and evaporated to remove the solvent. *N-(3-N',N'-Dimethylaminopropyl)-2-bromoisobutyramide* was isolated *in vacuo*. oil compound; yield 5.9 g (95 %), $^1$H NMR (500 MHz, DMSO-$d_6$) δ 1.56 (m, 2 H, (CH$_3$)$_2$NCH$_2$C*H*$_2$CH$_2$NHC=O), 1.84 (s, 6 H, C=OC(C*H*$_3$)$_2$Br), 2.11 (s, 6 H, (C*H*$_3$)$_2$NCH$_2$CH$_2$), 2.22 (t, 2 H, *J* = 7.0 Hz, (CH$_3$)$_2$NC*H*$_2$CH$_2$), 3.12 (td, 2 H, *J* = 5.5 Hz and *J* = 7.0 Hz, CH$_2$C*H*$_2$NHC=O), 8.20 (broad t, 1 H, *J* = 5.5 Hz, amide) ppm; $^{13}$C NMR (125 MHz, DMSO-$d_6$) δ 26.7, 31.6, 38.7, 45.5, 57.4, 61.5, 170.9 ppm; IR (NaCl plate) 3349, 2975, 2946, 2864, 2822, 2800, 1661, 1537, 1465, 1370, 1294, 1263, 1195, 1161 and 1113 cm$^{-1}$.

*Positively charged ATRP initiator synthesis:* *N*-(3-*N'*,*N'*-Dimethylaminopropyl)-2-bromoisobutyramide (1.9 g, 7.5 mmol) and 4-bromobutyryl-*N*-oxysuccinimide ester (2.0 g, 7.5 mmol) were added in dried acetonitrile (50 mL) and bubbled with nitrogen gas for 10 min. The mixture was sealed and stirred at 40 °C overnight. The positively charged ATRP initiator (**1**) was precipitated in a mixture of ethyl acetate and diethyl ether (1:1 volume ratio), and the oil compound was isolated *in vacuo*; yield 3.6 g (93 %) (**Figure 3.2**), $^1$H NMR (500 MHz, *D*$_2$O) δ 1.88 (s, 6 H, C=OC(C*H*$_3$)$_2$Br), 1.91 − 2.24 (m, 4 H, C=OCH$_2$C*H*$_2$CH$_2$N$^+$CH$_2$C*H*$_2$CH$_2$NHC=O), 2.83 − 2.93 (m, 9 H, succinimide and C=OC*H*$_2$CH$_2$CH$_2$N$^+$(C*H*$_3$)), 3.04 − 3.14 (m, 5 H, C=OCH$_2$CH$_2$C*H*$_2$N$^+$(C*H*$_3$) ), 3.28 − 3.41 (m, 4 H, N$^+$C*H*$_2$CH$_2$C*H*$_2$NHC=O) ppm (**Figure 3.3**); $^{13}$C NMR (125 MHz, *D*$_2$O) δ22.1, 24.0, 25.6, 30.6, 36.6, 42.9, 51.1, 55.4, 61.6, 62.1, 169.1, 173.2, 174.9 ppm (**Figure 3.4**); IR (NaCl plate) 3418, 2969, 2708, 1813, 1780, 1734, 1653, 1536, 1472, 1371, 1298, 1210, 1113 and 1074 cm$^{-1}$.
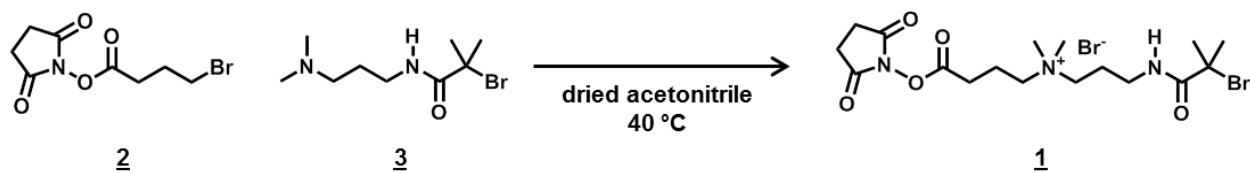


**Figure 3.2.** Positive initiator (1) synthesis.
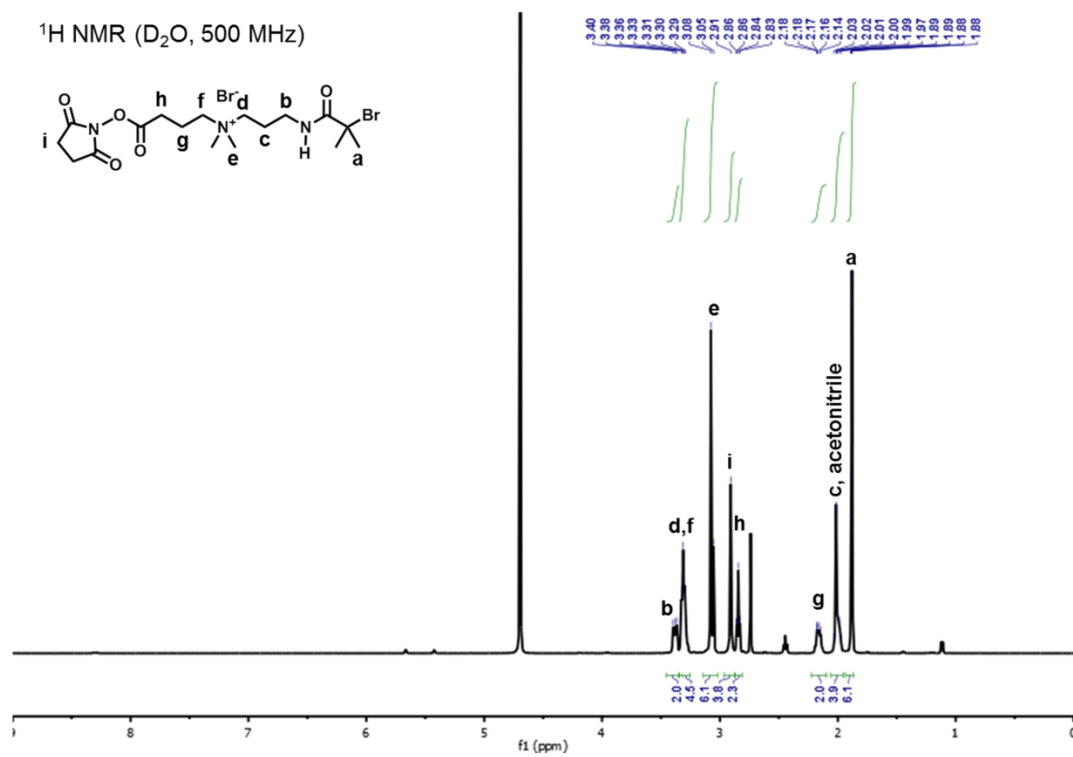
**Figure 3.3.** $^1$H NMR spectra of the positively charged initiator.
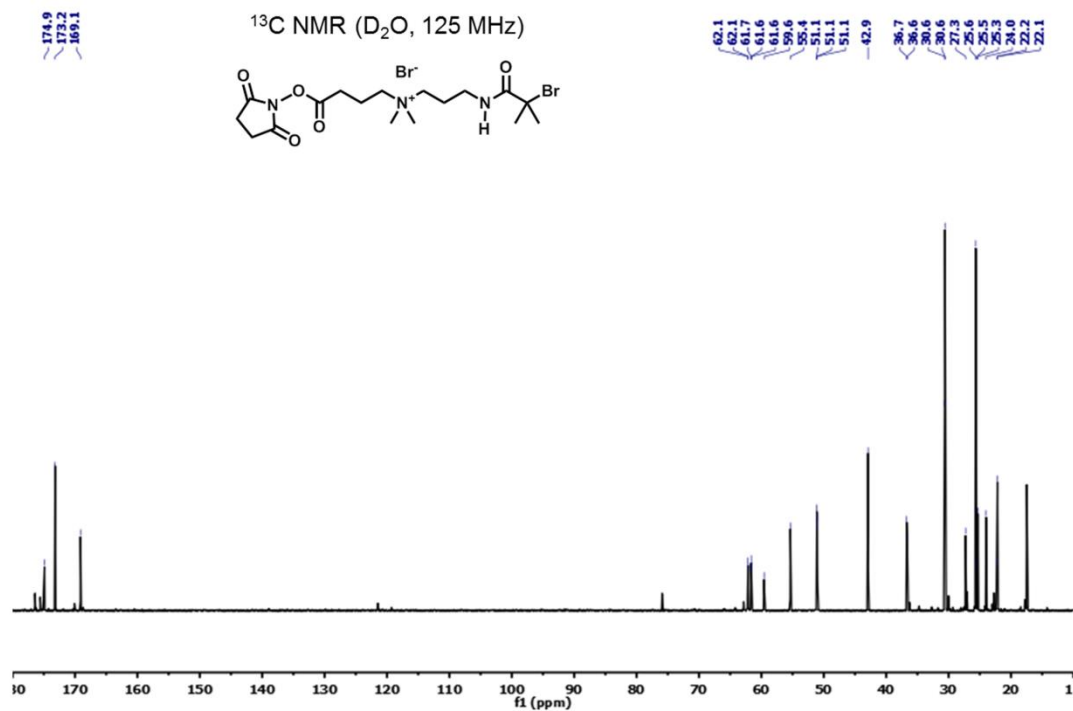
**Figure 3.4.** $^{13}$C NMR spectra of the positively charged initiator.

### 3.3.3 Electrospray ionization mass spectrometry (ESI-MS)

The positive initiator was characterized with ESI-MS using a Finnigan LCQ (Thermo Fisher) quadrupole field ion trap mass spectrometer with an electrospray ionization source (**Figure 3.5**). Each scan was acquired over 150-2000 m/z using a step of 0.5 u, dwell time of 1.5 ms, mass defect of 50 pu, and 80 V orifice potential. The positive initiator was dissolved in methanol at 100 μM and eluted using methanol at a flow rate of 15 μL/min.
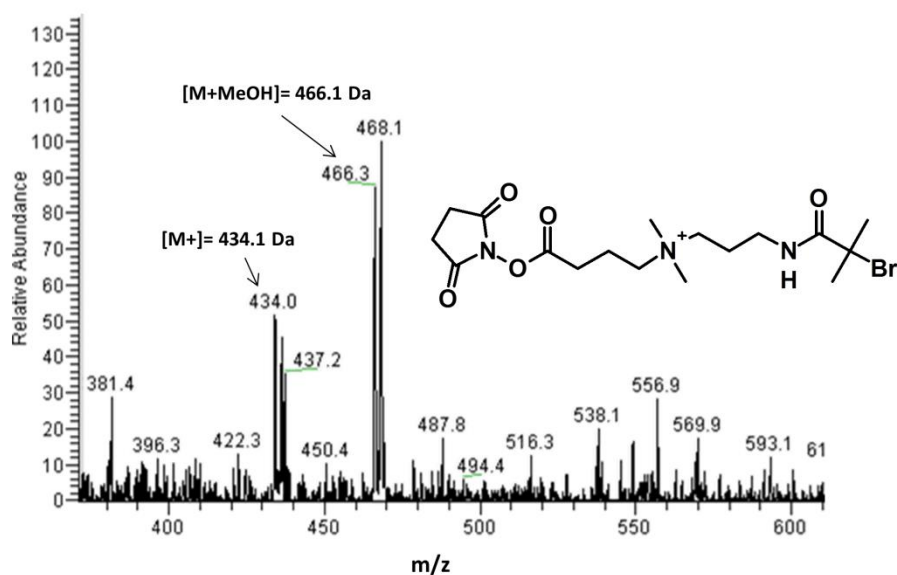
**Figure 3.5.** ESI-MS of the positively charged initiator with labeled peaks.

### 3.3.4 Protein-initiator synthesis and characterization

*Chymotrypsin (CT):* 200 μL of NHS-functionalized ATRP initiator solution in DMSO (168 μmol, 56 mg for neutral and 87 mg for positive initiator, respectively) was added to a CT solution (60 mg in 30 mL of 100 mM sodium phosphate buffer (pH 8.0)) and stirred at 4 °C for 2 h. CT-initiator conjugates were dialyzed in deionized water using a 15 kDa molecular mass cutoff dialysis tube in a refrigerator for 24 h and were then lyophilized.

*Lysozyme:* 200 μL of NHS-functionalized ATRP initiator solution in DMSO (172 μmol, 58 mg for neutral and 89 mg for positive initiator, respectively) was added to a lysozyme solution (70 mg in 30 mL of 100 mM sodium phosphate buffer (pH 8.0)) and stirred at room temperature for 2 h. Lysozyme-initiator conjugates were dialyzed in deionized water using an 8 kDa molecular mass cutoff dialysis tube in a refrigerator for 24 h and were then lyophilized.

86

*Avidin:* Neutral initiator (21 mg, 0.063 mmol) and avidin (20 mg, 0.0013 mmol protein, 0.013 mmol primary amine groups) were dissolved in 4 mL of 0.1 M sodium phosphate buffer (pH 8). The positively charged ATRP initiator (27 mg, 0.063 mmol) was dissolved in 50 µL of DMSO and added to a solution of avidin (20 mg, 0.013 mmol primary amine groups) in 4 mL of 0.1 M sodium phosphate buffer (pH 8). The solutions were stirred at 4°C for 2 h and avidin conjugates were purified by dialysis using 15 kDa molecular mass cutoff dialysis tube, in 25 mM sodium phosphate (pH 8), for 24 h at 4°C and were then lyophilized.

*Uricase:* 200 µL of NHS-functionalized ATRP initiator solution in DMSO (100 µmol, 34 mg for neutral and 52 mg for positive initiator, respectively) was added to a uricase solution (20 mg of uricase in 20 mL of 100 mM sodium phosphate buffer (pH 7.0)) and stirred at room temperature for 2 h. Uricase-initiator conjugates were dialyzed in 25 mM sodium phosphate (pH 7.0) using a 25 kDa molecular mass cutoff dialysis tube in a refrigerator for 24 h and were then lyophilized. The concentration of protein in the uricase-initiator conjugate was determined using a Micro BCA Assay Kit (ThermoFisher Scientific).

*Acetylcholinesterase (AChE):* 100 µL of NHS-functionalized ATRP initiator solution in DMSO (12.7 µmol, 4.3 mg for neutral and 5.5 mg for positive initiator, respectively) was added to an AChE solution (7 mg of AChE in 10 mL of 100 mM sodium phosphate buffer (pH 7.0)) and stirred at room temperature for 2 h. AChE-initiator conjugates were dialyzed in 25 mM sodium phosphate buffer (pH 7.0) using a 25 kDa molecular mass cutoff dialysis tube in a refrigerator for 24 h and were then lyophilized. The concentration of protein in the AChE-initiator conjugate was determined using a Micro BCA Assay Kit.

### 3.3.5 BCA protein assay

The concentration of protein in the solution was determined using a Micro BCA protein Assay Kit (ThermoFisher Scientific). The sample solution (25 µL) and Micro BCA working reagent (75 µL) were incubated at 60 °C for 1 h. After incubation, 900 µL of deionized water was added and the absorbance at 562 nm was recorded by an UV-VIS spectrometer (Lambda 45, Perkin Elmer). The standard curve was obtained using native protein.

### 3.3.6 Fluorescamine assay

A fluorescamine assay was used to determine the number of bound initiators on the protein surface. 40 µL of sample, 100 mM sodium phosphate buffer (40 µL, pH 8), and fluorescamine solution in DMSO (20 µL, 3 mg/mL) were added into a 96-well plate and incubated at room temperature for 15 min. Fluorescence intensities were measured at the excitation of 390 nm and emission of 470 nm with 10-nm bandwidths by a Safire Spike plate reader at the Molecular Biosensor and Imaging Center, Carnegie Mellon University. Initiator concentration was determined using a standard curve using native protein.

### 3.3.7 Trypsin digestion of protein-initiators

Trypsin digestion was performed on protein-initiators to generate peptide fragments to determine modification sites. Peptide fragments were analyzed using matrix-assisted laser desorption/ionization time-of-flight (MALDI-ToF) mass spectrometry. Native CT, CT(N), and CT(+) were digested according to the protocol described in the In-Solution Tryptic Digestion and Guanidination Kit. 20 µg of protein or protein-initiator constructs (10 µL of a 2 mg/mL protein solution in deionized water) were added to 15 µL of 50 mM ammonium bicarbonate with 1.5 µL of 100 mM dithiothreitol (DTT) in an Eppendorf tube. The reaction was incubated for 5 min at

95 °C. 3 µL of 100 mM iodoacetamide aqueous solution was then added and samples were incubated in the dark for 20 minutes at room temperature for thiol alkylation. Next, 1 µL of 100 ng/µL trypsin was added to the tube and the reaction was incubated at 37 °C for 3 hours. Then, an additional 1 µL of 100 ng/µL trypsin was subsequently added. The trypsin digestion was terminated after a total reaction time of 12 hours by the addition of trifluoroacetic acid (TFA). Digested samples were purified using ZipTipC$_{18}$ microtips and eluted with 2 µL of matrix solution (20 mg/mL sinapinic acid in 50 % acetonitrile with 0.1 % TFA) directly onto a MALDI-ToF plate. The molecular masses of the expected peptide fragments before and after digestion were predicted using PeptideCutter on UniProt P00766 (ExPASy Bioinformatics Portal, Swiss Institute of Bioinformatics). CT-initiator digests were compared to native CT digests. Modification at a particular amino group was determined by either the loss of a peak of the CT-initiator in comparison to native CT or by the appearance of a new peak that equaled the mass (or adducts) of the peptide fragment plus the mass of the initiator (neutral initiator: 220 Da, positive initiator: 320 Da). Fragments below the MALDI-ToF lower m/z=500 limit were not able to be detected.

### 3.3.8  MALDI-ToF

Protein solutions (1.0 mg/mL) were mixed with an equal volume of matrix (Sinapinic acid (20 mg/mL) in 50% acetonitrile with 0.4% trifluoroacetic acid) and 2 µL of the resulting mixture was loaded onto a silver sterling plate target. Apomyoglobin, cytochrome C, and aldolase were used as calibration standards. To determine the extent of initiator modification on protein-initiators, the m/z of the native protein was subtracted from the m/z of the protein-initiator. The difference in m/z was then divided by the mass of the initiator (neutral initiator: 220 Da, positive initiator: 320 Da; after attachment) to obtain the number of initiators per protein.

89

When analyzing trypsin digests of protein-initiators, Bradykinin fragment, angiotensin II (human) and insulin oxidized B chain (bovine) were used as calibration standards. MALDI-ToF data was collected on a PerSeptive Voyager STR MS with nitrogen laser (337 nm) and 20 kV accelerating voltage with a grid voltage of 90 %. 300 laser shots covering the complete spot were accumulated for each spectrum.

### 3.3.9   Isoelectric Focusing (IEF) gel

Criterion IEF precast gels (pH 3-10, 12+2 well, polyacrylamide gel, 13.3 x 8.7 cm) from Bio-Rad were used to determine the isoelectric point of proteins and protein-initiators. Protein solutions (concentration depended on sample) were mixed with 50% glycerol using a 1 to 10 ratio of protein sample to 50% glycerol. 30 μL were loaded into each well. The IEF standards were prepared and loaded according to the Bio-Rad instruction manual. The gel was run in a stepwise manner as follows: 100 V for 60 minutes, 250 V for 60 minutes, 500 V for 30 minutes. Gels were silver stained using the Pierce Silver Stain Kit following their instructions.

### 3.3.10  Protein-pCBMA and pSMA conjugate synthesis

A solution of monomer (230 mg for CBMA and 246 mg for SMA, 1.0 mmol respectively) and CT-initiator (23 mg for neutral and 25 mg for positive initiator, 10 μmol of initiator) in 100 mM sodium phosphate (20 mL, pH 7) was sealed and bubbled with nitrogen gas in an ice bath for 30 min. 2 mL of deoxygenated catalyst solution (described previously[45]) was added to the polymerization reactor under bubbling nitrogen. The mixture was sealed and stirred in a refrigerator for 1 h.  The conjugate was isolated by dialysis with a 25 kDa molecular mass cutoff dialysis tube in deionized water or 25 mM sodium phosphate buffer in a refrigerator for 24 h and then lyophilized.  Conjugate CT content was determined by BCA assay as described

previously.[32] Other protein-polymer conjugates were prepared using the same ATRP reactant ratios, but at ~5x lower concentration of all reactants, and analyzed by the same procedure as CT-polymers. Monomer concentrations to target DPs of 100 were used for all conjugates except avidin, which was targeted at 150. Monomer conversions are listed in **Table 3.2**.

**Table 3.2.** Monomer conversions estimated by the achieved degree of polymerization compared to the targeted degree of polymerization. Achieved degrees of polymerization were determined using cleaved polymer $M_n$ values. Lower concentrations of reactants for the additional proteins (besides CT) during ATRP resulted in lower monomer conversions.

|  | **Monomer Conversion** |
|---|---|
| CT(+)-pSMA | 88% |
| CT(N)-pSMA | 81% |
| CT(+)-pCBMA | 100% |
| CT(N)-pCBMA | 79% |
| Lyz(N)-pCBMA | 41% |
| Lyz(+)-pCBMA | 40% |
| Avidin(N)-pCBMA | 81% |
| Avidin(+)-pCBMA | 93% |
| Uri(N)-pCBMA | 38% |
| Uri(+)-pCBMA | 35% |
| AChE(N)-pCBMA | 34% |
| AChE(+)-pCBMA | 37% |

### 3.3.11 Acid hydrolysis and characterization of cleaved polymer

The grafted polymer was cleaved by acid hydrolysis from the conjugate. Protein-polymer conjugate (20 mg) and 6 N HCl aq. (5 mL) were placed in a hydrolysis tube. After three freeze−pump−thaw cycles, the hydrolysis was performed at 110 °C for 24 h *in vacuo*. The cleaved polymer was isolated by dialysis using a 1 kDa molecular mass cut off dialysis tube in deionized water and was then lyophilized. The molecular mass of the cleaved polymer was measured by GPC.

### 3.3.12 Dynamic light scattering

Dynamic light scattering data was collected on a Malvern Zetasizer nano-ZS located in the Department of Chemistry, Carnegie Mellon University, Pittsburgh, PA. The hydrodynamic diameters (number and volume distributions) of samples were measured three times (5 runs per measurement) at room temperature.

### 3.3.13 Prediction of logD

ChemAxon was used to draw the structure of and calculate the hydrophobicity (logD) of lysine side chains and lysine-initiators.

### 3.3.14 Activity Assays

*CT:* *N*-succinyl-Ala-Ala-Pro-Phe-*p*-nitroanilide (Suc-AAPF-*p*NA) was used as a substrate for CT. Substrate (0-20 mg/mL in DMSO, 30 μL) was added to a 1.5 mL cuvette with sodium phosphate buffer (pH 8, 100 mM). Native CT, CT-initiators, or CT-polymers (0.1 mg/mL protein, 4 μM, 10 μL) was added to the cuvette with substrate and buffer. The initial substrate hydrolysis rate was measured in triplicate by recording the increase in absorbance at 412 nm over the first 60 seconds after mixing using a Lambda 2 Perkin Elmer ultraviolet-visible spectrometer equipped with a temperature-controlled cell holder at 37 °C. Michaelis-Menten parameters were determined using nonlinear curve fitting of initial hydrolysis rate versus substrate concentration in GraphPad.

*Lysozyme:* Activities of native, lysozyme-initiator, and polymer conjugates were determined by turbidimetric assays. Lyophilized *Micrococcus lysodeikticus* (Sigma Aldrich) was used to monitor enzymatic catalysis of cell wall lysis. Absorption at 450 nm of suspended *M. lysodeikticus* (990 μL, 0.2 mg/mL) in 50 mM sodium phosphate (pH 6.0) was measured by an UV-VIS spectrometer. 10 μL of native and lysozyme-initiator solutions (1.4 μM in 50 mM

sodium phosphate (pH 6.0)) were added and the change of absorbance at 450 nm at room temperature was monitored.

*Avidin:* HABA is an azo-dye that binds to avidin and shows spectral changes, thus can be used for determination of avidin binding affinity[2]. The absorption at 500 nm of a 200 µM HABA solution in phosphate buffered saline without calcium or magnesium (986 µL, Lonza) was measured using an UV-VIS spectrometer. 16 µL of the conjugate solution (125 µM of avidin in deionized water) was added to the HABA solution and incubated at room temperature for 1 min, and then the absorption at 500 nm was measured. The change in absorbance at 500 nm was used to determine the amount of bound HABA to the conjugate. It has been previously shown that upon biotin binding, tryptophan fluorescence of avidin is decreased from 337 to 324 nm.[3] We detected changes in intrinsic tryptophan fluorescence confirming biotin binding and took biotin binding kinetic measurements using a stopped-flow spectrometer with fluorescence detection (Applied Photophysics SX20). The excitation wavelength was 295 nm with a 5 nm bandwidth. The instrument was permitted to collect 1000 data points throughout the reaction (0.1-450 s). For all experiments, the avidin concentration was 0.5 µM (final) and biotin concentration was 5.0 µM (final). Reactions were initiated by mixing equal volumes of avidin with its substrates in 0.1 M phosphate buffer, pH 8. Fluorescence was measured in volts. Data were fit to single exponential functions using the $F(t) = F_{\infty} - \Delta F \exp(-k_{obs}t)$ equation, where, $k_{obs}$ is the observed first-order rate constant, $F_{\infty}$ is the final value of fluorescence and $\Delta F$ is the amplitude. In case of native avidin kinetics, the data were fit to single exponential functions using $F(t) = F_{\infty} + \Delta F \exp(-k_{obs}t)$, where $k_{obs}$ is the observed first-order rate constant, $F_{\infty}$ is the final value of fluorescence, and $\Delta F$ is the amplitude.

*Uricase:* Uric acid (0 – 400 µL of 300 µM in 50 mM sodium tetraborate (pH 8.5)) was mixed with 50 mM sodium phosphate buffer (990 – 580 µL, pH 8.5). Native, initiator, and polymer conjugate solutions (10 µL, 20 µM of uricase) were added to the substrate solution. The initial rate was monitored by recording the decreasing in absorbance at 290 nm using an UV-VIS absorbance spectrometer with a temperature controlled cell holder at 37 °C. Michaelis-Menten parameters were determined by nonlinear curve fitting of initial rate versus substrate concentration plots using Prism 7 software (GraphPad).

*AChE:* Acetylthiocholine iodide (0 – 100 µL of 10 mM in 100 mM sodium phosphate buffer (pH 7.4)) and 10 µL of DTNB solution (50 mM in DMSO) were mixed with 100 mM sodium phosphate (980 – 880 µL, pH 7.4). Native, initiator, and polymer conjugate solutions (10 µL, 4.2 µM of AChE) were added to the substrate solution. The initial rate was monitored by recording the increase in absorbance at 412 nm using an UV-VIS absorbance spectrometer with a temperature controlled cell holder at 37 °C. Michaelis-Menten parameters were determined by nonlinear curve fitting of initial rate versus substrate concentration plots using Prism 7 software (GraphPad).

### 3.3.15  Residual activity assays

*CT:* Native CT, CT-initiators, and CT-polymers (1 mg/mL, 40 µM protein) were dissolved in sodium phosphate buffer (pH 8, 100 mM). In triplicate, samples were then diluted to 4 µM for incubation. For thermostability, samples were incubated at 50 °C and pH 8 in a circulating water bath. For acid stability, samples were incubated at pH 1(167 mM HCl) and 37 °C. At specified time points, aliquots of 10 µL were removed over 60 minutes and residual activity was measured using Suc-AAPF-pNA as a substrate (6 mg/mL, 30 µL, 288 µM in DMSO) in sodium phosphate buffer (pH 8, 100 mM, 37 °C, 960 µL). Initial hydrolysis rate was

measured as the increase in absorbance at 412 nm over 40 seconds and data was normalized to its optimal activity (pH 8, 37 °C) at time 0.

*Lysozyme*: Native lysozyme, initiator, and polymer conjugates (14 µM of lysozyme) in 50 mM sodium phosphate buffer (pH 6.0) were incubated at 80 °C. At given time points, aliquots (10 µL) were removed and activity was measured in 990 µL of suspended *M. lysodeikticus* (0.2 mg/mL) in 50 mM sodium phosphate (pH 6.0) at room temperature.  Rates were monitored by recording the decreasing in absorbance at 450 nm using an UV-VIS spectrometer.  The residual activity was calculated as a ratio of the initial rates of the reaction at the given time points over the initial activity at time zero.

*Uricase:* Native uricase, initiator, and polymer conjugates (20 µM of uricase) in 50 mM sodium borate buffer (pH 8.5) were incubated at 75 °C. At given time points, aliquots (10 µL) were removed and activity was measured in 990 µL of 100 µM uric acid in 50 mM sodium borate buffer (pH 8.5) at 37 °C.  Rates were monitored by recording the decrease in absorbance at 290 nm using an UV-VIS spectrometer.  The residual activity was calculated as a ratio of the initial rates of the reaction at the given time points over the initial activity at time zero.

*AChE:* Native, initiator, and polymer conjugates (1.4 µM of AChE) in 100 mM sodium phosphate buffer (pH 7.0) were incubated at 50 °C. At given time points, aliquots (10 µL) were removed and added to a mixture of 930 µL of 100 mM sodium phosphate (pH 7.4), 50 µL of acetylthiocholine iodide (10 mM in 100 mM sodium phosphate (pH 7.4) and 10 µL of DTNB solution (50 mM in DMSO) at 37 °C.  Activity rates were monitored by recording the increase in absorbance at 412 nm using an UV-VIS spectrometer.  The residual activity was calculated as a ratio of the initial rates of the reaction at the given time point over the initial activity at time zero.

### 3.3.16 Tryptophan Fluorescence

Fluorescence measurements were collected using a BioTek Synergy H1 Plate Reader. Native CT, CT-initiators, and CT-polymers (1 mg/mL, 40 μM protein) were dissolved in sodium phosphate buffer (pH 8, 100 mM). Samples were diluted to 0.1 mg/mL (4 μM protein) in a black round bottom 96 well plate in triplicate. For thermostability, samples were incubated at 45 °C (maximum temperature setting for the BioTek Synergy H1 plate reader) and pH 8. For acid stability, samples were incubated at pH 1 (167 mM HCl) and 37 °C. Fluorescence intensity was measured every 2 minutes over 60 minutes (excitation at 270 nm, emissions at 330 nm and 350 nm). The ratio of emission fluorescence intensities (350 nm/330 nm) was plotted over time with time 0 as the fluorescence intensity of the sample at pH 8 and 37 °C.

### 3.3.17 Molecular Dynamics Simulation

CT-positive initiator model was built with the Maestro Schrodinger build toolkit using the crystal structure of CT as the initial structure (PDB: 4CHA). Positive initiators were attached to the N-terminus and all 14 lysine residues to create a fully modified CT-positive initiator construct. The molecule was subjected to a 1 ns simulated annealing using Desmond. Simulated annealing was performed in 4 stages: linear increasing temperature from 300-400 K over 0-100 ps, constant temperature at 400 K from 100-400 ps, linear decreasing temperature from 400-300 K over 400-700 ps, and constant temperature at 300 K from 700-1000 ps. The simulation system was prepared in Desmond system builder and consisted of OPLS 2005 force field, SPC water model, orthorhombic minimized box, and NaCl ions to neutralize the box followed by the addition of 100 mM NaCl. NVT ensemble and Berendsen thermostat were used to control temperature with a 1 ps relaxation time. The van der Waals interaction had a cutoff of 9 Å and particle mesh Ewald was used for Coulomb interactions with a 9 Å switching distance. The

molecule was simulated using Desmond over 1 ns with a 1.2 ps recording energy interval and 5 ps trajectory recording. A molecular dynamics simulation production run was performed on the final structure from simulated annealing. The simulation was performed over 20 ns at 300 K with a time-step bonded of 2 fs and a NPT ensemble (trajectories were recorded every 1.2 ps and energy was recorded every 4.8 ps). "Nose-Hoover chain" thermostat and "Martyna-Tobia-Klein" Barostat methods were used with 2 ps relaxation time and isotropic coupling. The default relaxation protocol was used with a 9 Å cutoff for van der Waals interactions. The solute atoms were restrained first with a force constant of 50.0 kcal mol$^{-1}$Å$^{-1}$. Next, the solute heavy atoms were restrained with a force constant of 50.0 kcal mol$^{-1}$Å$^{-1}$. After the production run, the trajectory was then loaded into Visual Molecular Dynamics (VMD) software for further analysis. The VMD salt bridge plug-in was used to monitor salt bridge formation and location over the 20 ns trajectory caused by initiator-induced structural changes. Salt bridges were monitored between acidic and basic protein residues and not from charges originating from the initiator itself.

## 3.4    Results and Discussion

### 3.4.1    Bioconjugate Synthesis and Characterization

We first synthesized a positively charged ATRP-initiator (**Figure 3.2**). *N*-(3-*N',N'*-Dimethylaminopropyl)-2-bromoisobutyramide and 4-bromobutyryl-*N*-oxysuccinimide ester were synthesized and then reacted with each other to form a positively charged ATRP-initiator. The overall synthesis had a 68% yield. The positive charge was in the form of a quaternary ammonium, $NR_4^+$, which was located approximately halfway between the protein-reactive NHS group and the terminal alkyl halide. The positive charge on the initiator quaternary nitrogen atom is therefore extended by $5.6 \pm 0.2$ Å from the original charge on the lysine NZ atom. We selected a quaternary ammonium group as the source of the positive charge since it would remain

97

positively charged at all pH's and would have a higher propensity of providing stabilization due to its chaotropic cationic nature.

We have previously studied polymer-based protein engineering of the serine protease chymotrypsin. Therefore, we naturally began our exploration of the impact of a permanently positively charged initiator on enzyme structure, dynamics and function by measuring the kinetics and stability of chymotrypsin-initiator constructs and chymotrypsin-polymer conjugates. Our previous studies have shown that chymotrypsin loses activity but gains stability when poly(carboxybetaine methacrylate) (pCBMA) is grown from the surface. Conversely, poly(sulfonate methacrylate) (pSMA) rapidly destroys the function of chymotrypsin (**Figure 3.6**).[49,153]
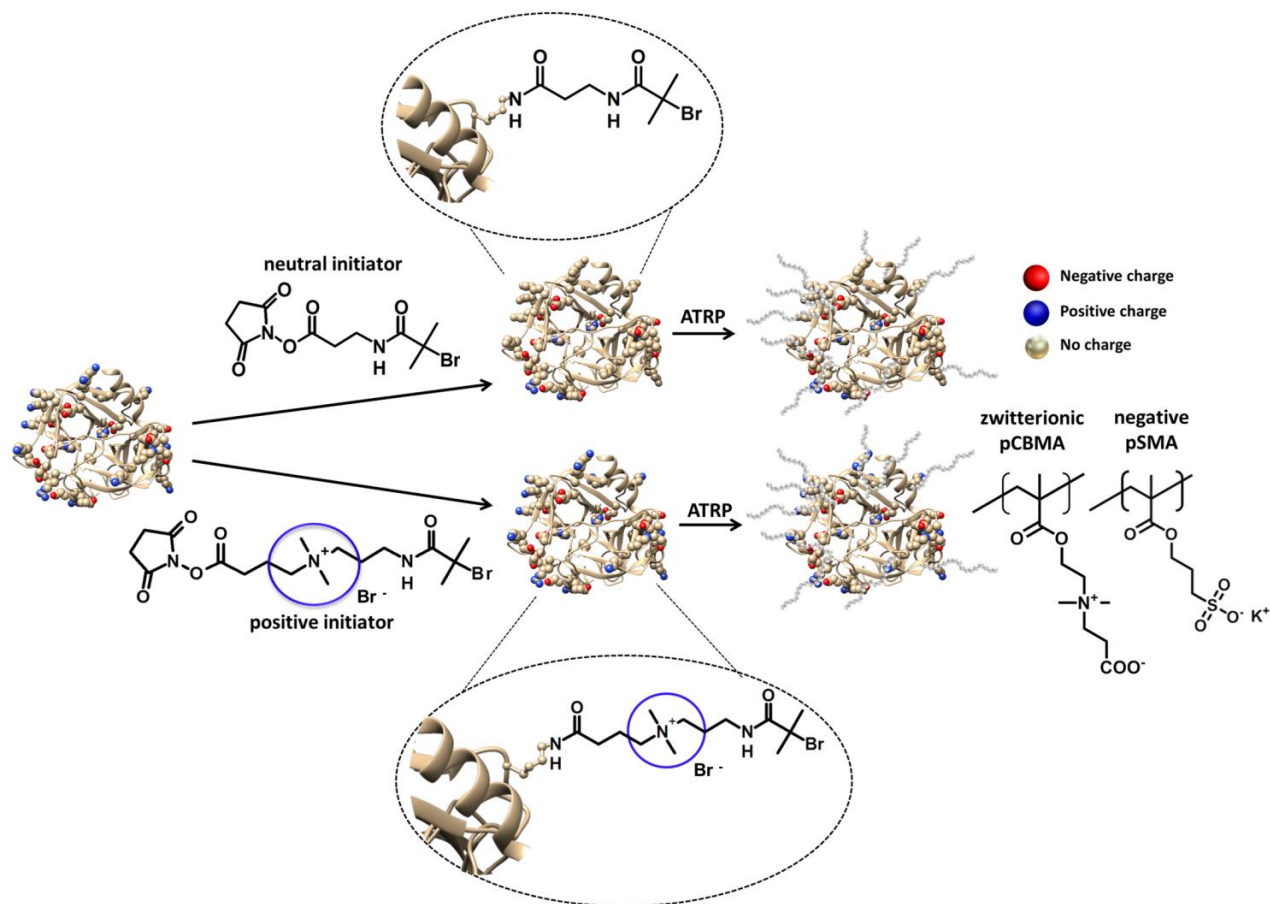
**Figure 3.6.** Synthetic approach to prepare grafted-from protein-polymer conjugates using neutral (N) or positively charged (+) initiators. The initiators reacted with primary amino groups on the protein surface through NHS chemistry. ATRP was then performed from the biomacroinitiators using a zwitterionic polymer, pCBMA, or a negatively charged polymer, pSMA.

The CT-initiator constructs were analyzed with matrix assisted laser desorption/ionization time-of-flight (MALDI-ToF) mass spectroscopy to determine the average number of amino groups that had been modified (**Figure 3.7**). CT has 15 total amino groups (N-terminus and 14 lysines). The average numbers of initiators attached to CT were 14.1 and 10.6 for the neutral (N) and positively charged (+) initiators, respectively. The slight decrease in total number of positive initiator modifications in comparison to the neutral initiator was likely due to its larger size and charge. The larger size could inhibit reactions with primary amines that have

decreased accessible surface areas while the positive charge could hinder reactions with primary amines in positively charged regions of CT.[34]
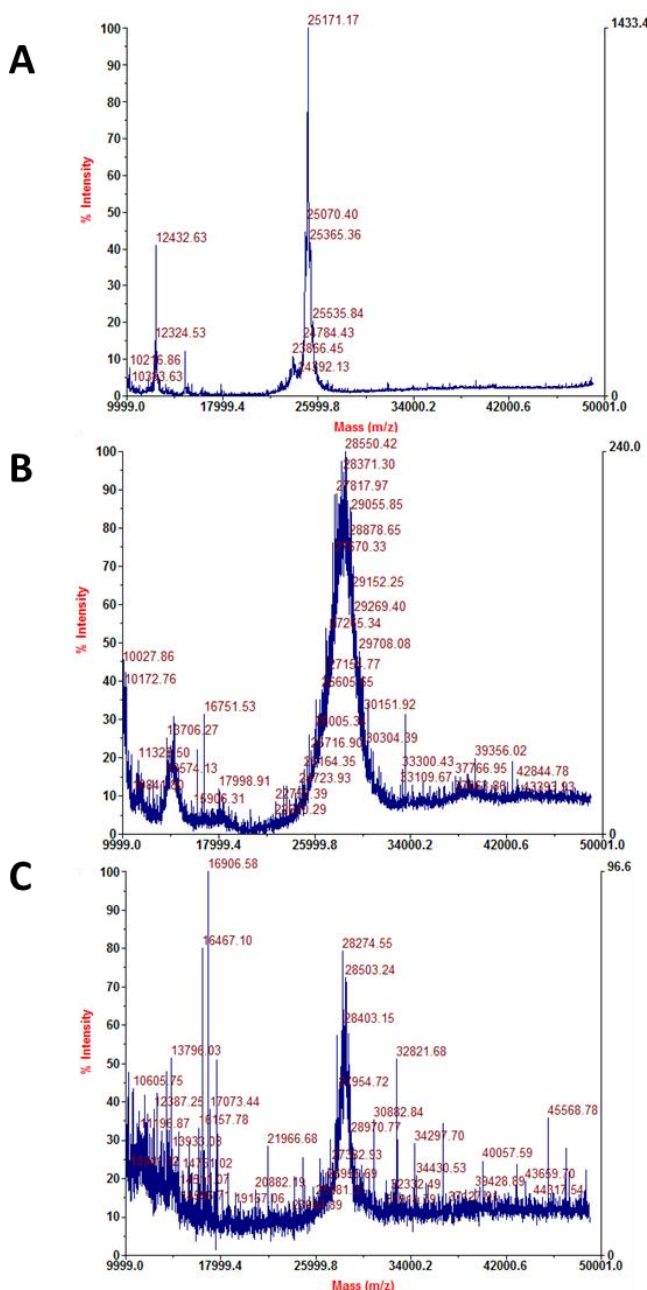


**Figure 3.7.** MALDI-ToF spectra of A) native CT, B) CT(+), and C) CT(N). Number of modifications was determined by taking the difference in m/z of the CT-initiators and native CT and dividing by the initiator molar mass without the –NHS group (positive initiator= 320 Da, neutral initiator= 220 Da). CT(+) had an average of 10.6 modifications and CT(N) had an average of 14.1 modifications.

In order to determine the sites of modification for each protein-initiator constructs, trypsin digestion followed by analysis of peptide fragments using MALDI-ToF was performed (**Figure 3.8 and Table 3.3, Table 3.4**).[34] The same sites were modified with the neutral and positively charged initiators except K82, K84, K90, K177, and K202. In general, these sites had decreased exposed surface areas which made them unable to be modified by the positively charged initiator, which was larger in size than the neutral initiator.[34]
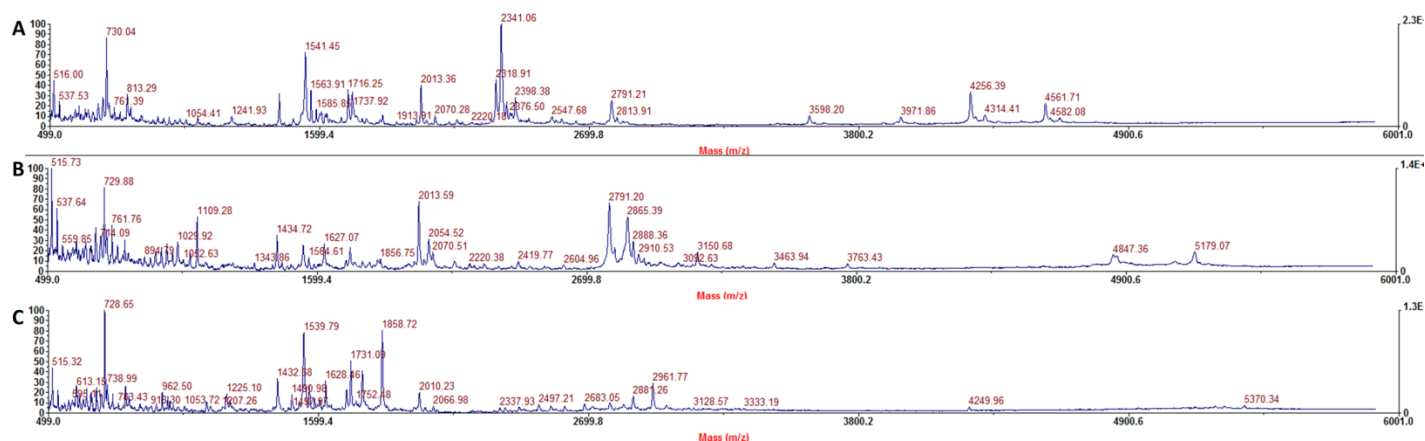


**Figure 3.8.** Trypsin digestion MALDI-ToF spectra of A) native CT, B) CT(N), and C) CT(+). Many peptide fragments were below the m/z limit of MALDI-ToF (500 m/z). Determination of modification at sites with small fragments was therefore not possible unless higher m/z adducts were present.

**Table 3.3.** Trypsin digestion fragments of CT(N).

| Peptide Fragment | Expected mass (m/z) | Observed mass (m/z) | Amino group modified |
|---|---|---|---|
| | **CT-neutral initiator** | | |
| CGVPAIQPVLSGLSR | 3463.42 | 3463.94 [2M+3H2O+2H] | N-terminus |
| IVNGEEAVPGSWPWQVSLQDK | 2602.5 | 2604.96 [M+ACN+H] | K36 |
| TGFHFCGGSLINENWVVTAAHCGVTTSDVVVAGEFDQGSSSEK | 4843.7 | 4843.36 [M+ACN+Na] | K79 |
| IQK | 672.4 | 672.88 [M+ACN+Na] | K82 |
| LK or IK | 962.0 | 963.6 [2M+H] | K84 or K177 |
| IAK | 615.3 | 616.2 [M+ACN+Na] | K87 |
| LSTAASFSQTVSAVCLPSASDDFAAGTTCVTTGWGLTR | 1342.6 | 1343.86 [M+2H+Na] | K175 |
| LQQASLPLLSNTNCKK | 2219.0 | 2220.38 [M+H] | K169+K170 |
| YWGTK | 917.0 | 916.4 [M+ACN+H] | K175 |
| DAMICAGASGVSSCMGDSGGPLVCK | 2791.6 | 2791.20 [M+2ACN+H] | K202 |

**Table 3.4.** Trypsin digestion fragments of CT(+).

| CT-positive initiator | | | |
|---|---|---|---|
| **Peptide Fragment** | **Expected mass (m/z)** | **Observed mass (m/z)** | **Amino group modified** |
| CGVPAIQPVLSGLSR | 1858.8 | 1858.72 [M+ACN+Na] | N-terminus |
| IVNGEEAVPGSWPWQVSLQDK | 2682.6 | 2683.05 [M+Na] | K36 |
| TGFHFCGGSLINENWVVTAAHCGVTTSDVV VAGEFDQGSSSEK | 1627.3 | 1628.46 [M+3H] | K79 |
| VFK | 1489.0 | 1487.89 [2M+ACN+Na] | K90 |
| YWGTK | 2011.4 | 2010.23 [2M+ACN+Na] | K175 |
| LQQASLPLLSNTNCKK | 2417.1 | 2416.52 [M+H] | K169 + K170 |

We were first interested in determining how the different CT-initiators impacted the isoelectric point (pI) of CT, which is the pH at which CT has no net electrical charge. We used isoelectric focusing (IEF) gel electrophoresis with a pH 3-10 gradient (**Figure 3.9**) to study the protein charge in the enzyme-initiator constructs. Native CT has a pI of approximately 8.75.[181] The pI of the CT(N) construct dropped to pI values ranging from ~3-6, with the majority of the band intensity at the limit of the gel around pH 3. There were three distinct bands: pI ~3, 5, and 6 which were most likely due to sub-populations of protein-initiators that had different numbers of reacted initiators. While MALDI-ToF provided an average number of modifications in the sample, the IEF gel allowed us to visualize the sub-populations with different degrees of modification. The decrease in pI for CT(N) was expected since the protein was losing positive charges and becoming more acidic. The pI values for CT(+) were increased to ~5-7.5 from CT(N), but were still decreased from native CT. pI values arise from an average of the individual residue $pK_a$ values, which are highly sensitive to their local electrostatic environment.[182] It is also

known that charge-charge interactions are the dominant factor that shift $pK_a$ values of ionizable groups on the protein surface.[183] Since our positively charged initiator did not have a $pK_a$, it made sense that the pI of CT(+) would be restored to intermediate values relative to native CT. After verifying that pI values for CT(+) were increased to ~5-7.5 from CT(N), protein-polymer conjugates were synthesized with incompatible (pSMA) and compatible (pCBMA) polymers (**Table 3.5**).
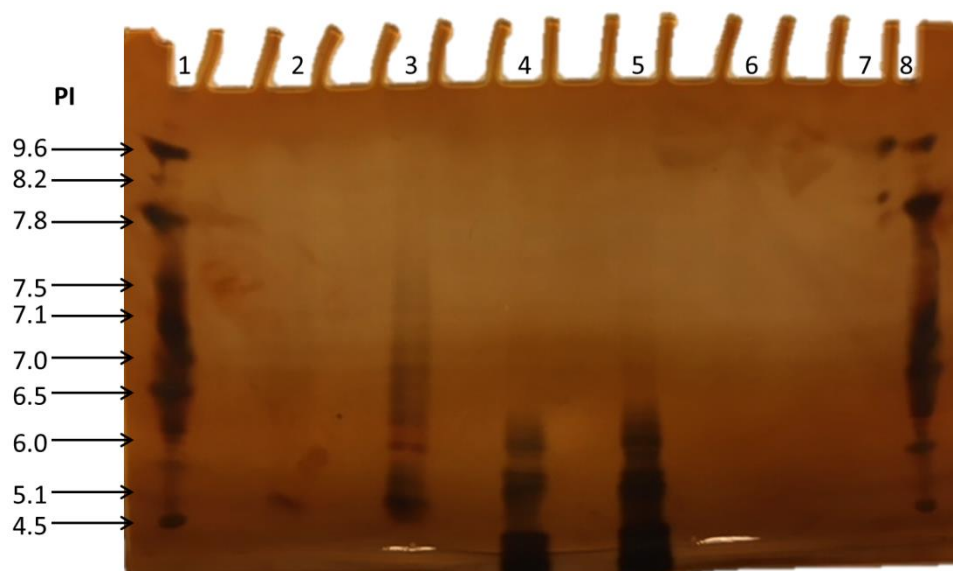


**Figure 3.9.** Isoelectric focusing gel to determine the change in pI of chymotrypsin upon modifications with neutral or positively charged ATRP-initiators. The gel has a pH gradient from 3-10. Lanes 1 and 8: ladders, Lane 2: CT(+) (low concentration, 0.6 µg/well), Lane 3: CT(+) (high concentration, 1.2 µg/well), Lane 4: CT(N) (low concentration, 0.6 µg/well), Lane 5: CT(N) (high concentration, 1.2 µg/well), Lane 6: CT (low concentration, 1.2 µg/well), Lane 7: CT (high concentration, 2.4 µg/well). The pI's of CT, CT-neutral initiator, and CT-positive initiator were ~9.6, <3-6, and 5-7.5, respectively. The multiple bands in the CT-initiator lanes were due to different populations of macroinitiators that varied in degree of modification.

**Table 3.5.** Characterization and activities of native CT, CT-initiators, and CT-polymers.

| | | Number of initiators | Cleaved polymer $M_n$ (kDa); Đ | Conjugate $M_n$ *(kDa);DP | $D_h$ (nm) Number Dist. | Turnover number, $k_{cat}$ (s$^{-1}$) | Michaelis Constant, $K_M$ (µM) | Catalytic Efficiency, $k_{cat}$/$K_M$ (µM$^{-1}$s$^{-1}$) |
|---|---|---|---|---|---|---|---|---|
| Chymotrypsin | **Native** | -- | -- | -- | 3.98 ± 0.48 | 26.6 ± 0.3 | 107 ± 5 | 0.25 ± 0.01 |
| | (+) | 10.6 | -- | -- | 4.18 ± 0.70 | 21.6 ± 0.6 | 60 ± 7 | 0.36 ± 0.03 |
| | (N) | 14.1 | -- | -- | 4.07 ± 0.31 | 18.9 ± 0.4 | 53 ± 5 | 0.36 ± 0.03 |
| | (+)-pSMA | 10.6 | 21.7; 1.44 | 256: 82 | 14.3 ± 7.5 | 22.2 ± 0.2 | 109 ± 3 | 0.20 ± 0.004 |
| | (N)-pSMA | 14.1 | 19.9; 1.54 | 306; 75 | 12.9 ± 6.9 | 3.0 ± 0.2 | 217 ± 35 | 0.01 ± 0.002 |
| | (+)-pCBMA | 10.6 | 23.8; 1.57 | 278; 104 | 18.3 ± 3.4 | 30.5 ± 0.6 | 73 ± 6 | 0.42 ± 0.02 |
| | (N)-pCBMA | 14.1 | 18.1; 1.54 | 281; 79 | 17.5 ± 7.7 | 25.6 ± 0.2 | 84 ± 3 | 0.30 ± 0.01 |

\* Conjugate $M_n$=(cleaved polymer $M_n$ × number of initiators) + molar mass of CT.

The molecular masses of the polymers were kept constant (targeted degree of polymerization of 100) in order to compare the activity and stability of each conjugate to that of the native enzyme.[103] After ATRP and purification of the conjugates via dialysis, protein-polymer conjugates were characterized with a bicinchoninic acid (BCA) assay to determine protein concentration from which conjugate molecular mass and degree of polymerization were estimated.[10] The polymers were also cleaved from the protein surface via acid hydrolysis and the isolated polymers were analyzed by gel permeation chromatography for relative molecular mass and polydispersity (Đ) from which conjugate molecular mass and degree of polymerization were also calculated. Conjugate number-average molecular masses reported in **Table 3.5** are derived from GPC data, however, BCA and GPC results agreed well. Number average hydrodynamic diameters ($D_h$) were also measured using dynamic light scattering and conjugates grew in size from 3.98 nm for native CT to approximately 13 nm for CT-pSMA  and approximately 18 nm for CT-pCBMA conjugates grown from either CT(+) or CT(N). CT-pCBMA conjugates had slightly larger hydrodynamic diameters because pCBMA is super-hydrophilic which would give CT-pCBMA a larger hydration layer than CT-pSMA conjugates. Only single peaks were

detected in DLS by number and volume distributions (**Figure 3.10, Figure 3.11, Figure 3.12, Figure 3.13)** and there were no signs of visible aggregation.
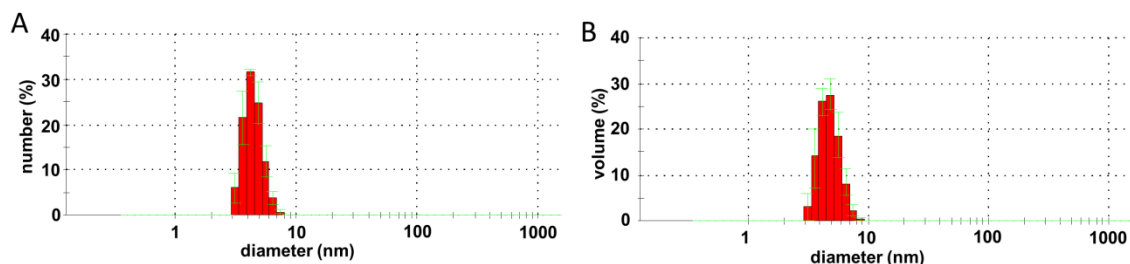


**Figure 3.10.** DLS of Native CT by A) number distribution and B) volume distribution.
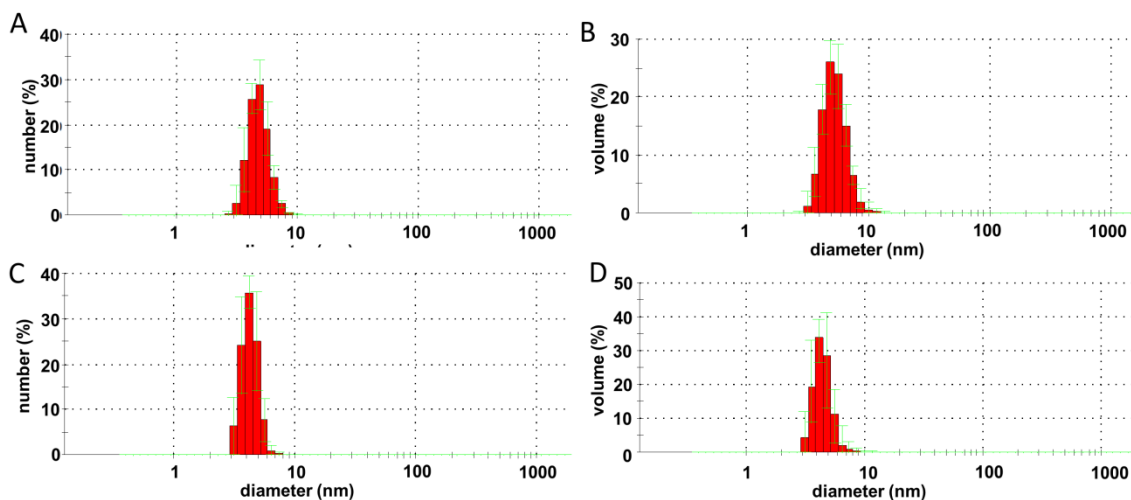


**Figure 3.11.** DLS of CT(+) by A) number distribution and B) volume distribution. DLS of CT(N) by C) number distribution and D) volume distribution.
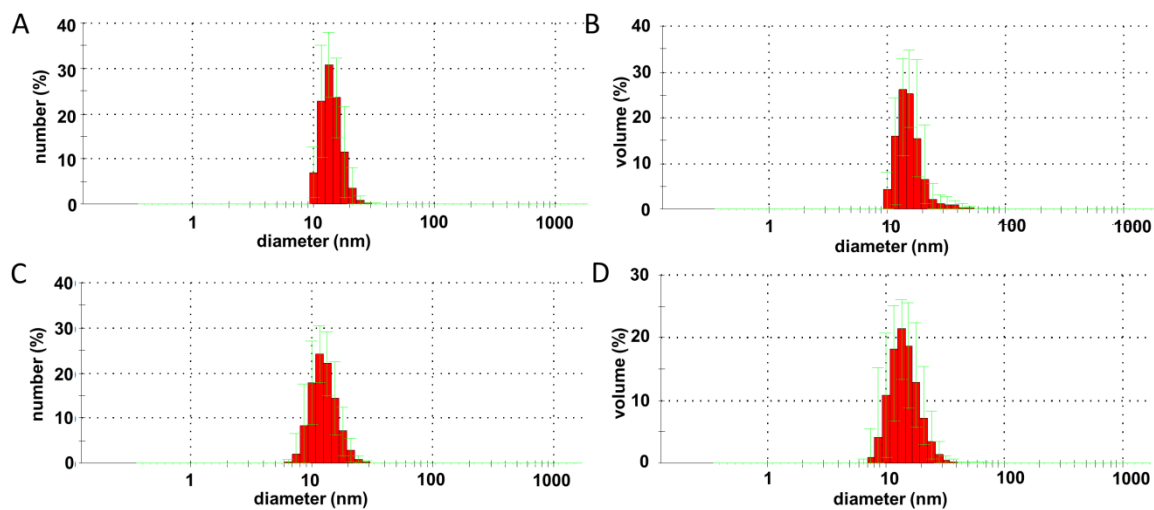
**Figure 3.12.** DLS of CT(+)-pCBMA by A) number distribution and B) volume distribution. DLS of CT(N)-pCBMA by C) number distribution and D) volume distribution.
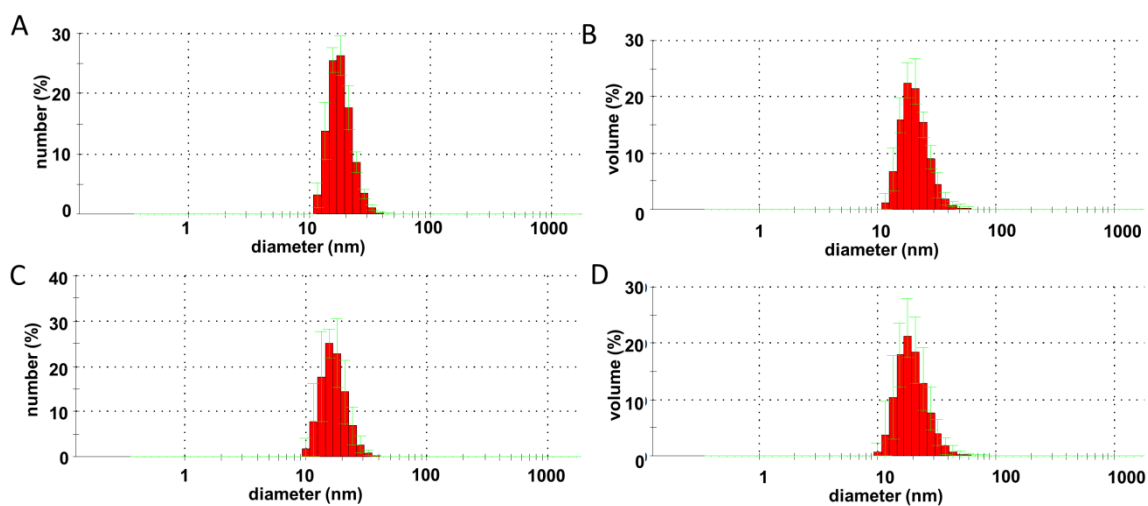


**Figure 3.13.** DLS of CT(+)-pSMA by A) number distribution and B) volume distribution. DLS of CT(N)-pSMA by C) number distribution and D) volume distribution.

### 3.4.2 Impact of charged initiator on activity of an incompatible protein-polymer conjugate

Attachment of polymers to proteins usually causes significant activity reductions, which have been attributed to protein structural stiffening.[57] The degree of protein modification and activity loss are also tightly correlated. Negatively charged polymers, such as pSMA, have been previously shown to inactivate CT rapidly.[153] Indeed, in the previous study, tryptophan fluorescence intensity at pH 8.0 increased after the CT(N)-pSMA conjugate was synthesized, indicating that the conjugate was already partially unfolded even in its most optimal environment.[153] We next explored whether maintaining enzyme surface charge, using a charged initiator, could protect the biocatalytic activity in CT-pSMA conjugates. Activities were measured by Michaelis-Menten kinetics at pH 8 and 37 °C using Succinyl-Ala-Ala-Pro-Phe-*p*-nitroanilide (Suc-AAPF-*p*NA), a hydrophobic and negatively charged substrate for CT, that binds to the hydrophobic $S_1$ binding pocket and is then cleaved by the catalytic triad (Ser 195, His 57, Asp 102). The turnover numbers ($k_{cat}$, s$^{-1}$), Michaelis constants ($K_M$, μM), and overall catalytic efficiencies ($k_{cat}/K_M$, μM$^{-1}$s$^{-1}$) were first determined for native CT and CT-pSMA conjugates grown from either neutral or positive initiators (**Table 3.5**). The growth of pSMA from CT(N) caused CT to lose 97% of its activity, matching results from previous work.[49,153] Unfortunately, this degree of activity loss is not unprecedented for protein-polymer conjugates in general. We were delighted to observe that the CT(+)-pSMA conjugate showed similar activities to native CT in terms of both $k_{cat}$ and $K_M$. It is important to note that the positively charged initiator modified less sites than the neutral initiator (10.6 vs. 14.1). In our prior work with chymotrypsin, however, we have shown that the activities of CT modified at 11 sites and 13 sites were similar[178], so we believe that the activity difference between the neutral and positively charged initiator was related to charge versus number of modifications.

We next considered *why* a simple charged initiator might have such a profound effect on protein surface electrostatics when surrounded by a vast array of negative charges in the polymer. After all, the CT(+)-pSMA conjugate retained 10 positive charges at its surface, but added over 1,000 negative charges to the molecular shell. Charged groups produce an electric field due to interactions with other charged particles in close proximity. The electric field strength at a surface with propagating point charges can be estimated using (**equation 3.1**),

$$E = \frac{kq}{r^2} \qquad \textbf{(equation 3.1)}$$

where E is electric field ($NC^{-1}$), $k$ is Coulomb's constant (9.0E9 $Nm^2C^{-2}$), $q$ is the signed magnitude of the point charge, and $r$ is the distance between the charges. Therefore, the electric field strength is proportional to the magnitude of the electric charge and inversely proportional to the squared distance. A CT(+)-pSMA conjugate of one polymer chain was modeled to estimate the electric field strength at the protein surface (**Figure 3.14**). Since the electric field is additive, even if there were 100 negative charges (DP=100) following the positive charge, the electric field strength at the protein surface would still be +0.77. This calculation assumes that the polymer backbone is in a linear conformation, which might not be true for all polymer types, but we have previously shown through molecular dynamics simulation that pSMA is a rather stiff, inflexible polymer, increasing the validity of the assumption.[153] This informative example highlights the importance of maintaining optimal surface charge prior to growth of charged polymers. Since the positively charged initiator was able to maintain high levels of activity of an incompatible polymer-protein conjugate, we next explored whether it may also improve conjugate stability when exposed to typical stressors, such as temperature and pH.
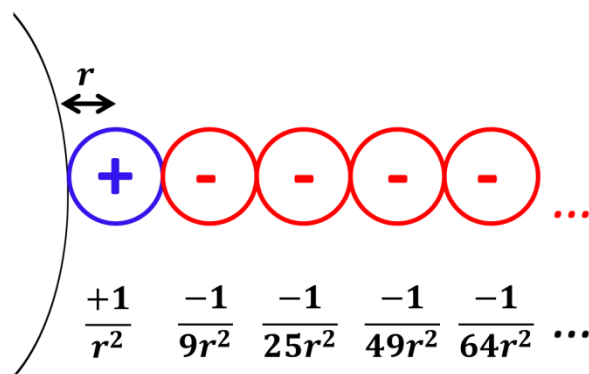
**Figure 3.14.** CT(+)-pSMA conjugate modeled as point charges. The positive charge is from the quarternary ammonium on the positive initiator while the remaining negative charges are the anionic sulfonate groups on SMA monomers. Even if there were 100 negative charges to the right of the positive charge, the electric field strength at the protein surface would still be +0.77.

### 3.4.3  Impact of charged initiator on stability of an incompatible protein-polymer conjugate

Various strategies have been used to stabilize protein solutions including adding excipients (polyols and salts)[155,184,185], immobilization onto solid supports,[186] encapsulation into reverse micelles[187], or by covalent attachment of polymer.[49] CT has a two-step deactivation mechanism where it undergoes complete deactivation via an intermediate transition state as follows (**equation 3.2**),[188]

$$F \overset{k_1}{\leftrightarrow} I \overset{k_2}{\to} U \qquad\qquad (\textbf{equation 3.2})$$

where F, I, and U are the folded, intermediate, and unfolded conformational states, and $k_1$ and $k_2$ are first order deactivation rate constants (min$^{-1}$). CT, when conjugated with polymer, resists inactivation by either not unfolding or refolding at a high rate.[188] We first determined the resistance of CT-pSMA conjugates to inactivation by heat (50 °C, pH 8) and acid (pH 1, 37 °C) (**Figure 3.15**). Deactivation via temperature and pH were chosen because they are two common stressors for protein structural stability and are valuable parameters for both industrial and therapeutic applications of enzymes. Covalently attached polymers have the ability to increase

110

the temperature and pH working ranges of the enzyme to increase their robustness during industrial processing. At specified time points, aliquots were taken from the incubating samples and activities were measured at pH 8 and 37 °C. CT(N)-pSMA irreversibly inactivated after just 10 minutes at 50 °C (**Figure 3.15A**). In another demonstration of the impact of the positive initiator, CT(+)-pSMA was remarkably stable as it retained 60% residual activity at 60 minutes. Our prior work has elucidated the mechanism of CT-polymer conjugate resistance to acid induced irreversible inactivation where the polymers trap proteins in partially unfolded intermediate states, prevent complete unfolding, and assist in refolding.[153] In acid, CT(+)-pSMA also displayed higher stability and was able to maintain 20% residual activity in comparison to CT(N)-pSMA, which had immediately irreversibly inactivated (**Figure 3.15B**). These data, in combination with Michaelis-Menten activity data, were the first observations to our knowledge of both high activity and stability with a negatively charged protein-polymer conjugate. The stability data further confirmed our view of the importance of net protein surface charge restoration when growing polymers from protein surfaces. Next, we began to dissect the interactions between the protein surface and the bio-macroinitiators.
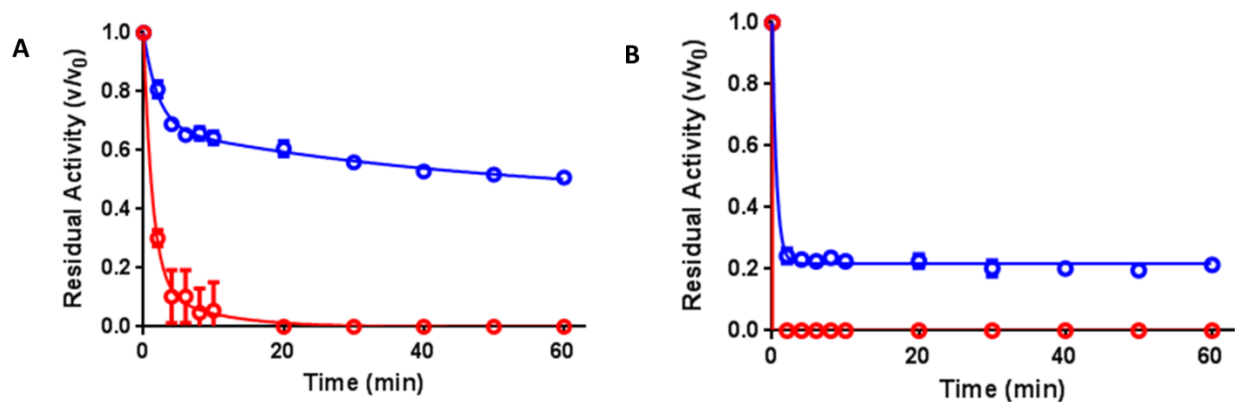
**Figure 3.15.** A) CT-pSMA thermal stabilities at 50 °C and pH 8 and B) CT-pSMA acid stabilities at pH 1 and 37 °C for conjugates grown from (N) or (+) initiators. CT(N)-pSMA (⊙), and CT(+)-pSMA (⊙). CT-pSMA conjugates synthesized using the positive initiator had increased thermal and acid stabilities in comparison to their neutral initiator conjugate counterparts. Residual activities were normalized to activity at time 0 which was the conjugate's optimal conditions for activity at pH 8 and 37 °C. Error bars in all plots represent the standard error of the mean from triplicate measurements.

### 3.4.4 Impact of charged initiator on activities and stabilities of protein-initiator constructs

Michaelis-Menten activities for CT-initiators were measured and are listed in **Table 3.5**. CT(N) and CT(+) had similar activities, but both had higher overall catalytic efficiencies than native CT due to a decrease in $K_M$. The observed decrease in $K_M$ upon neutral initiator attachment could have been the result of the hydrophobicity of the initiator. The octanol-water distribution coefficient (log D), which takes into account the hydrophobicity of different ionization states of a charged molecule, of a lysine side chain at pH 8.0 was -1.00 using ChemAxon. After covalent attachment of the neutral initiator, the calculated log D value of a lysine-initiator construct rose to 1.82. Considering that this reaction occurred on 14 out of the possible 15 amino groups, the surface of CT would have undoubtedly become more hydrophobic which would have strengthened the van der Waals interactions between the hydrophobic substrate and hydrophobic $S_1$ binding pocket to increase the affinity for the substrate. After attachment of the positive initiator, however, the calculated log D of the lysine-initiator construct

112

decreased to -1.98. The positive charge in the initiator likely maintained favorable electrostatic interactions with the negatively charged substrate to increase the binding affinity.

Since activities were comparable between CT(+) and CT(N), thermal and acid stabilities were probed next. Residual activities were further correlated with conformational tertiary changes by following increases in tryptophan fluorescence emissions over time during incubation at high temperature (45 °C, pH 8). CT(N) had irreversibly inactivated at elevated temperature (**Figure 3.16A**) and also at low pH (**Figure 3.16C**) within the first couple minutes. These profiles were drastically different than native CT which slowly deactivated over time. We were pleased to observed CT(+) had a similar thermal stability profile as native CT. When the data were fitted to the two-step inactivation model described by **equation 3.2** using GraphPad's 2-phase decay, CT(+) displayed a larger $k_1$ and a smaller $k_2$ than the native enzyme (**Table 3.6**). At elevated temperature, fluorescence intensity increased substantially over 60 min for CT(N) indicating protein unfolding and exposure of buried aromatic residues while CT(+) and native CT slightly increased to similar degrees, matching the residual activity profiles (**Figure 3.16B**).[63] In acid, both CT(N) and CT(+) irreversibly inactivated within the first 5 minutes by unfolding as seen in the tryptophan fluorescence immediate increases in intensities (**Figure 3.16D and Table 3.7**). Deactivation by heat is due to the breakage of hydrogen bonds with surface residues leading to disorder in the water molecule network around the protein allowing for increased vibrational dynamics and unfolding. Deactivation by pH, however, is due to disruption of the ionizable residues and electrostatic interactions on the protein surface which eventually leads to unfolding. Since modifying amino groups with the ATRP initiators changes the protein's ionizability and the positive initiator creates a non-ionizable positive charge, it was not surprising that unfolding was observed for both CT(N) and CT(+) in acid.
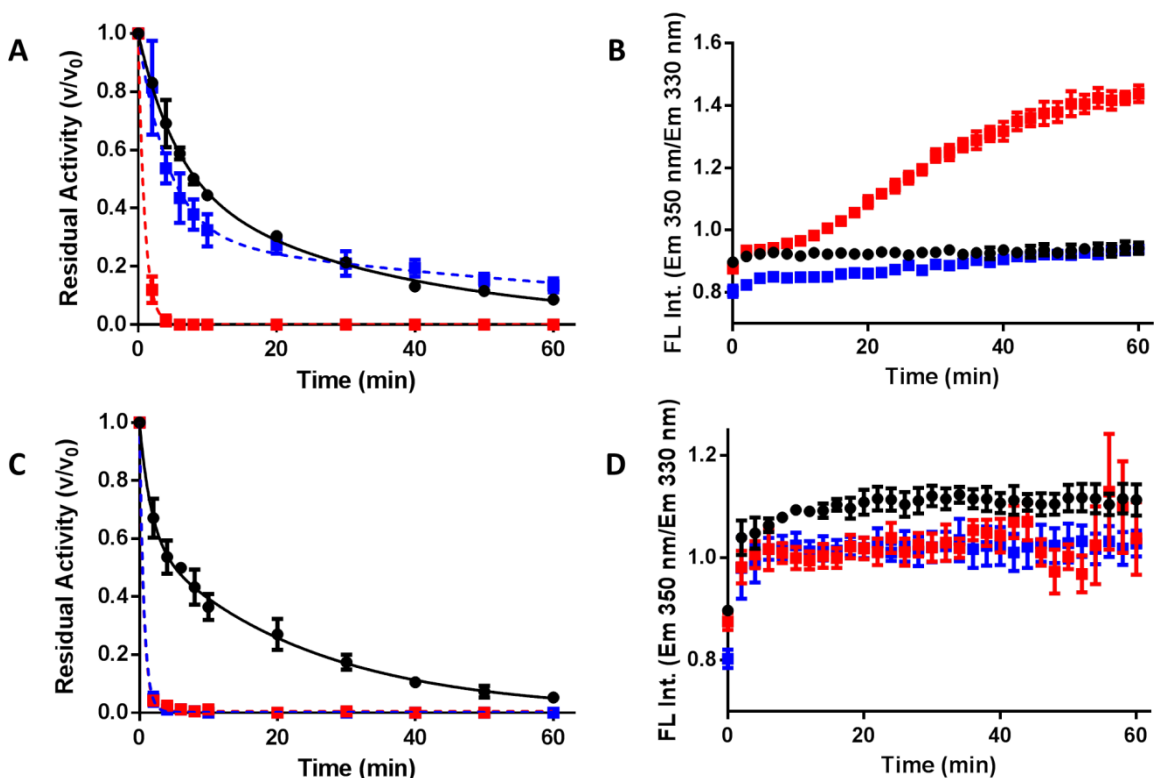
**Figure 3.16.** Thermal and acid stabilities of native CT and CT-initiators. Stabilities are normalized to time 0 which represents the most active form of CT (pH 8 and 37 °C). A) Residual activities at 50 °C and pH 8 and B) tryptophan fluorescence emission intensities at 45 °C and pH 8. Increases in fluorescence intensities indicate protein unfolding as buried aromatic residues become more exposed to the solvent. C) Residual activities and D) tryptophan fluorescence emission intensities at pH 1 and 37 °C. In all plots, native CT (●), CT(N) (■), and CT(+) (■). Connecting lines are nonlinear fits using GraphPad. At elevated temperature, the CT(N) lost all detectable activity within the first 5 minutes which correlated to rapid unfolding in the tryptophan fluorescence plot. CT(+) displayed similar residual activities and conformational stabilities to native CT indicating that surface charge is important for maintaining CT's stability. In acid, both CT(N) and CT(+) rapidly lost activity as confirmed with rapid unfolding via tryptophan fluorescence. Error bars in all plots represent the standard error of the mean from triplicate measurements.

**Table 3.6.** Deactivation rates at pH 8 and 50 °C.

| | 50 °C, pH 8 | | |
| --- | --- | --- | --- |
| | *One-phase decay* $k$ (min$^{-1}$) | *Two-phase decay* $k_1$(min$^{-1}$) | $k_2$ (min$^{-1}$) |
| **Native CT** | - | $0.18 \pm 0.05$ | $0.03 \pm 0.02$ |
| **CT(N)** | $1.06 \pm 0.03$ | - | - |
| **CT(+)** | - | $0.23 \pm 0.04$ | $0.01 \pm 0.02$ |
| **CT(+)-(N)-mix** | **$0.55 \pm 0.03$** | $0.64 \pm 0.11$ | $0.10 \pm 0.15$ |
| **CT(N)-pCBMA** | $0.19 \pm 0.04$ | - | - |
| **CT(+)-pCBMA** | $0.09 \pm 0.03$ | - | - |
| **CT(N)-pSMA** | - | $0.78 \pm 0.21$ | $0.12 \pm 0.15$ |
| **CT(+)-pSMA** | - | $0.48 \pm 0.06$ | $0.02 \pm 0.01$ |

**Table 3.7.** Deactivation rates at pH 1 and 37 °C.

| | pH 1, 37 °C | | |
| --- | --- | --- | --- |
| | *One-phase decay* $k$ (min$^{-1}$) | *Two-phase decay* $k_1$(min$^{-1}$) | $k_2$ (min$^{-1}$) |
| **Native CT** | | $0.59 \pm 0.14$ | $0.04 \pm 0.01$ |
| **CT(N)** | $1.63 \pm 0.09$ | | |
| **CT(+)** | $1.55 \pm 0.06$ | | |
| **CT(N)-pCBMA** | $1.51 \pm 0.76$ | | |
| **CT(+)-pCBMA** | $0.88 \pm 0.15$ | | |
| **CT(N)-pSMA** | - | | |
| **CT(+)-pSMA** | $1.69 \pm 0.19$ | | |

Next, we were interested if the increased thermal stability of CT(+) was due to altered short range (salt-bridge) or restoration of long range electrostatic interactions. We synthesized a CT-initiator construct that contained a random mixture of neutral and positive initiators around the protein surface. If a specific short-range interaction was causing the stabilization, then

random mixed modification should eliminate the possibility of that interaction occurring and the thermal stability of the mixed sample would be similar to that of the neutral initiated sample. Characterization through MALDI-ToF showed that the mixed constructs contained an average of 9 neutral and 5 positive initiators per CT (**Figure 3.17**).
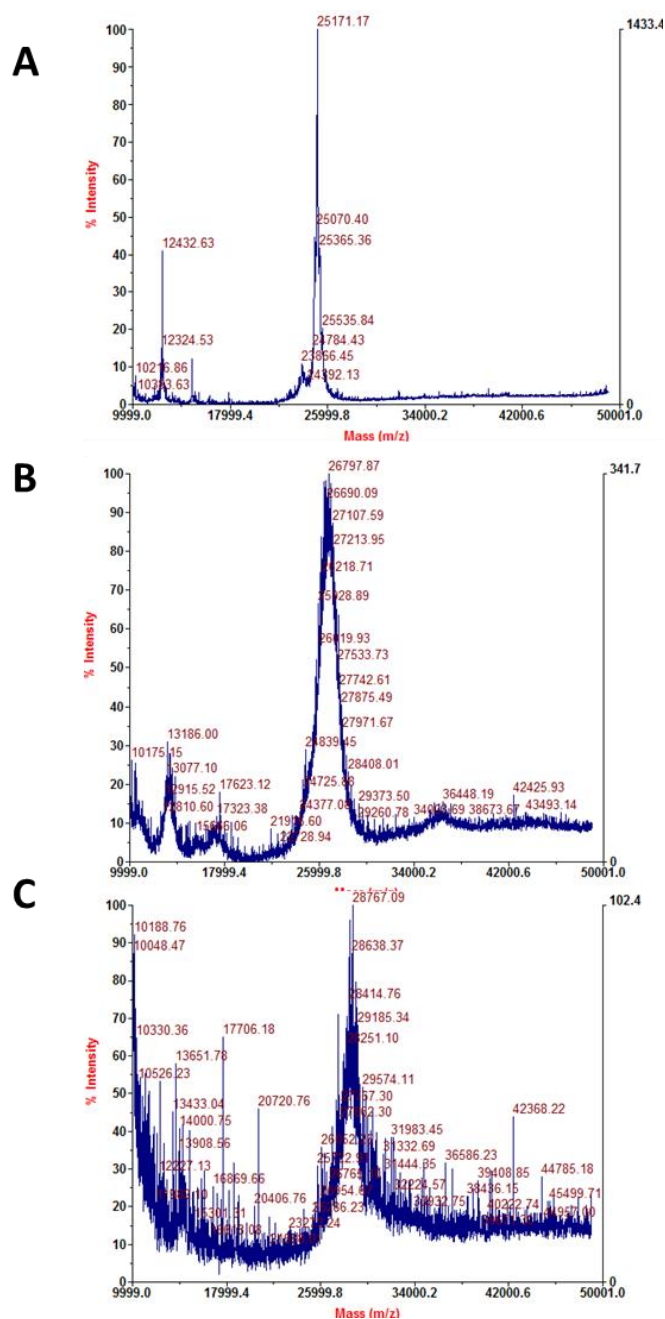
**Figure 3.17.** MALDI-ToF spectra of A) Native CT, B) CT(+), and C) CT-positive-neutral initiator. CT(+) was synthesized stoichiometrically and after purification and MALDI-ToF analysis, neutral initiator was reacted with the remaining amino groups followed by purification and MALDI-ToF. CT(+) showed 5.1 modifications and CT-positive-neutral initiator showed an additional modification of 9 neutral initiators.

For activity, the mixed construct had slightly lower Michaelis-Menten parameters than both CT(N) and CT(+) ($k_{cat}= 16.7 \pm 0.4$ s$^{-1}$, $K_M= 82 \pm 7$ μM, $k_{cat}/K_M= 0.20 \pm 0.01$ μM$^{-1}$s$^{-1}$) at pH

8 and 37 °C. For thermal stability at pH 8 and 50 °C, the mixed initiator construct had a stability curve that fell between CT(N) and CT(+) stability curves (**Figure 3.18)** while the deactivation rate of the CT-mixed initiator ($0.55 \pm 0.03$ min$^{-1}$) was approximately half of CT(N) ($1.06 \pm 0.03$ min$^{-1}$). These data implied that the stabilizing effect against heat-induced irreversible inactivation of the positive initiator construct was most likely due to maintenance of long-range surface charge electrostatic interactions versus specific short-range interactions.
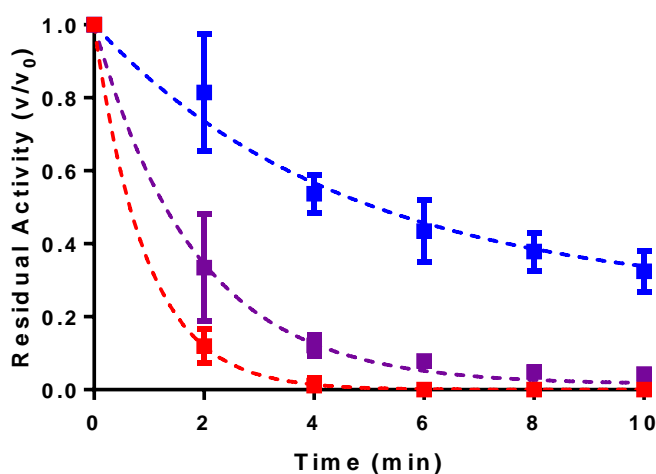


**Figure 3.18.** Residual activity of CT-mixed initiator (■) in relation to CT(N)( ■) and CT(+) (■). CT-mixed initiator was modified with approximately 9 neutral initiators and 5 positive initiators. CT-mixed initiator displayed a stability profile in between CT(N) and CT(+). Error bars are from standard deviations of triplicate measurements.

To verify that the stabilizing effects were due to long-range electrostatic interactions over short-range (salt bridges), we performed a 20 ns all-atom molecular dynamics (MD) simulation in a water box with periodic boundary conditions on a fully modified CT (PDB: 4CHA) with positive initiators. The simulation was performed to mimic experimental conditions by adjusting the protonation states of ionizable groups to pH 8 and adding 100 mM NaCl. The system was subjected to a 1 ns simulated annealing to place the molecule in its lowest energy state and

remove bias in initiator configuration before starting the 20 ns production run. MD simulations were performed using the OPLS2005 force field and the average radius of gyration was 1.85 nm which was validated against experimental hydrodynamic diameter data (**Figure 3.19**).
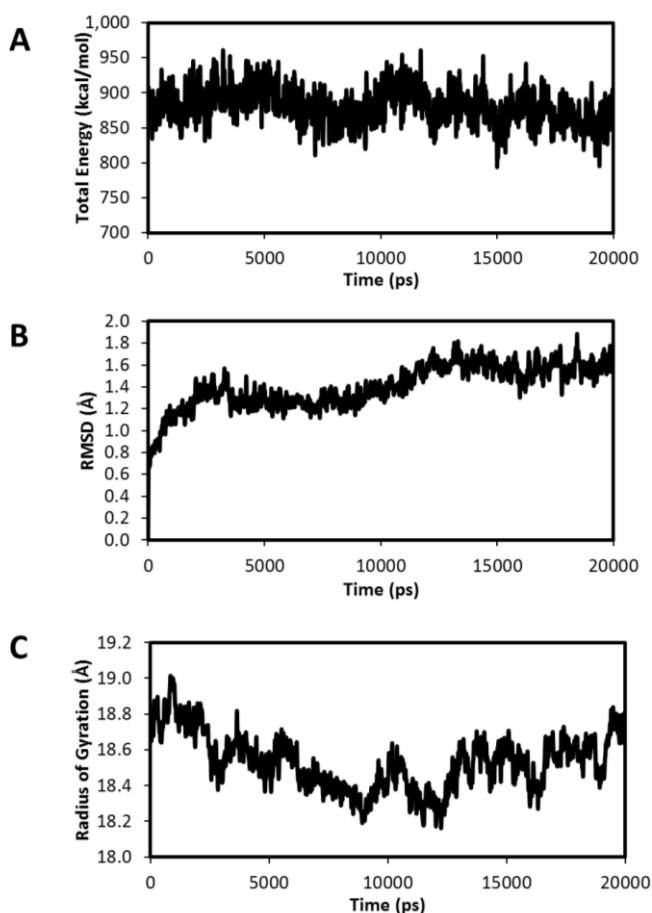


**Figure 3.19.** Molecular dynamics simulation analysis of a fully modified CT(+) molecule. A) Total energy (kcal/mol), B) root mean square deviation (RMSD) of the alpha carbons (Å), and C) Radius of gyration (Å) of the CT(+) construct over the 20 ns simulation.

Electrostatic interactions around the protein surface were monitored over the 20 ns trajectory by determining the number of salt bridge formations, which represent the short-range electrostatic interactions. Salt bridge formation was monitored using Visual Molecular Dynamics (VMD) software plugins. A salt bridge is formed when the distance between any of the oxygen

atoms of acidic residues (Asp, Glu) are within 3.2 Å of the nitrogens of basic residues (Arg, His, Lys, Hsp). Therefore, salt bridges were determined for the lysine portions of lysine-initiator moieties and induced tertiary structural changes to remaining acidic and basic residues, but not for the additional nitrogens on the initiator structure. Native CT has one known salt bridge (between the α-ammonium ion of Ile 16 and the carboxylate ion of Asp 194) and was chosen as the protein for comparison.[189] It was previously found that destabilization of this salt bridge decreased stability by 2.9 kcal mol$^{-1}$.[189] In the CT-positive initiator construct, we observed the formation of 4 different salt bridges throughout the 20 ns analysis: Asp 72-Arg 154, Glu 21-Arg 154, Asp 129-Arg 230, and Asp 128-Lys203 (**Figure 3.20A**). Arg 154 is located within close proximity of two acidic residues, Asp 72 and Glu 21, and formed salt bridges with both in the simulated model. The time spent in a salt bridge was also monitored over 20 ns (**Figure 3.20B**). The most dominant salt bridge was between Asp 72-Arg 154. Since there was only one salt bridge formed that was associated with the lysine portion of a modified lysine residue, it was possible that CT(N) could also form the majority of the salt bridges induced by conformational dynamics. Additionally, the stabilities (residual activities) of CT and CT(+) were similar indicating that the formation of additional salt bridges did not significantly enhance CT's stability. Rather, it was more likely that the maintained stability of CT(+) over CT(N) was due to long-range electrostatic interactions through restoring the charge balance, aligning with the findings of activity and stability of CT-mixed initiator.
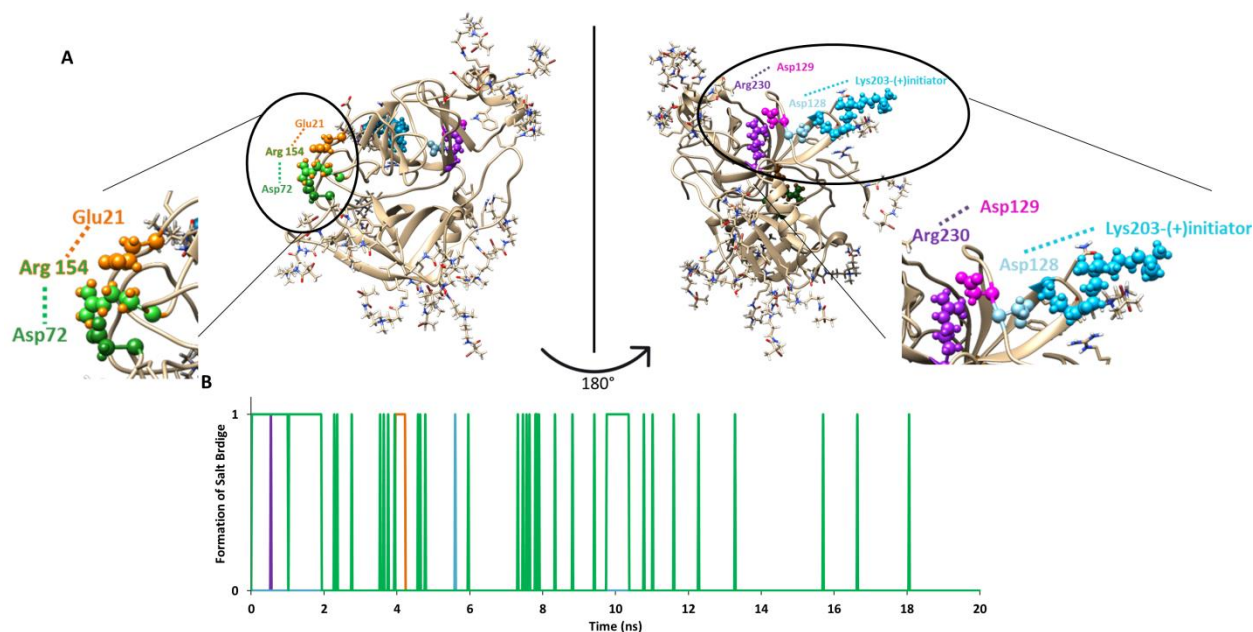
**Figure 3.20.** Formation of salt bridge analysis of CT fully modified with positive initiators from a 20 ns molecular dynamics simulation. A) Salt bridges between acidic and basic residues are color coded: Asp 72-Arg 154 (green), Glu 21-Arg 154 (orange), Asp 129-Arg 230 (purple), Asp 128-Lys203-positive initiator (light blue). B) Salt bridge formation indicated by a value of 1 on the y-axis. Four salt bridges were formed and the most dominant salt bridge occurred between Asp 72-Arg 154.

### 3.4.5 Impact of charged initiator on activity and stability of a compatible protein-polymer conjugate

Since the positive initiator generated a highly active and stable conjugate with an "incompatible" polymer, we hypothesized that maintaining natural surface charge may also be able to further improve the activity and stability of a highly compatible polymer, namely zwitterionic polymer, pCBMA. As stated above, almost all protein-polymer conjugates lose activity to some degree. We were curious whether maintaining surface charge would remove this limitation, or even unusually enhance conjugate function further. We have shown previously[153] that CT-pCBMA conjugates grown from neutral initiators are highly effective (with slightly improved $k_{cat}/K_M$ relative to the native enzyme[128]) (**Table 3.5**). When using the positive initiator, CT(+)-pCBMA had an increased $k_{cat}/K_M$ (0.30 ± 0.01 to 0.42 ± 0.02 $\mu M^{-1}s^{-1}$)

with increased $k_{cat}$ and decreased $K_M$ compared to CT(N)-pCBMA. We also observed that the overall catalytic efficiency of CT(+)-pCBMA was almost double that of native CT. The thermal stability of the CT(+)-pCBMA was also improved relative to native and neutral-initiated conjugate (even maintaining ~90% activity after exposure to high temperature for 60 minutes) (**Figure 3.21**). Although zwitterionic polymers are now setting the benchmark for modified protein stabilization[129,190,191], this "gold standard" can now be further improved with the use of a positively charged initiator.
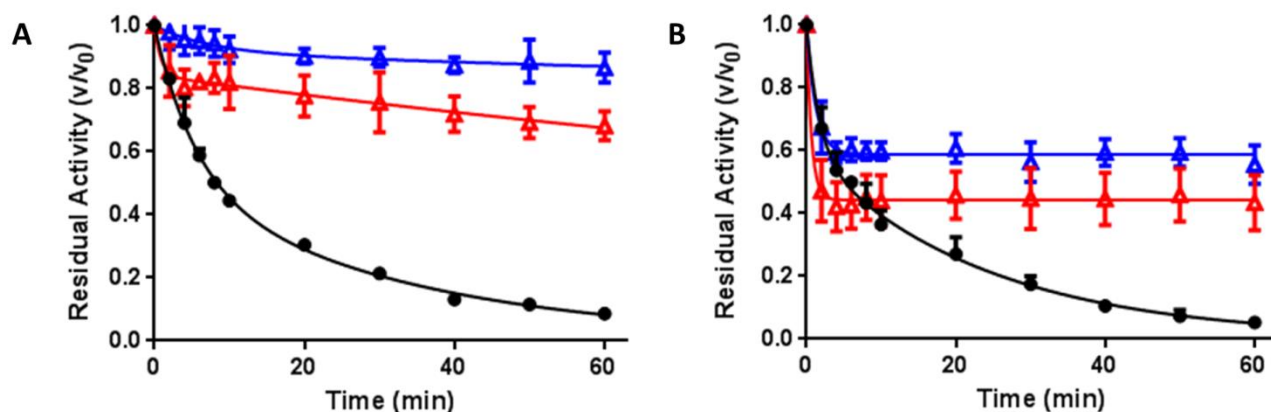


**Figure 3.21.** A) CT-pCBMA thermal stabilities at 50 °C and pH 8 and B) CT-pCBMA acid stabilities at pH 1and 37 °C for conjugates grown from (N) or (+) initiators. In both plots, CT(N)-pCBMA (△) , CT(+)-pCBMA (△), and native CT (●). Conjugates synthesized using the positive initiator had increased thermal and acid stabilities in comparison to their neutral initiator conjugate counterparts. Residual activities were normalized to activity at time 0 which was the conjugate's optimal conditions for activity at pH 8 and 37 °C. Error bars in all plots represent the standard error of the mean from triplicate measurements.

### 3.4.6 Impact of charged initiator on activity and stability of diverse protein-pCBMA conjugates

Since we discovered that the positively charged initiator could generate protein-polymer conjugates with significantly higher activities and stabilities than native chymotrypsin and neutral-initiated chymotrypsin, we decided to explore whether a diverse group of enzymes would also benefit from a positively charged initiator. To make this more challenging, we selected a

group of enzymes that are not all ideally suited to polymer-based protein engineering. We modified lysozyme (14.3 kDa, 7 amines), avidin (16.4 kDa, 10 amines), uricase (35 kDa, 25 amines), and acetylcholinesterase (70 kDa, 26 amines) with pCBMA grown from neutral and positively charged initiators. These enzymes have very different molecular masses, number of amino groups, active site mechanisms, multimeric characteristics (molecular masses and number of amines listed are per monomer), and susceptibilities to modification. The degree of initiator modification for each protein-initiator construct was determined using a fluorescamine assay, except for lysozyme and avidin samples, which were characterized by MALDI-ToF (**Figure 3.22 and Figure 3.23**). Polymers of CBMA were grown from each of the protein-initiator constructs with similar degrees of polymerization. After synthesis, conjugate molecular masses were estimated by the cleaved polymer molecular mass by GPC.
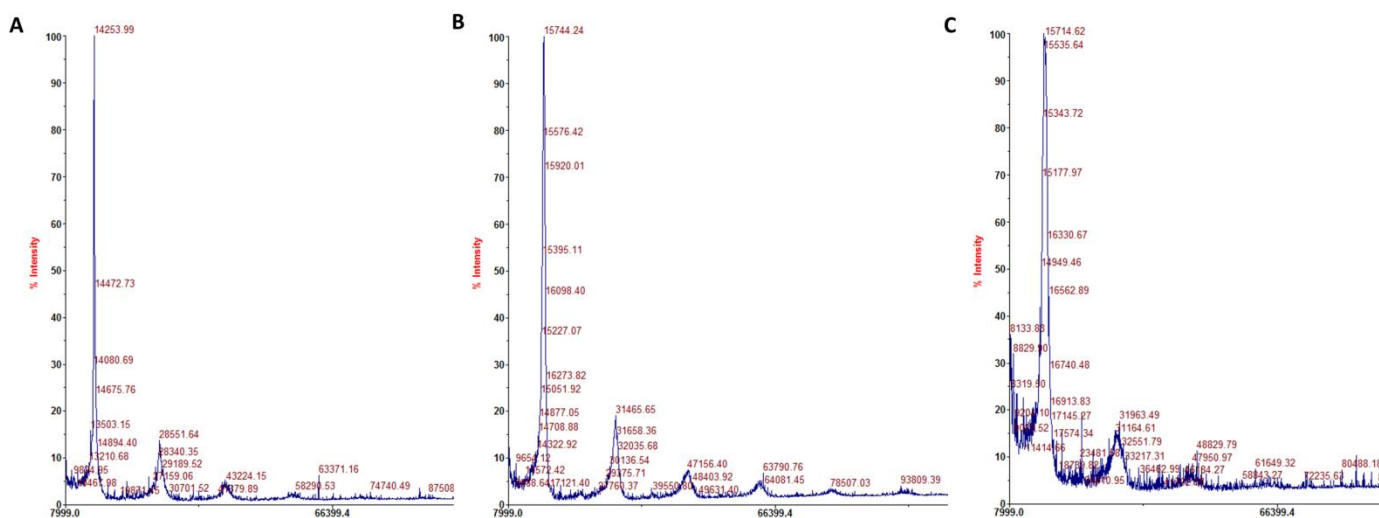


**Figure 3.22.** MALDI-ToF of A) native lysozyme, B) lysozyme(N), and C) lysozyme(+). Degree of modification was determined by taking the difference in m/z between the lysozyme-initiator and native lysozyme (monomeric forms) and then dividing by the molar mass of the initiator (neutral initiator: 220 Da, positive initiator: 320 Da). The $[M+H]^+$ peak (tallest peak) was used for the calculation. The other peaks correspond to $[2M+H]^+$, $[3M+H]^+$, $[4M+H]^+$, etc.

123
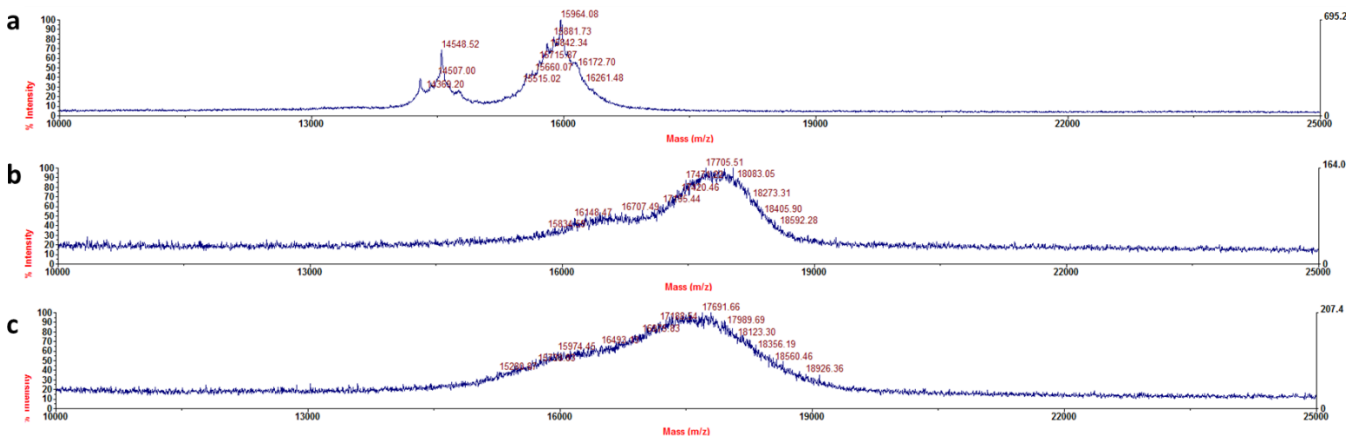
**Figure 3.23.** MALDI-ToF mass spectrometry of a) native avidin, b) avidin(N) and c) avidin(+). The monomer is detected at m/z=15.9 and the unglycosylated form of monomeric avidin is detected at m/z=14.5.

*Activity*

The reaction rates and attachment locations of neutral ATRP initiators with lysozyme, a small, single sub-unit protein that is an antimicrobial enzyme and is important for the immune system, have been dissected in detail.[34] Lysozyme hydrolyzes the β-1,4 glycosidic linkages between N-acetylmuramic acid and N-acetylglucosamine that are present in the cell wall of the bacteria. As seen with CT, the degree of initiator modification was slightly less for the positive initiator compared to the neutral initiator (4.6 versus 6.7) (**Table 3.8**). Lysozyme activity was measured by the change in absorbance at 450 nm over time when using *Micrococcus lysodeikticus* as a substrate. Lysozyme(N) was almost completely inactive (two orders of magnitude less activity than native lysozyme). The compelling results with CT were mirrored for lysozyme(+) and we observed almost complete restoration of activity for the positively charged protein-initiator construct compared to native. Growth of pCBMA from lysozyme(N) regained activity lost upon neutral initiator attachment while growth of pCBMA from lysozyme(+) only

124

showed moderate further increase in activity. Lysozyme(+)-pCBMA had double the activity of lysozyme(N)-pCBMA.

Avidin, a tetrameric protein (homo-tetramer) that is approximately 66 kDa in its tetrameric form and is found in the egg whites of birds, reptiles, and amphibians, was also modified by the positive initiator to a reduced amount (7.0 versus 7.9). Using a model system we have described previously[192], we determined that the conjugate with the positive initiator had an increased biotin binding rate and increased equilibrium HABA binding over the conjugate with the neutral initiator (**Table 3.8**).

In the liver, uricase catalyzes the oxidation of uric acid by gaseous molecular oxygen to produce 5-hydroxyisourate and hydrogen peroxide.[193,194] Uricase has a homo-tetrameric structure and the active sites of the monomers are located at dimeric interfaces. There is also a hydrophobic cavity on each monomer located next to its active site and the flexibility of this cavity is essential for catalysis.[195] The therapeutic utility of uricase makes it an ideal target for polymer-based protein engineering, but the enzyme has been found to lose almost all activity upon polymer modification when densely modified. As expected, uricase(N) was largely inactivated and very little activity was detectable. The loss in activity was due to a combined decrease in $k_{cat}$ and increase in $K_M$ compared to native. Surprisingly, growth of pCBMA did not recover the lost activity of uricase(N) and in fact, caused complete inactivation of uricase(N)-pCBMA. Initiation of uricase with the positively charged initiator resulted in an enzyme with detectable activity, though the activity was still significantly less than the native enzyme due to high modification. Growth of pCBMA from uricase(+) also yielded a protein-polymer conjugate with detectable activity. The large decrease in activity could be due to a combination of decreased flexibility (causing decreased $k_{cat}$), modification of Lys 10 in the active site (causing

inactivation), increased hydrophilicity of the cavity when using the positive initiator (causing increased $K_M$), or loss of tetrameric structure due to high modification densities. We are now optimizing uricase activity by targeting each of these issues.

Acetylcholinesterase (AChE) catalyzes the hydrolysis of acetylcholine to acetic acid and choline. The positively charged substrate binds to the anionic site of AChE and is then hydrolyzed by the catalytic triad (Ser 200, Glu 327, His 440).[196,197] AChE(N)-pCBMA had decreased activity over both AChE and AChE(N), due largely to a decrease in $k_{cat}$. Once again, however, the positively charged initiator-grown protein-polymer conjugate (AChE(+)-pCBMA) did not show any further activity loss after the growth of polymer.

**Table 3.8.** Characterizations and activities of a range of proteins and their subsequent protein-initiators, and protein-polymers. Conjugate data are calculated per monomer. Errors on activity data are calculated from standard deviations of triplicate measurements. U.D. stands for undetectable in cases where conjugation fully inactivated the protein.

| | | Number of initiators | Cleaved polymer $M_n$ (kDa); Đ | Conjugate $M_n$ (kDa) | $D_h$ (nm) | Activity | | |
|---|---|---|---|---|---|---|---|---|
| | | | | | | $\Delta A_{450}$ x$10^{-4}$ (s$^{-1}$) | | |
| Lysozyme | Native | -- | -- | -- | $2.6 \pm 0.9$ | $32.3 \pm 0.5$ | | |
| | (N) | 6.7 | -- | -- | $2.8 \pm 1.0$ | $1.0 \pm 0.1$ | | |
| | (+) | 4.6 | -- | -- | $2.9 \pm 1.0$ | $23.7 \pm 1.5$ | | |
| | (N)-pCBMA | 6.7 | 9.4; 1.38 | 77.0 | $9.5 \pm 1.6$ | $10.2 \pm 0.2$ | | |
| | (+)-pCBMA | 4.6 | 9.2; 1.34 | 56.3 | $8.6 \pm 1.0$ | $28.5 \pm 0.4$ | | |
| | | | | | | Biotin binding rate (s$^{-1}$) | HABA binding, $K_{assoc}$ (µM) | |
| Avidin | Native | -- | -- | -- | $5.8 \pm 0.5$ | $92.5 \pm 14.1$ | $2.13 \pm 0.09$ | |
| | (N) | 7.9 | -- | -- | $5.6 \pm 0.6$ | $1.09 \pm 0.07$ | $2.10 \pm 0.12$ | |
| | (+) | 7.0 | -- | -- | $6.3 \pm 1.8$ | $1.69 \pm 0.04$ | $2.11 \pm 0.10$ | |
| | (N)-pCBMA | 7.9 | 27.9; 1.82 | 237.4 | $26.8 \pm 2.5$ | $0.23 \pm 0.07$ | $0.56 \pm 0.01$ | |
| | (+)-pCBMA | 7.0 | 32.0; 1.93 | 241.0 | $26.9 \pm 3.4$ | $1.64 \pm 0.08$ | $0.71 \pm 0.01$ | |

| | | | | | | Turnover Number $k_{cat}$ (s$^{-1}$) | Michaelis Constant $K_M$ (µM) | Catalytic Efficiency $k_{cat}/K_M$ (µM$^{-1}$s$^{-1}$) |
|---|---|---|---|---|---|---|---|---|
| **Uricase** | **Native** | -- | -- | -- | 7.3 ± 3.0 | 3.42 ± 0.05 | 12.9 ± 0.6 | 0.266 ± 0.013 |
| | **(N)** | 25.3 | -- | -- | 8.5 ± 2.5 | 0.18 ± 0.01 | 119.4 ± 9.7 | 0.002 ± 0.0006 |
| | **(+)** | 19.8 | -- | -- | 8.7 ± 2.0 | 2.14 ± 0.04 | 25.4 ± 1.4 | 0.084 ± 0.005 |
| | **(N)-pCBMA** | 25.3 | 8.8: 1.41 | 257.6 | 16.1 ± 5.1 | U.D. | U.D. | U.D. |
| | **(+)-pCBMA** | 19.8 | 8.1: 1.36 | 195.4 | 17.3 ± 8.9 | 0.03 ± 0.003 | 22.0 ± 7.6 | 0.001 ± 0.0005 |
| **Acetylcholinesterase** | **Native** | -- | -- | -- | 8.6 ± 1.8 | 120.5 ± 3.3 | 309 ± 21 | 0.390 ± 0.029 |
| | **(N)** | 14.2 | -- | -- | 9.2 ± 2.7 | 98.6 ± 1.9 | 206 ± 12 | 0.479 ± 0.029 |
| | **(+)** | 10.2 | -- | -- | 9.4 ± 2.1 | 119.1 ± 2.7 | 337 ± 19 | 0.353 ± 0.021 |
| | **(N)-pCBMA** | 14.2 | 7.9; 1.35 | 184.0 | 12.3 ± 2.4 | 2.9 ± 0.1 | 275 ± 19 | 0.010 ± 0.007 |
| | **(+)-pCBMA** | 10.2 | 8.5; 1.34 | 158.5 | 11.9 ± 2.6 | 115.0 ± 3.2 | 329 ± 22 | 0.349 ± 0.026 |

*Stability*

The rates of heat-induced irreversible inactivation of lysozyme-initiators and subsequent lysozyme-polymer conjugates were assessed by measuring residual activities over time during incubation at 80 °C (**Figure 3.24A**). Lysozyme(N) had the lowest thermal stability and had lost approximately 60% of its original activity after 2 minutes at 80 °C. The stability of lysozyme(N) was regained upon growth of pCBMA and was similar to those of native, lysozyme(+), and lysozyme(+)-pCBMA. The rates of heat-induced irreversible inactivation of uricases were determined by measuring the residual activities over time at 75 °C. Uricase(N) stability was decreased in comparison to native uricase while uricase(+) was higher than native uricase (**Figure 3.24B**). Uricase(+)-pCBMA had a similar thermal stability as uricase(+). The rates of heat-induced irreversible inactivation of acetylcholinesterases were determined next by measuring the residual activities over time at 50 °C (**Figure 3.24C**). AChE(N) was irreversibly inactivated within the first 2 minutes of incubation at 50 °C. Stability was regained after growth

of pCBMA from AChE(N) and was comparable to the native enzyme. AChE(+) showed increased thermal stabilities over AChE(N) and was also comparable to native AChE. Conjugates of AChE(+)-pCBMA showed the highest thermal stabilities of all AChE samples retaining  approximately 70% activity after 60 minutes of incubation at elevated temperatures.
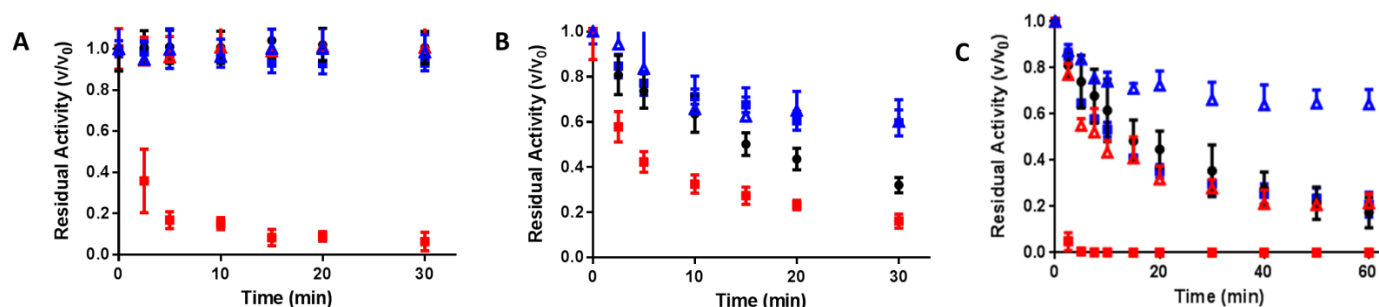


**Figure 3.24.** Thermal stabilities for grafted-from A) lysozyme samples (80 °C), B) uricase samples (75 °C), and C) acetylcholinesterase samples (50 °C) as residual activities over time normalized to activities at time 0. In all plots, native protein (●), protein(N) (■), protein(+) (■), protein(N)-pCBMA (△), and protein(+)-pCBMA (△). In general, samples prepared with the positive initiator had higher thermostabilities over their neutral counterparts. Error bars represent standard deviations from triplicate measurements.

## 3.5    Conclusions

Overall, conjugates grown from the positively charged bio-macroinitiator constructs all showed increased activities in comparison to their neutral bio-macroinitiator construct counterparts. All of the protein(+)-polymer conjugates also had increased thermostabilities in comparison to the protein(N)-polymer conjugates. As we had observed for CT, the stability curves of the protein(+) constructs were similar to, or better than, those for the native proteins.

Protein-polymer conjugate structure-function-dynamic relationships are important to understand in order to help guide future functional conjugate design. We have shown herein that the use of charged ATRP-initiators that restore surface charge close to native values is crucial to

maximizing activity and stability. Moreover, we are now able to safely grow incompatible homopolymers without deactivation or loss in stability, as demonstrated with CT. This can have many far-reaching implications. For example, many biomolecules have negatively charged surfaces/membranes. Having a therapeutic molecule coated with negatively charged polymers would increase repulsive electrostatic forces between these molecules to prevent unwanted interactions or uptake *in vivo*. Supramolecular assemblies could also be created using a bottom-up approach to fabricate higher ordered, reversible structures based on electrostatic interactions with negatively charged polymer conjugates. Additionally, negatively charged polymers containing carboxylic acids that are conjugated to biomolecules could be functionalized to attach drugs or targeting ligands using common carboxylic acid chemistries. Finally, conjugates that are highly negatively charged could increase the efficiency of purification and separation techniques that rely on electrostatic interactions such as ion-exchange chromatography. The idea of using a charge-maintaining initiator can further be generalized for other conjugation strategies. For example, when targeting residues that have negatively charged carboxylic acids, a negatively charged initiator might be beneficial. Additionally, the initiator structure can be designed in such a way that it places the charged group at a desired distance from the protein surface, which could tune activity. Taking inspiration from this work, we are now exploring the impact of amine-targeting positive charge retaining "grafting-to" strategies as a way to restore the activity of PEGylated proteins. Maintenance of long-range electrostatic interactions by surface charge retention protein-ATRP should be a general approach to enhancing the activity and stability of protein-polymer conjugates.

## Chapter 4. **Transforming protein-polymer conjugate purification by tuning protein solubility**

### 4.1 Chapter Summary

Almost all commercial therapeutic and industrial proteins are purified by processes that include salting-out precipitation in ammonium sulfate. Protein-polymer conjugates are generally synthesized from already pure starting materials and the struggle to separate the conjugates from polymer, native protein, and from differently modified variants has vexed scientists for decades. Since ammonium sulfate precipitation is exclusively used as an initial step in crude protein purifications, it has had little relevance in the delicate purification of protein-polymer conjugates. We have generated a family of protein-polymer conjugates with a variety of polymers, grafting densities, and polymer lengths using surface-initiated atom transfer radical polymerization. Covalently attached zwitterionic, positively charged, and negatively charged polymers increased solubility of the conjugates in ammonium sulfate and completely prevented precipitation even at 100% saturation (4.1M). Atomistic molecular dynamic simulations showed the impact was driven by an anti-polyelectrolyte effect from zwitterionic polymers. Zwitterionic polymer-protein conjugates even maintained activity in 4.1 M ammonium sulfate. Uncharged polymers exhibited polymer length-dependent decreased solubility in ammonium sulfate. We then used the newly discovered impact of growing polymers from the surface of the protein on salting-out to efficiently and simply purify mixtures of conjugates and native proteins into single species. Increasing a protein's solubility in salt through polymer conjugation, mimicking extreme halophiles found in nature, could also lead to many new applications of protein-polymer conjugates.

## 4.2 Introduction

Purification of proteins in biotechnology, typically by chromatography, accounts for 30-50% of manufacturing costs of high-value biopharmaceuticals[198] and is a major challenge that is often undervalued in this billion dollar industry. Purification via precipitation has been historically used for fractionation of biomolecules from blood plasma, but is becoming increasingly prevalent for other therapeutic biologics. Indeed, a recent study found that from 2010-2017, the number of precipitation patents has steadily increased totaling 246.[199] Most notably, the number of patents specifically for antibody purification via precipitation has shown the largest growth due to the ever-expanding fraction of antibodies being used therapeutically (both unmodified and PEGylated (PEG: polyethylene glycol) forms).[199] As such, large pharmaceutical companies including Amgen and Novartis, have increased their research and development investments to support this expansion.[199] There is an increasing demand for more efficient, simple, cost effective, and scalable protein purification methods, and precipitation methods have started to gain the most attention to help meet manufacturing needs.

Covalently attaching synthetic polymers to a protein, such as PEGylation, is one way to alter the bioactivity[14,46,48,101,103,150,200], stability[49,106,153,200,201], circulating half-life[3,5,7,64,157,162,202], and immunogenicity[97,165,203,204] of the resultant protein-polymer conjugate. Polymer attachment site,[34,100,179,180,205–207] number of attachments,[45,205] polymer type[48,49,153], polymer chain length[103,192,208], and conjugation chemistry[100,209–212] are all variables that can be tuned to optimize the conjugate's properties for a specific outcome, such as increased thermostability[111,152,213] or solubility. Protein solubility is especially important for therapeutic proteins which can require concentrations as high as 100 mg/mL for effective dose administration. High concentrations of proteins unfortunately enhance aggregation-based degradation.[214] Protein aggregation caused by poor solubility has also been linked to various disease states. For example, neurological diseases

such as Parkinson's or Alzheimer's are caused by protein aggregation.[215,216] Additionally, γD-crystallin's P23T (Pro23 to Thr) mutation reduces solubility and causes early onset of cataracts.[217,218] In industrial biotechnology, enzyme solubility in non-aqueous media is also of particular interest because new catalytic reactions become possible and more efficient due to increased solubilities of nonpolar substrates/products and reduction of unwanted hydrolytic side-reactions.[96,219–222]

Protein solubility depends on numerous intrinsic and extrinsic factors. The intrinsic chemical structure of the protein surface and the number of charged amino acids influence solubility.[223–225] In aqueous solutions, solubility is proportional to the number of charged amino acids on the protein surface.[223] Interestingly, proteins are least soluble at their isoelectric point (pI) where they have no net charge.[223] Therefore, chemical modification of the protein surface can alter solubility. Indeed, PEGylation of proteins and other hydrophobic drugs increases their solubility in water,[226] while conjugation of poly(2-(dimethylamino)ethyl methacrylate (pDMAEMA) was found to facilitate the molecular dissolution of α-chymotrypsin in acetonitrile.[227] Extrinsic factors including temperature, pH, ionic strength, and other additives can also impact solubility. It is difficult to accurately determine intrinsic protein solubility because many proteins are highly soluble requiring large amounts of lyophilized protein to reach saturation in a given volume. For this reason, additives such as salts, long-chain polymers, or organic solvents are often used to precipitate proteins to determine solubility.[224,225,228–230] Controlling protein solubility is at the very core of the biotechnology industry, since protein precipitation is an essential first step in almost all protein purification protocols.

The ability of a salt to precipitate a protein can be predicted by the Hofmeister series where kosmotropic salts stabilize protein structure and induce "salting out", while chaotropic

salts destabilize and promote "salting in".[225] Ammonium sulfate $((NH_4^+)_2SO_4^{2-})$ is strongly kosmotropic and has one of the highest solubilities in water (4.1 M at 25 °C) making it one of the most effective salts for protein precipitation without causing denaturation. In solution, proteins are always surrounded by a layer of water molecules known as the hydration layer. These water molecules interact with the protein surface through hydrogen bonding and electrostatic interactions and are essential for maintaining protein structure, dynamics, and bioactivity.[231] As the salt concentration is increased, the water molecules become attracted to the salt ions and are "pulled away" from the protein's surface. Eventually, the hydration layer is depleted which promotes protein-protein hydrophobic interactions and after enough aggregation, the proteins precipitate. The salting out point is different for each protein since each protein has a different surface charge composition and solubility. Ammonium sulfate precipitation is the principal technique in biotechnology used for both purification of a protein of interest from a crude mixture and for concentrating dilute solutions.[224,232,233]

Since proteins precipitate at a certain salt concentration, most organisms cannot survive in high salinity due to cytoplasmic protein aggregation. However, halophiles have adapted to living in areas containing high salts, such as the Dead Sea or the Great Salt Lake.[234–237] There are two mechanisms for how halophiles are able to do this. Halophiles accumulate osmolytes, such as betaines, in their cytoplasm that help control osmotic pressure while stabilizing proteins.[238,239] Halophiles have also evolved to control cellular salt fluxes and they have specially adapted intracellular proteins that withstand high salt concentrations.[234] Halophilic proteins have an abundance of negatively charged amino acids (aspartic acid, glutamic acid), short polar side chains, increased hydrophilicity, lower helical formation, and higher coil formation.[235,236] Halophiles have also been categorized depending on the NaCl concentration they survive in

where slight halophiles thrive in 0.34-0.85 M salt, moderate halophiles in 0.85-3.4 M salt, and extreme halophiles in 3.4-5.1 M salt.[237]

The intracellular betaine osmolytes used by some halophiles mimic the structure of zwitterionic polymer side chains originating from monomers such as 3-[[2-(methacryloyloxy) ethyl]dimethylammonio]propionate. Indeed, many studies have been performed to determine the behavior of zwitterionic polymers in salt solutions for applications in antifouling, antibacterial surfaces, surface wetting, and anti-icing.[240–244] We hypothesized that modifying the surface of a protein with rationally designed polymers would predictably tune protein solubility at high salt concentrations. In this Chapter, we used protein-initiated grafted-from atom transfer radical polymerization (ATRP) to create large families of protein-polymer conjugates with desired salting out behaviors. We varied the number of polymer chains (grafting density), polymer length (degree of polymerization, DP), and polymer type on a model protein, lysozyme (Lyz). Protein-polymer conjugate salting out points were determined by ammonium sulfate precipitation. We also determined changes in hydrodynamic diameters and stabilities over time in increasing ammonium sulfate concentrations using dynamic light scattering. Furthermore, we measured the enzymatic activities of the conjugates in 4.1 M ammonium sulfate. Atomistic molecular dynamic simulations provided mechanistic explanations for changes in conjugate solubility. Finally, we utilized the difference in salting out points of native protein and protein-polymer conjugates to purify the conjugates from a heterogeneous mixture.

## 4.3    Materials and Methods

Lysozyme (Lyz) from hen egg white, α-chymotrypsin (CT) from bovine pancreas, glycine, copper(II) chloride (Cu(II)Cl), sodium ascorbate (NaAsc), 1,1,4,7,10,10-hexamethyltriethylenetetramine (HMTETA), and poly(ethylene glycol) methyl ether

methacrylate (OEGMA$_{500}$) were purchased from Sigma-Aldrich (St. Louis, MO). 3-[[2-(Methacryloyloxy)ethyl]dimethylammonio] propionate (CBMA) was purchased from TCI America. HMTETA was purified using a basic alumina column. Pierce silver stain kit was purchased from ThermoFisher. SDS-PAGE gels (4-15% Mini-PROTEAN TGX precast gels) were purchased from Bio-Rad. All other chemicals were used without further purification and were purchased from Sigma Aldrich unless otherwise stated. The positively charged ATRP initiator was prepared as previously described.[212] Dialysis tubing for purification was purchased from Spectra/Por, Spectrum Laboratories Inc., CA.

### 4.3.1   Instrumentation

Ultraviolet-visible (UV-VIS) spectrophotometry (Lambda 45, PerkinElmer) was used to determine protein concentrations from bicinchoninic acid (BCA) assays. Number average ($M_n$), weight average ($M_w$), and dispersity (Đ) of polymers (cleaved and free) were determined by gel permeation chromatography (GPC) (Waters 2695 Series) with a data processor, three columns (Waters Ultrahydrogel Linier, 250 and 500), and a refractive index detector using a running buffer of Dulbecco's Phosphate Buffered Saline with 0.02 wt% sodium azide at a flowrate of 1.0 mL/min. Calibration was performed using Pullulan standards (Polymer Standards Service, Amherst, MA). Matrix-assisted laser desorption/ionization time-of-flight mass spectrometry (MALDI-ToF MS) data was acquired on a Perseptive Biosystems Voyager, Elite MALDI-ToF spectrometer located in the Center for Molecular Analysis at Carnegie Mellon University. Dynamic light scattering (DLS) hydrodynamic diameters were measured on a Malvern Zetasizer nano-ZS located in the Department of Chemistry at Carnegie Mellon University. Ammonium sulfate precipitation analysis and enzymatic activities were measured on a Synergy H1 Multi-Mode Plate Reader (BioTek Instruments, Winooski, VT).

### 4.3.2  ATRP Initiator modifications (1, 3, 5) on Lyz

**1 initiator modification.** To synthesize Lyz with an average of 1 initiator modification (Lyz(1+)), 100 mg (0.007 mmol Lyz, 0.049 mmol $NH_2$) of native Lyz was dissolved in 20 mL of 0.1 M sodium phosphate buffer, pH 8. 25 mg of positively charged ATRP initiator (0.049 mmol, 1 equivalent against the number of $NH_2$ groups) was dissolved in 100 μL of DMSO. The dissolved initiator was added to the Lyz solution and stirred at 4°C for 2 h. Lyz-initiator was then purified by dialysis (8 kDa MWCO) against deionized water at 4°C and was subsequently lyophilized.

**3 initiator modifications.** To synthesize Lyz with an average of 3 initiator modifications (Lyz(3+)), 150 mg (0.01 mmol Lyz, 0.073 mmol $NH_2$) of native Lyz was dissolved in 29 mL of 0.1 M sodium phosphate buffer, pH 8. 114 mg (0.221 mmol, 3 equivalents against the number of $NH_2$ groups) of positively charged initiator, dissolved in 1 mL DMSO, was added to the Lyz solution and stirred for 2 h at 4°C. Initiator modified Lyz was purified by dialysis as described above and was subsequently lyophilized.

**5 initiator modifications.** To synthesize Lyz with an average of 5 initiator modifications (Lyz(5+)), 500 mg (0.035 mmol Lyz, 0.245 mmol $NH_2$) of Lyz was dissolved in 100 mL of 0.1 M sodium phosphate buffer, pH 8. 631 mg of positively charged initiator (1.22 mmol, 5 equivalents against the number of $NH_2$ groups) was dissolved in 1 mL DMSO and was then added to the Lyz solution. The reaction solution was stirred at 4°C for 2 h. Initiator modified Lyz was purified by dialysis as described above and was subsequently lyophilized.

### 4.3.3  MALDI-ToF

Initiator modified Lyz (1 mg/mL) or native Lyz (1 mg/mL) was mixed with MALDI matrix (10 mg sinapinic acid, 250 μL of 0.1% trifluoroacetic acid and 250 μL of 50%

acetonitrile) in 1:1 ratio. 2 μL of mixed sample was loaded onto a sterling silver MALDI target plate. MALDI-TOF MS measurements were recorded using a Perseptive Voyager STR MS with a nitrogen laser (337 nm) and 20 kV accelerating voltage with a grid voltage of 90%. A total of 500 laser shots covering the complete spot were accumulated for each spectrum. Cytochrome C, apomyoglobin, and aldolase were used as calibration samples. The average number of initiator attached to Lyz was determined by taking the difference in peak m/z vales between native Lyz and Lyz-initiators and dividing by the mass of the reacted initiator (without NHS group) (321 Da).

### 4.3.4   ATRP from Lyz-initiator

**ATRP from Lyz(1+).** 20 mg of Lyz(1+) (1.4 μmol ATRP initiator groups) and 7.8 mg CBMA for target DP of 25, 62 mg CBMA for target DP of 200, 17 mg OEGMA for target DP of 25, and 136 mg OEGMA for target DP of 200 were dissolved in 1120 μL of 0.1 M sodium phosphate, pH 8. Lyz(1+) and monomer solutions were bubbled under argon for approximately 7 min. Concurrently, 336 μL of 50 mM Cu(II)Cl in deionized water was bubbled under argon in a separate flask for  2 minutes. Next, 16.8 μL of 100 mM sodium ascorbate was added to the Cu(II)Cl solution. After that, 5.3 μL of HMTETA was added to reduced Cu(II) to Cu(I) and the solution was bubbled for an additional minute. Next, 280 μL of the Cu/ligand solution was added to the Lyz-initiator/monomer solution using a syringe and the sealed solution was stirred for 1 h. The reaction was stopped by exposure to air and then the conjugates were purified using dialysis (8 kDa MWCO) against deionized water for 24 h and were subsequently lyophilized.

**ATRP from Lyz(3+).** 30 mg of Lyz(3+) (6.4 μmol initiator groups) was dissolved in 5760 μL of 0.1 M sodium phosphate, pH 8. 37 mg CBMA or 81 mg OEGMA (target DP 25) and 295 mg CBMA or 644 mg OEGMA (target DP 200) were added to Lyz(3+) and bubbled for 15

min under argon. In a separate flask, 768 µL of 100 mM Cu(II)Cl solution was bubbled under argon for 2 min. Next, 77 µL of 100 mM sodium ascorbate solution was added to the bubbling Cu(II)Cl solution. Then, 25 µL HMTETA ligand was added to reduced Cu(II) to Cu(I) and the solution was bubbled for an additional minute. Next, 640 µL of the Cu/ligand solution was transferred via syringe to the Lyz-initiator/monomer solution. The polymerization was stopped by exposure to air after 1 h of stirring. The conjugates were purified using dialysis (8 kDa MWCO) against deionized water for 24 h and were subsequently lyophilized.

**ATRP of CBMA from Lyz(5+).** 30 mg (9.5 µmol initiator groups) of Lyz(5+) was dissolved in 18 mL of 0.1 M sodium phosphate, pH 8. 54 mg, 109 mg, 217 mg, 326 mg, and 434 mg CBMA (for the target DP of 25, 50, 100, 150 and 200, respectively) were added to Lyz(5+) and were bubbled under argon for 45 min. In a separate flask, 2.4 mL of 50 mM Cu(II)Cl solution was bubbled for 10 min. Next, 114 µL of 100 mM sodium ascorbate was added to reduce Cu(II) to Cu(I) and then 37 µL of HMTETA ligand was added. After that, 2 mL of the Cu/ligand solution was added to Lyz-initiator/CBMA solution. The reaction was stopped upon exposure to air after 1 h for stirring and the Lyz(5+)pCBMA conjugates were purified using dialysis (8 kDa MWCO) against deionized water for 24 h and were subsequently lyophilized.

**ATRP of OEGMA from Lyz(5+).** 32 mg (10 µmol initiator groups) of Lyz(5+) and 126 mg, 252 mg, 505 mg, 758 mg and 1010 mg OEGMA (for the target DP of 25, 50, 100, 150 and 200, respectively) were dissolved in 9 mL of 0.1 M sodium phosphate, pH 8. The Lyz(5+)/monomer solution was bubbled for 30 min under argon. In a separate flask, 1.2 mL of 100 mM Cu(II)Cl solution was bubbled for 10 min. Next, 120 µL of 100 mM sodium ascorbate was added to reduce Cu(II) to Cu(I) and then 39 µL of HMTETA ligand was added. Then, 1 mL of the Cu/ligand solution was added to the Lyz(5+)/OEGMA solution. The reaction was stopped

upon exposure to air after 1 h or stirring and the Lyz(5+)pOEGMA conjugates were purified using dialysis (8 kDa MWCO) against deionized water for 24 h and were subsequently lyophilized.

### 4.3.5    Free polymer synthesis

4.7 mg (0.92 mM final concentration) of neutral initiator (synthesized as previously described[47]) and 442 mg CBMA (target DP 100) or 894 µL OEGMA (target DP 100) were dissolved in 20 mL of deionized water and were bubbled under argon for 30 min. In a separate flask, 78 mg of Cu(II)Cl in 3 mL of deionized water was bubbled under argon. Next, 573 µL of a 20 mg/mL sodium ascorbate solution was added to reduce Cu(II) to Cu(I) and the solution was bubbled for 5 min before adding 186 µL of HMTETA, followed by additional bubbling for 1 minute. Next, 1 mL of the Cu/ligand solution was transferred to the initiator/monomer solution via syringe and the sealed flask was stirred for 1 h at 25 °C. The final concentrations in the ATRP reaction were 92 mM monomer, 0.92 mM initiator, 9.2 mM Cu(II) (reduced), 11 mM HMTETA, and 0.92 mM NaAsc. The polymerization was stopped by exposure to air and the polymers were purified by dialysis (1 kDa MWCO) against deionized water for 24 h at 25 °C. Purified polymers were then lyophilized and analyzed by GPC for molecular masses and dispersities.

### 4.3.6    BCA assay to determine protein concentration

To determine the protein content in the conjugates, 1-3 mg/mL of Lyz-polymer samples were prepared in deionized water. 25 µL of the sample was then mixed with 1 mL of BCA solution (50:1 vol:vol of BCA and Cu(II)SO$_4$) and incubated at 60°C for 15 min. The absorbance was recorded at 562 nm. Protein concentration was determined against a standard curve of native

Lyz (0.8-0.012 mg/mL) in deionized water. Lyz-polymer conjugates molecular masses and degree of polymerizations were estimated as previously described.[47]

### 4.3.7 Dynamic light scattering to determine conjugate size in PBS

Hydrodynamic diameters of Lyz samples were determined on a Malvern Zetasizer nano-ZS. Lyz samples (native, initiator modified, and polymer modified) were dissolved at 1 mg/mL in 0.1 M sodium phosphate buffer, pH 8. Samples were filtered using a 0.45 μM cellulose acetate syringe filter and measured three times (15 runs per measurement). Reported values are number distribution hydrodynamic diameters.

### 4.3.8 Acid hydrolysis and GPC

10-15 mg of Lyz-polymer conjugates were dissolved in hydrolysis tubes using 6N HCl (5 mL). After three repetitions of freeze-pump-thaw cycles, the samples were place in an oil bath at 110°C under vacuum for 20 h. Cleaved polymers were purified by dialysis (1 kDa MWCO) against deionized water and were then lyophilized. Cleaved polymers were analyzed by GPC for molecular masses and dispersities using pullulan standards as previously described.

### 4.3.9 Ammonium sulfate precipitation

Native protein, protein-initiators, and protein-polymers were dissolved at 2 mg/mL protein concentration (starting volume was 1 mL) in 50 mM NaPhos buffer, pH 7. The initial concentrations of protein in the samples were measured by the absorbance 280 nm using a Synergy H1 plate reader. Absorbance values were converted to concentrations based on a standard curve of native protein (0 to 2 mg/mL). Solid amounts of ammonium sulfate were added to the solutions to reach the desired percent saturation as calculated from EnCor Biotechnology's online calculator at 25 °C (http://www.encorbio.com/protocols/AM-SO4.htm). After each

ammonium sulfate addition, samples were vortexed to ensure full dissolution of the ammonium sulfate. The samples were then allowed to sit on the benchtop for 15 min followed by centrifugation at 16, 800$\times$g for 20 min to pellet any precipitated protein. The protein concentration in the supernatant was measured in triplicate by the absorbance at 280 nm. The supernatant used to determine protein concentration was place back into the sample and the next solid mass of ammonium sulfate was added. The process of mixing, sitting, centrifuging, and measuring protein concentration was repeated after each ammonium sulfate addition until 100% saturation (4.1 M) was reached. The addition of ammonium sulfate increased the solution volume to 1.42 mL at 100% saturation.

Ammonium sulfate was also performed for native protein in the presence of free pCBMA or pOEGMA. In this case, native Lyz was dissolved at 2 mg/mL (1 mL starting volume) in 50 mM NaPhos buffer, pH 7. Lyophilized pCBMA or pOEGMA was added to match the amount (by mass), as estimated from the BCA results, of polymer present during the precipitation experiment of Lyz(5+)pCBMA DP 91 and Lyz(5+)pOEGMA DP 164. The process of ammonium sulfate precipitation was then carried out as previously described.

### 4.3.10 Dynamic light scattering to determine conjugate size in ammonium sulfate

Native protein, protein-initiators, and protein-polymers were dissolved at 1 mg/mL protein concentration (starting volume was 1 mL) in 50 mM NaPhos buffer, pH 7. Solutions were filtered using a 0.45 µM cellulose acetate syringe filter. The process used for ammonium sulfate precipitation, as described above, was repeated, but instead of measuring protein concentration in the supernatant, the hydrodynamic diameters were measured in triplicate (15 runs per measurement). Hydrodynamic diameters were measured at increasing ammonium sulfate concentrations until 100% saturation was reached. The changes in solution refractive

index,[245] dielectric constant,[246] and viscosity[247] with increasing salt did not affect the hydrodynamic diameter output.

### 4.3.11 Dynamic light scattering to measure size stability

Lyz(5+)pCBMA DP 14 and DP 91 were dissolved at 1 mg/mL in 50 mM NaPhos buffer, pH 7. 0.77 mg of solid ammonium sulfate was added and dissolved to reach 100% saturation. Samples were filtered using a 0.45 µM cellulose acetate syringe filter. Immediately after filtering, hydrodynamic diameters were measured over 6 h, then again after 1 week, 2 weeks, and 2.5 months. Number and volume distributions were recorded from 15 scans per measurement.

### 4.3.12 Dynamic light scattering to measure size reversibility

Lyz(5+)pCBMA DP 91 was dissolved in 100% saturated ammonium sulfate at 1 mg/mL and the hydrodynamic diameter was measured. The sample was then diluted to 50% saturation (0.5 mg/mL) and 25% saturation (0.25 mg/mL) and hydrodynamic diameters were measured after each dilution as previously described. Size reversibility was also tested by cycling between 50% and 100% saturation. Lyz(5+)pCBMA DP 91 was dissolved in 50% saturated ammonium sulfate at 1 mg/mL. The hydrodynamic diameter was measured and then solid ammonium sulfate was added to reach 100% saturation, followed by another hydrodynamic diameter measurement. The solution was then diluted to 50% saturation again (0.5 mg/mL), measured by DLS, then ammonium sulfate was added to reach 100% saturation again. This process was repeated one more time for a total of 3 complete cycles. Hydrodynamic diameters were measured as described previously.

### 4.3.13 Molecular Dynamic Simulations

Lyz's crystallographic structure (PDB ID "1AKI") was used to build the native protein structure. The reduce code in Ambertools[248] was used to determine amino acid protonation states. The structures of free pCBMA (DP 18) and free pOEGMA (DP 25) were generated using the PySimm[120] software package's forcefield assisted linear self- avoiding random walk. The initiator structure was the positively charged ATRP initiator used experimentally in this study. Initiator-polymer structures were attached to the NZ atoms of Lyz at 5 sites: K1, K13, K33, K97, K116 which were determined from a rules-based prediction.[34] Lyz was modeled using the CHARMM C36m force field and initiators/polymers were modeled using analog parameters from CGenFF. [122,249,250] Topology files were generated using the psfgen tool within VMD software.[121] TIP3P water model, as implemented in NAMD, was used for solvation with a buffering distance of 14 Å. The system was neutralized by the addition of $Na^+$ and $Cl^-$ counterions. NaCl was additionally added at increasing molar concentrations (0.0, 0.15, 0.3, 1.0, 1.5, 2.0, 2.5, 3.0, and 5.0). The CUDA accelerated namd 2.13 was used to perform the atomistic MD simulations which was available in the high performance cluster, hipergator2, at the University of Florida.[124]

The conjugates were subjected to gradient energy minimizations over 10,000 steps while restraining the protein. The systems were further minimized for an additional 10,000 steps without restraint. Next, the conjugates were heated to 310.15 K in 20 ps intervals and 50 K increments using a NVT ensemble followed by 500 ps of additional simulation. After that, the NPT ensemble was applied to each system at 1 bar with a nonbonded cut-off of 12 Å and a force switching at 10 Å. Particle Mesh Ewald summation was used for long-range electrostatic interactions. Bond lengths involving hydrogen atoms were constrained using a 2 fs time step with the SETTLE algorithm. Simulations were performed for 500 ns for pCBMA and 200 ns for

pOEGMA and analyses were performed using in-house VMD tcl scripts. 200 ns was enough simulation time to see the collapse of pOEGMA for a relatively long time.

### 4.3.14 Enzymatic Activity Assay

Enzymatic activities of native Lyz, Lyz-initiators, and Lyz-pCBMA conjugates were measured using 4-Methylumbelliferyl β-D-N,N′,N″-triacetylchitotrioside, a small molecule fluorescent substrate ($\lambda_{ex}$ = 360 nm, $\lambda_{em}$ = 455 nm). Lyz solutions were prepared at 1 mg/mL (Lyz concentration) in 50 mM NaPhos, pH 6.0. The substrate was dissolved in DMSO at 5 mg/mL (6.4 mM). To start the reaction, 29 µL of the 1 mg/mL Lyz solutions (2 µM final concentration) was added with 8 µL of substrate solution (50 µM final concentration) and 963 mL of either 50 mM NaPhos (pH 6.0) or 100% saturated ammonium sulfate. Reactions were incubated at 37 °C in a water bath. At increasing time points over 4 hours, 50 µL of the reaction mixture was mixed with 150 µL of stop buffer (100 mM glycine-NaOH, pH 11) in a 96 well plate. The fluorescence intensities (relative fluorescence units: RFU) were then measured in triplicate. Reaction rates were corrected by blanks of the substrate (8 µL) in either NaPhos, pH 6.0 and 100% saturated ammonium sulfate (992 µL). RFU versus reaction time plots were fit to linear regressions in GraphPad.

### 4.3.15 Purification and SDS-PAGE gel analysis (pCBMA and pOEGMA)

Native Lyz and Lyz(5+)pOEGMA, and Lyz(5+)pCBMA DP 91 were prepared at 1 mg/mL in deionized water. Native Lyz and conjugates were mixed at a 1:99 volume ratio (10 µL native Lyz and 990 µL conjugate). Solid ammonium sulfate was added to reach 100% saturation for pCBMA (0.77 g) or 40% saturation for pOEGMA (0.25 g). The mixtures were allowed to sit for 1 h on the benchtop, followed by centrifugation at 16,800×*g* for 1 h. The supernatants were

aspirated and the precipitates were re-dissolved in 1 mL of deionized water. Supernatants and precipitates were dialyzed in deionized water to remove ammonium sulfate for 24 h at 4 °C. Ultrafiltration (3 kDa MWCO) was performed on dialyzed samples to concentrate them back to starting concentrations. SDS-PAGE analysis was performed on native Lyz, Lyz(5+)pCBMA DP 91, Lyz(5+)pOEGMA DP 164, supernatants, precipitates, the starting mixture (prior to salt addition), and standards. 25 µL of samples were mixed with 25 µL of sample buffer (190 µL of 2X Lamaelli sample buffer with 10 µL of 2-mercaptoethanol). Samples were heated at 95 °C for 10 min in an oil bath. Running buffer was composed of 1X Tris/Glycine/SDS buffer. Samples (20 µL or 10 µL of ladder) were loaded into the wells of a 4-15% precast gel and electrophoresis was run at 100 V, 4 W, 40 mA for 40 min. Gels were then silver stained following the protocol provided by the Pierce Silver Stain kit.

### 4.3.16  Chymotrypsin-polymer conjugate synthesis and characterization

Chymotrypsin (CT)-polymers that were previously synthesized and characterized[153] were used in the current study for ammonium sulfate precipitation analysis. Briefly, CT was modified with 12 neutral initiators and long chained polymers of zwitterionic poly(carboxybetaine methacrylate) (pCBMA), neutral poly(oligoethylene glycol methacrylate) (pOEGMA), neutral to positive poly(dimethylaminoethyl methacrylate) (pDMAEMA), positive poly(quarternary ammonium meth- acrylate) (pQA), or negative poly(sulfonate methacrylate) (pSMA) were grown from the surface of CT-neutral initiator using ATRP. Conjugates were characterized with a BCA assay and dynamic light scattering. Additionally, acid hydrolysis was performed to cleave polymers followed by GPC analysis.

## 4.4 Results and Discussion

### 4.4.1 Conjugate Synthesis and Characterization

Lysozyme-polymer conjugates were synthesized with a high grafting density and varied polymer chain lengths using grafting-from ATRP (**Figure 4.1**). Two polymers at five chain lengths each were chosen to study the effect of polymer attachment on solubility: zwitterionic poly(carboxybetaine methacrylate) (pCBMA) and neutral poly(oligo(ethylene glycol) methacrylate) (pOEGMA). These polymers also have significantly different octanol-water distribution coefficients (logD) where the logD of CBMA monomer is approximately -2.35 and OEGMA is approximately 0.84.[153] Clearly, CBMA is more hydrophilic than OEGMA and while both are net neutral, CBMA is highly charged. Small molecule positively charged ATRP initiators[212] were first reacted with the available 7 amino groups on Lyz's surface. The number of reacted initiators was determined by the change in mass of Lyz-initiator compared to native Lyz analyzed by matrix-assisted laser desorption/ionization time of flight (MALDI-ToF) mass spectroscopy (**Figure 4.2**). The average of 5 attached initiators (5+) were the sources for polymer growth via ATRP. Polymer chain length was increased by increasing the monomer to initiator ratio in the ATRP reaction (targeted DPs from 25 to 200). Lyz-polymer conjugates were purified via dialysis and were then lyophilized.

## 1. ATRP Initiator Attachment
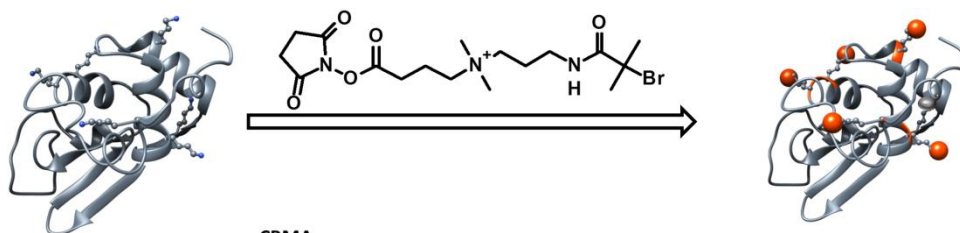


## 2. ATRP
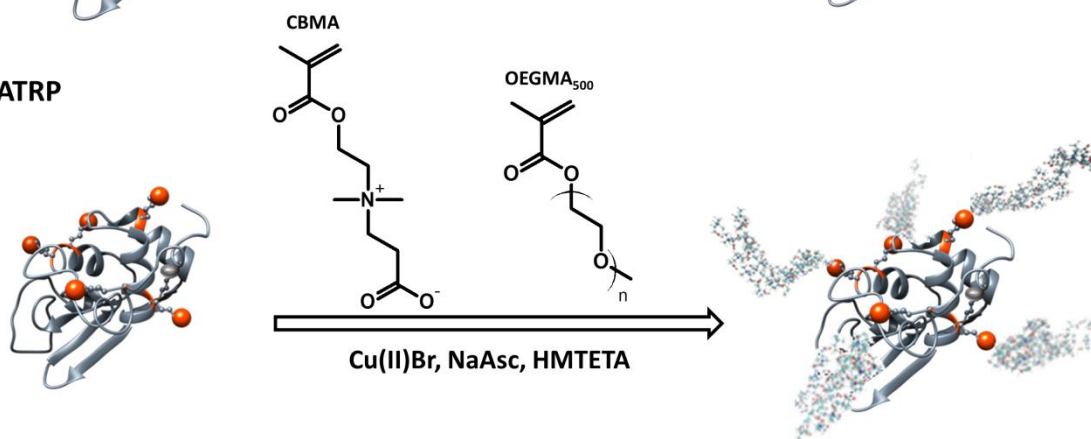


**Figure 4.1.** Grafting-from Lyz-polymer conjugate synthesis using ATRP. A positively charged ATRP initiator was first reacted with accessible amino groups on Lyz's surface. Next, ATRP was used to grow polymers of zwitterionic CBMA or neutral OEGMA at increasing polymer lengths. Additional acronyms: sodium ascorbate (NaAsc), 1,1,4,7,10,10-Hexamethyltriethylenetetramine (HMTETA).
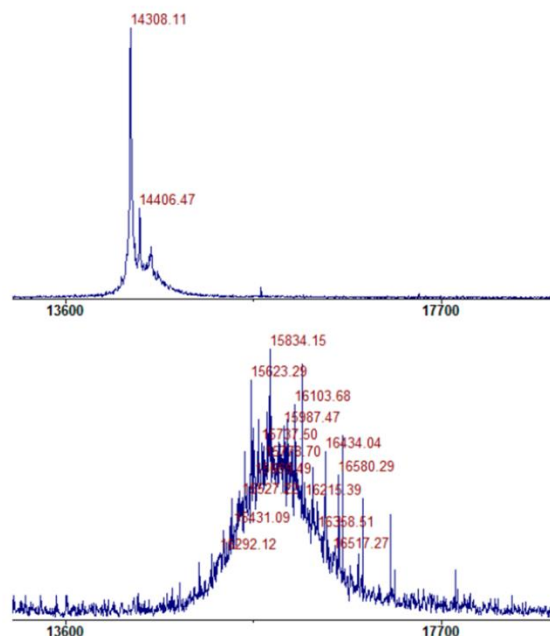
**Figure 4.2.** MALDI-ToF spectra of native Lyz (top) and Lyz-initiator (bottom). The number of attached initiators was calculated by the difference in m/z between Lyz-initiator and native Lyz divided by the mass of the initiator (321 Da). The average number of attached initiators was 4.8.

A bicinchoninic acid (BCA) protein assay was used to determine protein concentration in the conjugate samples from which polymer concentration, molecular mass, and degree of polymerization were estimated.[47] Targeted DPs during ATRP were 25, 50, 100, 150, and 200, yielding measured DPs of 18, 32, 56, 79, and 91 for pCBMA conjugates and 25, 43, 90, 105, 164 for pOEGMA conjugates, respectively (**Table 4.1**).

Conjugates were next characterized by dynamic light scattering (number distributions) in phosphate buffered saline (PBS) to determine how an increase in chain length correlated with increased conjugate size (**Figure 4.3**). Native Lyz had a hydrodynamic diameter of $3.6 \pm 0.1$ nm, Lyz-pCBMA conjugates increased in hydrodynamic diameters from $7.9 \pm 0.4$ nm (DP 18) to $16.8 \pm 0.8$ nm (DP 91), and Lyz-pOEGMA conjugates increased in hydrodynamic diameters from $9.2 \pm 0.8$ nm (DP 25) to $26.2 \pm 3.0$ nm (DP 164) (**Table 4.1**). Additionally, polymers were

148

cleaved from Lyz by acid hydrolysis and were analyzed by gel permeation chromatography (GPC) for molecular mass ($M_n$) and dispersity (Đ). Polymer $M_n$ increased from 8.1 kDa (Đ 1.4) to 38.7 kDa (Đ 1.9) for pCBMA and from 17.5 kDa (Đ 1.7) to 85.4 kDa (Đ 1.7) for pOEGMA (**Table 4.1, Figure 4.4, Figure 4.5**).

**Table 4.1.** Lyz-polymer characterization using a bicinchoninic acid (BCA) assay to estimate degree of polymerization (DP), dynamic light scattering number distribution to measure hydrodynamic diameter ($D_h$), and acid hydrolysis with gel permeation chromatography (GPC) to calculate number-average molecular mass ($M_n$) and dispersity (Đ) of cleaved polymer.

| Sample* | Estimated DP* | $D_h$ (nm) | Cleaved polymer $M_n$ (kDa) | Đ |
|---|---|---|---|---|
| **Lyz** | -- | $3.6 \pm 0.1$ | -- | -- |
| **Lyz(5+)pCBMA$_{25}$** | 18 | $7.9 \pm 0.4$ | 8.1 | 1.4 |
| **Lyz(5+)pCBMA$_{50}$** | 32 | $11.0 \pm 1.0$ | 11.9 | 1.6 |
| **Lyz(5+)pCBMA$_{100}$** | 56 | $13.4 \pm 0.9$ | 20.9 | 1.7 |
| **Lyz(5+)pCBMA$_{150}$** | 79 | $15.4 \pm 0.8$ | 30.8 | 1.8 |
| **Lyz(5+)pCBMA$_{200}$** | 91 | $16.8 \pm 0.8$ | 38.7 | 1.9 |
| **Lyz(5+)pOEGMA$_{25}$** | 25 | $9.2 \pm 0.8$ | 17.5 | 1.7 |
| **Lyz(5+)pOEGMA$_{50}$** | 43 | $12.6 \pm 1.1$ | 26.9 | 1.8 |
| **Lyz(5+)pOEGMA$_{100}$** | 90 | $20.2 \pm 1.7$ | 46.6 | 1.9 |
| **Lyz(5+)pOEGMA$_{150}$** | 105 | $22.2 \pm 2.9$ | 53.2 | 1.8 |
| **Lyz(5+)pOEGMA$_{200}$** | 164 | $26.2 \pm 3.0$ | 85.4 | 1.7 |

*Subscript numbers represent the targeted DP from the ATRP reaction. Estimated DPs are calculated from the BCA assay.[47] The (5+) represents the number of positively charged initiators on the conjugate.
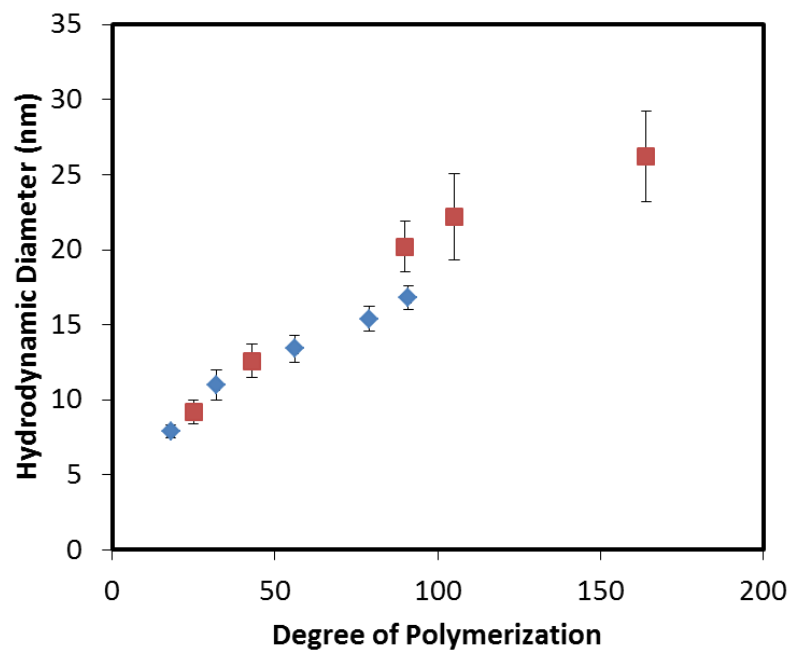
**Figure 4.3.** Dynamic light scattering hydrodynamic diameters, by number distribution, for Lyz(5+)pCBMA (blue diamonds) and Lyz(5+)pOEGMA (red squares) conjugates of increasing polymer length (DP).
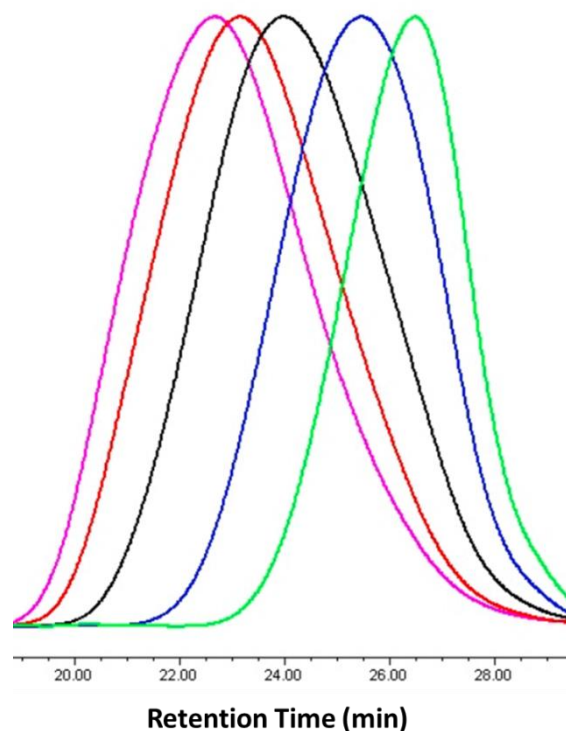
**Figure 4.4.** Gel permeation chromatography spectra of cleaved pCBMA from conjugates. Polymers were cleaved by acid hydrolysis (6N HCl) at 110 °C under vacuum overnight and then dialyzed in deionized water. Polymers increased in molecular mass as DP increased. DP 18 (green), DP 32 (blue), DP 56 (black), DP 79 (red), DP 91 (pink).
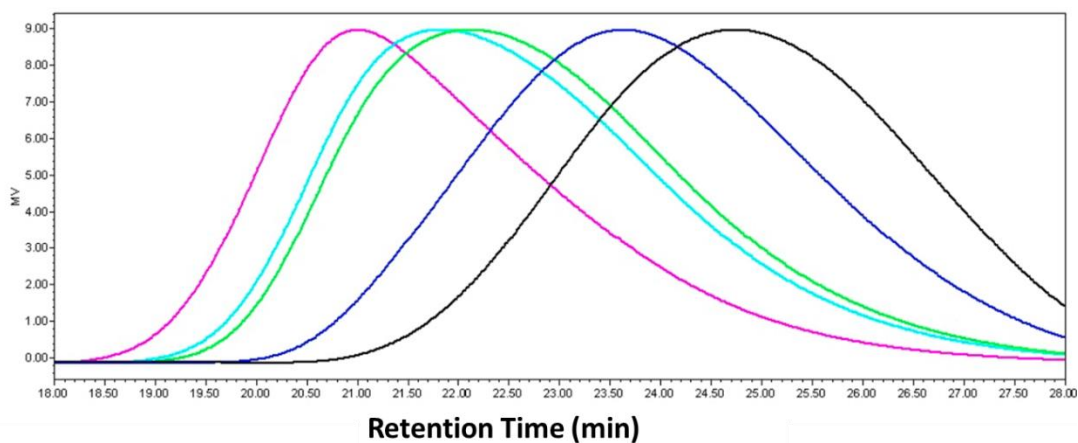


**Figure 4.5.** Gel permeation chromatography spectra of cleaved pOEGMA from conjugates. Polymers were cleaved by acid hydrolysis (6N HCl) at 110 °C under vacuum overnight and then dialyzed in deionized water. Polymers increased in molecular mass as DP increased. DP 25 (black), DP 43 (blue), DP 90 (green), DP 105 (cyan), DP 164 (pink).

151

### 4.4.2 Effect of Polymer Length on Conjugate Solubility

Native Lyz, Lyz-initiator, and Lyz-polymer conjugates were subjected to precipitation by ammonium sulfate at pH 7.0 to determine their salting out points (**Figure 4.6**). Lyz has been shown to salt out as predicted by the anion Hofmeister series at basic pH values and high ionic strength, but salt out according to the reversed anion Hofmeister series at neutral to acidic pH and moderate ionic strength.[251,252] Additionally, Lyz solubility can be predicted from the cation Hofmeister series when pH < pI (Lyz pI: ~11).[253] Native Lyz, as expected[223], precipitated around 60% saturated ammonium sulfate (2.5 M)  (**Figure 4.6A,B**). Lyz-initiator also precipitated around 60% saturation. A charge-preserving ATRP initiator[212] was used to synthesize the Lyz-conjugates so that the  positive charges on amino groups were retained after initiator attachment. Therefore, the net numbers of positive and negative charges on the protein surface were preserved after initiator attachment causing Lyz-initiator to salt out at a similar salt concentration to native Lyz.
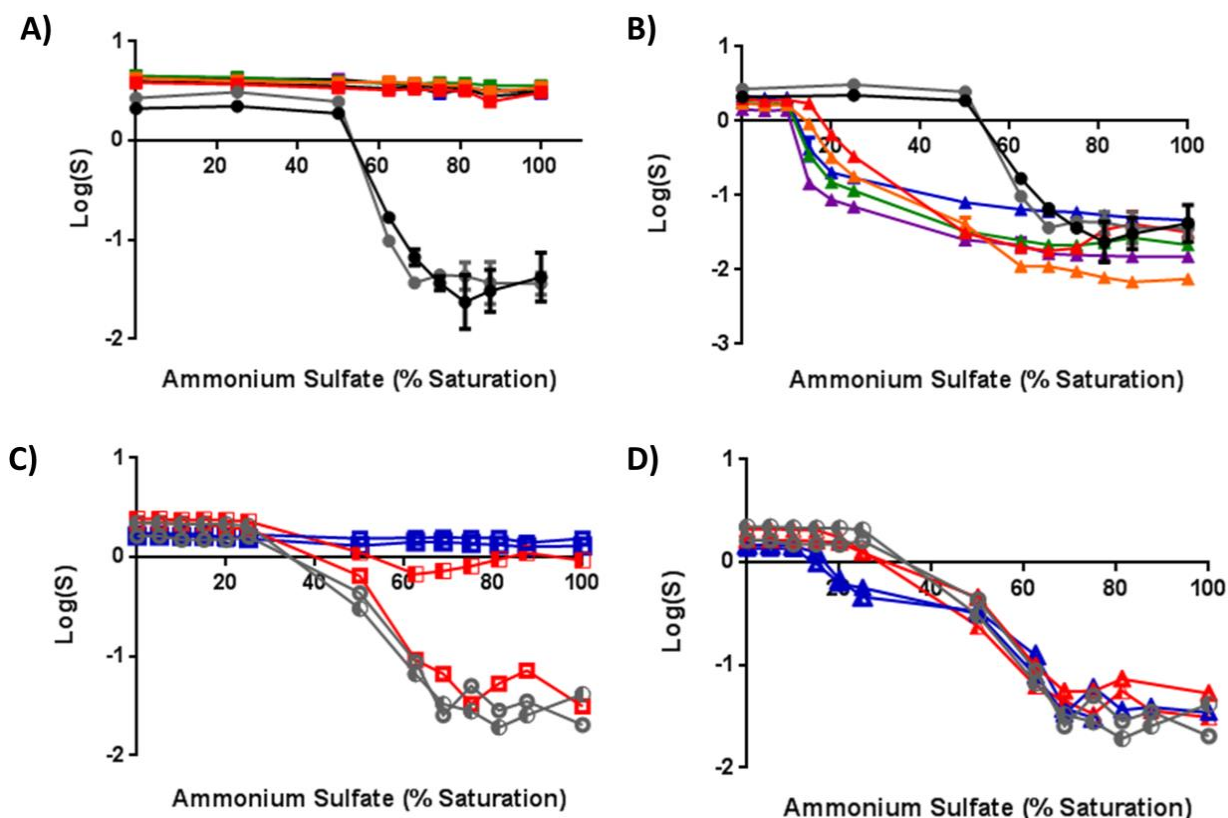
**Figure 4.6.** A-B) Ammonium sulfate precipitation of native Lyz (black circle), Lyz(5+) (gray circle), and Lyz-polymer conjugates. Plots are solubility (log of the supernatant protein concentration) versus ammonium sulfate percent saturation. 100% saturation corresponds to 4.1 M salt concentration. A) Lyz(5+)pCBMA conjugates with DP 18 (red square), DP 32 (orange square), DP 56 (green square), DP 79 (blue square), and DP 91 (purple square). B) Lyz(5+)pOEGMA conjugates with DP 25 (red triangle), DP 43 (orange triangle), DP 90 (green triangle), DP 105 (blue triangle), and DP 164 (purple triangle). pCBMA increased Lyz's solubility while pOEGMA decreased Lyz's solubility depending on DP. C-D) Ammonium sulfate precipitation of native Lyz(1+) (gray open circle), Lyz(3+) (gray half open circle), and Lyz-polymer conjugates with lower grafting densities and low/high DP. C) pCBMA conjugates of Lyz(1+) DP 14 (red open square), Lyz(1+) DP 44 (blue open square), Lyz(3+) DP 20 (red half open square), and Lyz(3+) DP 66 (blue half open square). The only pCBMA conjugate that precipitated was the lowest grafting density and lowest DP. D) pOEGMA conjugates of Lyz(1+) DP 9 (red open triangle), Lyz(1+) DP 93 (blue open triangle), Lyz(3+) DP 16 (red half open triangle), and Lyz(3+) DP 57 (blue half open triangle). pOEGMA length affected solubility more than grafting density. Error bars represent the standard deviations from triplicate measurements.

We expected that increasing pCBMA length would increase conjugate hydrophilicity and should therefore increase the salt concentration needed to salt out Lyz-pCBMA conjugates since free zwitterionic polymers are highly solvated in water and solvation increases with salt concentration.[254,255] Lyz(5+)pCBMA conjugates actually exhibited no salting out behavior,

independent of DP, even up to 100% saturation (4.1 M) (**Figure 4.6A**). Very few native proteins are soluble in 100% ammonium sulfate and most precipitate in the range of 40-60% saturation. Saturated ammonium sulfate is, after all, approximately 7 times the ionic strength of seawater. Conversely, Lyz(5+)pOEGMA conjugates exhibited a length-dependent reduction in salting out concentration (**Figure 4.6B**). Although the net surface charge on Lyz-pOEGMA was similar to native Lyz, the dense molecular shell of uncharged, amphiphilic polymers undoubtedly increased the hydrophobicity of the entire complex. Increasing the pOEGMA chain length decreased the conjugate's solubility. Long-chained Lyz(5+)pOEGMA with a DP of 164 precipitated around 10% saturation and the salting out point increased according to DP where short-chained DP 25 Lyz(5+)pOEGMA didn't precipitate until about 20% saturation. We surmised that conjugate hydrophobicity increased with pOEGMA length.[256]

We were interested in whether the observed differences in solubilities were due to covalent polymer conjugation versus the presence of polymer in solution since proteins have been precipitated non-covalently by some PEG's.[257,258] A more recent study found that unattached (free) charged polymers with the size 25 times larger than the protein's diameter could induce protein precipitation by wrapping themselves around the protein to neutralize surface charges.[259] We therefore synthesized free pCBMA and pOEGMA and performed ammonium sulfate precipitation of native Lyz in the presence of free polymers (**Figure 4.7 and Figure 4.8).** The concentrations of free polymers used matched the mass concentrations of polymers in the long-chained Lyz(5+)pCBMA (DP 91) and Lyz(5+)pOEGMA (DP 164) ammonium sulfate precipitation samples. The presence of free polymers did not affect Lyz solubility and Lyz precipitated around 60% saturation in the presence of both pCBMA and

pOEGMA, showing that covalent attachment of the polymer to the protein was required in order

to tune the solubility of the conjugates in salt solutions.
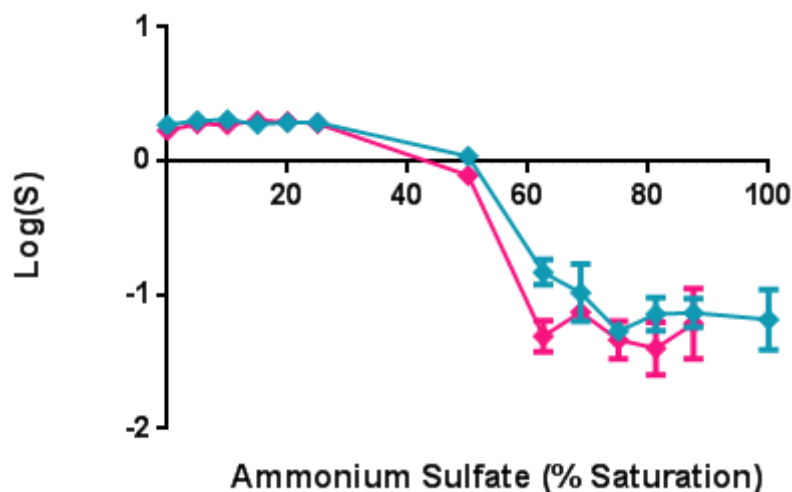


**Figure 4.7.** Ammonium sulfate precipitation of free native Lyz in solution with free pCBMA (cyan) or pOEGMA (pink). The amount of free polymer added was the same amount of polymer that was present in the Lyz-pCBMA DP 91 or Lyz-pOEGMA DP 164 samples during the conjugate ammonium sulfate precipitation experiment.
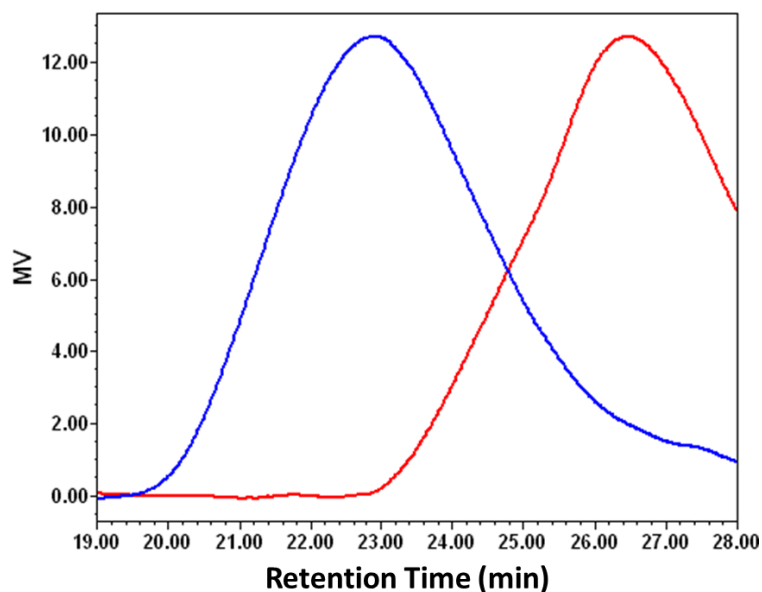


**Figure 4.8.** Gel permeation chromatography spectra of free pCBMA (red) and pOEGMA (blue).

155

### 4.4.3   Effect of Grafting Density on Conjugate Solubility

Since all of the Lyz(5+)pCBMA conjugates remained soluble up to 100% saturation and Lyz(5+)pOEGMA conjugates precipitated at relatively low percent saturations, we next investigated whether there was a minimum amount of polymer that would elicit a change in the salting out point from native Lyz. We synthesized Lyz-pCBMA and Lyz-pOEGMA conjugates with lower grafting densities, namely 1 and 3 average initiator modifications (**Figure 4.9**). From each Lyz-initiator, short and long chained pCBMA and pOEGMA were grown. Conjugates were characterized using a BCA assay to estimate DP[47] and DLS to determine hydrodynamic diameter (**Table 4.2**). Lyz with 1 initiator had pCBMA's of DP 14 (5.2 ± 0.8 nm) or DP 44 (6.0 ± 0.8 nm) and pOEGMA's of DP 9 (5.9 ± 0.8 nm) or DP 93 (14.0 ± 2.5 nm). Lyz with 3 initiators had pCBMA's of DP 20 (5.3 ± 1.1 nm) or DP 66 (12.7 ± 1.5 nm) and pOEGMA's of DP 16 (7.9 ± 1.5 nm) or DP 57 (18.0 ± 3.3 nm).
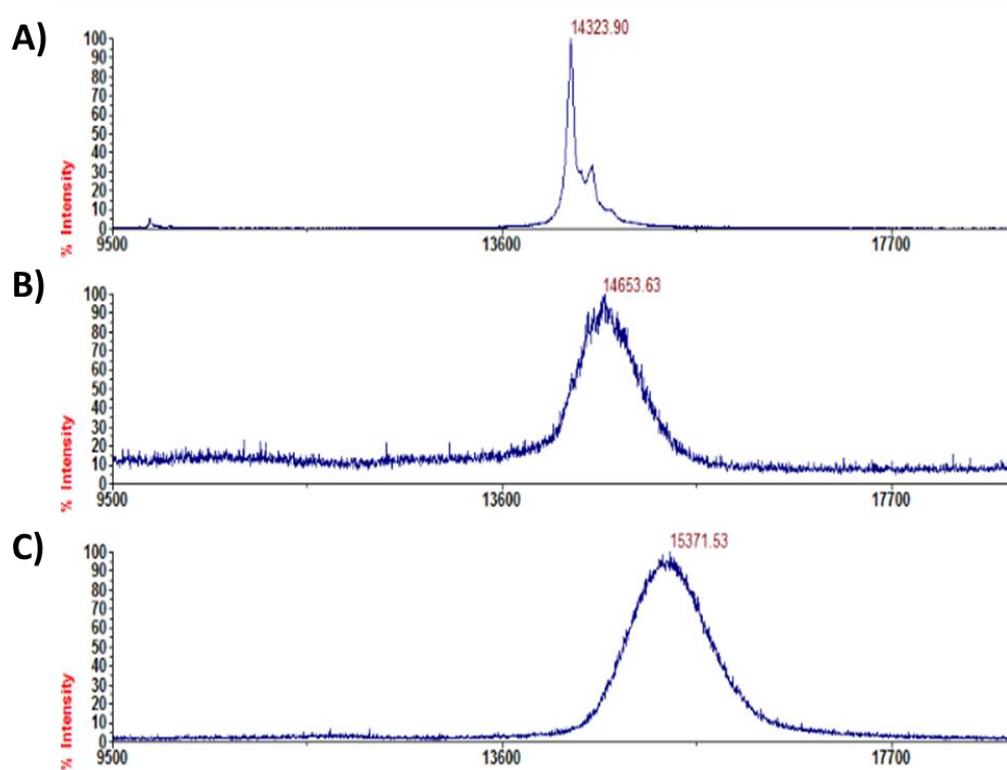


**Figure 4.9.** MALDI-ToF spectra of A) native Lyz, B) Lyz(1+), and C) Lyz(3+).

**Table 4.2.** Lyz-polymer characterization table for conjugates with 1 initiator (1+) or 3 initiators (3+).

| | Estimated DP* | $D_h$ (nm; number dist.) |
|---|---|---|
| **Lyz(1+)** | -- | $3.3 \pm 0.3$ |
| **Lyz(3+)** | -- | $3.7 \pm 0.2$ |
| **Lyz(1+) pCBMA** | 14 | $5.2 \pm 0.8$ |
| | 44 | $6.0 \pm 0.8$ |
| **Lyz(1+) pOEGMA** | 9 | $5.9 \pm 0.8$ |
| | 93 | $14.0 \pm 2.5$ |
| **Lyz(3+) pCBMA** | 20 | $5.3 \pm 1.1$ |
| | 66 | $12.7 \pm 1.5$ |
| **Lyz(3+) pOEGMA** | 16 | $7.9 \pm 1.5$ |
| | 57 | $18.0 \quad \pm 3.3$ |

*DP was estimated from BCA results.

Ammonium sulfate precipitation of the variable grafting density conjugates (**Figure 4.6C,D**) showed that the conjugate with the least amount of polymer, Lyz(1+)pCBMA DP 14 did not remain soluble in saturated ammonium sulfate. For Lyz-pOEGMA, polymer length, rather than grafting density, influenced the salting out point. Long chain pOEGMA conjugates with 1 or 3 initiators precipitated first (around 20% saturation) while short chained pOEGMA conjugates precipitated similarly to Lyz-initiator (at around 60% saturation). The range of concentrations over which the pOEGMA conjugates precipitated could have been related to heterogeneity within the samples (not every conjugate molecule has the same number of polymer chains attached). Indeed, ammonium sulfate precipitation should be an excellent route to fractionating heterogeneous polymer-protein conjugate solutions.

### 4.4.4   Zwitterionic Conjugate Stability in Ammonium Sulfate

Since all Lyz(5+)pCBMA conjugates had solubilities up to 100% saturated ammonium sulfate, we next investigated how their hydrodynamic diameters changed with increasing salt concentration and whether the size of the conjugates changed over time. Ammonium sulfate precipitation was performed again on Lyz(5+)pCBMA conjugates and DLS measurements of the supernatants were taken at each increasing ammonium sulfate concentration (**Figure 4.10A**). The hydrodynamic diameters of native Lyz and Lyz-initiator were relatively stable up to 50% saturation. Beyond this point, the samples precipitated and DLS measurements of the supernatants were not able to be performed. Lyz(5+)pCBMA conjugates, however, displayed reversible (**Figure 4.11**) increases in hydrodynamic diameters up to 100% saturation where the hydrodynamic diameters of all conjugates were around 60 nm by number distribution. Additionally, the standard deviation in the measurements increased as salt concentration increased.

Next, we determined the polymer length effect on the rate of change in conjugate $D_h$ during storage in saturated ammonium sulfate solution (**Figure 4.10B**).   The hydrodynamic diameters of both the short DP 18 and long DP 91 conjugates were stable for up to 2.5 months. Storage of protein solutions, especially for pharmaceuticals, in ammonium sulfate is of great interest because it inhibits bacterial growth and prevents contamination during shelf storage.[260]
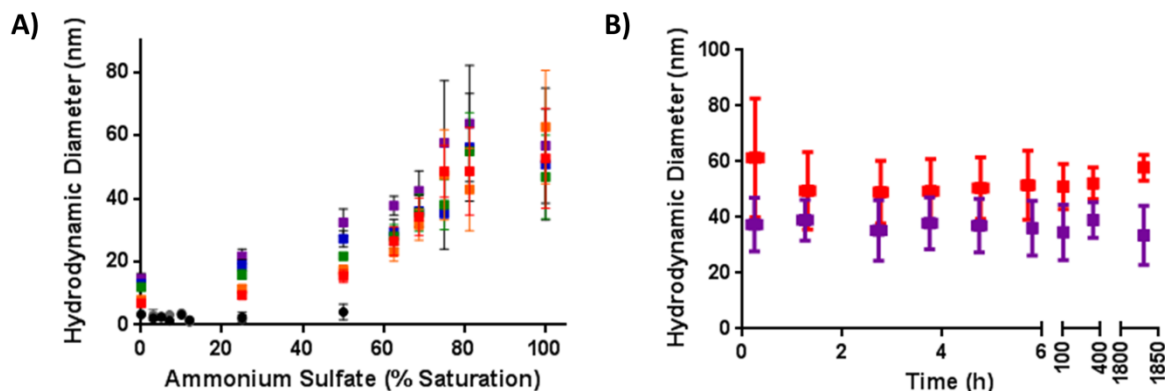
**Figure 4.10.** Dynamic light scattering data to measure hydrodynamic diameters (number distribution averages and errors) of A) Lyz(5+)pCBMA conjugates in increasing ammonium sulfate saturation for DP 18 (red square), DP 32 (orange square), DP 56 (green square), DP 79 (blue square), and DP 91 (purple square). All conjugates increased in hydrodynamic diameter with increased ammonium sulfate concentration. Native Lyz (black circle) and Lyz(5+) (gray circle) hydrodynamic diameters were not able to be measured after 50% saturation because samples precipitated. B) Lyz(5+)pCBMA DP 18 (red square) and DP 91 (purple square) hydrodynamic diameter stability over 2.5 months in 100% saturated ammonium sulfate.
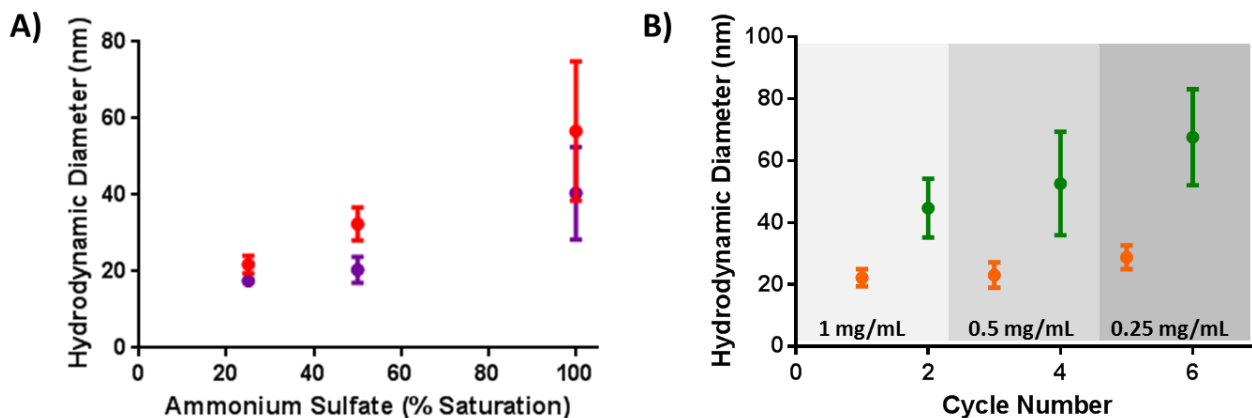


**Figure 4.11.** Hydrodynamic diameters (number distribution averages and errors) of Lyz(5+)pCBMA DP 91 in A) increasing (red circle) or decreasing (purple circle) ammonium sulfate concentrations and B) cycling between 50% (orange circle) and 100% saturation (green circle) over 3 complete cycles. This data shows that the change in hydrodynamic diameter with ammonium sulfate concentration is reversible.

The increases in pCBMA conjugate size with salt concentration could be attributed to either micro-aggregation or an actual change in conjugate size. Although single peaks were

detected in number distributions up to 100% saturation, multimodal peaks became prominent in the volume distributions at 70% saturation (**Figure 4.12**). At approximately this salt concentration, we also noted the increase in the standard deviations of the DLS measurements. This was indicative of a small degree of micro-aggregation, which did not result in precipitation, at ammonium sulfate concentrations above 70%. An actual change in conjugate size could have resulted from the anti-polyelectrolyte effect. The anti-polyelectrolyte effect of zwitterionic polymers has been studied in depth for non-fouling biomaterials, but has not been studied for the polymers bound to proteins.[241–243,254,261–265] Zwitterionic polymers are composed of an equal number of positive and negative charges. Intra- and inter-chain electrostatic interactions cause the polymer to adopt a more collapsed conformation in water. As salt concentration is increased, the salt ions neutralize the electrostatic interactions and allow the polymer chains to extend in solution and become more hydrated. Although the data reported herein would be the first direct observation of this effect in a protein-polymer conjugate, the anti-polyelectrolyte chain extension could have contributed to the observed increase in hydrodynamic diameter. Changes in polymer conformation caused by anti-polyelectrolyte effects would also increase intrinsic viscosity.[262,263] DLS actually measures the diffusion coefficient of a particle in solution due to Brownian motion and converts this parameter to a hydrodynamic diameter using the Stokes-Einstein equation. Therefore, an increase in intrinsic viscosity would decrease the diffusion coefficient of a particle and increase hydrodynamic diameter.[243,255] We therefore sought to determine whether zwitterionic polymer chains might extend as a function of salt concentration, and how such behavior would differ from pOEGMA-protein conjugates at the atomistic level.
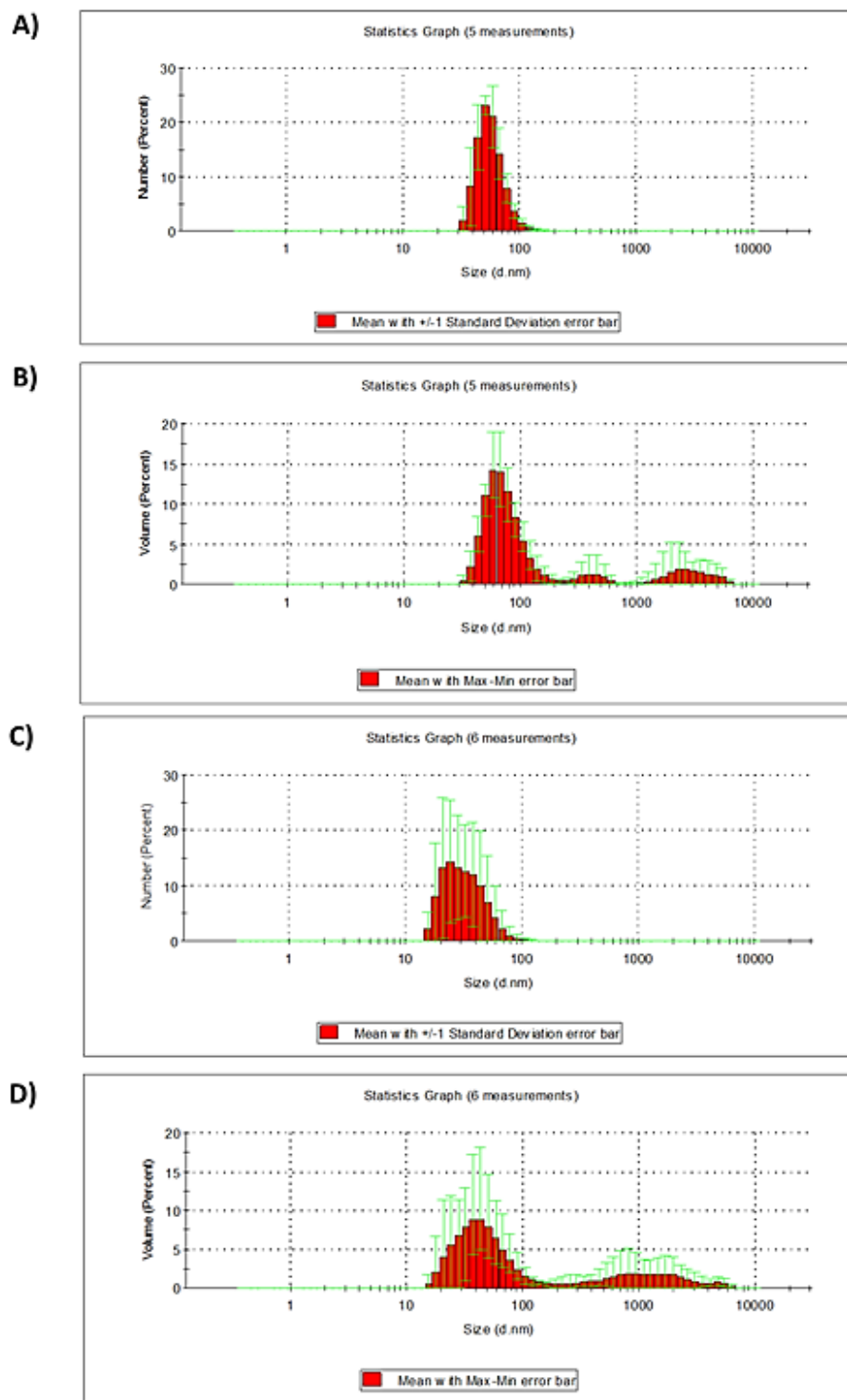
**Figure 4.12.** Hydrodynamic diameters in 100% ammonium sulfate saturation of Lyz(5+)pCBMA DP 18 by A) number distribution and B) volume distribution and DP 91 by C) number distribution and B) volume distribution after storage for 2.5 months. Multimodal peaks are present in volume distributions indicating micro-aggregation.

161

### 4.4.5 Atomistic Molecular Dynamics Simulations of Polymer Conformation on Protein-Polymer Conjugates as a Function of Salt Concentration

To determine the molecular basis for why zwitterionic polymers conjugated to proteins prevented salting out, atomistic molecular dynamics (MD) simulations were performed. On one hand, the conjugated zwitterionic polymers could have prevented depletion of the hydration layer around the protein. Alternatively, the hydration layer could be depleted, but the shell of highly charged zwitterionic polymers prevented proteins from aggregating and precipitating. We additionally sought to determine the mechanism for the early precipitation of Lyz-pOEGMA from MD.

Models of short-chained Lyz(5+)pCBMA (DP 18) and Lyz(5+)pOEGMA (DP 25) were built *in silico* attached to K1, K13, K33, K97, and K116, which were the lysine residues with the most exposed surface areas from a tertiary structure-based prediction.[34] Simulations were performed over 500 ns and 200 ns for Lyz-pCBMA and Lyz-pOEGMA, respectively, in increasing NaCl concentrations from 0.0 to 5.0 M. Simulations were also performed on free, unconjugated pCBMA chains (DP 18) and free pOEGMA chains (DP 25) (with positively charged initiators). First, the radii of gyrations ($R_g$'s) of free polymers were determined in increasing NaCl concentrations to determine the effect of salt on polymer conformations. pCBMA's average $R_g$ was approximately $12 \pm 1.5$ Å and while the average fluctuated slightly with NaCl concentration, there was no observable correlation indicating that pCBMA polymer chains sampled similar conformations (**Figure 4.13A**). Conversely, there was a significant change in the $R_g$ of pOEGMA as a function of increasing salt concentration (**Figure 4.13B**). At 0 M NaCl, pOEGMA's average $R_g$ was approximately 20 Å and the $R_g$ steadily decreased to 16 Å at 5 M NaCl. This indicated that pOEGMA chains were collapsing with increasing salt

concentration. These trends were consistent between the free polymer and conjugate simulations (**Figure 4.14 and Figure 4.15**).
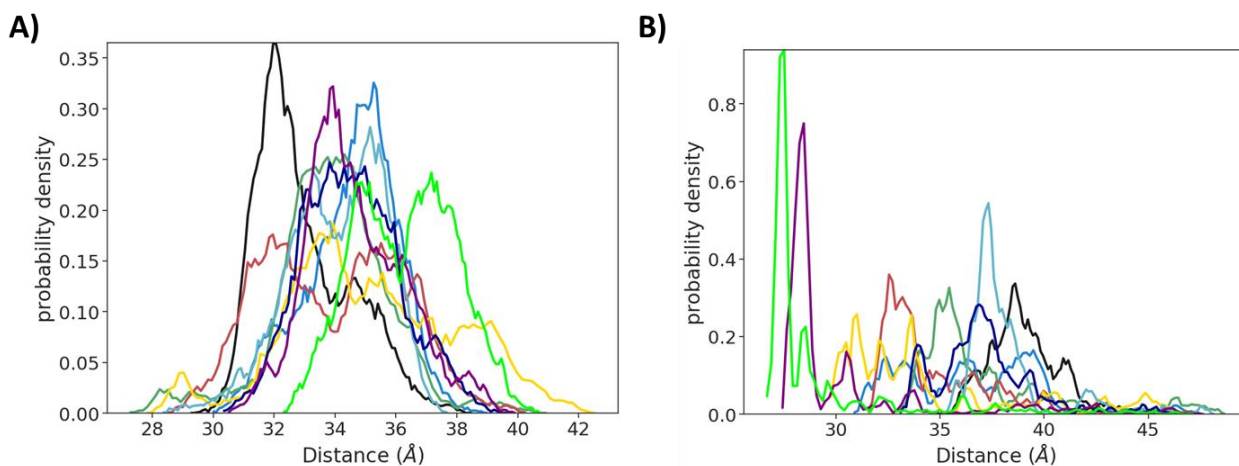


**Figure 4.13.** $R_g$ of A) Lyz(5+)pCBMA and B) Lyz(5+)pOEGMA in increasing  NaCl: 0.0 M (black), 0.15 M (blue), 0.3 M (green), 1.0 M (red), 1.5 M (yellow), 2.0 M (light blue), 2.5 M (dark blue), 3.0 M (purple), and 5.0 M (lime green).
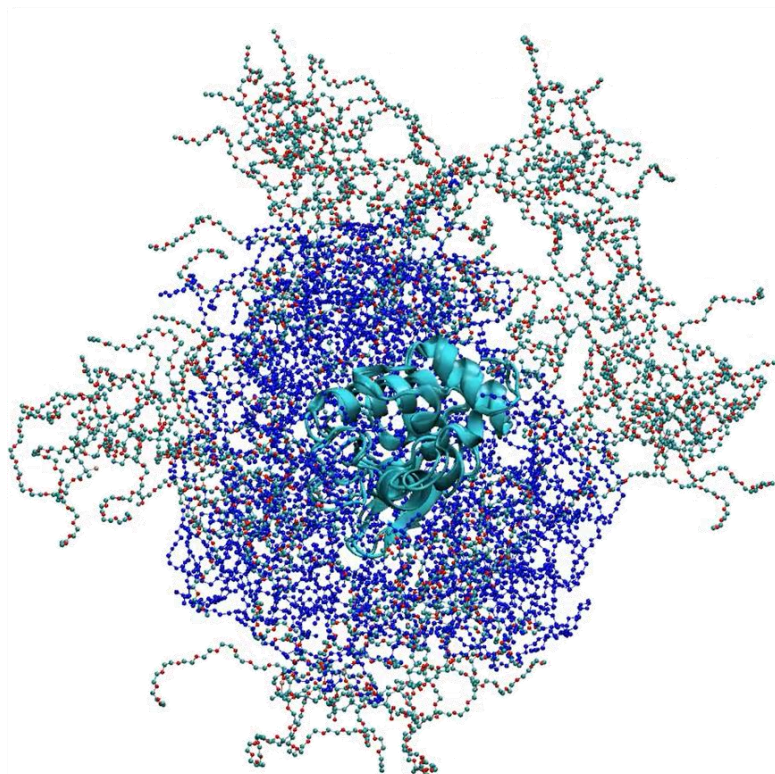
**Figure 4.14.** Overlaid snapshot of Lyz(5+)pOEGMA DP 25 in 0.0 M NaCl and 5.0 M NaCl. The dark blue pOEGMA chains at 5.0 M are collapsed around the protein surface.

In order to determine the local arrangement of solvent molecules (water, Na$^+$ and Cl$^-$ ions) near the conjugates, radial distribution function (RDF) analyses were performed between the solvent molecules and the O$^-$ atoms in pCBMA side-chains or PEG's in the pOEGMA side-chains. Essentially, these calculations determined the probability of finding solvent molecules within a certain distance of the polymer chains. For Lyz(5+)pCBMA, as the NaCl concentration increased, an additional solvation layer emerged corresponding to the appearance of a peak around 3.5 Å while maintaining the additional peaks at distances up to ~10.0 Å (**Figure 4.15C**). Furthermore, the dominant peak around 2.5 Å decreased in intensity as NaCl concentration increased indicating that some of the water molecules that were previously in the 1$^{st}$ hydration layer moved further away to form the additional hydration layers. Moreover, as salt

164

concentration increased, the presence of nearby $Cl^-$ ions increased and $Na^+$ ions decreased. This can be effectively seen by the increase in the peak intensity around 3.5 Å at 5.0 M NaCl (**Figure 4.15D and Figure 4.16).** This phenomenon aligns well with the anti-polyelectrolyte effect and further validates the trend of increasing hydrodynamic diameters (**Figure 4.10A**). The increase in hydrodynamic diameter was therefore not due to pCBMA chain extension. Additionally, the change in hydration layers of Lyz(5+)pCBMA matched that of free pCBMA showing that pCBMA-solvent interactions are similar in response to increased NaCl concentrations whether free in solution or attached to a protein surface (**Figure 4.17**). We have previously shown, through MD simulations, that poly(carboxy betaine) acrylamide chains were highly dynamic and did not interact strongly with a protein surface.[153] This is also seen qualitatively in the Lyz(5+)pCBMA conjugate snapshot (**Figure 4.18**) in low and high salt concentrations. Therefore, although Lyz's surface is highly decorated with different charged amino acids, the presence of this complex interface did not affect the salt-induced changes in pCBMA conformation. The extension of polymer chains away from Lyz's surface left much of Lyz's surface exposed, confirming that the altered solubility of Lyz-polymer conjugates was derived from changes in Lyz's physicochemical properties rather than polymer wrapping around the protein to mask Lyz's surface properties.

Hydration layers were also determined for Lyz(5+)pOEGMA and free pOEGMA in increasing NaCl concentration. RDFs were consistent between free and conjugated simulations. There were two discernable hydration layers around the PEG units in pOEGMA (2.5 and 5.0 Å) and while the total number of hydration layers remained constant, the likelihood of finding a water molecule in those layers decreased with increasing NaCl concentration (**Figure 4.15E**). Additionally, the probability of finding a $Cl^-$ or $Na^+$ ion near pOEGMA decreased (**Figure 4.15F**

**and Figure 4.16**). It is important to note that both $R_g$ and level of hydration start to significantly decrease after 1.5 M salt concentration, corresponding to 36% saturated ammonium sulfate, which is the point at which almost all of Lyz(5+)pOEGMA has precipitated (**Figure 4.6B**). Overall, the salting out of Lyz-pCBMA conjugates was prevented because the hydration layers around the conjugate increased with increasing salt concentration. Lyz-pOEGMA conjugates collapsed and displayed a decreased hydration which could have promoted precipitation.
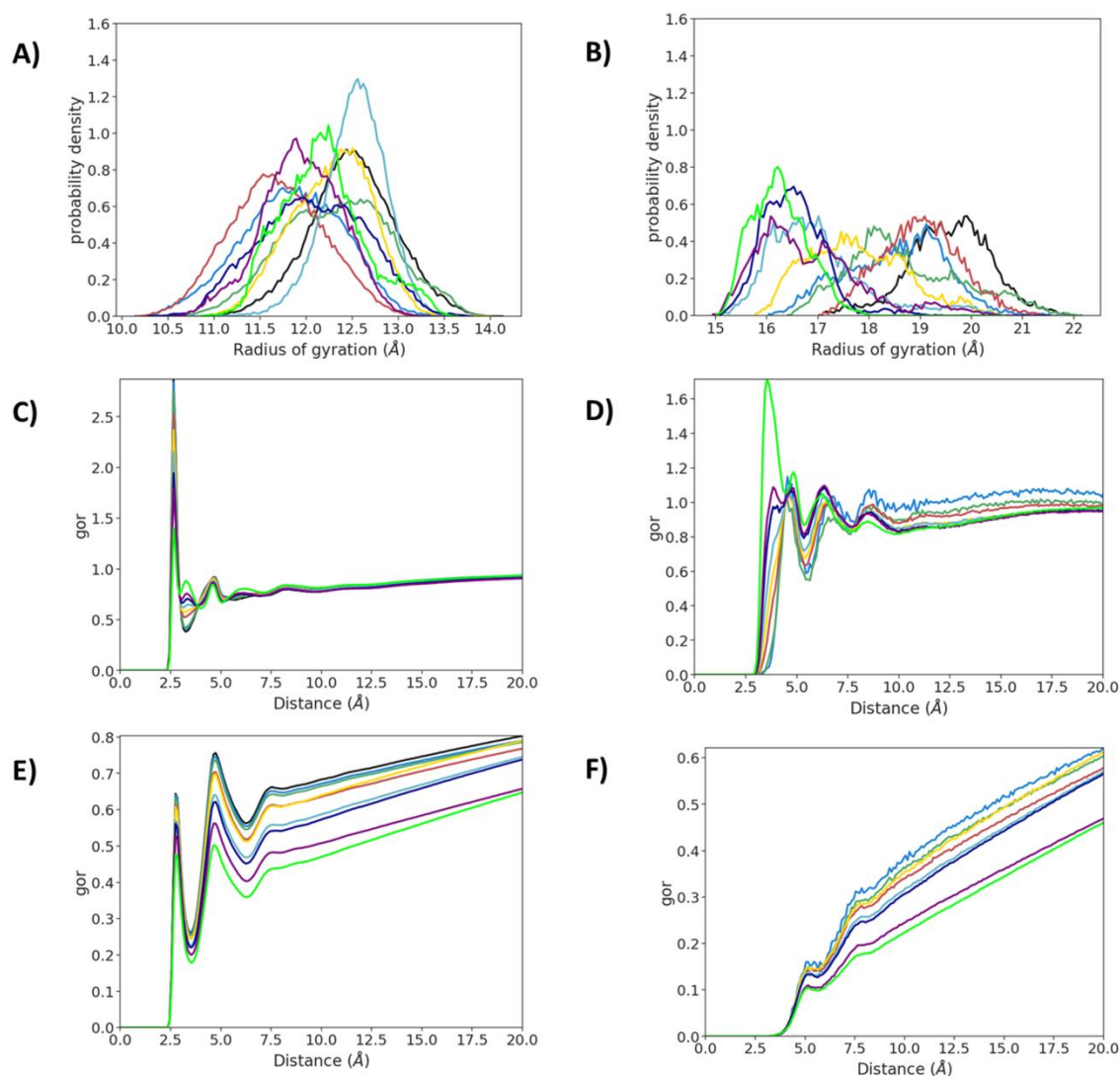


**Figure 4.15.** Radius of gyration of A) free pCBMA and B) free pOEGMA in increasing NaCl concentration. Radial distribution functions (RDF) for Lyz(5+)pCBMA DP 18 between C) water molecules and O⁻ atoms of pCBMA and D) Cl⁻ ions and O⁻ atoms of pCBMA in increasing NaCl

166

concentrations. Hydration layer increases as NaCl concentration increases and both water molecules and $Cl^-$ ions become more ordered. Radial distribution function analyses for Lyz(5+)pOEGMA DP 25 between E) water molecules and PEG in the pOEGMA monomer side-chain and F) $Cl^-$ ions and PEG in the pOEGMA monomer side-chain in increasing NaCl. Hydration decreases with increasing salt for Lyz(5+)pOEGMA. Legend: 0.0 M (black), 0.15 M (blue), 0.3 M (green), 1.0 M (red), 1.5 M (yellow), 2.0 M (light blue), 2.5 M (dark blue), 3.0 M (purple), and 5.0 M (lime green).
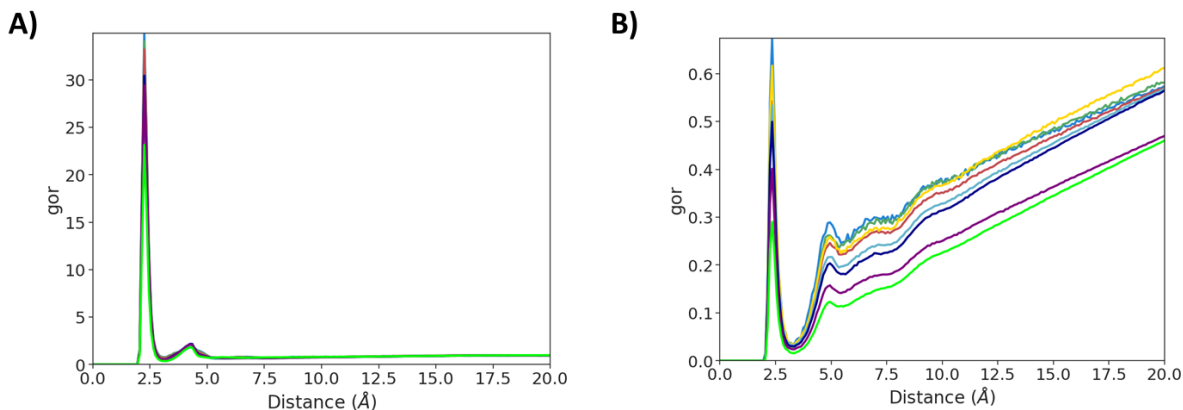


**Figure 4.16.** Radial distribution function analyses between $Na^+$ ions and $O^-$ atoms of A) Lyz(5+)pCBMA and PEG's of B) Lyz(5+)pOEGMA. NaCl: 0.15 M (blue), 0.3 M (green), 1.0 M (red), 1.5 M (yellow), 2.0 M (light blue), 2.5 M (dark blue), 3.0 M (purple), and 5.0 M (lime green).
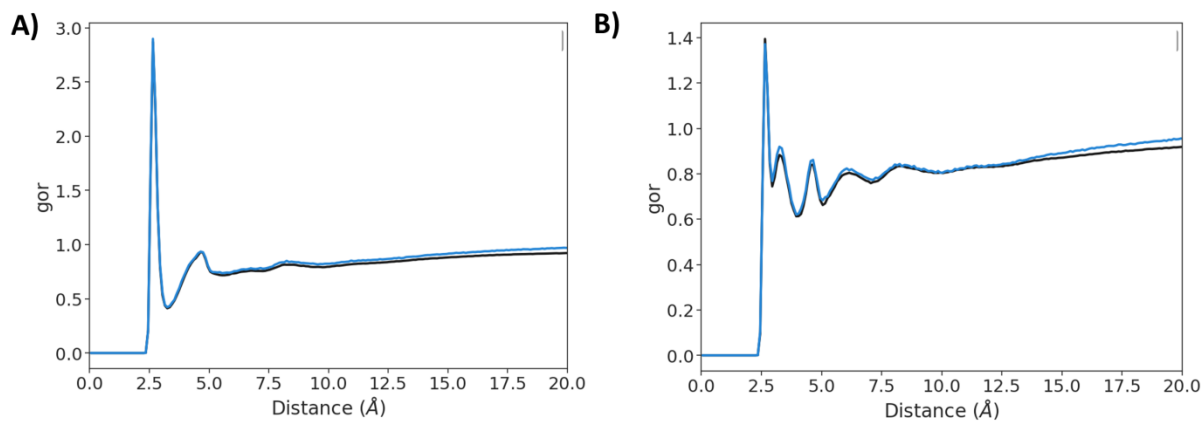


**Figure 4.17.** Radial distribution function analyses between water molecules and $O^-$ atoms of pCBMA at A) 0.15 M NaCl and B) 5.0 M NaCl: Lyz(5+)pCBMA (black) and free pCBMA (blue). RDF analyses are similar whether pCBMA is free in solution or bound to a protein surface.
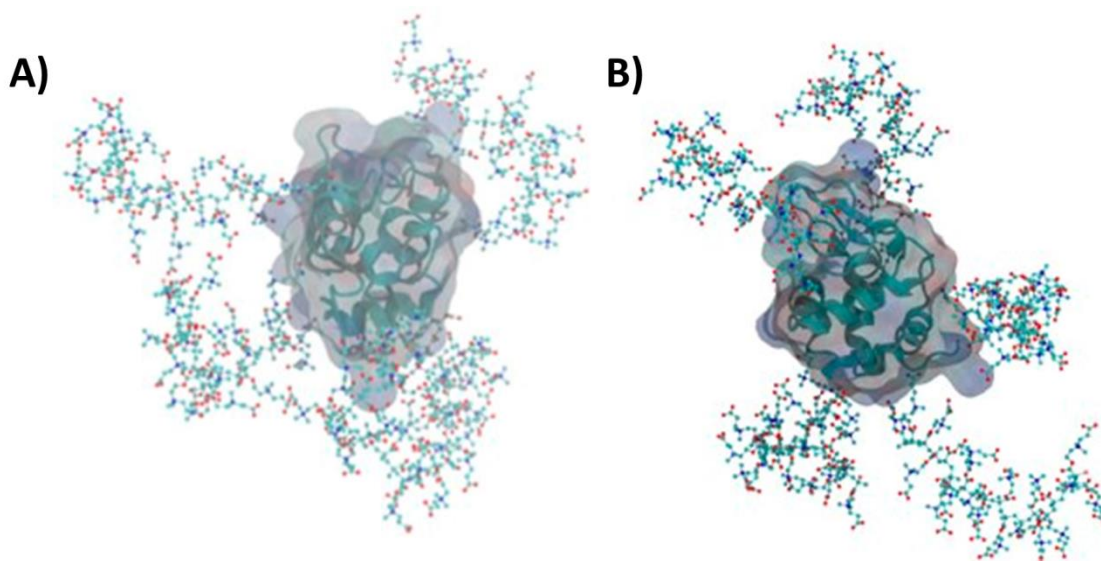
**Figure 4.18.** Snapshot of Lyz(5+)pCBMA DP 18 during the MD simulation showing extension of polymer chains away from the protein surface and high degrees of protein surface exposure in A) 0.0 M and B) 5.0 M NaCl.

### 4.4.6   Conjugate Activity in 100% Saturated Ammonium Sulfate

The newly discovered solubility of a protein in saturated salt solutions raises the interesting question of whether functional activity can be retained in this environment. A challenge in most precipitation methods is loss of protein function. We therefore determined the activities of Lyz-pCBMA conjugates containing 1, 3, and 5 polymer chains in saturated ammonium sulfate using a small molecule fluorescent substrate, 4-methylumbelliferyl β-D-N,N′,N″-triacetylchitotrioside. There was no correlation between activity and pCBMA length in either 50 mM sodium phosphate (NaPhos) or saturated ammonium sulfate (**Table 4.3 and Figure 4.19**). Lyz remained active after initiator attachment and pCBMA growth. Lyz(5+)pCBMA conjugates had increased activities in 100% saturated ammonium sulfate and were up to 1.6 times higher than the corresponding activities in NaPhos buffer, even at slightly lower pH (pH 6.0 versus pH 5.5). Interestingly, Lyz-initiator displayed the highest activity in ammonium sulfate (4.2 times more than in NaPhos buffer). Activities of Lyz-pCBMA conjugates

with 1 and 3 initiators were also measured. The conjugates remained active after polymer growth and were again, more active in 100% ammonium sulfate. Additionally, Lyz(1+) and Lyz(3+) were 1.8 and 2.4 times more active in ammonium sulfate than NaPhos, respectively. Lyz-initiator should be aggregated at 100% ammonium sulfate saturation. Aggregation typically leads to unfolding and loss of activity. The ammonium cation is highly kosmotropic, however, and stabilizes the protein structure during precipitation to keep Lyz active. The chemical structure of the initiator contains a positively charged quaternary ammonium. This could have strongly attracted sulfate anions and slightly changed the arrangement of the active site residues to strengthen the active site-substrate interaction to increase activity in ammonium sulfate.[266]

**Table 4.3.** Enzymatic activities of Lyz, Lyz-initiators, and Lyz-pCBMA conjugates of increasing DP in 50 mM NaPhos buffer and 100% saturated ammonium sulfate (4.1 M). Activity was measured using the fluorescent substrate 4-Methylumbelliferyl β-D-N,N′,N″-triacetylchitotrioside over 4 h. Data were fit to linear regressions to obtain the reaction rate. Error represents the standard deviations from triplicate measurements.

| | | Reaction Rate (RFU min$^{-1}$) | | |
|---|---|---|---|---|
| | | 50 mM NaPhos (pH 6.0) | 4.1 M Ammonium Sulfate (pH 5.5) | Ratio (Ammonium Sulfate: NaPhos) |
| | Lyz | 26.5 ± 1.5 | 25.6 ± 1.5 | 1.0 |
| *5 initiators* | Lyz(5+) | 18.8 ± 3.8 | 78.4 ± 4.3 | 4.2 |
| | DP 18 | 19.3 ± 1.3 | 30.7 ± 2.0 | 1.6 |
| | DP 32 | 33.9 ± 4.4 | 36.3 ± 1.6 | 1.1 |
| | DP 56 | 21.3 ± 2.6 | 26.6 ± 1.1 | 1.2 |
| | DP 79 | 21.3 ± 0.2 | 28.2 ± 0.9 | 1.3 |
| | DP 91 | 17.9 ± 2.2 | 24.2 ± 0.7 | 1.4 |
| *3 initiators* | Lyz(3+) | 30.6 ± 0.6 | 74.1 ± 1.5 | 2.4 |
| | DP 20 | 35.8 ± 0.3 | 73.2 ± 2.3 | 2.0 |
| | DP 66 | 19.0 ± 0.1 | 30.1 ± 0.6 | 1.6 |
| *1 initiator* | Lyz(1+) | 30.1 ± 0.1 | 53.4 ± 1.3 | 1.8 |
| | DP 14 | 43.7 ± 0.3 | 78.6 ± 1.4 | 1.8 |
| | DP 44 | 28.3 ± 1.2 | 48.5 ± 0.8 | 1.7 |
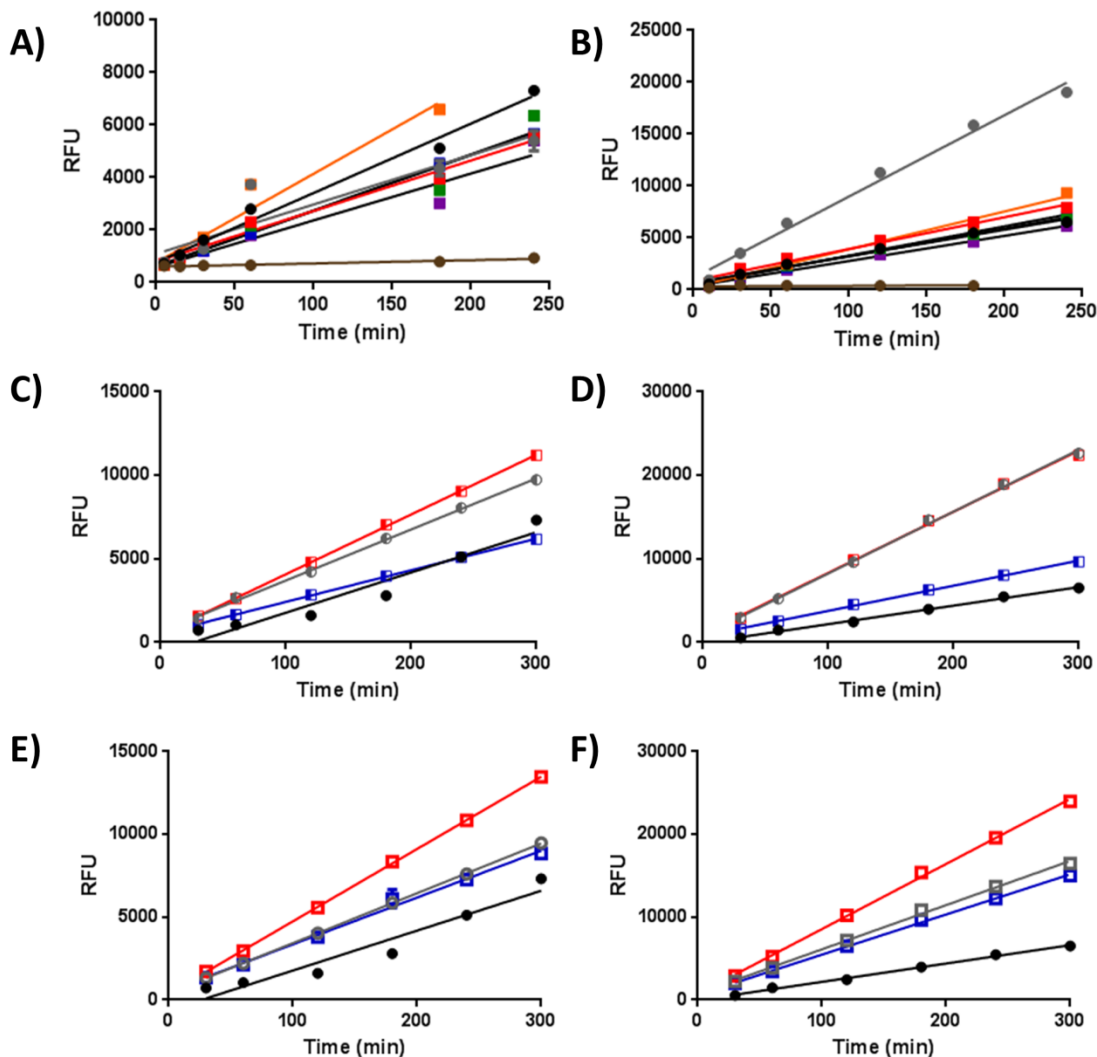
**Figure 4.19.** Enzymatic reaction rates of Lyz-pCBMA conjugates in 50 mM NaPhos buffer (pH 6.0) (1st column) and 100% saturated ammonium sulfate (pH 5.5) (2nd column). Conjugates with 5 initiators in A) NaPhos and B) 100% ammonium sulfate for native Lyz (black circle), Lyz(5+) (gray circle), DP 18 (red square), DP 32 (orange square), DP 56 (green square), DP 79 (blue square), and DP 91 (purple square). Conjugates with 3 initiators in C) NaPhos and D) 100% ammonium sulfate for native Lyz (black circle), Lyz(3+) (gray half open circle), DP 20 (red half open square), and DP 66 (blue half open square). Conjugates with 1 initiator in E) NaPhos and F) 100% ammonium sulfate for native Lyz (black circle), Lyz(1+) (gray open circle), DP 14 (red open square), and DP 44 (blue open square). Blanks from auto hydrolysis of substrate are shown in NaPhos and 100% ammonium sulfate (brown circles) in plots A) and B), respectively.

### 4.4.7 Purification by Utilizing Different Salting Out Points

After verifying that ammonium sulfate did not deactivate the conjugates, the differences in solubilities were utilized to purify a mixture of conjugates and minute amounts of native Lyz (10 μg/mL). A hurdle in protein-polymer conjugate synthesis and characterization is

171

heterogeneity. This makes characterization difficult[207] and it also impedes accurate measurements of activity and stability since unmodified protein may remain in the sample. Various chromatography techniques are typically used to purify conjugates including size exclusion, ion exchange, or high performance reverse phase chromatography, which all require instrumentation and user-knowledge. Ammonium sulfate, however, is inexpensive and does not require high-end analytical equipment. We therefore mixed long chained pCBMA and pOEGMA conjugates with native Lyz in a 1:99 volume ratio of native Lyz to conjugate (5 initiators), preferentially precipitated one of the species, then performed SDS-PAGE analysis of the supernatant and precipitate. Native Lyz and Lyz-pOEGMA DP 164 precipitated around 60% and 15%, respectively, while Lyz-pCBMA DP 91 did not precipitate at all. Therefore, to purify a mixture of native Lyz and Lyz-pOEGMA, ammonium sulfate was added at 40% saturation to preferentially precipitate the conjugate and to purify a mixture of native Lyz and Lyz-pCBMA, ammonium sulfate was added at 100% saturation to preferentially precipitate native Lyz. After preferential precipitation, samples were dialyzed in deionized water to remove the salt and then ultrafiltration was performed to obtain samples with the concentration of the starting mixture. Lyz(5+)pCBMA and Lyz(5+)pOEGMA gel lanes show the typical band broadening after polymer conjugation and increases in molecular mass over native Lyz (**Figure 4.20**). Both native Lyz and Lyz(5+)pCBMA can be seen in the starting mixture, and after preferential precipitation, the band for native Lyz in the supernatant noticeably decreased (**Figure 4.20A**). The gel was analyzed in ImageJ to compare the intensities of the native Lyz band before and after purification to estimate a final concentration of 0.003 mg/mL from a starting concentration of 0.01 mg/mL. A second round of preferential precipitation was performed on that supernatant and after another SDS-PAGE analysis, no native Lyz was detected in the supernatant (**Figure 4.21**). For

Lyz(5+)pOEGMA, both the conjugate and native Lyz bands can be seen in the starting mixture (**Figure 4.20B**). After purification with 40% ammonium sulfate, the conjugate was preferentially precipitated and native Lyz was not detected in the precipitate indicating successful purification. Additionally, Image J was used to compare the band intensities of the conjugate in the starting mixture and the conjugate in the precipitate. The purification yield was estimated as 61%. Although there was a decrease in yield, the broadening of the band was decreased so that a more homogenous conjugate was purified. This method of purification based on differences in solubilities was very useful for conjugates of high modification where the salting out point was much different than the native protein. We believe this method can be utilized for other polymer types as well.
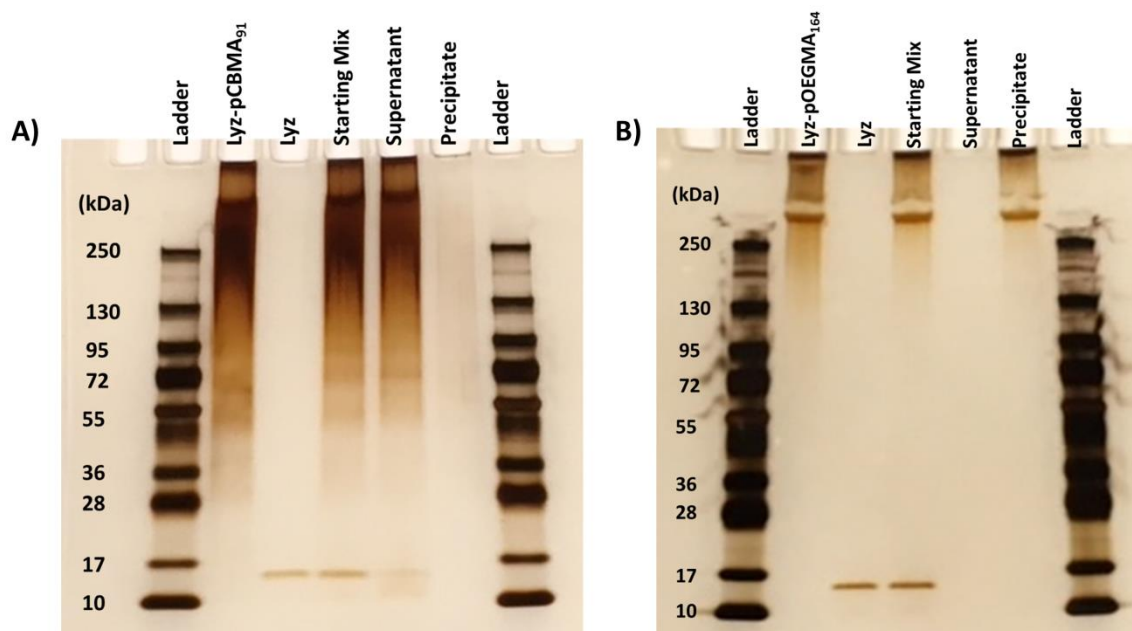


**Figure 4.20.** Silver stained SDS-PAGE gels to show purification of a mixture of native Lyz and A) Lyz(5+)pCBMA DP 91 or B) Lyz(5+)pOEGMA DP 164. Samples were mixed in a 1 to 99 volume ratio of native Lyz to conjugate (starting mix) and ammonium sulfate was added to preferentially precipitate native Lyz from Lyz-pCBMA (100% saturation) or to precipitate Lyz-pOEGMA from native Lyz (40% saturation). Supernatants and precipitates were dialyzed in deionized water to remove salt and were then concentrated back to starting concentrations using ultrafiltration prior to SDS-PAGE analysis.
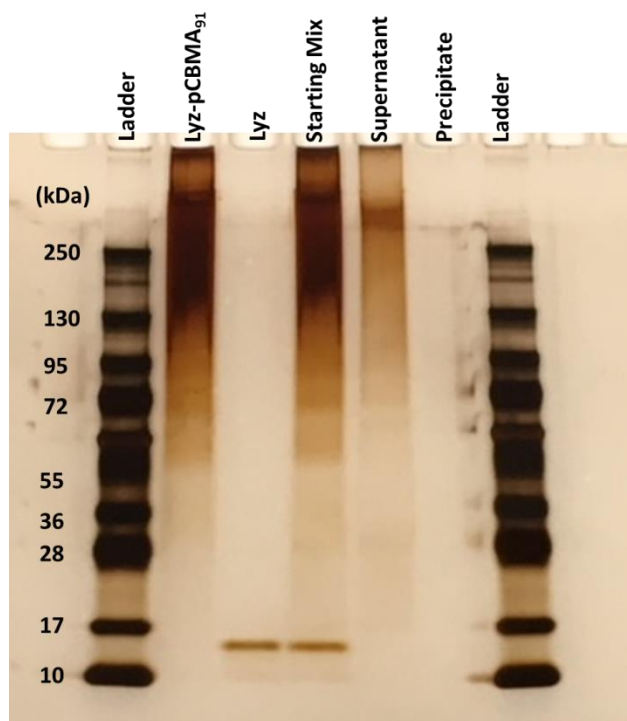
**Figure 4.21.** Silver stained SDS-PAGE analysis from a second round of purification of Lyz(5+)pCBMA DP 91 from a mixture with native Lyz. The supernatant from Figure 6A was purified again by the addition of 100% saturated ammonium sulfate and the same processing was performed as in Figure 6A. No native Lyz remained in the supernatant after the 2$^{nd}$ purification.

## 4.4.8 Effect of Other Charged Polymers on Conjugate Solubility

Finally, we exemplified the range of conjugates that purification by ammonium sulfate precipitation could be useful. α-Chymotrypsin (CT)-polymer conjugates that were previously synthesized and characterized[153] were studied. Briefly, twelve long-chained polymers of zwitterionic pCBMA (DP 112), neutral pOEGMA (DP 97), neutral/positive poly(dimethylaminoethyl methacrylate) (pDMAEMA) (DP 89), positively charged poly(quaternary ammonium methacrylate) (pQA) (DP 89), and negatively charged poly(sulfonate methacrylate) (pSMA) (DP 113) were grown from the surface of CT that had been modified with 12 neutral initiators, on average.[153] Ammonium sulfate precipitation was

performed on native CT, CT-initiator, and CT-polymer conjugates (**Figure 4.22**). Native CT

precipitated near 60% saturation and CT-initiator precipitated around 20% saturation. This is

much different than the case with Lyz where native Lyz and Lyz-initiator precipitated around the

same point. Lyz conjugates were synthesized with a positively charged initiator that preserved

the positive charge that was previously on the amino group. CT conjugates, however, were

synthesized with a neutral initiator where covalent attachment converts the positively charged

amino group to a non-ionizable amide bond thereby increasing the negative to positive charge

ratio on the local protein surface to increase hydrophobicity. This decrease in charge density

caused the CT-initiator to precipitate at much lower ammonium sulfate concentrations. It also

precipitated slowly over the range of 20 to 60% saturation, which again, could be potentially

useful for sample fractionation to synthesize homogenous conjugates. Since the advantages of

using a charged initiator were only published recently[212], the majority of grafted-from initiators

in the current literature are still uncharged and target protein amino groups.[100,209,210] Therefore,

the precipitation of protein-initiator before the native protein is advantageous for separating

unmodified from modified protein after the initiator reaction. As with Lyz, growth of pCBMA

increased CT's solubility up to 100% saturation while growth of pOEGMA decreased solubility

to 15% saturation. Interestingly, the positively charged pQA, positively charged pDMAEMA,

and negatively charged pSMA conjugates all remained soluble up to 100% saturation, as well.

pDMAEMA has a pKa around $6.2^{153}$ and at pH 7, would be 15% protonated and positively

charged which was enough charge to keep CT soluble. Typical polyelectrolyte polymers collapse

in high salt concentrations by screening of electrostatic interactions, but remain hydrated, which

would have prevented precipitation.[267] There are many other types of monomers, both

commercially available and that can be synthesized in-house, that are amenable to grafting from

techniques, namely ATRP or reversible addition-fragmentation chain-transfer (RAFT) polymerization. Therefore, polymers can be specifically designed to tune the solubility of a protein-polymer conjugate to ease purification.
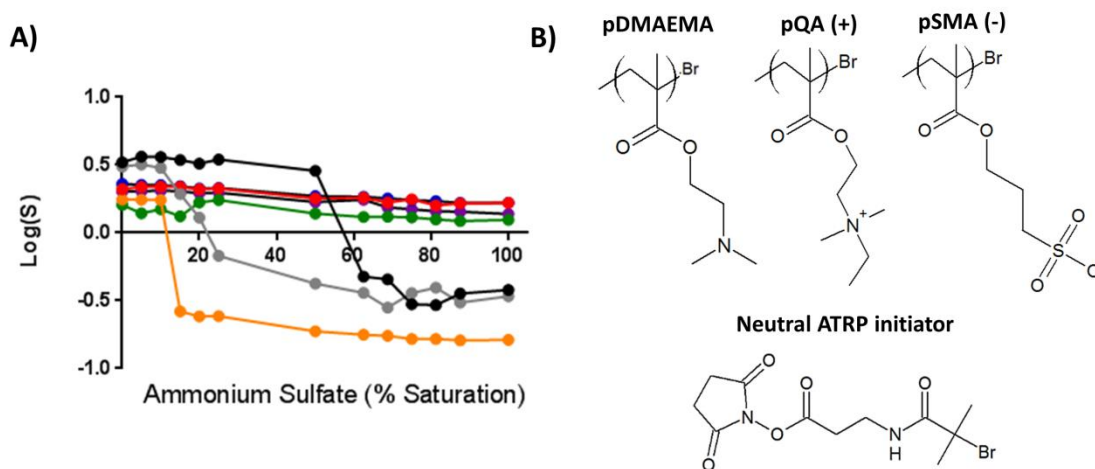


**Figure 4.22.** A) Ammonium sulfate precipitation of native CT, CT-neutral initiator, and CT-polymer conjugates. Native CT (black circle), CT-neutral initiator (gray circle), CT-pCBMA DP 112 (red circle), CT-pOEGMA DP 97 (orange circle), CT-pDMAEMA DP 89 (green circle), CT-pQA DP 89 (blue circle), and CT-pSMA DP 113 (purple circle). B) The various structures of charged polymers that were grown from CT using the neutral ATRP initiator. Error bars (within the symbols) represent the standard deviations from triplicate measurements.

## 4.5    Conclusions

Covalent attachment of polymers to a protein can significantly alter the protein's solubility, which can be tuned by changing the polymer type, grafting density, and polymer length. The grafting-from approach to conjugate synthesis easily allows for each of those variables to be tuned independently. Highly charged polymers (zwitterionic, positive, and negative) increase the solubility up to 100% ammonium sulfate saturation and prevent salting-out while uncharged, amphiphilic polymers decrease solubility. Zwitterionic polymer conjugates that are soluble in 100% ammonium sulfate remain active and are stable for at least 2.5 months of storage. Experimental and simulation results showed that zwitterionic polymers, when bound to the protein surface, display the anti-polyelectrolyte effect with increasing salt concentration

176

similar to the behavior of unbound zwitterionic polymers in salt solutions. Due to this effect, the conjugates are highly solvated at high ammonium sulfate concentrations. The differences in solubilities between conjugates and either native protein or protein-initiator can be utilized for simple purification and fractionation of heterogeneous mixtures.

The protein-polymer conjugates that were soluble in 100% ammonium sulfate (4.1 M) would fall into the category of extreme halophilic proteins that are able to survive in the harshest of salt conditions which further shows how polymer conjugation can increase the robustness of a protein to survive in non-native environments. The addition of ammonium sulfate to a protein solution can have many uses since it is kosmotropic and promotes stabilization. In general, polymer conjugation to a protein can cause structural changes and deactivation of the protein. Since ammonium sulfate has been shown to help refold misfolded/unfolded proteins, it could also be used to re-structure protein-polymer conjugates or help maintain the protein structure (prevent unfolding) throughout conjugate synthesis (initiator attachment and polymer growth). Additionally, polymer attachment has been shown to increase the thermostability of a protein. Ammonium sulfate has also been shown to increase a protein's thermostability. Therefore, the addition of ammonium sulfate to a protein-polymer conjugate solution could potentially increase the thermostability of a protein beyond the increase provided by the polymer. Another potential application is in the purification of a target protein from cell lysate, enabled through the use of non-natural amino acids. The target protein can be genetically engineered with a specific reactive group on a non-natural amino acid. Zwitterionic polymers can then by reacted to (or grown from) the non-natural amino acid followed by ammonium sulfate precipitation. The target protein will remain soluble while all other cell lysate contaminants will precipitate. The non-natural amino acid can also be engineered to contain a reversible/cleavable group so that the zwitterionic

177

polymer can be cleaved after purification to yield the native target protein. This approach could have significant impact in antibody purification as an alternative to Protein A chromatography. In general, we now have the ability to keep proteins soluble in high concentrations of salts by polymer conjugation which can be utilized for many new and unforeseen applications.

# Chapter 5.   Future Directions and Overall Conclusions

## 5.1   Future Directions

Recent advances in polymer-based protein engineering present considerable opportunities to realize new directions for controlling biomacromolecule structure and function with polymers. Through increasing the breadth of monomers that may be employed for controlled polymerization methods, proteins may be modified with increasingly diverse polymers, which can be used to impart new functions to proteins and control protein function in new ways. Additionally, the development of oxygen-tolerant polymerization techniques has opened doors to grow polymer chains from living biomacromolecules, including cells and tissues. New characterization techniques to analyze these hybrid complexes will also be important moving forward. In this section, we will discuss each of these advances and their implications for emerging applications of polymer-based protein engineering that highlight new and exciting directions.

### 5.1.1   Diversification of Polymers for Biomacromolecule Modification

Combining the broad range of available monomers, initiators, and catalysts for ATRP and RAFT with the growth of *in situ* methods for grafting polymers from proteins has led to intriguing possibilities. In particular, the convergence of materials and biological worlds has enabled the exploration of more complex polymers and polymer architectures in the context of protein-polymer conjugates. For example, PEG is slowly being replaced with other polymers, including, namely, zwitterionic polymers such as poly(carboxybetaine methacrylate), which has been grown from the surface of proteins and shown to impart superior stability relative to PEG.[64] The replacement of PEG by other polymers has also lead to novel functions, including drug delivery and *in vivo* targeting. Cummings and co-workers[49] recently showed that the growth of

cationic polymers (*e.g.*, poly(quaternary ammonium methacrylate)) can enhance binding of proteins to mucin in the gastrointestinal tract.

A related area that remains to be explored entails the use of novel membrane-permeable polymers to deliver CRISPR/Cas9 machinery into cells for genome-editing. Specifically, it is interesting to consider the extent to which polymer modification could permit the safe and efficient delivery of Cas9 to mammalian cells, which currently represents a major challenge in this exploding field. Furthermore, while temperature sensitive polymers (*e.g.*, poly(*N*-isopropylacrylamide)) have been grown from proteins, the growth of polymers that respond to other stimuli (e.g., light, mechanical forces, electrical current, magnetic field) remains an underexplored field. Similarly, while the vast majority of polymers that have been grown from proteins have consisted of homopolymers, the growth of heteropolymers may permit new functions to be accessed.[268] Interestingly, although not conjugated to proteins, Panganiban et al.[60] recently reported that random copolymers with similar degrees of chemical heterogeneity as that of proteins can significantly improve protein solubility and stability in organic solvents.

## 5.1.2   Emerging Characterization and Purification Techniques

*Asymmetric flow field-flow fractionation coupled with multi-angle laser light scattering*

Current protein-polymer conjugate characterization techniques to calculate molecular mass, such as GPC, have limitations and can only provide an estimated value rather than an intrinsic value. Molecular mass by GPC is always calculated in reference to calibration standards, which may interact with the column differently than the protein-polymer conjugate sample and affect the molecular mass calculation. Therefore, new techniques are needed to obtain more accurate characterizations. As an alternative to GPC, asymmetrical flow field-flow fractionation (AF4) is a channel-based separation technique that separates based on differences

in Brownian motion, does not use a column for separation, and more accurately reflects the physical properties of a sample in solution. Additionally, it is non-destructive to the sample and does not suffer from strong shear forces. AF4 has been successfully used to characterize free polymers[269], but has not yet been explored for protein-polymer conjugates. When AF4 is coupled to multi-angle laser light scattering (MALLS), the intrinsic molecular mass can be calculated using the Rayleigh ratio, without the need to use standards. MALLS can provide further information including radius of gyration ($R_g$), hydrodynamic radius ($R_h$), shape factor ($R_g/R_h$), aggregation state, and degree of branching (if using branched polymers). Therefore, most of the conjugate's intrinsic physical properties can be determined from a single, rapid measurement.

### *Aqueous two-phase systems*

Liquid-liquid extraction is a method to separate mixtures of solutes into single components based on their individual partitioning to two different immiscible phases, typically water and an organic solvent. Proteins, and other biomolecules, have poor solubility and stability in organic solvents making this purification method unsuitable. Phase separation can also be achieved, however, where both phases are aqueous and these are known as aqueous two-phase systems (ATPS). In ATPS, the phases are typically composed of polymer-polymer (PEG-dextran) or polymer-salt (PEG-phosphate), making both of these systems amenable for biomolecules. Additionally, PEG-salt systems are slightly more attractive because simple dialysis can be used to remove excess salt after separation; however, protein precipitation at high salt concentration may be of concern. Many studies have been performed to determine the mechanisms of protein partitioning in ATPS as a function of protein physicochemical properties including size, surface charge, and hydrophobicity,[270–274] all of which are properties that are easily altered by polymer modification. Therefore, in a mixture of unmodified protein and

protein-polymer conjugate, their partitioning behavior should be different, allowing for separation into more pure components (**Figure 5.1**). ATPS extractions may also be used in series to achieve higher degrees of purity with each additional extraction.
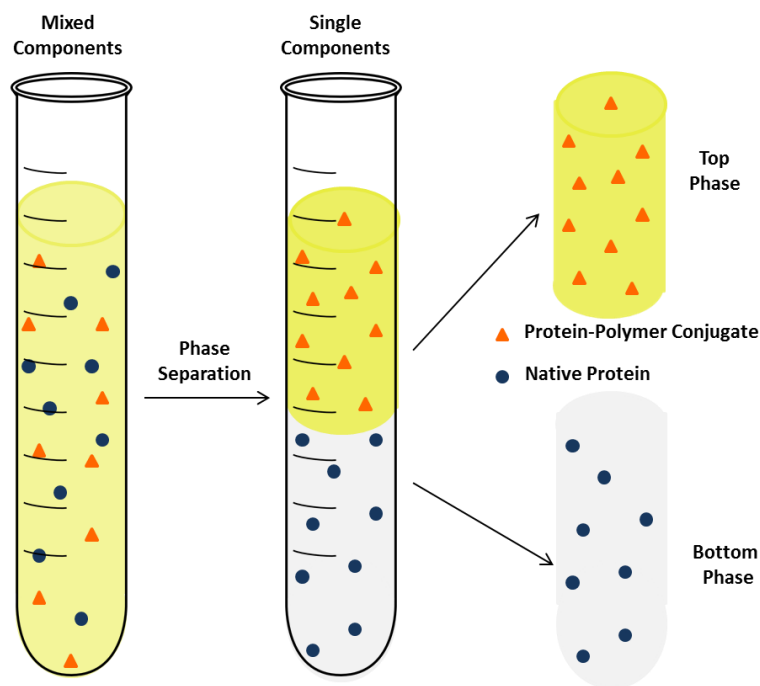


**Figure 5.1.** Example of how aqueous-two phase systems can potentially be used to purify protein-polymer conjugates.

As a preliminary study, the Lyz(5+)pCBMA conjugates that were synthesized for the ammonium sulfate precipitation study (**Table 4.1**) were placed in ATPS of PEG-NaPhos or PEG-dextran and their partition coefficients were compared to the partition coefficients of native Lyz and Lyz(5+). The partition coefficient is the protein concentration in the top phase (PEG, 4 kDa) divided by the protein concentration in the bottom phase (NaPhos (pH 7) or dextran (500 kDa) measured by the absorbance at 280 nm. Therefore, a partition coefficient of 1.0 would indicate that the sample partitioned equally to both phases. Briefly, the ATPS were composed of

13 wt% PEG-7 wt% NaPhos (**Figure 5.2**) or 6 wt% PEG-8 wt% dextran (**Figure 5.3**) in order to keep the volume of each phase equal. Next, protein-polymer conjugates, native protein, or protein-initiator samples were added to the ATPS at 0.5 mg/mL. The systems were vortexed, centrifuged at 1200×g for 5 minutes, and were then allowed to equilibrate at room temperature overnight. Aliquots from each phase were taken to measure protein concentration and further calculate the partition coefficients.

In the PEG-NaPhos ATPS (**Figure 5.2**), native Lyz and Lyz(5+)pCBMA conjugates strongly partitioned to the NaPhos phase while Lyz(5+) strongly partitioned to PEG phase. Additionally, the partition coefficient decreased slightly with increasing DP. Therefore, a mixture of Lyz(5+) and Lyz(5+)pCBMA could be purified into individual components.
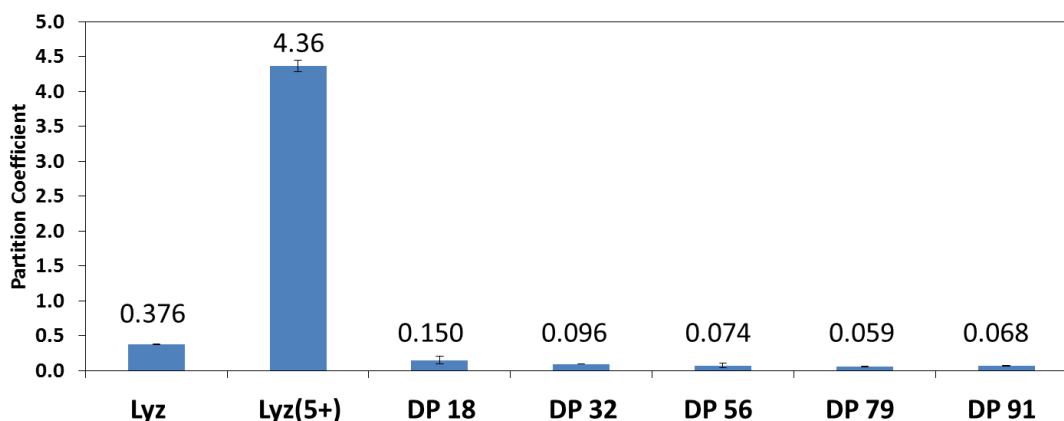


**Figure 5.2.** Partition coefficients of pCBMA samples in an ATPS of 13 wt% PEG-7 wt% NaPhos. Lyz, partitioned slightly more to the NaPhos phase, Lyz(5+) strongly partitioned to the PEG phase, and Lyz(5+)pCBMA samples of increasing DP strongly partitioned to the NaPhos phase.

In the PEG-dextran ATPS, Lyz(5+) preferentially partitioned to the PEG phase, native Lyz and Lyz(5+)pCBMA DP 18 partitioned almost equally into both phases, and increasing DP's preferentially partitioned to the dextran phase. The partitioning behavior of these

conjugates were stronger in the PEG-NaPhos system in comparison to the PEG-dextran system. Interestingly, it has been previously shown that PEG-phosphase systems are more sensitive to protein surface charge while PEG-dextran systems are more sensitive to protein molecular mass.[271,274]
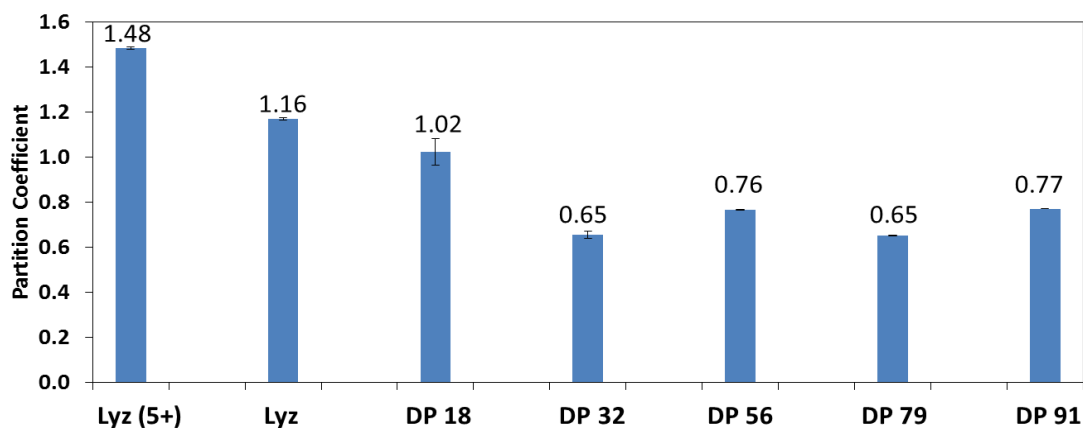


**Figure 5.3.** Partition coefficients of pCBMA samples in an ATPS of 6 wt% PEG-8 wt% dextran. Lyz(5+) preferentially partitioned to the PEG phase, native Lyz and DP 18 partitioned almost equally into both phases, and DP 32 through DP 91 preferentially partitioned to the dextran phase.

In general, the partition behaviors of native Lyz, Lyz-initiator, and Lyz-polymer conjugates are different from each other and depend on the composition of the ATPS. Although this was a preliminary study, the results indicate that ATPS could be a viable method for protein-polymer conjugate purification, and potentially for sample fractionation or characterization. For example, if conjugates were found to partition correlating strongly with size, a standard curve could be made and used for size determination of an unknown conjugate of a similar polymer type. It is also interesting to think about how ATPS and other water/organic phase systems can further be used in the realm of protein-polymer conjugates. When differences in substrate and product solubility occur for an enzymatic reaction, catalysis of the substrate can be performed in

the aqueous phase while product can be recovered in the non-aqueous phase. Moreover, enzyme-polymer conjugates can be synthesized to be soluble and active in organic solvents and the opposite phenomena can occur. Also, other types of ATPS or multi-phase systems can be synthesized using various polymers, salts, and surfactants. One could imagine a multi-phase system that can be used for an enzymatic chain reaction. An enzyme in the top phase could catalyze a reaction so that its product is the substrate for a second enzymatic reaction in the phase below, and so on. Ultimately, there are many new applications for protein-polymer conjugates in this area that warrant further investigation.

## 5.2   Overall Conclusions

Today, engineering biomacromolecular function and delivery is an art that is dependent on molecular biology. The techniques are exquisitely powerful but are also limited to the synthetic space in which biology works. Combining the power of synthetic chemistry with biology provides a new set of tools that can drive new science and overcome the limitations of biomacromolecular systems that exist today. To open the door to that new field of science and technology, we need to combine rational design of next generation biomolecule-polymer hybrids with a fundamental understanding of the parameters that predict and control reactivity between growing polymers and biomolecules. We have developed an understanding of structure-function-dynamics relationships between polymers and enzymes that has resulted in new applications. In the last decade, we and others have learned how to covalently couple or display multiple small molecule initiators onto a protein and then grow polymers from those sites. Using this approach, we have engineered protein-polymer hybrids that had increased stabilities at low pH, high temperature, and high salinity while maintaining biologic activities. While such advances

demonstrate the potential of this field, only the very tip of this field has begun to be explored, and the impact this field may have is only beginning to be understood. The continued advancement of this field is necessary to aid in the realization of this impact and, moreover, will likely lead to even new science and breakthroughs that expand the genetic code (*e.g.*, post-translational modifications, including phosphorylation, glycosylation, acetylation, and sumoylation) by which nature uses to control biomolecular function.

# References

(1)     Davis, F. F. The Origin of Pegnology. *Adv. Drug Deliv. Rev.* **2002**, *54* (4), 457–458.

(2)     Abuchowski, A.; van Es, T.; Palczuk, N. C.; Davis, F. F. Alteration of Immunological Properties of Bovine Serum Albumin by Covalent Attachment of Poly(ethylene Glycol). *J. Control. Rel.* **1977**, *252* (11), 3578–3581.

(3)     Abuchowski, A.; McCoy, J. R.; Palczuk, N. C.; van Es, T.; Davis, F. F. Effect of Covalent Attachment of Polyethylene Glycol on Immunogenicity and Circulating Life of Bovine Liver Catalase. *J. Biol. Chem.* **1977**, *252* (11), 3582–3586.

(4)     Harris, J. M. *Poly(ethylene Glycol) Chemistry : Biotechnical and Biomedical Applications*; 1992.

(5)     Harris, J. M.; Chess, R. B. Effect of Pegylation on Pharmaceuticals. *Nat. Rev. Drug Discov.* **2003**, *2* (3), 214–221.

(6)     Pasut, G.; Veronese, F. M. State of the Art in PEGylation: The Great Versatility Achieved after Forty Years of Research. *J. Control. Release* **2012**, *161* (2), 461–472.

(7)     Jevševar, S.; Kunstelj, M.; Porekar, V. G. PEGylation of Therapeutic Proteins. *Biotechnol. J.* **2010**, *5* (1), 113–128.

(8)     Alconcel, S. N. S.; Baas, A. S.; Maynard, H. D. FDA-Approved Poly(ethylene Glycol)–protein Conjugate Drugs. *Polym. Chem.* **2011**, *2* (7), 1442.

(9)     J., C. Conjugation Reactions. *Concepts Drug Metab.* **1980**, No. A, 211–250.

(10)   Lele, B. S.; Murata, H.; Matyjaszewski, K.; Russell, A. J. Synthesis of Uniform

Protein−Polymer Conjugates. *Biomacromolecules* **2005**, *6* (6), 3380–3387.

(11)   Bhalchandra, L. S.; Russell, A. J. Enhancing Enzyme Stability Against TiO2-UV Induced Inactivation. *Biomacromolecules* **2005**, *6* (1), 475–482.

(12)   Lee, S. B.; Koepsel, R. R.; Morley, S. W.; Matyjaszewski, K.; Sun, Y.; Russell, A. J. Permanent, Nonleaching Antibacterial Surfaces, 1. Synthesis by Atom Transfer Radical Polymerization. *Biomacromolecules* **2004**, *5* (3), 877–882.

(13)   Lee, S. B.; Russell, A. J.; Matyjaszewski, K. ATRP Synthesis of Amphiphilic Random, Gradient, and Block Copolymers of 2-(Dimethylamino)ethly Methacrylate and N-Butyl Methacrylate in Aqueous Media. *Biomacromolecules* **2003**, *4* (5), 1386–1393.

(14)   Bontempo, D.; Maynard, H. D. Streptavidin as a Macroinitiator for Polymerization: In Situ Protein−Polymer Conjugate Formation. *J Am Chem Soc* **2005**, *127* (18), 6508–6509.

(15)   Lee, H.; Pietrasik, J.; Sheiko, S. S.; Matyjaszewski, K. Stimuli-Responsive Molecular Brushes. *Prog. Polym. Sci.* **2010**, *35* (1-2), 24–44.

(16)   Hui, C. M.; Pietrasik, J.; Schmitt, M.; Mahoney, C.; Choi, J.; Bockstaller, M. R.; Matyjaszewski, K. Surface-Initiated Polymerization as an Enabling Tool for Multifunctional (Nano-)Engineered Hybrid Materials. *Chem. Mater.* **2014**, *26* (1), 745–762.

(17)   Cobo, I.; Li, M.; Sumerlin, B. S.; Perrier, S. Smart Hybrid Materials by Conjugation of Responsive Polymers to Biomacromolecules. *Nat. Mater.* **2015**, *14* (2), 143–159.

(18)   Wu, Y.; Ng, D. Y. W.; Kuan, S. L.; Weil, T. Protein–polymer Therapeutics: A Macromolecular Perspective. *Biomater. Sci.* **2015**, *3* (2), 214–230.

(19)  Averick, S.; Mehl, R. A.; Das, S. R.; Matyjaszewski, K. Well-Defined Biohybrids Using Reversible-Deactivation Radical Polymerization Procedures. *J. Control. Release* **2015**, *205*, 45–57.

(20)  Matyjaszewski, K. Atom Transfer Radical Polymerization (ATRP): Current Status and Future Perspectives. *Macromolecules* **2012**, *45* (10), 4015–4039.

(21)  Matyjaszewski, K.; Tsarevsky, N. V. Macromolecular Engineering by Atom Transfer Radical Polymerization. *J. Am. Chem. Soc.* **2014**, *136* (18), 6513–6533.

(22)  Cummings, C.; Murata, H.; Koepsel, R.; Russell, A. J. Tailoring Enzyme Activity and Stability Using Polymer-Based Protein Engineering. *Biomaterials* **2013**, *34* (30), 7437–7443.

(23)  Simakova, A.; Averick, S. E.; Konkolewicz, D.; Matyjaszewski, K. Aqueous ARGET ATRP. *Macromolecules* **2012**, *45* (16), 6371–6379.

(24)  Konkolewicz, D.; Magenau, A. J. D.; Averick, S. E.; Simakova, A.; He, H.; Matyjaszewski, K. ICAR ATRP with Ppm Cu Catalyst in Water. *Macromolecules* **2012**, *45* (11), 4461–4468.

(25)  Sumerlin, B. S. Proteins as Initiators of Controlled Radical Polymerization: Grafting-from via ATRP and RAFT. *ACS Macro Lett.* **2012**, *1* (1), 141–145.

(26)  De, P.; Li, M.; Gondi, S. R.; Sumerlin, B. S. Temperature-Regulated Activity of Responsive Polymer−Protein Conjugates Prepared by Grafting-from via RAFT Polymerization. *J. Am. Chem. Soc.* **2008**, *130* (34), 11288–11289.

(27)  Cyrille Boyer; Volga Bulmus, *; Jingquan Liu; Thomas P. Davis, *; Martina H. Stenzel,

A.; Barner-Kowollik, C. Well-Defined Protein−Polymer Conjugates via in Situ RAFT Polymerization. *J Am Chem Soc* **2007**, *129* (22), 7145–7154.

(28)    Li, X.; Wang, L.; Chen, G.; Haddleton, D. M.; Chen, H. Visible Light Induced Fast Synthesis of Protein–polymer Conjugates: Controllable Polymerization and Protein Activity. *Chem. Commun.* **2014**, *50* (49), 6506–6508.

(29)    Xu, J.; Jung, K.; Corrigan, N. A.; Boyer, C. Aqueous Photoinduced Living/controlled Polymerization: Tailoring for Bioconjugation. *Chem. Sci.* **2014**, *5* (9), 3568.

(30)    Tucker, B. S.; Coughlin, M. L.; Figg, C. A.; Sumerlin, B. S. Grafting-From Proteins Using Metal-Free PET–RAFT Polymerizations under Mild Visible-Light Irradiation. *ACS Macro Lett.* **2017**, *6* (4), 452–457.

(31)    Averick, S.; Simakova, A.; Park, S.; Konkolewicz, D.; Magenau, A. J. D.; Mehl, R. A.; Matyjaszewski, K. ATRP under Biologically Relevant Conditions: Grafting from a Protein. *ACS Macro Lett.* **2012**, *1* (1), 6–10.

(32)    Axelsen, P. H.; Harel, M.; Silman, I.; Sussman, J. L. Structure and Dynamics of the Active Site Gorge of Acetylcholinesterase: Synergistic Use of Molecular Dynamics Simulation and X-Ray Crystallography. *Protein Sci.* **2008**, *3* (2), 188–197.

(33)    Silman, I.; Harel, M.; Axelsen, P.; Raves, M.; Sussman, J. L. Three-Dimensional Structures of Acetylcholinesterase and of Its Complexes with Anticholinesterase Agents. *Biochem. Soc. Trans.* **1994**, *22* (3), 745–749.

(34)    Carmali, S.; Murata, H.; Amemiya, E.; Matyjaszewski, K.; Russell, A. J. Tertiary Structure-Based Prediction of How ATRP Initiators React with Proteins. *ACS Biomater.*

*Sci. Eng.* **2017**, *3* (9), 2086–2097.

(35)   Murata, H.; Carmali, S.; Baker, S. L.; Matyjaszewski, K.; Russell, A. J. Solid-Phase

Synthesis of Protein-Polymers on Reversible Immobilization Supports. *Nat. Commun.*

**2018**, *9* (1), 845.

(36)   Baslé, E.; Joubert, N.; Pucheault, M. Protein Chemical Modification on Endogenous

Amino Acids. *Chem. Biol.* **2010**, *17* (3), 213–227.

(37)   Krall, N.; da Cruz, F. P.; Boutureira, O.; Bernardes, G. J. L. Site-Selective Protein-

Modification Chemistry for Basic Biology and Drug Development. *Nat. Chem.* **2016**, *8*

(2), 103–113.

(38)   Peeler, J. C.; Woodman, B. F.; Averick, S.; Miyake-Stoner, S. J.; Stokes, A. L.; Hess, K.

R.; Matyjaszewski, K.; Mehl, R. A. Genetically Encoded Initiator for Polymer Growth

from Proteins. *J. Am. Chem. Soc.* **2010**, *132* (39), 13575–13577.

(39)   Averick, S. E.; Paredes, E.; Grahacharya, D.; Woodman, B. F.; Miyake-Stoner, S. J.;

Mehl, R. A.; Matyjaszewski, K.; Das, S. R. A Protein–Polymer Hybrid Mediated By

DNA. *Langmuir* **2012**, *28* (4), 1954–1958.

(40)   Plaks, J. G.; Falatach, R.; Kastantin, M.; Berberich, J. A.; Kaar, J. L. Multisite Clickable

Modification of Proteins Using Lipoic Acid Ligase. *Bioconjug. Chem.* **2015**, *26* (6), 1104–

1112.

(41)   Mao, H.; Hart, S. A.; Schink, A.; Pollok, B. A. Sortase-Mediated Protein Ligation:  A

New Method for Protein Engineering. *J. Am. Chem. Soc.* **2004**, *126* (9), 2670–2671.

(42)   Qi, Y.; Amiram, M.; Gao, W.; McCafferty, D. G.; Chilkoti, A. Sortase-Catalyzed Initiator

Attachment Enables High Yield Growth of a Stealth Polymer from the C Terminus of a Protein. *Macromol. Rapid Commun.* **2013**, *34* (15), 1256–1260.

(43)   Chapman, R.; Gormley, A. J.; Herpoldt, K.-L.; Stevens, M. M. Highly Controlled Open Vessel RAFT Polymerizations by Enzyme Degassing. *Macromolecules* **2014**, *47* (24), 8541–8547.

(44)   Enciso, A. E.; Fu, L.; Russell, A. J.; Matyjaszewski, K. A Breathing Atom-Transfer Radical Polymerization: Fully Oxygen-Tolerant Polymerization Inspired by Aerobic Respiration of Cells. *Angew. Chemie Int. Ed.* **2018**, *57* (4), 933–936.

(45)   Schulz, J. D.; Patt, M.; Basler, S.; Kries, H.; Hilvert, D.; Gauthier, M. A.; Leroux, J. C. Site-Specific Polymer Conjugation Stabilizes Therapeutic Enzymes in the Gastrointestinal Tract. *Adv. Mater.* **2016**, *28* (7), 1455–1460.

(46)   Falatach, R.; Li, S.; Sloane, S.; Mcglone, C.; Berberich, J. A.; Page, R. C.; Averick, S.; Konkolewicz, D. Why Synthesize Protein-Polymer Conjugates? The Stability and Activity of Chymotrypsin-Polymer Bioconjugates Synthesized by RAFT. *Polym. (United Kingdom)* **2015**, *72*, 382–386.

(47)   Murata, H.; Cummings, C. S.; Koepsel, R. R.; Russell, A. J. Polymer-Based Protein Engineering Can Rationally Tune Enzyme Activity, pH-Dependence, and Stability. *Biomacromolecules* **2013**, *14* (6), 1919–1926.

(48)   Lucius, M.; Falatach, R.; McGlone, C.; Makaroff, K.; Danielson, A.; Williams, C.; Nix, J. C.; Konkolewicz, D.; Page, R. C.; Berberich, J. A. Investigating the Impact of Polymer Functional Groups on the Stability and Activity of Lysozyme-Polymer Conjugates.

*Biomacromolecules* **2016**, *17* (3), 1123–1134.

(49) Cummings, C. S.; Campbell, A. S.; Baker, S. L.; Carmali, S.; Murata, H.; Russell, A. J. Design of Stomach Acid-Stable and Mucin-Binding Enzyme Polymer Conjugates. *Biomacromolecules* **2017**, *18* (2), 576–586.

(50) Cobo, I.; Li, M.; Sumerlin, B. S.; Perrier, S. Smart Hybrid Materials by Conjugation of Responsive Polymers to Biomacromolecules. *Nat. Mater.* **2014**, *14* (2), 143–159.

(51) Li, M.; De Priyadarsi; Gondi, S. R.; Sumerlin, B. S. Responsive Polymer-Protein Bioconjugates Prepared by RAFT Polymerization and Copper-Catalyzed Azide-Alkyne Click Chemistry. *Macromol. Rapid Commun.* **2008**, *29* (12-13), 1172–1176.

(52) Moatsou, D.; Li, J.; Ranji, A.; Pitto-Barry, A.; Ntai, I.; Jewett, M. C.; O'Reilly, R. K. Self-Assembly of Temperature-Responsive Protein-Polymer Bioconjugates. *Bioconjug. Chem.* **2015**, *26* (9), 1890–1899.

(53) Cummings, C.; Murata, H.; Koepsel, R.; Russell, A. J. Tailoring Enzyme Activity and Stability Using Polymer-Based Protein Engineering. *Biomaterials* **2013**, *34* (30), 7437–7443.

(54) Cummings, C.; Murata, H.; Koepsel, R.; Russell, A. J. Dramatically Increased pH and Temperature Stability of Chymotrypsin Using Dual Block Polymer-Based Protein Engineering. *Biomacromolecules* **2014**, *15* (3), 763–771.

(55) Kurinomaru, T.; Kuwada, K.; Tomita, S.; Kameda, T.; Shiraki, K. Noncovalent PEGylation through Protein-Polyelectrolyte Interaction: Kinetic Experiment and Molecular Dynamics Simulation. *J. Phys. Chem. B* **2017**, *121* (28), 6785–6791.

(56)  Yang, C.; Lu, D.; Liu, Z. How PEGylation Enhances the Stability and Potency of Insulin: A Molecular Dynamics Simulation. *Biochemistry* **2011**, *50* (13), 2585–2593.

(57)  Rodríguez-Martínez, J. A.; Solá, R. J.; Castillo, B.; Cintrón-Colón, H. R.; Rivera-Rivera, I.; Barletta, G.; Griebenow, K. Stabilization of α-Chymotrypsin upon PEGylation Correlates with Reduced Structural Dynamics. *Biotechnol. Bioeng.* **2008**, *101* (6), 1142–1149.

(58)  Lee, H.; Venable, R. M.; Mackerell, A. D.; Pastor, R. W.; Pastor, R. W. Molecular Dynamics Studies of Polyethylene Oxide and Polyethylene Glycol: Hydrodynamic Radius and Shape Anisotropy. *Biophys. J.* **2008**, *95* (4), 1590–1599.

(59)  Siewert J. Marrink; H. Jelger Risselada; Serge Yefimov; D. Peter Tieleman; Vries, A. H. de. The MARTINI Force Field: Coarse Grained Model for Biomolecular Simulations. *J. Phys. Chem. B* **2007**, *111* (27), 7812–7824.

(60)  Panganiban, B.; Qiao, B.; Jiang, T.; DelRe, C.; Obadia, M. M.; Nguyen, T. D.; Smith, A. A. A.; Hall, A.; Sit, I.; Crosby, M. G.; et al. Random Heteropolymers Preserve Protein Function in Foreign Environments. *Science* **2018**, *359* (6381), 1239–1243.

(61)  Condon, J. E.; Martin, T. B.; Jayaraman, A. Effect of Conjugation on Phase Transitions in Thermoresponsive Polymers: An Atomistic and Coarse-Grained Simulation Study. *Soft Matter* **2017**, *13* (16), 2907–2918.

(62)  Stanzione, F.; Jayaraman, A. Hybrid Atomistic and Coarse-Grained Molecular Dynamics Simulations of Polyethylene Glycol (PEG) in Explicit Water. *J. Phys. Chem. B* **2016**, *120* (17), 4160–4173.

(63)   Williams, C.; Dougherty, M. L.; Makaroff, K.; Stapleton, J.; Konkolewicz, D.; Berberich, J. A.; Page, R. C. *Strategies for Biophysical Characterization of Protein–Polymer Conjugates*, 1st ed.; 2017; Vol. 590.

(64)   Bhattacharjee, S.; Liu, W.; Wang, W. H.; Weitzhandler, I.; Li, X.; Qi, Y.; Liu, J.; Pang, Y.; Hunt, D. F.; Chilkoti, A. Site-Specific Zwitterionic Polymer Conjugates of a Protein Have Long Plasma Circulation. *ChemBioChem* **2015**, *16* (17), 2451–2455.

(65)   Cattani, G.; Vogeley, L.; Crowley, P. B. Structure of a PEGylated Protein Reveals a Highly Porous Double-Helical Assembly. *Nat. Chem.* **2015**, *7* (10), 823–828.

(66)   Fiaux, J.; Bertelsen, E. B.; Horwich, A. L.; Wüthrich, K. NMR Analysis of a 900K GroEL GroES Complex. *Nature* **2002**, *418* (6894), 207–211.

(67)   Callaway, E. Molecular-Imaging Pioneers Scoop Nobel. *Nature* **2017**, *550* (7675), 167.

(68)   Liu, Z.; Dong, C.; Wang, X.; Wang, H.; Li, W.; Tan, J.; Chang, J. Self-Assembled Biodegradable Protein-Polymer Vesicle as a Tumor-Targeted Nanocarrier. *ACS Appl. Mater. Interfaces* **2014**, *6* (4), 2393–2400.

(69)   Liu, X.; Gao, W. In Situ Growth of Self-Assembled Protein-Polymer Nanovesicles for Enhanced Intracellular Protein Delivery. *ACS Appl. Mater. Interfaces* **2017**, *9* (3), 2023–2028.

(70)   Cummings, C. S.; Fein, K.; Murata, H.; Ball, R. L.; Russell, A. J.; Whitehead, K. A. ATRP-Grown Protein-Polymer Conjugates Containing Phenylpiperazine Selectively Enhance Transepithelial Protein Transport. *J. Control. Release* **2017**, *255* (January), 270–278.

(71)   Hoffman, J. M.; Stayton, P. S.; Hoffman, A. S.; Lai, J. J. Stimuli-Responsive Reagent System for Enabling Microfluidic Immunoassays with Biomarker Purification and Enrichment. *Bioconjug. Chem.* **2015**, *26* (1), 29–38.

(72)   Liu, Z.; Chen, N.; Dong, C.; Li, W.; Guo, W.; Wang, H.; Wang, S.; Tan, J.; Tu, Y.; Chang, J. Facile Construction of Near Infrared Fluorescence Nanoprobe with Amphiphilic Protein-Polymer Bioconjugate for Targeted Cell Imaging. *ACS Appl. Mater. Interfaces* **2015**, *7* (34), 18997–19005.

(73)   Cingil, H. E.; Storm, I. M.; Yorulmaz, Y.; Te Brake, D. W.; De Vries, R.; Cohen Stuart, M. A.; Sprakel, J. Monitoring Protein Capsid Assembly with a Conjugated Polymer Strain Sensor. *J. Am. Chem. Soc.* **2015**, *137* (31), 9800–9803.

(74)   Campbell, A. S.; Islam, M. F.; Russell, A. J. Intramolecular Electron Transfer through Poly-Ferrocenyl Glucose Oxidase Conjugates to Carbon Electrodes: 1. Sensor Sensitivity, Selectivity and Longevity. *Electrochim. Acta* **2017**, *248*, 578–584.

(75)   Hoffman, A. S. Stimuli-Responsive Polymers: Biomedical Applications and Challenges for Clinical Translation. *Adv. Drug Deliv. Rev.* **2013**, *65* (1), 10–16.

(76)   Bayramoglu, G.; Arica, M. Y. Activity and Stability of Urease Entrapped in Thermosensitive poly(N-Isopropylacrylamide-Co-Poly(ethyleneglycol)-Methacrylate) Hydrogel. *Bioprocess Biosyst. Eng.* **2014**, *37* (2), 235–243.

(77)   Shakya, A. K.; Sami, H.; Srivastava, A.; Kumar, A. Stability of Responsive Polymer–protein Bioconjugates. *Prog. Polym. Sci.* **2010**, *35* (4), 459–486.

(78)   Murata, H.; Cummings, C. S.; Koepsel, R. R.; Russell, A. J. Polymer-Based Protein

Engineering Can Rationally Tune Enzyme Activity, pH-Dependence, and Stability. *Biomacromolecules* **2013**, *14* (6), 1919–1926.

(79)   Cummings, C.; Murata, H.; Koepsel, R.; Russell, A. J. Dramatically Increased pH and Temperature Stability of Chymotrypsin Using Dual Block Polymer-Based Protein Engineering. *Biomacromolecules* **2014**, *15* (3), 763–771.

(80)   Kovaliov, M.; Allegrezza, M. L.; Richter, B.; Konkolewicz, D.; Averick, S. Synthesis of Lipase Polymer Hybrids with Retained or Enhanced Activity Using the Grafting-from Strategy. *Polymer (Guildf).* **2018**, *137*, 338–345.

(81)   Grotzky, A.; Nauser, T.; Erdogan, H.; Schlüter, A. D.; Walde, P. A Fluorescently Labeled Dendronized Polymer–Enzyme Conjugate Carrying Multiple Copies of Two Different Types of Active Enzymes. *J. Am. Chem. Soc.* **2012**, *134* (28), 11392–11395.

(82)   Zore, O. V.; Pande, P.; Okifo, O.; Basu, A. K.; Kasi, R. M.; Kumar, C. V. Nanoarmoring: Strategies for Preparation of Multi-Catalytic Enzyme Polymer Conjugates and Enhancement of High Temperature Biocatalysis. *RSC Adv.* **2017**, *7* (47), 29563–29574.

(83)   Konieczny, S.; Leurs, M.; Tiller, J. C. Polymer Enzyme Conjugates as Chiral Ligands for Sharpless Dihydroxylation of Alkenes in Organic Solvents. *ChemBioChem* **2015**, *16* (1), 83–90.

(84)   Cummings, C. S.; Murata, H.; Matyjaszewski, K.; Russell, A. J. Polymer-Based Protein Engineering Enables Molecular Dissolution of Chymotrypsin in Acetonitrile. *ACS Macro Lett.* **2016**, *5* (4), 493–497.

(85)   Zhu, J.; Zhang, Y.; Lu, D.; Zare, R. N.; Ge, J.; Liu, Z. Temperature-Responsive Enzyme–

polymer Nanoconjugates with Enhanced Catalytic Activities in Organic Media. *Chem. Commun.* **2013**, *49* (54), 6090.

(86) Hu, Y.; Liang, B.; Fang, L.; Ma, G.; Yang, G.; Zhu, Q.; Chen, S.; Ye, X. Antifouling Zwitterionic Coating via Electrochemically Mediated Atom Transfer Radical Polymerization on Enzyme-Based Glucose Sensors for Long-Time Stability in 37 °C Serum. *Langmuir* **2016**, *32* (45), 11763–11770.

(87) Campbell, A. S.; Murata, H.; Carmali, S.; Matyjaszewski, K.; Islam, M. F.; Russell, A. J. Polymer-Based Protein Engineering Grown Ferrocene-Containing Redox Polymers Improve Current Generation in an Enzymatic Biofuel Cell. *Biosens. Bioelectron.* **2016**, *86*, 446–453.

(88) Huang, A.; Qin, G.; Olsen, B. D. Highly Active Biocatalytic Coatings from Protein–Polymer Diblock Copolymers. *ACS Appl. Mater. Interfaces* **2015**, *7* (27), 14660–14669.

(89) Wu, Y.; Ng, D. Y. W.; Kuan, S. L.; Weil, T. Protein–polymer Therapeutics: A Macromolecular Perspective. *Biomater. Sci.* **2015**, *3* (2), 214–230.

(90) Veronese, F. M.; Pasut, G. PEGylation, Successful Approach to Drug Delivery. *Drug Discov. Today* **2005**, *10* (21), 1451–1458.

(91) Heredia, K. L.; Bontempo, D.; Ly, T.; Byers, J. T.; Halstenberg, S.; Maynard, H. D. In Situ Preparation of Protein - "Smart" polymer Conjugates with Retention of Bioactivity. *J. Am. Chem. Soc.* **2005**, *127* (48), 16955–16960.

(92) Hills, G. Industrial Use of Lipases to Produce Fatty Acid Esters. *Eur. J. Lipid Sci. Technol.* **2003**, *105* (10), 601–607.

(93)   Bi, Y. H.; Duan, Z. Q.; Li, X. Q.; Wang, Z. Y.; Zhao, X. R. Introducing Biobased Ionic Liquids as the Nonaqueous Media for Enzymatic Synthesis of Phosphatidylserine. *J. Agric. Food Chem.* **2015**, *63* (5), 1558–1561.

(94)   Choi, J. M.; Han, S. S.; Kim, H. S. Industrial Applications of Enzyme Biocatalysis: Current Status and Future Aspects. *Biotechnol. Adv.* **2015**, *33* (7), 1443–1454.

(95)   Klibanov, A. M. Enzymatic Catalysis in Anhydrous Organic-Solvents. *Trends.in Biochem.* **1989**, *14* (4), 141–144.

(96)   Klibanov, A. M. Improving Enzymes by Using Them in Organic Solvents. *Nature* **2001**, *409* (6817), 241–246.

(97)   Abuchowski, A.; Mccoy, J. R.; Palczuk, N. C.; van Es, T.; Davis, F. F. Effect of Covalent Attachment of Polyethylene Glycol on Immunogenicity and Circulating Life of Bovine Liver Catalase *. *J. Biol. Chem.* **1976**, *252* (11), 3582–3586.

(98)   Kulkarni, S.; Schilli, C.; Grin, B.; Müller, A. H. E.; Hoffman, A. S.; Stayton, P. S. Controlling the Aggregation of Conjugates of Streptavidin with Smart Block Copolymers Prepared via the RAFT Copolymerization Technique. *Biomacromolecules* **2006**, *7* (10), 2736–2741.

(99)   Grover, G. N.; Maynard, H. D. Protein-Polymer Conjugates: Synthetic Approaches by Controlled Radical Polymerizations and Interesting Applications. *Curr. Opin. Chem. Biol.* **2010**, *14* (6), 818–827.

(100)  Wilson, P. Synthesis and Applications of Protein/Peptide-Polymer Conjugates. *Macromol. Chem. Phys.* **2017**, *218* (9), 1600595.

(101) Lele, B. S.; Murata, H.; Matyjaszewski, K.; Russell, A. J. Synthesis of Uniform Protein-Polymer Conjugates. *Biomacromolecules* **2005**, *6* (6), 3380–3387.

(102) Pelegri-O'Day, E. M.; Maynard, H. D. Controlled Radical Polymerization as an Enabling Approach for the Next Generation of Protein-Polymer Conjugates. *Acc. Chem. Res.* **2016**, *49* (9), 1777–1785.

(103) Murata, H.; Cummings, C. S.; Koepsel, R. R.; Russell, A. J. Rational Tailoring of Substrate and Inhibitor Affinity via ATRP Polymer-Based Protein Engineering. *Biomacromolecules* **2014**, *15* (7), 2817–2823.

(104) Averick, S.; Simakova, A.; Park, S.; Konkolewicz, D.; Magenau, A. J. D.; Mehl, R. A.; Matyjaszewski, K. ATRP under Biologically Relevant Conditions: Grafting from a Protein. *ACS Macro Lett.* **2012**, *1* (1), 6–10.

(105) Campbell, A. S.; Murata, H.; Carmali, S.; Matyjaszewski, K.; Islam, M. F.; Russell, A. J. Polymer-Based Protein Engineering Grown Ferrocene-Containing Redox Polymers Improve Current Generation in an Enzymatic Biofuel Cell. *Biosens. Bioelectron.* **2016**, *86*, 446–453.

(106) Gaertner, H. F.; Puigserver, A. J. Increased Activity and Stability of Poly(ethylene Glycol)-Modified Trypsin. *Enzyme Microb. Technol.* **1992**, *14* (2), 150–155.

(107) Nodake, Y.; Yamasaki, N. Some Properties of a Macromolecular Conjugate of Lysozyme Prepared by Modification with a Monomethoxypolyethylene Glycol Derivative. *Biosci. Biotechnol.* **2000**, *8451* (December).

(108) Treetharnmathurot, B.; Dieudonné, L.; Ferguson, E. L.; Schmaljohann, D.; Duncan, R.;

Wiwattanapatapee, R. Dextrin-Trypsin and ST-HPMA-Trypsin Conjugates: Enzyme Activity, Autolysis and Thermal Stability. *Int. J. Pharm.* **2009**, *373* (1-2), 68–76.

(109) Natalello, A.; Ami, D.; Collini, M.; D'Alfonso, L.; Chirico, G.; Tonon, G.; Scaramuzza, S.; Schrepfer, R.; Doglia, S. M. Biophysical Characterization of Met-G-CSF: Effects of Different Site-Specific Mono-Pegylations on Protein Stability and Aggregation. *PLoS One* **2012**, *7* (8), 1–9.

(110) Cao, L.; Shi, X.; Cui, Y.; Yang, W.; Chen, G.; Yuan, L.; Chen, H. Protein–polymer Conjugates Prepared via Host–guest Interactions: Effects of the Conjugation Site, Polymer Type and Molecular Weight on Protein Activity. *Polym. Chem.* **2016**, *7* (32), 5139–5146.

(111) Morgenstern, J.; Baumann, P.; Brunner, C.; Hubbuch, J. Effect of PEG Molecular Weight and PEGylation Degree on the Physical Stability of PEGylated Lysozyme. *Int. J. Pharm.* **2017**, *519* (1-2), 408–417.

(112) García-Arellano, H.; Valderrama, B.; Saab-Rincón, G.; Vazquez-Duhalt, R. High Temperature Biocatalysis by Chemically Modified Cytochrome c. *Bioconjug. Chem.* **2002**, *13* (6), 1336–1344.

(113) Mu, Q.; Hu, T.; Yu, J. Molecular Insight into the Steric Shielding Effect of PEG on the Conjugated Staphylokinase: Biochemical Characterization and Molecular Dynamics Simulation. *PLoS One* **2013**, *8* (7), 1–10.

(114) Farhadian, S.; Shareghi, B.; Saboury, A. A.; Babaheydari, A. K.; Raisi, F.; Heidari, E. Molecular Aspects of the Interaction of Spermidine and Alpha-Chymotrypsin. *Int. J. Biol. Macromol.* **2016**, *92*, 523–532.

(115) Yang, W.; Zhu, L.; Cui, Y.; Wang, H.; Wang, Y.; Yuan, L.; Chen, H. Improvement of Site-Directed Protein-Polymer Conjugates: High Bioactivity and Stability Using a Soft Chain-Transfer Agent. *ACS Appl. Mater. Interfaces* **2016**, *8* (25), 15967–15974.

(116) Pandey, B. K.; Smith, M. S.; Torgerson, C.; Lawrence, P. B.; Matthews, S. S.; Watkins, E.; Groves, M. L.; Prigozhin, M. B.; Price, J. L. Impact of Site-Specific PEGylation on the Conformational Stability and Folding Rate of the Pin WW Domain Depends Strongly on PEG Oligomer Length. *Bioconjug. Chem.* **2013**, *24* (5), 796–802.

(117) Plesner, B.; Westh, P.; Nielsen, A. D. Biophysical Characterisation of GlycoPEGylated Recombinant Human Factor VIIa. *Int. J. Pharm.* **2011**, *406* (1-2), 62–68.

(118) Wright, T. A.; Lucius Dougherty, M.; Schmitz, B.; Burridge, K. M.; Makaroff, K.; Stewart, J. M.; Fischesser, H. D.; Shepherd, J. T.; Berberich, J. A.; Konkolewicz, D.; et al. Polymer Conjugation to Enhance Cellulase Activity and Preserve Thermal and Functional Stability. *Bioconjug. Chem.* **2017**, *28* (10), 2638–2645.

(119) Tsukada, H.; Blow, D. M. Structure of Chymotrypsin Refined at 1.68 A Resolution. *J. Mol. Biol.* **1985**, *184*, 703–711.

(120) Fortunato, M. E.; Colina, C. M. Pysimm: A Python Package for Simulation of Molecular Systems. *SoftwareX* **2017**, *6*, 7–12.

(121) Humphrey, W.; Dalke, A.; Schulten, K. VMD: Visual Molecular Dynamics. *J. Mol. Graph.* **1996**, *14* (1), 33–38.

(122) Huang, J.; Rauscher, S.; Nawrocki, G.; Ran, T.; Feig, M.; De Groot, B. L.; Grubmüller, H.; MacKerell, A. D. CHARMM36m: An Improved Force Field for Folded and

Intrinsically Disordered Proteins. *Nat. Methods* **2016**, *14* (1), 71–73.

(123) Vanommeslaedhe, K.; Hatcher, E.; Acharya, C.; Kundu, S.; Zhong, S.; Shim, J.; Darian, E.; Guvench, O.; Lopes, P.; Vorobyov, I.; et al. CHARMM General Force Field: A Force Field for Drug-Like Molecules Compatible with the CHARMM All-Atom Additive Biological Force Fields. *J. Comput. Chem.* **2009**, *31*, 671–690.

(124) Phillips, J. C.; Braun, R.; Wang, W.; Gumbart, J.; Tajkhorshid, E.; Villa, E.; Chipot, C.; Skeel, R. D.; Kalé, L.; Schulten, K. Scalable Molecular Dynamics with NAMD. *J. Comput. Chem.* **2005**, *26* (16), 1781–1802.

(125) Darden, T.; York, D.; Pedersen, L. Particle Mesh Ewald: An N·log(N) Method for Ewald Sums in Large Systems. *J. Chem. Phys.* **1993**, *98* (12), 10089–10092.

(126) Thomas, P.; Russell, A.; Fersht, A. Tailoring the pH Dependence of Enzyme Catalysis Using Protein Engineering. *Nature* **1985**, *318* (28), 375–376.

(127) Hedstrom, L. Serine Protease Mechanism and Specificity. *Chem. Rev.* **2002**, *102* (12), 4501–4523.

(128) Cao, Z.; Jiang, S. Super-Hydrophilic Zwitterionic Poly(carboxybetaine) and Amphiphilic Non-Ionic Poly(ethylene Glycol) for Stealth Nanoparticles. *Nano Today* **2012**, *7* (5), 404–413.

(129) Keefe, A. J.; Jiang, S. Poly(zwitterionic)protein Conjugates Offer Increased Stability without Sacrificing Binding Affinity or Bioactivity. *Nat. Chem.* **2011**, *4* (1), 59–63.

(130) Pokala, N.; Handel, T. M. Review: Protein Design - Where We Were, Where We Are, Where We're Going. *J. Struct. Biol.* **2001**, *134* (2-3), 269–281.

(131) Strickler, S. S.; Gribenko, A. V.; Gribenko, A. V.; Keiffer, T. R.; Tomlinson, J.; Reihle, T.; Loladze, V. V.; Makhatadze, G. I. Protein Stability and Surface Electrostatics: A Charged Relationship. *Biochemistry* **2006**, *45* (9), 2761–2766.

(132) Sogbein, O. O.; Simmons, D. A.; Konermann, L. Effects of pH on the Kinetic Reaction Mechanism of Myoglobin Unfolding Studied by Time-Resolved Electrospray Ionization Mass Spectrometry. *J. Am. Soc. Mass Spectrom.* **2000**, *11* (4), 312–319.

(133) Rami, B. R.; Udgaonkar, J. B. pH-Jump-Induced Folding and Unfolding Studies of Barstar: Evidence for Multiple Folding and Unfolding Pathways. *Biochemistry* **2001**, *40* (50), 15267–15279.

(134) Khan, F.; Ahmad, A.; Khan, M. I. Chemical, Thermal and pH-Induced Equilibrium Unfolding Studies of Fusarium Solani Lectin. *IUBMB Life* **2007**, *59* (1), 34–43.

(135) Wood, J. L. pH-Controlled Hydrogen-Bonding ( Short Communication ). *Biochem. J.* **1974**, *143* (3), 775–777.

(136) Damodaran, S.; Kinsella, J. E. The Effects of Neutral Salts on the Stability of Macromolecules. A New Approach Using a Protein-Ligand Binding System. *J. Biol. Chem.* **1981**, *256* (7), 3394–3398.

(137) Sterling, H. J.; Prell, J. S.; Cassou, C. A.; Williams, E. R. Protein Conformation and Supercharging with DMSO from Aqueous Solution. *J. Am. Soc. Mass Spectrom.* **2011**, *22* (7), 1178–1186.

(138) Lu, D.; Wu, J.; Liu, Z. Dynamic Control of Protein Folding Pathway with a Polymer of Tunable Hydrophobicity. *J. Phys. Chem. B* **2007**, *111* (42), 12303–12309.

(139) Rubenstein, B. M.; Coluzza, I.; Miller, M. A. Controlling the Folding and Substrate-Binding of Proteins Using Polymer Brushes. *Phys. Rev. Lett.* **2012**, *108* (20), 208104–208108.

(140) Taverna, D. M.; Goldstein, R. A. Why Are Proteins Marginally Stable? *Proteins* **2002**, *46* (1), 105–109.

(141) Calligari, P. A.; Calandrini, V.; Ollivier, J.; Artero, J.-B.; Härtlein, M.; Johnson, M.; Kneller, G. R. Adaptation of Extremophilic Proteins with Temperature and Pressure: Evidence from Initiation Factor 6. *J. Phys. Chem. B* **2015**, *119* (25), 7860–7873.

(142) de Champdoré, M.; Staiano, M.; Rossi, M.; D'Auria, S. Proteins from Extremophiles as Stable Tools for Advanced Biotechnological Applications of High Social Interest. *J. R. Soc. Interface* **2007**, *4* (13), 183–191.

(143) Coker, J. A. Extremophiles and Biotechnology: Current Uses and Prospects. *F1000Research* **2016**, *5*.

(144) Radestock, S.; Gohlke, H. Exploiting the Link between Protein Rigidity and Thermostability for Data-Driven Protein Engineering. *Eng. Life Sci.* **2008**, *8* (5), 507–522.

(145) Parrott, M. C.; DeSimone, J. M. Drug Delivery: Relieving PEGylation. *Nat. Chem.* **2011**, *4* (1), 13–14.

(146) Huang, A.; Qin, G.; Olsen, B. D. Highly Active Biocatalytic Coatings from Protein-Polymer Diblock Copolymers. *ACS Appl. Mater. Interfaces* **2015**, *7* (27), 14660–14669.

(147) Shakya, A. K.; Nandakumar, K. S. An Update on Smart Biocatalysts for Industrial and Biomedical Applications. *J. R. Soc. Interface* **2018**, *15*, 1–15.

(148) Cummings, C. S.; Campbell, A. S.; Baker, S. L.; Carmali, S.; Murata, H.; Russell, A. J. Design of Stomach Acid-Stable and Mucin-Binding Enzyme Polymer Conjugates. *Biomacromolecules* **2017**, *18* (2), 576–586.

(149) Lozano, P.; de Diego, T.; Guegan, J. P.; Vaultier, M.; Iborra, J. L. Stabilization of Alpha-Chymotrypsin by Ionic Liquids in Transesterification Reactions. *Biotechnol. Bioeng.* **2001**, *75* (5), 563–569.

(150) Heredia, K. L.; Maynard, H. D. Synthesis of Protein-Polymer Conjugates. *Org. Biomol. Chem.* **2007**, *5* (1), 45–53.

(151) Trzebicka, B.; Szweda, R.; Kosowski, D.; Szweda, D.; Otulakowski, Ł.; Haladjova, E.; Dworak, A. Thermoresponsive Polymer-Peptide/protein Conjugates. *Prog. Polym. Sci.* **2017**, *68*, 35–76.

(152) Gauthier, M. a.; Klok, H.-A. Polymer–protein Conjugates: An Enzymatic Activity Perspective. *Polym. Chem.* **2010**, *1* (9), 1341–1520.

(153) Baker, S. L.; Munasinghe, A.; Murata, H.; Lin, P.; Matyjaszewski, K.; Colina, C. M.; Russell, A. J. Intramolecular Interactions of Conjugated Polymers Mimic Molecular Chaperones to Stabilize Protein–Polymer Conjugates. *Biomacromolecules* **2018**, *19*, 3798–3813.

(154) Russell, A. J.; Baker, S. L.; Colina, C. M.; Figg, C. A.; Kaar, J. L.; Matyjaszewski, K.; Simakova, A.; Sumerlin, B. S. Next Generation Protein-Polymer Conjugates. *AIChE J.* **2018**, *64* (9), 3230–3246.

(155) Baldwin, R. L. How Hofmeister Ion Interactions Affect Protein Stability. *Biophys. J.*

**1996**, *71* (4), 2056–2063.

(156) Payne, R. W.; Murphy, B. M.; Manning, M. C. Product Development Issues for PEGylated Proteins. *Pharm. Dev. Technol.* **2011**, *16* (5), 423–440.

(157) Alconcel, S. N. S.; Baas, A. S.; Maynard, H. D. FDA-Approved Poly(ethylene Glycol)-Protein Conjugate Drugs. *Polym. Chem.* **2011**, *2* (7), 1442–1448.

(158) Sarkissian, C. N.; Gamez, A.; Wang, L.; Charbonneau, M.; Fitzpatrick, P.; Lemontt, J. F.; Zhao, B.; Vellard, M.; Bell, S. M.; Henschell, C.; et al. Preclinical Evaluation of Multiple Species of PEGylated Recombinant Phenylalanine Ammonia Lyase for the Treatment of Phenylketonuria. *Proc. Natl. Acad. Sci.* **2008**, *105* (52), 20894–20899.

(159) Gámez, A.; Sarkissian, C. N.; Wang, L.; Kim, W.; Straub, M.; Patch, M. G.; Chen, L.; Striepeke, S.; Fitzpatrick, P.; Lemontt, J. F.; et al. Development of Pegylated Forms of Recombinant Rhodosporidium Toruloides Phenylalanine Ammonia-Lyase for the Treatment of Classical Phenylketonuria. *Mol. Ther.* **2005**, *11* (6), 986–989.

(160) Baker, D. P.; Lin, E. Y.; Lin, K.; Pellegrini, M.; Petter, R. C.; Chen, L. L.; Arduini, R. M.; Brickelmaier, M.; Wen, D.; Hess, D. M.; et al. N-Terminally PEGylated Human Interferon-1a with Improved Pharmacokinetic Properties and in Vivo Efficacy in a Melanoma Angiogenesis Model §. *Bioconjug. Chem.* **2006**, *17*, 179–188.

(161) EMA/CHMP/782768/2017. *Committee for Medicinal Products for Human Use (CHMP) Assessment Report*; 2017.

(162) Turecek, P. L.; Bossard, M. J.; Graninger, M.; Gritsch, H.; Höllriegl, W.; Kaliwoda, M.; Matthiessen, P.; Mitterer, A.; Muchitsch, E.-M.; Purtscher, M.; et al. BAX 855, a

PEGylated rFVIII Product with Prolonged Half-Life. Development, Functional and Structural Characterisation. *Hamostaseologie* **2012**, *32*, 29–38.

(163) Weber, A.; Engelmaier, A.; Hainzelmayer, S.; Minibeck, E.; Anderle, H.; Schwarz, H. P.; Turecek, P. L. Development, Validation, and Application of a Novel Ligand-Binding Assay to Selectively Measure PEGylated Recombinant Human Coagulation Factor VIII (BAX 855). *Bioconjug. Chem.* **2015**, *26*, 2133–2142.

(164) FDA; CBER. *May 31, 2017 Summary Basis for Regulatory Action - REBINYN*; 2017.

(165) Turecek, P. L.; Bossard, M. J.; Schoetens, F.; Ivens, I. A. PEGylation of Biopharmaceuticals: A Review of Chemistry and Nonclinical Safety Information of Approved Drugs. *J. Pharm. Sci.* **2016**, *105*, 460–475.

(166) Pace, C. N.; Scholtz, J. M.; Grimsley, G. R. Forces Stabilizing Proteins. *FEBS Lett.* **2014**, *588* (14), 2177–2184.

(167) Dill, K. A. Dominant Forces in Protein Folding. *Biochemistry* **1990**, *29* (31), 7133–7155.

(168) Zhang, Z.; Witham, S.; Alexov, E. On the Role of Electrostatics in Protein-Protein Interactions. *Phys. Biol.* **2011**, *8* (3), 035001.

(169) Pace, C. N.; Shirley, B. A.; McNutt, M.; Gajiwala, K. Forces Contributing to the Conformational Stability of Proteins. *FASEB J.* **1996**, *10* (1), 75–83.

(170) Sanchez-Ruiz, J. M.; Makhatadze, G. I. To Charge or Not to Charge? *Trends Biotechnol.* **2001**, *19* (4), 132–135.

(171) Loladze, V. V; Ibarra-Molero, B.; Sanchez-Ruiz, J. M.; Makhatadze, G. I. Engineering a

Thermostable Protein via Optimization of Charge-Charge Interactions on the Protein Surface. *Biochemistry* **1999**, *38*, 16419–16423.

(172) Marshall, S. A.; Morgan, C. S.; Mayo, S. L. Electrostatics Significantly Affect the Stability of Designed Homeodomain Variants. *J. Mol. Biol.* **2002**, *316* (1), 189–199.

(173) Park, S.; Yang, X.; Saven, J. G. Advances in Computational Protein Design. *Curr. Opin. Struct. Biol.* **2004**, *14* (4), 487–494.

(174) Dwyer, M. A.; Looger, L. L.; Hellinga, H. W.; Misura, K.; Baker, D. Computational Design of a Biologically Active Enzyme. *Science (80-. ).* **2004**, *304* (5679), 1967–1971.

(175) Chi-Fung Lee, George I. Makhatadze,  and K.-B. W. Effects of Charge-to-Alanine Substitutions on the Stability of Ribosomal Protein L30e from Thermococcus Celer. *Biochemistry* **2005**, *44*, 16817–16825.

(176) Koide, A.; Jordan, M. R.; Horner, S. R.; Batori, V.; Koide, S. Stabilization of a Fibronectin Type III Domain by the Removal of Unfavorable Electrostatic Interactions on the Protein Surface. *Biochemistry* **2001**, *40* (34), 10326–10333.

(177) Loladze, V. V; Makhatadze, G. I. Removal of Surface Charge-Charge Interactions from Ubiquitin Leaves the Protein Folded and Very Stable. *Protein Sci.* **2002**, *11* (1), 174–177.

(178) Murata, H.; Carmali, S.; Baker, S. L.; Matyjaszewski, K.; Russell, A. J. Solid-Phase Synthesis of Protein-Polymers on Reversible Immobilization Supports. *Nat. Commun.* **2018**, *9*.

(179) Le Droumaguet, B.; Nicolas, J. Recent Advances in the Design of Bioconjugates from Controlled/living Radical Polymerization. *Polym. Chem.* **2010**, *1* (5), 563.

(180) Broyer, R. M.; Grover, G. N.; Maynard, H. D. Emerging Synthetic Approaches for Protein–polymer Conjugations. *Chem. Commun.* **2011**, *47* (8), 2212–2226.

(181) Ui, N. Isoelectric Points and Conformation of Proteins II. Isoelectric Focusing of Alpha-Chymotrypsin and Its Inactive Derivative. *Biochim. Biophys. Acta* **1971**, *229*, 582–589.

(182) Isom, D. G.; Castañeda, C. A.; Cannon, B. R.; García-Moreno, B. Large Shifts in pKa Values of Lysine Residues Buried inside a Protein. *Proc. Natl. Acad. Sci. U. S. A.* **2011**, *108* (13), 5260–5265.

(183) Laurents, D. V.; Huyghues-Despointes, B. M. P.; Bruix, M.; Thurlkill, R. L.; Schell, D.; Newsom, S.; Grimsley, G. R.; Shaw, K. L.; Treviño, S.; Rico, M.; et al. Charge–Charge Interactions Are Key Determinants of the pK Values of Ionizable Groups in Ribonuclease Sa (pI=3.5) and a Basic Variant (pI=10.2). *J. Mol. Biol.* **2003**, *325* (5), 1077–1092.

(184) Lozano, P.; Combes, D.; Iborra, J. L. Effect of Polyols on Alpha-Chymotrypsin Thermostability: A Mechanistic Analysis of the Enzyme Stabilization. *J. Biotechnol.* **1994**, *35* (1), 9–18.

(185) Levitsky VYu; Panova, A. A.; Mozhaev, V. V. Correlation of High-Temperature Stability of Alpha-Chymotrypsin with "Salting-In" Properties of Solution. *Eur. J. Biochem.* **1994**, *219* (1-2), 231–236.

(186) Mozhaev, V. V.; Sergeeva, M. V.; Belova, A. B.; Khmelnitsky, Y. L. Multipoint Attachment to a Support Protects Enzyme from Inactivation by Organic Solvents: α-Chymotrypsin in Aqueous Solutions of Alcohols and Diols. *Biotechnol. Bioeng.* **1990**, *35* (7), 653–659.

(187) Dorovska-Taran, V. N.; Veeger, C.; Visser, A. J. W. G. Comparison of the Dynamic Structure of Alpha-Chymotrypsin in Aqueous Solution and in Reversed Micelles by Fluorescent Active-Site Probing. *Eur. J. Biochem.* **1993**, *211* (1-2), 47–55.

(188) Lozano, P.; De Diego, T.; Iborra, J. L. Dynamic Structure/function Relationships in the Alpha-Chymotrypsin Deactivation Process by Heat and pH. *Eur. J. Biochem.* **1997**, *248* (1), 80–85.

(189) Fersht, A. R. Conformational Equilibria in α- and δ-Chymotrypsin: The Energetics and Importance of the Salt Bridge. *J. Mol. Biol.* **1972**, *64* (2), 497–509.

(190) Shao, Q.; Jiang, S. Molecular Understanding and Design of Zwitterionic Materials. *Adv. Mater.* **2015**, *27* (1), 15–26.

(191) Liu, S.; Jiang, S. Zwitterionic Polymer-Protein Conjugates Reduce Polymer-Specific Antibody Response. *Nano Today* **2016**, *11* (3), 285–291.

(192) Kaupbayeva, B.; Murata, H.; Lucas, A.; Matyjaszewski, K.; Minden, J. S.; Russell, A. J. Molecular Sieving on the Surface of a Nano-Armored Protein. *Biomacromolecules* **2019**, *20* (3), 1235–1245.

(193) Girard, E.; Marchal, S.; Perez, J.; Finet, S.; Kahn, R.; Fourme, R.; Marassio, G.; Dhaussy, A.-C.; Prangé, T.; Giffard, M.; et al. Structure-Function Perturbation and Dissociation of Tetrameric Urate Oxidase by High Hydrostatic Pressure. *Biophys. J.* **2010**, *98* (10), 2365–2373.

(194) Gabison, L.; Prangé, T.; Colloc'h, N.; El Hajji, M.; Castro, B.; Chiadmi, M. Structural Analysis of Urate Oxidase in Complex with Its Natural Substrate Inhibited by Cyanide:

Mechanistic Implications. *BMC Struct. Biol.* **2008**, *8* (1), 32.

(195) Colloc'h, N.; Prangé, T. Functional Relevance of the Internal Hydrophobic Cavity of Urate Oxidase. *FEBS Lett.* **2014**, *588* (9), 1715–1719.

(196) Axelsen, P. H.; Harel, M.; Silman, I.; Sussman, J. L. Structure and Dynamics of the Active Site Gorge of Acetylcholinesterase: Synergistic Use of Molecular Dynamics Simulation and X-Ray Crystallography. *Protein Sci.* **1994**, *3* (2), 188–197.

(197) Dvir, H.; Silman, I.; Harel, M.; Rosenberry, T. L.; Sussman, J. L. Acetylcholinesterase: From 3D Structure to Function. *Chem. Biol. Interact.* **2010**, *187* (1-3), 10–22.

(198) Aldridge, S. Protein Purification Rules. *Pharm. Technol. Eur.* **2007**, *19* (9).

(199) Martinez, M.; Spitali, M.; Norrant, E. L.; Bracewell, D. G. Precipitation as an Enabling Technology for the Intensification of Biopharmaceutical Manufacture. *Trends Biotechnol.* **2019**, *37* (3), 237–241.

(200) Gao, W. W.; Zhang, F. X.; Zhang, G. X.; Zhou, C. H. Key Factors Affecting the Activity and Stability of Enzymes in Ionic Liquids and Novel Applications in Biocatalysis. *Biochem. Eng. J.* **2015**, *99*, 67–84.

(201) Kumar, A.; Venkatesu, P. Overview of the Stability of Alpha Chymotrypsin in Different Solvent Media. *Chem. Rev.* **2012**, *112* (7), 4283–4307.

(202) Srivastava, A.; O'Connor, I. B.; Pandit, A.; Gerard Wall, J. Polymer-Antibody Fragment Conjugates for Biomedical Applications. *Prog. Polym. Sci.* **2014**, *39* (2), 308–329.

(203) Schellekens, H.; Hennink, W. E.; Brinks, V. The Immunogenicity of Polyethylene Glycol:

Facts and Fiction. *Pharm. Res.* **2013**, *30* (7), 1729–1734.

(204) Panza, J. L.; Wagner, W. R.; Role, H. L. R.; Rao, R. H.; Beckman, E. J.; Russell, A. J. Treatment of Rat Pancreatic Islets with Reactive PEG. *Biomaterials* **2000**, *21* (11), 1155–1164.

(205) Carmali, S.; Murata, H.; Matyjaszewski, K.; Russell, A. J. Tailoring Site Specificity of Bioconjugation Using Step-Wise Atom-Transfer Radical Polymerization on Proteins. *Biomacromolecules* **2018**, *19* (10), 4044–4051.

(206) De Graaf, A. J.; Kooijman, M.; Hennink, W. E.; Mastrobattista, E. Nonnatural Amino Acids for Site-Specific Protein Conjugation. *Bioconjug. Chem.* **2009**, *20* (7), 1281–1295.

(207) Russell, A. J.; Baker, S. L.; Colina, C. M.; Figg, C. A.; Kaar, J. L.; Matyjaszewski, K.; Simakova, A.; Sumerlin, B. S. Next Generation Protein-Polymer Conjugates. *AIChE J.* **2018**, *64* (9), 3230–3246.

(208) Jönsson, M.; Linse, P. Structure and Thermodynamics of Protein-Polymer Solutions: Effects of Spatially Distributed Hydrophobic Surface Residues. *J. Phys. Chem. B* **2005**, *109* (31), 15107–15117.

(209) Zhao, W.; Liu, F.; Chen, Y.; Bai, J.; Gao, W. Synthesis of Well-Defined Protein-Polymer Conjugates for Biomedicine. *Polym. (United Kingdom)* **2015**, *66*, A1–A10.

(210) Grover, G. N.; Maynard, H. D. Protein–polymer Conjugates: Synthetic Approaches by Controlled Radical Polymerizations and Interesting Applications. *Curr. Opin. Chem. Biol.* **2010**, *14* (6), 818–827.

(211) Murata, H.; Carmali, S.; Baker, S. L.; Matyjaszewski, K.; Russell, A. J. Solid-Phase

Synthesis of Protein-Polymers on Reversible Immobilization Supports. *Nat. Commun.* **2018**, *9* (1), 1–10.

(212) Baker, S. L.; Murata, H.; Kaupbayeva, B.; Tasbolat, A.; Matyjaszewski, K.; Russell, A. J. A Charge-Preserving ATRP Initiator Rescues the Lost Function of Negatively Charged Protein-Polymer Conjugates. *Biomacromolecules* **2019**, *20* (6), 2392–2405.

(213) Yang, Z.; Domach, M.; Auger, R.; Yang, F. X.; Russell, A. J. Polyethylene Glycol-Induced Stabilization of Subtilisin. *Enzyme Microb. Technol.* **1996**, *18* (2), 82–89.

(214) Shire, S. J.; Shahrokh, Z.; Liu, J. U. N. Challenges in the Development of High Protein Concentration Formulations. *J. Pharm. Sci.* **2004**, *93* (6), 1390–1402.

(215) Kumar, V.; Sami, N.; Kashav, T.; Islam, A.; Ahmad, F.; Hassan, M. I. Protein Aggregation and Neurodegenerative Diseases: From Theory to Therapy. *Eur. J. Med. Chem.* **2016**, *124*, 1105–1120.

(216) Ross, C. A.; Poirier, M. A. Protein Aggregation and Neurodegenerative Disease. *Nat. Med.* **2004**, *10*, S10–S17.

(217) Evans, P.; Wyatt, K.; Wistow, G. J.; Bateman, O. A.; Wallace, B. A.; Slingsby, C. The P23T Cataract Mutation Causes Loss of Solubility of Folded γD-Crystallin. *J. Mol. Biol.* **2004**, *343* (2), 435–444.

(218) Jung, J.; Byeon, I.-J. L.; Wang, Y.; King, J.; Gronenborn, A. M. The Structure of the Cataract-Causing P23T Mutant of Human γD-Crystallin Exhibits Distinctive Local Conformational and Dynamic Changes. *Biochemistry* **2009**, *48* (12), 2597–2609.

(219) Konieczny, S.; Krumm, C.; Doert, D.; Neufeld, K.; Tiller, J. C. Investigations on the

Activity of poly(2-Oxazoline) Enzyme Conjugates Dissolved in Organic Solvents. *J. Biotechnol.* **2014**, *181*, 55–63.

(220) Gupta, M. N. Enzyme Function in Organic Solvents. *Eur. J. Biochem.* **1992**, *203* (1992), 25–32.

(221) Ogino, H.; Ishikawa, H. Enzymes Which Are Stable in the Presence of Organic Solvents. *J. Biosci. Bioeng.* **2001**, *91* (2), 109–116.

(222) Konieczny, S.; Fik, C. P.; Averesch, N. J. H.; Tiller, J. C. Organosoluble Enzyme Conjugates with poly(2-Oxazoline)s via Pyromellitic Acid Dianhydride. *J. Biotechnol.* **2012**, *159* (3), 195–203.

(223) Kramer, R. M.; Shende, V. R.; Motl, N.; Pace, C. N.; Martin Scholtz, J. Toward a Molecular Understanding of Protein Solubility: Increased Negative Surface Charge Correlates with Increased Solubility. *Biophys. J.* **2012**, *102*, 1907–1915.

(224) Duong-Ly, K. C.; Gabelli, S. B. Salting out of Proteins Using Ammonium Sulfate Precipitation. In *Methods in Enzymology*; 2014; pp 85–94.

(225) Hyde, A. M.; Zultanski, S. L.; Waldman, J. H.; Zhong, Y.-L.; Shevlin, M.; Peng, F. General Principles and Strategies for Salting-Out Informed by the Hofmeister Series. *Org. Process Res. Dev.* **2017**, *21*, 1355–1370.

(226) Milla, P.; Dosio, F.; Cattel, L. PEGylation of Proteins and Liposomes: A Powerful and Flexible Strategy to Improve the Drug Delivery. *Curr. Drug Metab.* **2012**, *13* (1), 105–119.

(227) Cummings, C. S.; Murata, H.; Matyjaszewski, K.; Russell, A. J. Polymer-Based Protein

Engineering Enables Molecular Dissolution of Chymotrypsin in Acetonitrile. *ACS Macro Lett.* **2016**, *5* (4), 493–497.

(228) Yoshikawa, H.; Hirano, A.; Arakawa, T.; Shiraki, K. Mechanistic Insights into Protein Precipitation by Alcohol. *Int. J. Biol. Macromol.* **2012**, *50* (3), 865–871.

(229) Schubert, P. F.; Finn, R. K. Alcohol Precipitation of Proteins: The Relationship of Denaturation and Precipitation for Catalase. *Biotechnol. Bioeng.* **1981**, *23*, 2569–2590.

(230) Ingham, K. C. Precipitation of Proteins with Polyethylene Glycol. *Methods Enzymol.* **1990**, *182*, 301–306.

(231) Zhang, L.; Wang, L.; Kao, Y.-T.; Qiu, W.; Yang, Y.; Oghaghare, O.; Zhong, D. Mapping Hydration Dynamics around a Protein Surface. *PNAS* **2007**, *104* (47), 18461–18466.

(232) Perosa, F.; Carbone, R.; Ferrone, S.; Dammacco, F. Purification of Human Immunoglobulins by Sequential Precipitation with Caprylic Acid and Ammonium Sulphate. *J. Immunol. Methods* **1990**, *128* (1), 9–16.

(233) Coelho, D. F.; Silveira, E.; Pessoa Junior, A.; Tambourgi, E. B. Bromelain Purification through Unconventional Aqueous Two-Phase System (PEG/ammonium Sulphate). *Bioprocess Biosyst. Eng.* **2013**, *36*, 185–192.

(234) Lanyi, J. K. Salt-Dependent Properties of Proteins from Extremely Halophilic Bacteria. *Bacteriol. Rev.* **1974**, *38* (3), 272–290.

(235) Ortega, G.; Diercks, T.; Millet, O. Halophilic Protein Adaptation Results from Synergistic Residue-Ion Interactions in the Folded and Unfolded States. *Chem. Biol.* **2015**, *22* (12), 1597–1607.

(236) Paul, S.; Bag, S. K.; Das, S.; Harvill, E. T.; Dutta, C. Molecular Signature of Hypersaline Adaptation: Insights from Genome and Proteome Composition of Halophilic Prokaryotes. *Genome Biol.* **2008**, *9* (4), R70.

(237) Ollivier, B.; Caumettte, P.; Garcia, J.-L.; Mah3, R. A. Anaerobic Bacteria from Hypersaline Environments. *Microbiol. Rev.* **1994**, *58* (1), 27–38.

(238) Santos, H.; da Costa, M. S. Compatible Solutes of Organisms That Live in Hot Saline Environments. *Environ. Microbiol.* **2002**, *4* (9), 501–509.

(239) Nyyssola, A.; Kerovuo, J.; Kaukinen, P.; von Weymarn, N.; Reinikainen, T. Extreme Halophiles Synthesize Betaine from Glycine by Methylation. *J. Biol. Chem.* **2000**, *275* (29), 22196–22201.

(240) Chen, H.; Yang, J.; Xiao, S.; Hu, R.; Bhaway, S. M.; Vogt, B. D.; Zhang, M.; Chen, Q.; Ma, J.; Chang, Y.; et al. Salt-Responsive Polyzwitterionic Materials for Surface Regeneration between Switchable Fouling and Antifouling Properties. *Acta Biomater.* **2016**, *40*, 62–69.

(241) Xiao, S.; Ren, B.; Huang, L.; Shen, M.; Zhang, Y.; Zhong, M.; Yang, J.; Zheng, J. Salt-Responsive Zwitterionic Polymer Brushes with Anti-Polyelectrolyte Property. *Curr. Opin. Chem. Eng.* **2018**, *19*, 86–93.

(242) Yang, J.; Chen, H.; Xiao, S.; Shen, M.; Chen, F.; Fan, P.; Zhong, M.; Zheng, J. Salt-Responsive Zwitterionic Polymer Brushes with Tunable Friction and Antifouling Properties. *Langmuir* **2015**, *31*, 9125–9133.

(243) Lezov, A. A.; Lezov, A. V.; Vlasov, P. S.; Polushina, G. E.; Domnina, N. S. Molecular

Properties of Poly(carboxybetaine) in Solutions with Different Ionic Strengths and pH Values. *Polym. Sci. Ser. A* **2011**, *53* (11), 1012–1018.

(244) Chernyy, S.; Ja, M.; Shimizu, K.; Swerin, A.; Uttrup Pedersen, S.; Daasbjerg, K.; Makkonen, L.; Claesson, P.; Iruthayaraj, J. Superhydrophilic Polyelectrolyte Brush Layers with Imparted Anti-Icing Properties: Effect of Counter Ions. *Appl. Mater. Interfaces* **2014**, *6*, 6487–6496.

(245) Urréjola, S.; Sánchez, A.; Hervello, M. F. Refractive Indices of Sodium, Potassium, and Ammonium Sulfates in Ethanol-Water Solutions. *J. Chem. Eng. Data* **2010**, *55*, 2924–2929.

(246) Gavish, N.; Promislow, K. *Dependence of the Dielectric Constant of Electrolyte Solutions on Ionic Concentration-a Microfield Approach*; 2016; Vol. 22.

(247) Nikam, P. S.; Aher, J. S.; Kharat, S. J. Viscosities of Ammonium Sulfate, Potassium Sulfate, and Aluminum Sulfate in Water and Water + N,N-Dimethylformamide Mixtures at Different Temperatures. *J. Chem. Eng. Data* **2008**, *53*, 2469–2472.

(248) Case, D. A.; Babin, V.; Berryman, J.; Betz, R. M.; Cai, Q.; Cerutti, D. S.; Cheatham III, T. E.; Darden, T. A.; Duke, R. E.; Gohlke, H.; et al. Amber 14. University of California 2014.

(249) Vanommeslaeghe, K.; Raman, E. P.; MacKerell, A. D. Automation of the CHARMM General Force Field (CGenFF) II: Assignment of Bonded Parameters and Partial Atomic Charges. *J. Chem. Inf. Model.* **2012**, *52* (12), 3155–3168.

(250) Vanommeslaeghe, K.; Hatcher, E.; Acharya, C.; Kundu, S.; Zhong, S.; Shim, J.; Darian,

E.; Guvench, O.; Lopes, P.; Vorobyov, I.; et al. CHARMM General Force Field: A Force Field for Drug-like Molecules Compatible with the CHARMM All-Atom Additive Biological Force Fields. *J. Comput. Chem.* **2009**, *31* (4), NA – NA.

(251) Zhang, Y.; Cremer, P. S.; Somorjai, G. A. The Inverse and Direct Hofmeister Series for Lysozyme. *Pnas* **2009**, *106*, 15249–15253.

(252) Bostr€, M.; Parsons, D. F.; Salis, A.; Ninham, B. W.; Monduzzi, M. Possible Origin of the Inverse and Direct Hofmeister Series for Lysozyme at Low and High Salt Concentrations. **2011**, *27*, 9504–9511.

(253) Watanabe, E. O.; Popova, E.; Miranda, E. A.; Maurer, G.; Filho, P. de A. P. Phase Equilibria for Salt-Induced Lysozyme Precipitation: Effect of Salt Type and Temperature. *Fluid Phase Equilib.* **2009**, *281* (1), 32–39.

(254) Shao, Q.; He, Y.; Jiang, S. Molecular Dynamics Simulation Study of Ion Interactions with Zwitterions. *J. Phys. Chem. B* **2011**, *115*, 8358–8363.

(255) Wang, F.; Yang, J.; Zhao, J. Understanding Anti-Polyelectrolyte Behavior of a Well-Defined Polyzwitterion at the Single-Chain Level. *Polym. Int.* **2015**, *64* (8), 999–1005.

(256) Müller, E.; Josic, D.; Schröder, T.; Moosmann, A. Solubility and Binding Properties of PEGylated Lysozyme Derivatives with Increasing Molecular Weight on Hydrophobic-Interaction Chromatographic Resins. *J. Chromatogr. A* **2010**, *1217* (28), 4696–4703.

(257) Juckles, I. R. M. Fractionation of Proteins and Viruses with Polyethylene Glycol. *Biochim. Biophys. Acta - Protein Struct.* **1971**, *229* (3), 535–546.

(258) Polson, A.; Potgieter, G. M.; Largier, J. F.; Mears, G. E. F.; Joubert, F. J. The

Fractionation of Protein Mixtures by Linear Polymers of High Molecular Weight. *Biochim. Biophys. Acta - Gen. Subj.* **1964**, *82* (3), 463–475.

(259) Capito, F.; Kolmar, H.; Stanislawski, B.; Skudas, R. Required Polymer Lengths per Precipitated Protein Molecule in Protein-Polymer Interaction. *J. Polym. Res.* **2014**, *21* (2).

(260) Wingfield, P. T. Protein Precipitation Using Ammonium Sulfate. *Curr Protoc Protein Sci* **2001**, *3*, 1–10.

(261) Gao, M.; Gawel, K.; Stokke, B. T. Polyelectrolyte and Antipolyelectrolyte Effects in Swelling of Polyampholyte and Polyzwitterionic Charge Balanced and Charge Offset Hydrogels. *Eur. Polym. J.* **2014**, *53*, 65–74.

(262) Georgiev, G. S.; Kamenska, E. B.; Vassileva, E. D.; Kamenova, I. P.; Georgieva, V. T.; Iliev, S. B.; Ivanov, I. A. Self-Assembly, Antipolyelectrolyte Effect, and Nonbiofouling Properties of Polyzwitterions. *Biomacromolecules* **2006**, *7*, 1329–1334.

(263) Zhang, Z.; Vaisocherová, H.; Cheng, G.; Yang, W.; Xue, H.; Jiang, S. Nonfouling Behavior of Polycarboxybetaine-Grafted Surfaces: Structural and Environmental Effects. *Biomacromolecules* **2008**, *9* (10), 2686–2692.

(264) Matsuoka, H.; Yamakawa, Y.; Ghosh, A.; Saruwatari, Y. Nanostructure and Salt Effect of Zwitterionic Carboxybetaine Brush at the Air/Water Interface. *Langmuir* **2015**, *31*, 4827–4836.

(265) De Grooth, J.; Ogieglo, W.; De Vos, W. M.; Gironès, M.; Nijmeijer, K.; Benes, N. E. Swelling Dynamics of Zwitterionic Copolymers: The Effects of Concentration and Type of Anion and Cation. *Eur. Pharm. Rev.* **2014**, *55*, 57–65.

(266) IMOTO, T.; DOI, Y.; HAYASHI, K.; FUNATSU, M. Characterization of Enzyme-Substrate Complex of Lysozyme. *J. Biochem.* **1969**, *65* (5), 667–671.

(267) Higaki, Y.; Inutsuka, Y.; Ono, H.; Yamada, N. L.; Ikemoto, Y.; Takahara, A. Counteranion-Specific Hydration States of Cationic Polyelectrolyte Brushes. *Ind. Eng. Chem. Res* **2018**, *57*, 4.

(268) Li, H.; Li, M.; Yu, X.; Bapat, A. P.; Sumerlin, B. S. Block Copolymer Conjugates Prepared by Sequentially Grafting from Proteins via RAFT. *Polym. Chem.* **2011**, *2* (7), 1531.

(269) Fuentes, C.; Castillo, J.; Vila, J.; Nilsson, L. Application of Asymmetric Flow Field-Flow Fractionation (AF4) and Multiangle Light Scattering (MALS) for the Evaluation of Changes in the Product Molar Mass during PVP-B-PAMPS Synthesis. *Anal. Bioanal. Chem.* **2018**, *410* (16), 3757–3767.

(270) Albertsson, P.-P.; Cajarville, A.; Brooks, D. E.; Tjerneld, F. *Partition of Proteins in Aqueous Polymer Two-Phase Systems and the Effect of Molecular Weight of the Polymer*; 1987; Vol. 926.

(271) Andrews, B. A.; Asenjo, J. A. Theoretical and Experimental Evaluation of Hydrophobicity of Proteins to Predict Their Partitioning Behavior in Aqueous Two Phase Systems: A Review. *Sep. Sci. Technol.* **2010**, *45*, 2165–2170.

(272) Asenjo, J. A.; Andrews, B. A. Aqueous Two-Phase Systems for Protein Separation: A Perspective. *J. Chromatogr. A* **2011**, *1218*, 8826–8835.

(273) Schmidt, A. S.; Andrews, B. A.; Asenjo, J. A. Correlations for the Partition Behavior of

Proteins in Aqueous Two-Phase Systems: Effect of Overall Protein Concentration. *Biotechnol. Bioeng.* **1996**, *50* (6), 617–626.

(274) Andrews, B. A.; Schmidt, A. S.; Asenjo, J. A. Correlation for the Partition Behavior of Proteins in Aqueous Two-Phase Systems: Effect of Surface Hydrophobicity and Charge. *Biotechnol. Bioeng.* **2005**, *90* (3), 380–390.